HUMBOLDT-UNIVERSITÄT ZU BERLIN

The Circadian Clock Modulates Tumour Progression and Drug Response in Colorectal Cancer Cells through Metabolic Phenotype Rewiring

D I S S E R T A T I O N

zur Erlangung des akademischen Grades

doctor rerum naturalium

(Dr. rer. nat.)

im Fach Biologie

Spezialisierung: Molekularbiologie

eingereicht an der

Lebenswissenschaftlichen Fakultät der Humboldt-Universität zu Berlin

von

M.Sc. Luise Anna Fuhr

Präsidentin der Humboldt-Universität zu Berlin

Prof. Dr.-Ing. Dr. Sabine Kunst

Dekan der Lebenswissenschaftlichen Fakultät der Humboldt-Universität zu Berlin

Prof. Dr. Bernhard Grimm

Gutachter/innen:

1. PD Dr. Angela Relógio

2. Prof. Dr. Claudia Baldus

3. Prof. Dr. Thomas F. Meyer

Tag der mündlichen Prüfung: 21.10.2019

The work presented in this thesis was developed between November 2014 and December 2017 in the group of Dr. Angela Relógio (Systems Biology of Cancer) at the Institute for Theoretical Biology (ITB) and the Molecular Cancer Research Centre (MKFZ) Charité-Universitätsmedizin Berlin, Humboldt-Universität zu Berlin, Berlin Institute of Health. The work was funded by the German Federal Ministry of Education and Research (BMBF, eBio-CIRSPLICE, FKZ031A316), and by the Berlin School of Integrative Oncology (BSIO) of the Charité–Universitätsmedizin Berlin.

Parts of this dissertation have been published [1], [2]:

L. Fuhr *et al.*, "The Circadian Clock Regulates Metabolic Phenotype Rewiring Via HKDC1 and Modulates Tumor Progression and Drug Response in Colorectal Cancer," *EBioMedicine*, vol. 33, pp. 105–121, Jul. 2018.

R. El-Athman, **L. Fuhr**, and A. Relógio, "A Systems-Level Analysis Reveals Circadian Regulation of Splicing in Colorectal Cancer," *EBioMedicine*, vol. 33, pp. 68–81, Jul. 2018.

Contents

Summary

The circadian clock is an internal timing system that allows the entrainment of physiological and behavioural processes to the geophysical time with a periodicity of about 24 hours. It consists of a central pacemaker in the suprachiasmatic nucleus (SCN) and peripheral clocks in every cell. In mammals, a distinct set of genes is interconnected in regulatory feedback loops, thereby generating oscillations in gene expression in the core-clock itself as well as in numerous target genes. Known clock target genes are, among others, involved in cellular processes connected to tumour development and progression, including metabolic pathways, drug response pathways and the cell cycle. Malfunctions of the circadian clock are associated with different pathologies including cancer and studies link the disruption of the clock to an enhanced susceptibility to develop cancer, bad treatment response and poor prognosis. Attempts have already been made to apply chronotherapy in cancer treatment. However, to date studies fail to give clear messages due to tumour heterogeneity, genetic complexity and the missing knowledge about the involvement of the circadian clock in stage-specific tumour signatures.

The aim of this project was to study the role of the circadian clock in tumour development and progression with a focus on cancer metabolism and treatment response. The role of a deregulated clock was investigated in an *in vitro* model of colorectal cancer progression, namely, SW480 cells derived from a primary tumour and SW620 cells derived from a lymph node metastasis of the same patient. The investigated cell lines showed clear differences with respect to their clock phenotypes. A time course analysis of both cell lines on the transcriptome level revealed a global shift of 24 h oscillating genes as well as distinct alterations in metabolic pathways such as glycolysis and oxidative phosphorylation. Within these pathways a set of candidate genes, including the glycolytic gene *Hkdc1*, was identified that might mediate clock-driven metabolic alterations in tumourigenesis. A knockdown (KD) of the core-clock gene *Bmal1* was introduced to study the effects of a disrupted clock on gene expression and cell metabolism. *Bmal1*-KD in SW480 cells induced a metastatic phenotype similar to SW620 wild type (WT) cells, as indicated by faster proliferation, lower apoptosis rate and a highly energetic metabolic phenotype. Furthermore, *Bmal1*-KD induced metabolic phenotype rewiring as seen by altered glycolytic activity and mitochondrial respiration, a change in time-dependent metabolic profile, gene expression changes in the tested candidate genes and modified treatment

response to metabolism-targeting anticancer treatment. A reciprocal interplay between *Bmal1* and the glycolytic gene *Hkdc1* seems to be a possible mechanism of clock-driven metabolic reprogramming in tumorigenesis. Findings from the model system could partly be confirmed in two primary cell systems, primary fibroblasts isolated from normal colon (NF) and colon adenocarcinoma (CAF) of the same patient and human fallopian tube organoids. Furthermore, co-culture experiments with NFs and CAFs and cancer cell lines showed that cell-to-cell communication influences both the clock phenotype and cell metabolism. The results obtained in this project reinforce the postulated role of *Bmal1* as a tumour suppressor and elucidate a reciprocal interplay between the circadian clock and cancer metabolism with implications in metabolic phenotype rewiring during tumour progression. Novel connections between both systems identified in this project may play a pivotal role in colorectal cancer progression and in response to anticancer therapy.

Zusammenfassung

Die zirkadiane Uhr ist ein endogenes Zeitmesssystem, das die Anpassung physiologischer Prozesse und Verhaltensweisen von Lebewesen an die geophysikalische Zeit mit einer Periodizität von etwa 24 Stunden ermöglicht. Die zirkadiane Uhr besteht aus einem zentralen Schrittmacher im suprachiasmatischen Kern (SCN) und peripheren Uhren in jeder Zelle. Bei Säugetieren ist eine bestimmte Anzahl sogenannter Uhr-Gene in regulatorischen Rückkopplungsschleifen miteinander verbunden, wodurch Oszillationen in der Expression der Uhr-Gene selbst sowie in zahlreichen Zielgenen erzeugt werden. Zielgene der zirkadianen Uhr sind unter anderem an zellulären Prozessen beteiligt, die eine Rolle bei der Tumorentstehung und -progression spielen. Dazu gehören eine Vielzahl von Stoffwechselwegen, Arzneimittelreaktionswege sowie der Zellzyklus. Funktionsstörungen der zirkadianen Uhr stehen im Zusammenhang mit verschiedenen Krankheitsbildern, unter anderem Krebs. Studienergebnisse konnten eine Funktionsstörung der zirkadianen Uhr mit einer erhöhten Anfälligkeit für Krebserkrankungen, einer schlechten Behandlungsreaktion und einer ungünstigen Prognose in Zusammenhang bringen. Es gibt bereits Therapieansätze, welche die zirkadiane Uhr des Patienten bei der Behandlung von Tumoren einbeziehen, die sogenannte Chronotherapie. Bisherige Studien konnten jedoch aufgrund der Tumorheterogenität, der genetischen Komplexität und des fehlenden Wissens über die Beteiligung der zirkadianen Uhr an spezifischen Stadien der Tumorprogression keine klaren Aussagen über die Anwendung und den Erfolg von chronotherapeutischen Behandlungsansätzen liefern.

Ziel dieses Projekts war es, die Rolle der zirkadianen Uhr bei der Tumorentstehung und -entwicklung zu untersuchen. Der Fokus lag dabei auf tumorspezifischen Stoffwechselwegen. Die Rolle einer deregulierten zirkadianen Uhr wurde in einem *in-vitro* Zellmodel untersucht. Die SW480 Zelllinie wurde aus einem Primärtumor isoliert und die SW620 Zelllinie aus einer Lymphknotenmetastase desselben Patienten, sodass diese Zelllinien zwei Tumorstadien repräsentieren und als Verlaufsmodel von kolorektalen Karzinomen genutzt werden konnten. Die untersuchten Zelllinien zeigten deutliche Unterschiede in Bezug auf ihre Uhr Phänotypen. Eine Zeitreihenanalyse beider Zelllinien auf Transkriptomebene offenbarte eine globale Verschiebung von oszillierenden Genen mit einer Periode von 24 Stunden, sowie deutliche Unterschiede in verschiedenen Stoffwechselwegen wie der Glykolyse und oxidativer Phosphorylierung. Innerhalb dieser veränderten Stoffwechselwege wurden Kandidatengene

identifiziert, die eine Rolle bei der Vermittlung von Uhr gesteuerten metabolischen Veränderungen in der Tumorgenese spielen könnten. Darunter war auch das glykolytische Gen *Hkdc1*. Um die Auswirkungen einer gestörten zirkadianen Uhr auf Genexpressions- und Zellstoffwechselebene zu untersuchen, wurde eine Runterregulation des Uhr-Gens *Bmal1* durchgeführt. Die Runterregulation von *Bmal1* führte in SW480 Zellen zu einem metastatischen Phänotyp, der stark dem von SW620 Wildtypzellen ähnelte, was durch eine schnellere Proliferation, eine niedrigere Apoptoserate und einen hochenergetischen Stoffwechselphänotyp ersichtlich war. Darüber hinaus führte die Runterregulation von *Bmal1* zu einer Veränderung des metabolischen Phänotyps, zu Genexpressionsveränderungen in den getesteten Kandidatengenen und zu einer modifizierten Antwort auf die Behandlung mit einem Glykolyseinhibitor. Des Weiteren wurde das zeitabhängige Stoffwechselprofil durch die Runterregulation von *Bmal1* in den getesteten Zelllinien verändert. Ein Mechanismus der uhrgesteuerten Reprogrammierung des Zellstoffwechsels während der Tumorgenese scheint das gegenseitige Wechselspiel zwischen *Bmal1* und dem glykolytischen Gen *Hkdc1* zu sein. Die Ergebnisse, die mit dem verwendeten Modellsystem gewonnen wurden, konnten teilweise in zwei primären Zellsystemen bestätigt werden. Zum einen in primären Fibroblasten, die aus normalem Kolon (NFs) und Kolonkarzinomzellen (CAFs) desselben Patienten isoliert wurden und zum anderen in humanen Eileiterorganoiden. Co-Kultur Experimente mit NFs und CAFs und Krebszelllinien verdeutlichten außerdem, dass die Zell-zu-Zell Kommunikation den Uhr Phänotyp sowie den Zellstoffwechsel beeinflusst. Die in diesem Projekt erzielten Ergebnisse unterstützen die postulierte Rolle von *Bmal1* als Tumorsuppressor und verdeutlichen das reziproke Wechselspiel zwischen der zirkadianen Uhr und dem Stoffwechsel von Krebszellen und zeigen mögliche Auswirkungen einer deregulierten Uhr auf den Zellmetabolismus während der Tumorentwicklung. Neue Verbindungen zwischen beiden Systemen, die in diesem Projekt identifiziert wurden, könnten eine wichtige Rolle beim Verlauf von Darmkrebs und bei der Reaktion auf Krebstherapien spielen.

Acknowledgements

I am thankful to my advisor Dr. Angela Relógio for giving me the opportunity to freely develop my research, for supporting me with guidance and discussions, and for reviewing this thesis. Additionally, I thank Prof. Thomas F. Meyer for providing me with organoids and technical support, for being part of my PhD commission and for reviewing this work. Thank you to Prof. Claudia Baldus for being part of my PhD commission and for reviewing this work.

I want to thank all members of the "Systems Biology of Cancer" group for the friendly atmosphere and scientific discussions.

My special thank goes to my colleagues in the lab, who made working in the lab so easy and fruitful.

I am deeply grateful to my parents who took care of my son while I was writing. Without them, it would not have been possible to write this thesis.

Last but not least, I want to thank my husband and my lovely son Levi for their endless support and love. Every day with you is a good day!

Selbstständigkeitserklärung

Hiermit erkläre ich, die Dissertation selbstständig und nur unter Verwendung der angegebenen Hilfen und Hilfsmittel angefertigt zu haben. Ich habe mich anderwärts nicht um einen Doktorgrad beworben und besitze keinen entsprechenden Doktorgrad. Ich erkläre, dass ich die Dissertation oder Teile davon nicht bereits bei einer anderen wissenschaftlichen Einrichtung eingereicht habe und dass sie dort weder angenommen noch abgelehnt wurde. Ich erkläre die Kenntnisnahme der dem Verfahren zugrunde liegende Promotionsordnung der Lebenswissenschaftlichen Fakultät der Humboldt-Universität zu Berlin vom 05.03.2015. Weiterhin erkläre ich, dass keine Zusammenarbeit mit gewerblichen Promotionsberaterinnen/Promotionsberatern stattgefunden hat und dass die Grundsätze der Humboldt-Universität zu Berlin zur Sicherung guter wissenschaftlicher Praxis eingehalten wurden.

Declaration

I hereby declare that I completed the doctoral thesis independently based on the stated resources and aids. I have not applied for a doctoral degree elsewhere and do not have a corresponding doctoral degree. I have not submitted the doctoral thesis, or parts of it, to another academic institution and the thesis has not been accepted or rejected. I declare that I have acknowledged the Doctoral Degree Regulations which underlie the procedure of the Faculty of Life Sciences of Humboldt-Universität zu Berlin, as amended on 05.03.2015. Furthermore, I declare that no collaboration with commercial doctoral degree supervisors took place, and that the principles of Humboldt-Universität zu Berlin for ensuring good academic practice were abided by.

Berlin, _____

_____

Luise Anna Fuhr

List of Figures

List of supplementary Figures

List of Tables

List of supplementary Tables

List of abbreviations

Table 1: List of abbreviations

Abbreviation	Description
2-DG	2-Deoxyglucose
3-BrPa	3-Bromopyruvate
5-FU	5-Fluorouracil
Acetyl-CoA	Acetyl coenzyme A
AKT	Protein kinase B
Aldh3a2	Aldehyde Dehydrogenase 3 Family Member A2
Aldoc	Aldolase, Fructose-Bisphosphate C
ALL	Acute lymphoblastic leukaemia
ANOVA	Analysis of variance
Arntl	Aryl Hydrocarbon Receptor Nuclear Translocator Like
ATP	Adenosine triphosphate
BLH	*Bmal1*-promoter-Luciferase-Hygromycin
Bmal1	Brain and muscle ARNT-like protein
CAF	Cancer-associated fibroblasts
cAMP	Cyclic adenosine monophosphate
CCG	Clock controlled genes
CCN	Core-clock network
Clock	circadian locomotor output cycles kaput
c-Myc	MYC Proto-Oncogene
CO_2	Carbon dioxide
CRC	Colorectal cancer
CREB	cAMP response element binding protein
Cry	Cryptochrome
Ctrl	Control
Dbp	D-Box Binding PAR BZIP Transcription Factor
Dex	Dexamethasone
DHEA	Dehydroepiandrosterone
DMEM	Dulbecco's Modified Eagle's Medium
DMSO	Dimethyl sulfoxide
DNA	Deoxyribonucleic acid
dNTP	Deoxyribonucleoside triphosphate
EBI	European Bioinformatics Institute
ECAR	Extracellular acidification rate
ECCN	Extended core-clock network
EGF	Epidermal growth factor
EMBL	European Molecular Biology Laboratory
ETC	Electron transport chain
FASPS	Familial advanced sleep-phase syndrome
FBS	Foetal bovine serum
FCCP	Carbonyl cyanide-4 (trifluoromethoxy)

	phenylhydrazone
FGF	Fibroblast growth factor
Fors	Forskolin
G418	Geneticin
Gapdh	Glycerinaldehyd-3-phosphat-Dehydrogenase
GLUT1	Glucose transporter 1
GO	Gene Ontology
h	Hour
H_2O	Water
HAST	Histone acetyl transferase
HEPES	4-(2-hydroxyethyl)-1-piperazineethanesulfonic acid
HK2	Hexokinase 2
Hkdc1	Hexokinase Domain Containing 1
HTA 2.0	Human Transcriptome Array 2.0
IARC	International Agency for Research on Cancer
KD	Knockdown
KEGG	Kyoto Encyclopaedia of Genes and Genomes
LB	Lysogeny broth
lfc	log fold change
MCF	Michigan Cancer Foundation
MCS	L-methyl selenocysteine
Med	Medium
MEM	Minimum essential medium
mRNA	Messenger RNA
n	Number of replicates
NAD	Nicotinamide adenine dinucleotide
NADPH	Nicotinamide adenine dinucleotide phosphate
NCRG	Network of circadian-regulated genes
NF	Normal fibroblasts
NF-κB	Nuclear factor kappa-light-chain-enhancer of activated B cells
Npas	Neuronal PAS Domain Protein 2
Nr1d1/Nr1d2	nuclear receptor subfamily 1 group D member 1/2
OCR	Oxygen consumption rate
p	p-value
P21	Cyclin Dependent Kinase Inhibitor 1A
P53	Tumour Protein P53
PBS	Phosphate buffered saline
Pck2	Phosphoenolpyruvate Carboxykinase 2
Pdhb	Pyruvate Dehydrogenase E1 Beta Subunit
PEP	Phosphoenolpyruvate
Per	Period
PI3K	Phosphoinositide 3-kinase
PKM2	Pyruvate Kinase M1/2
PLB	*Per2*-promoter-Luciferase-Blasticidin
PPAR	Peroxisome proliferator-activated receptor

qPCR	Quantitative polymerase chain reaction
RAIN	Rhythmicity Analysis Incorporating Non-Parametric Methods
Rev-erb	nuclear receptor, reverse strand of ERBA
RFU	Relative fluorescence units
RHT	Retinohypothalamic tract
RLU	Relative luminescence units
RMA	Robust Multichip Average
RNA	Ribonucleic acid
ROCK	Rho-associated protein kinase
Ror	RAR-related orphan receptor
ROS	Reactive oxygen species
Rpm	Revolutions per minute
RPMI	Roswell Park Memorial Institute medium
RSPO1	R-spondin-1
SAD	Seasonal affective disorder
SCN	Suprachiasmatic nucleus
SEM	Standard error of the mean
shRNA	Short hairpin RNA
SOB	Super optimal broth
T	Period
Tbp	TATA-binding protein
TCA	Tricarboxylic acid
TE	Tris-EDTA
TGF-β RI	Transforming growth factor beta receptor 1
Wee1	WEE1 G2 Checkpoint Kinase
Wnt3a	Wingless-Type MMTV Integration Site Family, Member 3A
WT	Wild type
WZB117	3-Fluoro-1,2-phenylene bis(3-hydroxybenzoate)

1. Introduction

1.1 The circadian clock – a powerful time-generating system

After a recovering night of sleep, we wake up in the morning, undergo our everyday routines, eat regular meals, and fall asleep in the evening to sleep during another night. A precise internal timing system is responsible for this rhythmic behaviour. To anticipate the light/dark cycles of the earth, most organisms evolved an internal timing system which adapts physiology and behaviour to the geophysical time – the circadian clock [3].

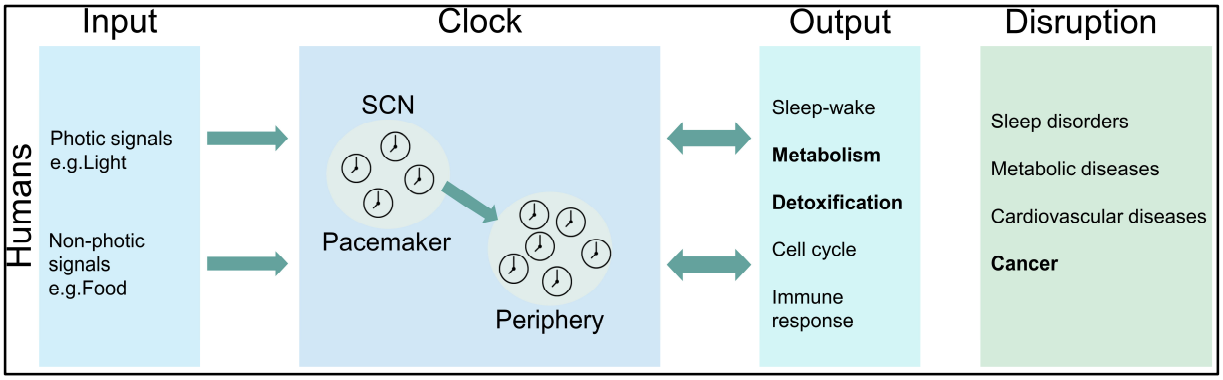

Figure 1: Organisation of the circadian timing system
The circadian timing system is organised in input pathways, clock mechanism and output pathways. In consequence of a deregulated clock, different pathologies may arise. Adapted from Albrecht [4].

The word circadian derives from the Latin words *circa diem*, which means about a day. As indicated by the name, the period of the circadian clock does not exactly measure 24 h. When organisms are kept under constant conditions such as constant light or temperature, physiological and behavioural cycles last only approximately 24 h. In humans, the free-running period length of the circadian clock is about 24.3 h [5]. Therefore, the circadian clock needs to be synchronised with the geophysical time periodically [6].

The circadian clock drives a large number of physiological and behavioural processes, which consequently follow a rhythm of around 24 h and allow an adaption to external daily rhythms [3]. Processes regulated by the circadian clock include cerebral activity, sleep-wake cycles,

metabolism, energy homeostasis, heart rate, blood pressure, body temperature, renal activity, hormone secretion and cytokine secretion [3] (**Figure 1**).

Although circadian research started already hundreds of years ago, the research field of chronobiology only came into focus during the last decades partly due to a new awareness of the role of the circadian clock in health and disease. Already in 1729 evidence for the existence of circadian rhythms was provided based on the research on leaf movements of the heliotrope plant, *Mimosa pudica,* which persisted in constant darkness and suggested the existence of an endogenous time-generating mechanism, in line with the geophysical time [7]. 200 years later, the first evidence for a genetic basis of circadian rhythms was provided by the German biologist Erwin Bünning, who reported that in common beans, the period lengths of the offspring ranged between the extremes of period lengths of the parent generation [7]. The first clock gene *Period* was identified in 1971 [8] and in 1990 the suprachiasmatic nucleus (SCN), a brain region located in the hypothalamus, was identified as the central pacemaker of the circadian clock [9]. Since then 14 core-clock genes have been identified in mammals, which generate a complex network of transcriptional and translational feedback loops, that drive oscillations in gene expression and thereby have systemic effects at the organismic level that influence numerous cellular processes [10]. The circadian clock can be described by several key characteristics. It is self-sustained, meaning that the circadian rhythm persists in the absence of environmental inputs. It is entrainable, meaning that the oscillator can be reset or phase-shifted by exposure to different time cues (e.g. light) which allows the synchronisation to the light/dark cycle. It is temperature-compensated, meaning that the circadian period only slightly changes under different physiological temperatures. Another characteristic of the circadian clock is the ability to transmit a time-signal to peripheral oscillators, thereby resetting them to the dominant zeitgeber [11].

1.1.1 Architecture of the circadian timing system

The mammalian circadian clock is hierarchically organised in three main components: input signalling pathways coming from the environment, the central pacemaker in the brain and output signalling pathways with peripheral clocks in virtually every cell. The central pacemaker is the SCN in the brain. It is built by two neuronal clusters and is located in the hypothalamus above the optic chiasm [3] (**Figure 2**). Each neuron harbours a self-sustained, cell-autonomous

molecular oscillator. The neurons of the SCN communicate with each other through synaptic and paracrine mechanisms or gap junctions to maintain phase coherence between their clocks. Additionally, peripheral clocks that have the same compositions as the ones in neurons can be found in virtually every body cell [3].

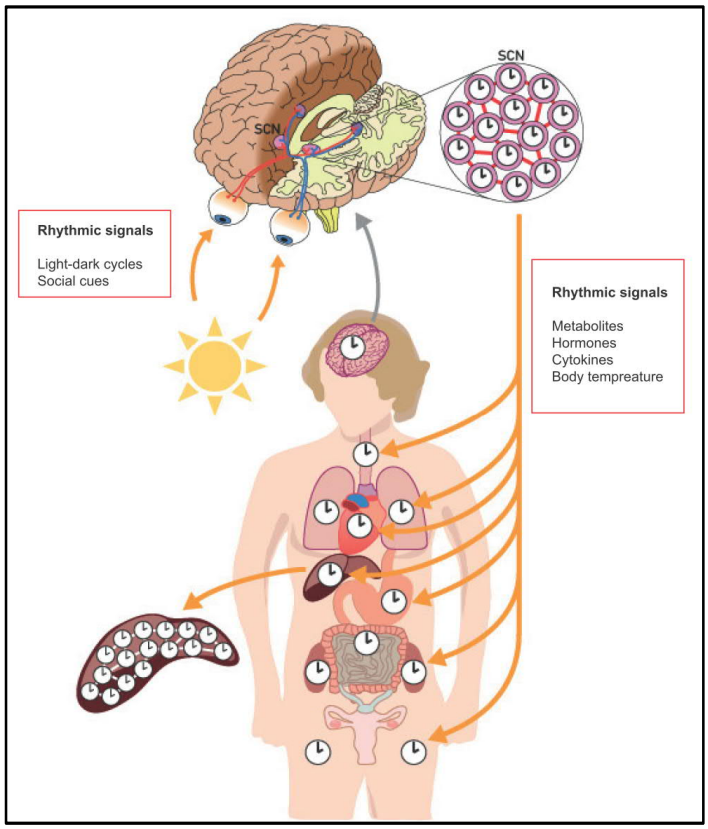

Figure 2: Architecture of the circadian timing system
The circadian timing system consists of a central pacemaker, the suprachiasmatic nucleus in the brain and peripheral clocks in virtually every cell. The phase of the SCN is synchronised to the geophysical time every day. Peripheral clocks in all cells are synchronised by the SCN through systemic signals, including metabolites, hormones, cytokines, body temperature, and neuronal signals from the peripheral nervous system. Adapted from Bollinger and Schibler [3].

The SCN coordinates rest-activity cycles and synchronises peripheral clocks but is only able to generate cycles of approximately, but not exactly 24 h. To generate cycles with a period of 24 h, it must be synchronised daily by the photoperiod to stay in synchrony with the geophysical time [3]. For this purpose, input signals are received from the environment and propagated via the input pathway to the SCN. These signals are called zeitgebers or timing cues. They are used to synchronise the pacemaker oscillations with the solar day-night cycle. Light is consequently the strongest zeitgeber, but temperature, noise, food, exercise and melatonin can act as zeitgebers as well [12], [13].

More precisely, light signals are received by rhodopsin and conopsin expressing photoreceptor cells and by intrinsically melanopsin expressing photosensitive ganglion cells in the inner layer of the retina and transmitted to the SCN via the retinohypothalamic tract (RHT) [4]. Light stimulation of the retina leads to neurotransmitter release, including glutamate, at the terminal synapses of the RHT, and the signal is then propagated to the SCN [4]. In the SCN glutamate activates NMDA-receptors, leading to a calcium influx in postsynaptic neurons. The influx results in the phosphorylation and activation of several signalling pathways that induce chromatin remodelling and the induction of immediate early genes and clock genes and the activation of protein kinases and the cAMP response element binding protein (CREB), a transcription factor which subsequently strongly activates *Per* transcription, one of the core-clock genes [13], [14]. The rapid increase of PER inhibits its own transcription as well as the transcription of *Cry*. As a result, the transcriptional rhythm of *Per* and *Cry* is reset and the clock phase is changed [3], [15]. Upon signal reception, the SCN generates and sustains rhythms that are subsequently diffused to the peripheral organs via output pathways such as the glucocorticoid pathway [16]. The SCN also transmits its rhythmic information signals to other cells within the brain and peripheral organs by other mechanisms, for example through endocrine signals (e.g. cortisol), body temperature, cytokines (e.g. transforming growth factor-β), metabolites (e.g. nicotinamide adenine dinucleotides) and neuronal signals from the peripheral nervous system [6]. The transmission of rhythmic information through neural and humoral output signals ultimately leads to the synchronisation of downstream physiology and behaviour such as sleep/wake rhythms, body temperature and hormone secretion [17].

1.1.2 The core-clock network

Clock genes are defined as genes that interact with each other to make up an auto-regulatory feedback loop, in which its activation and repression cycle takes about one day [4]. In mammals a defined number of core-clock genes interacts with one another to generate oscillations in gene expression. A sequential activation of genes leads to an auto-regulatory feedback loop with a circadian periodicity [4]. The mammalian molecular core-clock network existing in the SCN and peripheral cells is formed by a set of 14 genes interconnected in regulatory transcriptional and translational feedback loops, building the core-clock network (CCN), that accounts for the generation of circadian rhythms within individual cells [12]. These core-clock genes are members of the *Per* (period), *Cry* (cryptochrome), *Bmal* (brain and muscle ARNT-like protein),

C*lock* (circadian locomotor output cycles kaput, NPAS2 in neuronal tissue), *Ror* (RAR-related orphan receptor) and *Rev-Erb* (nuclear receptor, reverse strand of ERBA) gene and protein families [18].

During the early time of the circadian day, the CLOCK/ BMAL1 heterodimer complex is formed and regulates the transcription of all other CCN genes, by binding to E-Box sequences within the promoter regions of the target genes, *Ror*, *Rev-Erb*, *Per* and *Cry* [12], [18].

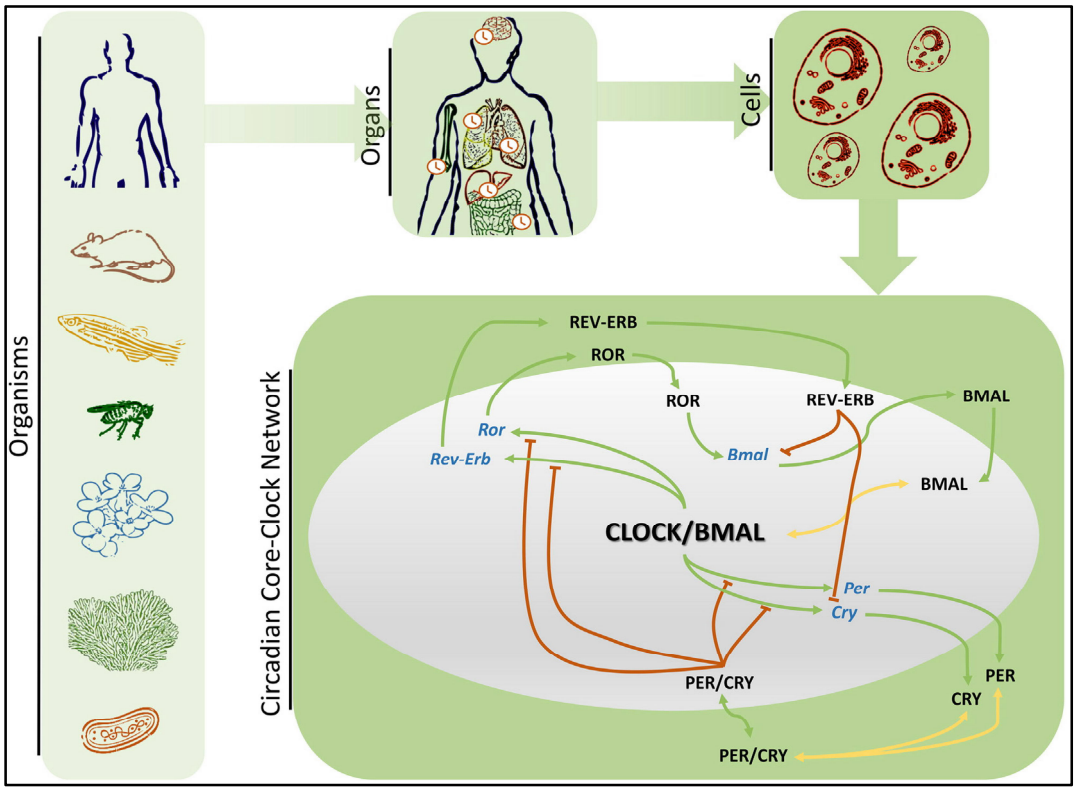

Figure 3: The circadian clock is a precise internal timing system
The circadian clock is present in a large variety of organisms from simple unicellular organisms to complex mammalian systems. In mammals, a main pacemaker is located in the SCN, and peripheral clocks exist in each organ which regulate the timing of physiological processes. Virtually every cell has its own clock that are synchronised by signals received from the main pacemaker. At the cellular level the complex CLOCK/BMAL regulates a set of positive (green) and negative (orange) interactions which form feedback-loops, thereby generating oscillations in gene expression. Adapted from **Fuhr** *et al.* [11].

More detailed, the human circadian clock consists of two regulatory feedback loops, the RORs/*Bmal*/REV-ERBs (RBR) loop and the PERs/CRYs (PC) loop [18]. In the PC feed-back loop, the rhythmically active transcription factors BMAL1 and CLOCK form heterodimers in the cytoplasm and enter the nucleus, where they bind to E-box sequences in promoters of the clock genes *Per* (Period 1-3) and *Cry*(Cryptochrome 1-2), thereby activating the expression of these genes [19]. PER and CRY proteins translocate into the cytoplasm where they form

PER/CRY complexes which translocate back into the nucleus where they act as corepressor complexes and inhibit CLOCK/BMAL- mediated transcription. They bind to CLOCK/BMAL1 heterodimers and when these complexes reach a certain concentration, they inhibit the activity of CLOCK/BMAL1 complexes. Consequently, *Per* and *Cry* transcription is no longer activated, the amounts of PER/CRY complexes decrease until they cannot longer interfere with CLOCK/BMAL1 heterodimers and a new PER/CRY accumulation cycle begins [3]. Hence, they inhibit their own transcription [19]. The second feed-back loop, the RBR loop is necessary for the robustness of the system and seems to be able to generate rhythms by itself [18]. For robustness of the circadian system, both feedback loops need to be interconnected [20] (**Figure 3**). In the RBR loop, BMAL1 and CLOCK regulate their own transcription. The CLOCK/BMAL1 complex binds to E-boxes in the promoter regions of *Rev-Erb α, β* and *Ror α, β, γ,* thereby activating their transcription. The nuclear receptors REV-ERB and ROR both compete for ROR elements (RORE) in the *Bmal1*-promoter and have antagonistic effects on *Bmal1* thereby finetuning its expression. Binding of ROR activates *Bmal1* expression, whereas binding of REV-ERB represses *Bmal1* expression. When activation prevails, the BMAL1 protein is produced which can again build heterodimers with CLOCK in the cytoplasm. These heterodimers translocate to the nucleus and initiate the next cycle of gene expression of both loops [19] (**Figure 3**).

Apart from the transcriptional network of core-clock genes, different posttranscriptional modifications on clock proteins are necessary to maintain oscillations of 24 hours. These include protein phosphorylation or acetylation as well as the histone acetyl transferase (HAT) of CLOCK [3], [19]. The acetylation of histones supports the transcription of other clock genes and makes the transcription machinery accessible, by opening condensed chromatin. The HAT activity is for example important for the transcriptional activation of *Per* and *Cry*, which are in turn key players for the maintenance of endogenous circadian rhythms [19].

1.1.3 The extended core-clock network

The CCN regulates the transcription of a large group of target genes, the so-called clock-controlled genes (CCG). To define an extended core-clock network (ECCN) a text-mining approach was used by our group. The ECCN contains 14 core-clock genes as well as their direct interacting target genes leading to a total number of 43 genes in the ECCN. Members of the

ECCN belong to pathways involved in cancer, cell cycle, immune defence, metabolism, xenobiotic detoxification and drug response [10]. Using different bioinformatic approaches, the ECCN was extended by a set of 118 genes that interact with the ECCN, leading to the network of circadian-regulated genes (NCRG), containing 161 genes in total [10], [21]. Members of the NCRG are involved in diverse biological processes, such as immune defence, apoptosis and metabolism, as well as the regulation of several miRNAs [21]. The deregulation of genes belonging to the NCRG is associated with cancer development and progression [22] (**Figure 4**).

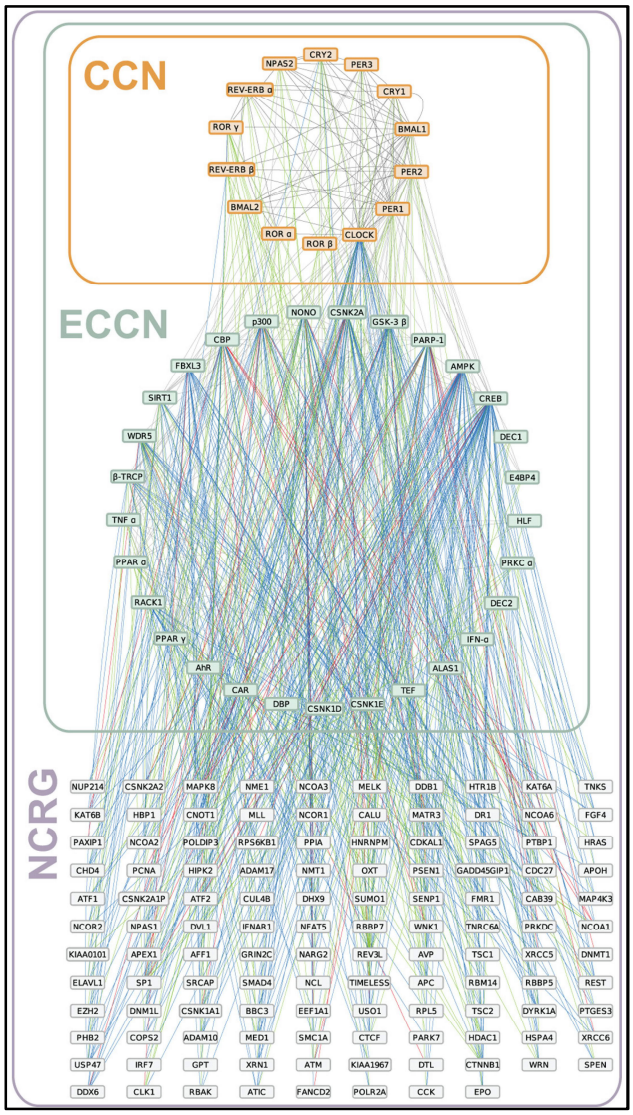

Figure 4: The network of circadian-regulated genes
Boxes represent individual genes. Connecting lines indicate interactions that are known (grey), predicted by co-expression (blue), text-mining (green) or by both (red). The CCN (orange), ECCN (green) and NCRG (purple) are indicated by rectangles. Adapted from Lehmann *et al.* [21].

Overall, about 10% of the genome is under circadian control [12], although recent studies in mice suggest that up to 50% of all genes show circadian oscillations in at least one tissue [23]. The circadian control of gene expression is highly tissue specific and only a small number of oscillating genes is present in different tissues of an organism [13]. Based on the large number of oscillating genes, it comes as no surprise that the circadian clock is involved in the regulation of a large number of processes such as the immune system [24], the metabolism of several metabolites [25], bone formation [26], sleep-awake cycles [27], memory consolidation [28], blood pressure, body temperature, cell division and proliferation [29], hormone regulation [30], apoptosis and senescence [31]. Therefore, in consequence of a deregulated clock several pathologies may arise.

1.2 The circadian clock in disease

As described above, the circadian clock regulates several biological pathways and processes. Unsurprisingly, a deregulated clock is involved in the onset of many diseases. Although it is still not completely understood how the circadian clock gets disrupted, night shift work, melatonin release, artificial light, diet and molecular deregulations or genetic disorders based on clock genes and clock-regulated genes have been identified as potential causes [32]. Altered circadian rhythms induced by clock gene knockdown (KD) lead to perturbations that have effects on the cellular and the organismic level [33], [34]. Pathologies that were already shown to be related with disrupted circadian rhythms include sleeping disorders (familial advanced sleep-phase syndrome (FASPS), sleep problems in the elderly) [18], [27], neuropsychiatric disturbances (seasonal affective disorder (SAD), bipolar disorders) [3], [18], metabolic diseases (diabetes and obesity) [35], [36], cardiovascular disorders [32] and cancer development [37]. Nonetheless, the mechanisms by which a disrupted clock leads to disease remain poorly understood. Furthermore, in many cases it is difficult to discriminate between direct effects of circadian clock disruption and a deregulated clock as a result of a certain disease.

1.2.1 The circadian clock in cancer

One connection under intensive study is the interplay between the circadian clock and cancer. The link between a disrupted clock and cancer was strengthened by several publications [37], [38] and shift work that involves circadian disruption was listed as a probable carcinogen by

the World Health Organization's International Agency for Research on Cancer (IARC) in 2007 [39]. Cancer types that were connected to night shift work by epidemiological studies include colorectal cancer [40], breast cancer [41], prostate cancer [42], endometrial cancer [43] and non-Hodgkin`s lymphoma [44]. The reason for increased cancer risk among night shift workers might be disrupted neuroendocrine function due to frequent phase shifts of external cues. This is supported by the fact that blind people display a lower cancer risk, probably because they are dependent on the endogenous clock without environmental light stimuli [39].

The dysregulation of core-clock genes can occur on different levels, including promoter methylation-induced epigenetic silencing, transcriptional and post-transcriptional modifications and structural variations of clock proteins [39]. Clock gene mutations were observed in different cancer types and as the circadian clock regulates cell cycle, DNA damage response and metabolism, disrupted circadian rhythms may lead to a deregulation of the beforementioned processes, eventually leading to tumourigenesis [37]. As an example, a study found the expression of *Per* genes to be disrupted in 95% of the examined female patients with breast cancer [45]. Various *in vitro* studies point to a tumour suppressor role of the *Per* family, as its overexpression leads to growth inhibition and apoptosis in different cancer types [45]-[47]. Furthermore, *Per2* expression levels are downregulated in lymphoma and acute myeloid leukaemia cell lines [49]. Moreover, low levels of *Per1* and *Per2* expression are linked to poor prognosis in gastric cancer [50]. Other core-clock genes that were shown to be disrupted in different cancer types include *Bmal1*, *Clock*, *Npas2* and *Cry* genes [37], [39]. *Clock* was shown to be involved in colorectal cancer, glioma and breast cancer [50]. These findings suggest a role of the circadian clock in cancer development and progression and point to a tumour suppressor role for several core-clock genes. Various studies suggest the possibility that not only one but several members of the circadian clock might be deregulated in different cancer types [39]. Depending on the experimental model used, the results gained from studies on the circadian clock and tumourigenesis are diverse. Furthermore, it partly remains unclear whether the impact of the circadian clock disruption in cancer development is directly due to the disruption of circadian rhythms itself or indirectly due to other regulatory features of core-clock genes such as regulation of the cell cycle, DNA damage responses and cellular metabolism [37].

Clock gene disruption leads to an activation of numerous oncogenic signalling pathways by activation of NF-κB, c-MYC, p53 and other elements. Additionally, a disrupted clock affects

several pathways involved in carcinogenesis. These include cell proliferation, metabolism, senescence, apoptosis, DNA damage response, DNA repair and replication and drug resistance [39]. This is underlined by the fact that a disrupted clock particularly increases the risk for tumours in systems that need constant cell proliferation for proper function, namely the immune system, the reproductive system and the digestive system [39], [51]. Another way by which the circadian clock is involved in tumourigenesis is via the regulation of the cell cycle. The circadian clock regulates the cell cycle at the G1/S and the G2/M checkpoints. Furthermore, several cell cycle-regulating genes are under circadian control, for example *Wee1*, c-*Myc*, *Cyclin-D1*, *p20* and *p21* [50], [52].

Although many studies connect the circadian clock to cancer, it is still debatable if a deregulated clock rather acts as a cause or consequence of cancer development. Furthermore, when studying the role of the circadian clock in cancer development and progression, it needs to be taken into account that *in vitro* experiments are not able to completely represent the complexity of circadian rhythms in animals [53].

1.2.1.1 The circadian clock in colorectal cancer

Different processes in the gastrointestinal tract display circadian rhythms, including motility, activity of mucosal enzymes and proliferation rate of different cell types. Therefore, disrupted circadian rhythms and gastrointestinal diseases such as cancer are likely to be tightly connected and a deregulated clock has been implicated in colorectal cancer (CRC)[54]. Colorectal cancer is the third most common cancer and a main cause of death in western societies [55]. The major cause of death related with CRC is the development of lung and liver metastases. Most of the patients with metastatic CRC remain incurable and have a median survival of two years [55].

The results of multiple studies suggest a role for the circadian clock in CRC. A study with colorectal cancer cell lines showed that *Bmal1* overexpression inhibits cell proliferation and improves oxaliplatin sensitivity in colorectal cancer [56]. *Bmal1*-knockdown studies in murine colon cancer cells revealed reduced expression levels of *Per1*, *Per2*, *Per3*, *Wee1* and *tp53*, decreased apoptosis and decreased cisplatin-induced DNA damage leading to enhanced tumour growth [54]. The circadian rhythmicity in the expression profiles of *Per1*, *Per2*, *Rev-erbα* and *Dbp* were reduced in chemically induced primary colorectal tumours as compared to normal colon and rhythmicity in *Bmal1* expression was completely abolished. While *Bmal1*

rhythmicity was also abolished in the surrounding colon tissue, the circadian expression profiles of *Per1*, *Per2*, *Rev-erbα* and *Dbp* were still existent [57]. *Per1*, *Per2*, *Per3* and *Cry2* were shown to be significantly downregulated in colorectal tumours and lower survival rates could be observed for colorectal cancers with low *Per1* and *Per3* expression [58]. A recent study using droplet digital PCR to study the expression of clock genes in human colorectal cancer reports that abnormal expression levels of *Per1* and *Per3* may be used as diagnostic and prognostic markers for colorectal cancer. Decreased levels of *Per1* and *Per3* were reported, however *Bmal1*, *Per2* and *Clock* expression were not changed [59]. Apart from that, other contradicting studies regarding the expression of clock genes exist that report upregulated clock gene expression in colorectal cancer, namely *Clock1* and *Bmal1* and *Cry* [60].

In summary, findings to date point to a role of the circadian clock in tumour suppression and the deregulation of the circadian system seems to play a role in cancer development and progression, as well as in treatment response and tolerability [3]. Nevertheless, it is difficult to interpret the partially contradicting results gained from animal models, human cell lines and patient samples, because the effects of a deregulated clock depend on the experimental model used. Additionally, as already mentioned, it is still controversial whether the impact of the circadian clock disruption in cancer development is due to the disruption of circadian rhythms itself or due to other regulatory features of core-clock genes such as regulation of the cell cycle, DNA damage responses and cellular metabolism [37].

1.2.1.2 Fundamentals of cancer metabolism

Metabolism includes all biochemical reactions that convert molecules to generate energy and structural building blocks [61]. Metabolic activity is adapted to respond to external cues which is crucial in a constantly changing environment. Discrepancies between metabolic requirements and the metabolic capacity of an organism are linked to a wide variety of pathologies, including metabolic syndrome, type 2 diabetes and cancer [61]. Cancer cells must fulfil a certain number of requirements that are essential for cell survival and proliferation. These include the generation of energy for biochemical reactions, the generation of biochemical components via biosynthetic pathways that are essential for cell division and growth and the maintenance of biochemical homeostasis. Besides the well-known hallmarks of cancer [62], cells need to fulfil these requirements to develop into malignant tumour cells [63].

In addition to the above described connection between the circadian clock and cancer, tumourigenesis is also linked to imbalanced metabolic homeostasis and to the deregulation of different metabolic pathways and specialised altered metabolic pathways may contribute to tumourigenesis [64]. Cancer cells show a vast number of metabolic alterations and specific metabolic pathways are likely to play a role in cell transformation. Metabolic alterations associated with tumourigenesis occur on all stages of cell-metabolite interaction. Consequently, the metabolic influx is affected, and allows the acquisition of necessary nutrients. The way that nutrients are allocated to different metabolic pathways contributing to tumourigenesis is altered. Metabolic alterations lead to long-term effects on cellular fate, for example changes in tumour cell differentiation or components of the tumour microenvironment [64].

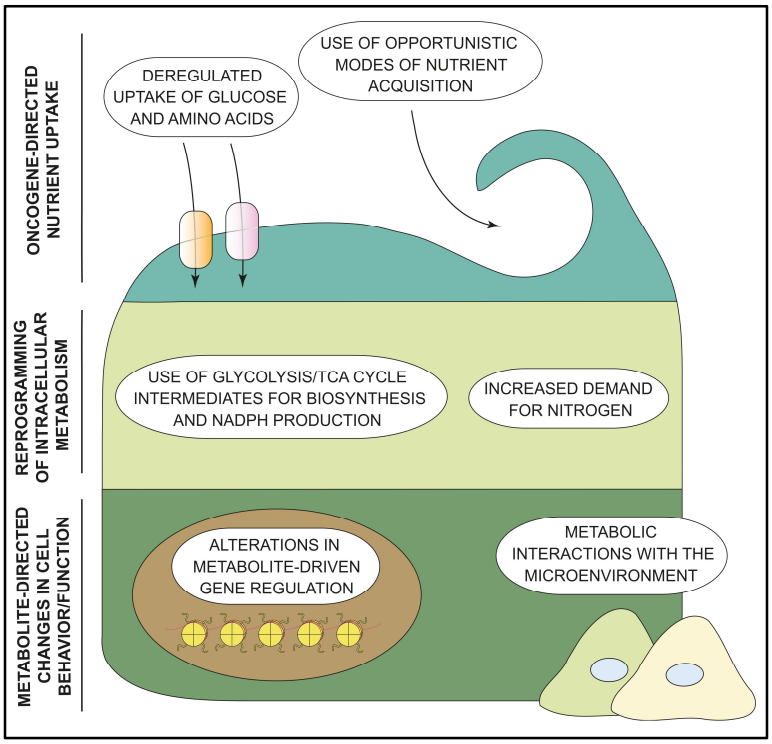

Figure 5: The emerging hallmarks of cancer metabolism
Based on metabolic alterations that occur in cancer cells, six hallmarks of cancer metabolism were defined. Namely, a deregulated uptake of glucose and amino acids, use of opportunistic modes of nutrient acquisition, use of glycolysis/TCA cycle intermediates for biosynthesis and NADPH production, increased demand for nitrogen, alterations in metabolite-driven gene regulation and metabolic interactions with the microenvironment Adapted from Pavlova and Thompson [64].

As a continuation of the well-known hallmarks of cancer [62], six metabolic alterations in cancer cells have been recently defined as the emerging hallmarks of cancer metabolism [64]. A deregulated uptake of glucose and amino acids, the use of opportunistic modes of nutrient acquisition, the use of glycolysis and the tricarboxylic acid (TCA) cycle intermediates for

biosynthesis and NADPH production, an increased demand for nitrogen, alterations in metabolite-driven gene regulation, and metabolic interactions with the microenvironment [64] (**Figure 5**). Tumours might show all six hallmarks or only some of them. These hallmarks can be used to better classify individual tumour and improve treatment [64].

One metabolic characteristic of many cancer cells is the preservation of high rates of glycolysis and concurrent oxidative phosphorylation to supply other pathways that generate macromolecules to fulfil metabolic demands of proliferating cells [65], [66]. In the glycolytic pathway, glucose enters the cell and is converted into pyruvate through a cascade of enzymatic reactions. Pyruvate can then either enter the TCA cycle or be processed to lactate. The TCA cycle is the link between glycolysis and oxidative phosphorylation. In normal cells, most of the pyruvate is processed to acetyl coenzyme A (acetyl-CoA) which enters the TCA cycle and is used for ATP production via the electron transport chain [67]. In cancer, an altered glucose metabolism is required to fulfil the anabolic demands of tumour cells [65]. Although enhanced aerobic glycolysis has been used as a marker to distinguish cancer cells from normal cells already decades ago, an elevated glucose metabolism has only very recently been defined as one of the hallmarks of cancer [64]. Aerobic glycolysis also known as the Warburg effect is an adaptation of cancer cells to the nutrient-poor tumour microenvironment and helps cancer cells to optimise nutrient uptake and metabolisation to macromolecules needed for cell growth and proliferation [68]. Already in 1956, Otto Warburg observed that cells process glucose to CO_2 and H_2O via low rates of glycolysis and subsequent oxidation of pyruvate in the TCA cycle in mitochondria. Though, cancer cells mainly use glucose for energy production by high rates of glycolysis and subsequently by lactic acid fermentation in the cytosol even in the presence of oxygen. Latter studies discovered that cancer cells show a variety of metabolic abnormalities and that oncoproteins as well as tumour suppressors influence the switch between aerobic glycolysis and the use of the TCA cycle to generate ATP. Still, the question remains, why cells use glycolysis as the preferred process which brings less energy instead of oxidative phosphorylation. Processing glucose via glycolysis produces two ATP molecules, whereas the processing by oxidative phosphorylation produces up to 36 ATP molecules [67]. The high rates of aerobic glycolysis lead to high levels of reactive oxygen species (ROS), a major cause of DNA damage promoting cancer and aging [39], but on the other hand glucose supplies other metabolic pathways with building blocks that are needed for the synthesis of lipids, nucleic acids, proteins and complex sugars, all needed for fast growing and dividing tumour cells [67].

Many members of the glycolytic pathway are associated with cancer, including glucose transporters, hexokinase 2 (HK2) and the pyruvate kinase PKM2 [67] (**Figure 6**). Furthermore, many oncogenic signalling pathways target metabolic pathways, thereby influencing tumour cell metabolism. For example, the oncogenic transcription factor MYC regulates the expression of several metabolic genes including PKM2, the predominant pyruvate kinase in cancer, the glucose transporter GLUT1, and the hexokinase HK2 [67]. Another example is the PI3K/AKT pathway. AKT leads to an upregulation of glucose transporter expression and induces glycolytic enzyme activity by phosphorylation of HK2, thereby promoting a glycolytic phenotype in cancer cells [67]. Besides the characteristic elevated use and uptake of glucose of many tumour cells, the uptake and use of acetate was described more recently as well. Acetate can be used for energy production and as a component for lipid biosynthesis. Additionally, glutamine as a substrate for energy production and glutathione synthesis came into focus very recently as elevated glutamine metabolism was shown in cancer cells [63].

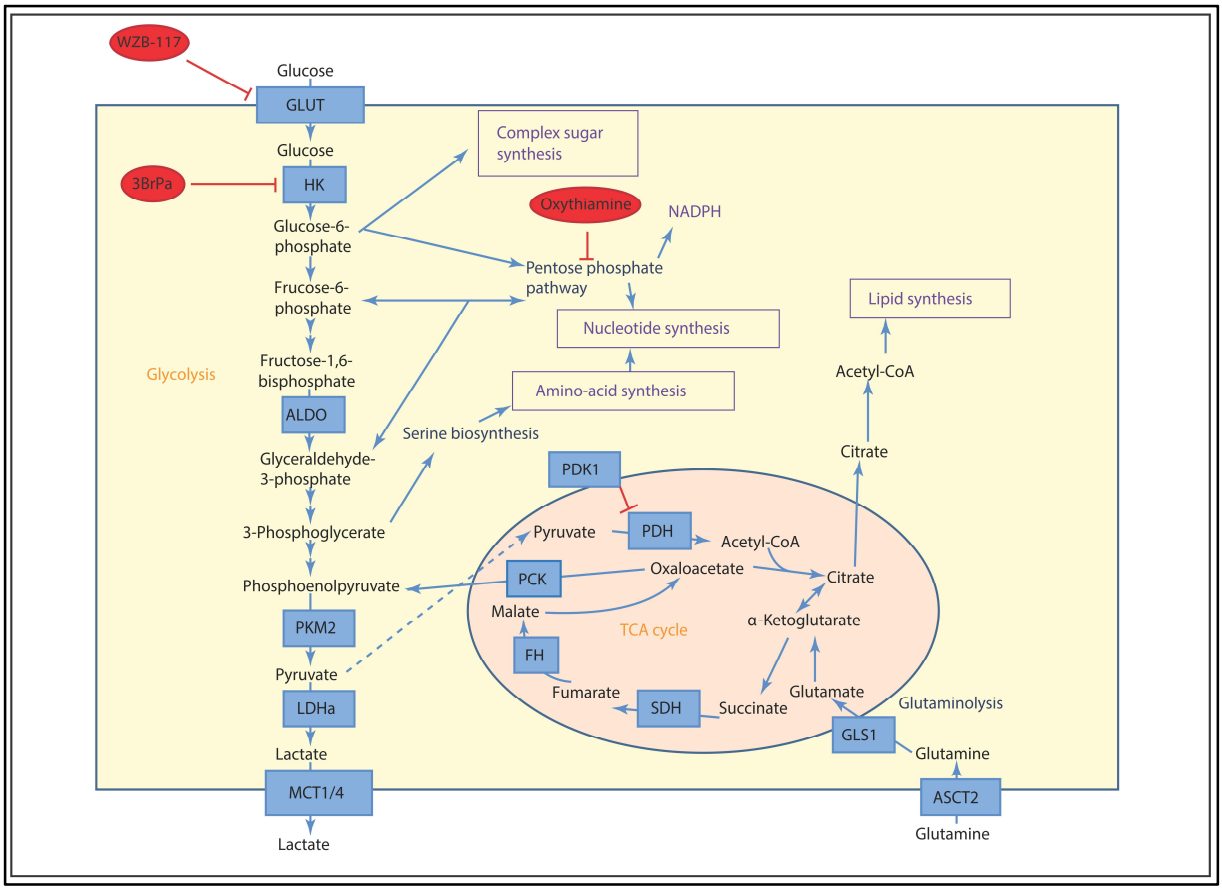

Figure 6: Targeting cancer metabolism
Metabolic pathways, key pathway interactions and enzymes (blue boxes) are shown together with key metabolic endpoints (purple boxes) necessary for proliferation and survival (biosynthetic intermediates and NADPH) as well as compounds targeting cancer metabolism (red circles). Adapted from Jones and Schulze [67].

1.2.2 Targeting cancer metabolism

Altered metabolic demands of proliferating tumour cells provide potential targets for new treatment strategies. Targeting metabolism in general is difficult and likely to cause severe side effects in patients because of the targeting of other fast-dividing cells in the bone marrow, hair follicles or intestinal crypts [69]. Although metabolic alterations of tumour cells were already observed a century ago, studies on cancer metabolism only came into renewed focus again during the last years. Concomitant, different molecular targets within metabolic pathways were tested with respect to their anticancer effects but to date most of them are still in preclinical development [70], [71]. The use of huge amounts of glucose and the metabolisation into lactate even in the presence of oxygen, known as aerobic glycolysis or Warburg effect, is a characteristic that distinguishes cancer cells from normal cells. Therefore, targeting enhanced glycolysis is a potential target for cancer therapy and research is made in this direction as well as the attempt to inhibit lactate production and excretion [69]. An example for targeting glycolysis in cancer therapy is the use of 2-deoxyglucose (2-DG), which is phosphorylated by hexokinase to 2-deoxyglucose-6-phosphate and cannot be further metabolised. Consequently, it accumulates and competitively inhibits hexokinase, therefore slowing down glucose uptake [69]. Although anti-proliferative effects of 2-DG were shown by several studies, its use in cancer therapy is limited due to severe side effects when used in effective doses [69]. Other agents tested include 3-Bromopyruvate (3-BrPa) that blocks the glycolytic flux by targeting HK2 [67]. 3-BrPa diminishes ATP reserves in the cell which is seen as a key factor for chemoresistance in cancer cells [70]. Another tested metabolism-targeting anticancer drug is oxythiamine that blocks the non-oxidative pentose phosphate pathway by targeting Transketolase[67]. Other potential targets are glucose transporters as the first rate-limiting step in glucose metabolism. WZB117 is a GLUT1 inhibitor which blocks glucose uptake and consequently decreases ATP levels and glycolytic enzyme leading to reduced glycolysis and cellular growth [70], [72]. Furthermore WZB117 has been found to repress tumour growth in nude mice [72]. WZB117 was also used in combination with 5-Fluorouracil (5-Fu) in colon cells to overcome 5-Fu resistance [73] (**Figure 6**).

1.3 Circadian regulation of metabolism – an impact in cancer?

The circadian clock regulates metabolic homeostasis and tight links between the circadian clock and the regulation of metabolism have been described previously. Time course microarray studies on different mammalian tissues revealed that a large proportion of the transcriptome (3%-20%) showed rhythmic expression in these tissues [74]. Many of the oscillating genes are members of biosynthetic and metabolic processes, such as cholesterol and lipid metabolism, glycolysis, gluconeogenesis, oxidative phosphorylation and detoxification, suggesting a tight control of metabolic pathways by the circadian clock. Noteworthy, in many cases, the rate-limiting enzymes were under circadian control [74], [75]. A publication from our group revealed a connection between the circadian clock and metabolism as well as detoxification pathways [76]. Furthermore, a reciprocal interplay of the circadian clock and mitochondrial respiratory activity has been shown recently [77], [78]. One essential link between the circadian clock and metabolism are feeding/fasting cycles. Peripheral clocks can be entrained by food intake and feeding time changes have consequences on cell metabolism [79].

One way how the circadian clock regulates metabolic homeostasis is by targeting key metabolic genes that have functions in nutrient uptake, energy storage, mitochondria biosynthesis and intracellular redox levels, including genes that are associated with the Warburg effect, namely glucose-6-phosphatase, pyruvate kinase and glucose transporter 2 [39]. Several metabolism-associated genes show circadian expression patterns, for example genes encoding for the glucagon receptor, glucokinase, glucagon, glucose transporter 2, glucose-6-phosphatase, pyruvate kinase, pyruvate dehydrogenase and HMG-CoA reductase [37], [80]. Furthermore, numerous metabolites have been shown to oscillate in a circadian manner including glucose, lipids and fatty acids with peaking levels during wakefulness and activity [61], [80], [81]. In nocturnal rodents, amino acid and xenobiotic metabolites peak during the night, while carbohydrate, lipid and nucleotide metabolites peak during the daily resting period [82]. These observations strengthen the role of the circadian clock as a regulator of metabolism.

While the circadian clock regulates multiple metabolic pathways, in turn, metabolite availability and feeding behaviour regulate the circadian clock, indicating a bidirectional interaction [37]. This reciprocal interplay provides the circadian clock with the required flexibility to adjust physiology to the metabolic requirements of cells, tissues and the whole organism [61]. Interactions between small metabolites and their cellular binding partners seem

to be one way how the feedback regulation works. So-called metabolic sensor proteins perceive fluctuations in nutrient, energy and redox levels and consequently adjust gene expression. Furthermore, systemic metabolite levels act as peripheral Zeitgebers. Circadian-regulated metabolites such as glucose [83], amino acids [84], insulin [85], glucagon [86] and glucocorticoids [87] also have Zeitgeber capacity. Different feedback mechanisms exist to adjust the circadian clock to the metabolic state of a cell, including various metabolic genes such as members of insulin and folate metabolism that affect the core-clock oscillator [61]. The strong interconnection between the circadian clock and metabolism is reinforced by the observation that circadian disruption due to environmental factors as well as genetic aberrations can lead to metabolic disorders [80]. As an example, night shift work is associated with cardiovascular disease, increased body mass, and elevated plasma glucose and lipid levels [80]. Animal experiments were performed to better understand the mechanisms of internal synchronisation and revealed that plasma glucose rhythmicity was lost in rodents that "worked" during their sleep phase and the levels of serum triglycerides was reversed with peaks during the sleep phase [88]. Furthermore, evidence suggests that a deregulated clock can promote the development of metabolic disorders, including hyperlipidaemia, fatty liver, obesity, type 2 diabetes mellitus and some types of cancer [89]. For example, animals with *Clock* or *Bmal1* knockout have been shown to develop hyperglycaemia, glucose intolerance and ultimately obesity and metabolic syndrome [61].

Besides their direct role in the core-clock network, several core-clock genes also have reported functions associated with metabolic processes. PER2 does not only bind to REV-ERBα but also to the nuclear receptors PPARα and PPARγ, thereby controlling metabolic processes in white adipose and liver tissue [80]. *Bmal1* knockout mice do not only show complete abolishment of circadian rhythms, they also display a severe metabolic phenotype, namely impaired glucose metabolism as well as insulin hypersensitivity [90]. Furthermore, several tissues in these animals show an age-dependent size reduction in accordance with elevated ROS levels [91]. Additionally, glucose and triglyceride levels are not oscillating, and gluconeogenesis is impaired in *Bmal1*-deficient mice [92]. Although *Clock*- and *Per2*-mutant mice show metabolic alterations in several studies, inconsistent findings were reported probably based on differences in the specific type of mutation and the genetic background [90].

The interplay between the circadian clock and cell metabolism has already thoroughly been studied and the connection between the circadian clock, metabolism and cancer came more and more into focus during the last years. However, the role of the circadian clock in cancer metabolism is still an area of active investigation. Studies in mice have shown that carrying mutations in individual clock genes lead to a higher susceptibility to lymphoma. Additionally, these mutant mice have increased rates of lymphoma and hepatocellular carcinoma after irradiation [93]. Furthermore, the MYC oncogene was reported to be involved in the regulation of rhythmic metabolism in cultured U2OS cells, further strengthening the connection between metabolism, cancer and the circadian clock [93]. Based on the knowledge gained so far and given the fundamental role of the circadian clock in regulating metabolism, it is very likely that the circadian clock is involved in the regulation of metabolic processes also in the context of cancer. Hence, tumourigenesis, the circadian clock and metabolism seem to be tightly interconnected. Although the reasons and the role for metabolic disruption in tumourigenesis are not fully understood, there is increasing evidence, that the circadian clock plays a crucial role [37]. Findings to date point to a role for the circadian clock in energy homeostasis and metabolism. As cancer cells consume high rates of energy, the loss of circadian metabolic regulation may lead to uncontrolled proliferation in cancer cells [50]. However detailed knowledge about the mechanisms by which the circadian clock regulates cellular metabolism in cancer is still missing. In addition to the influence of the circadian clock on metabolic pathways, drug response pathways that influence pharmacokinetics and pharmacodynamics are under circadian control as well [94]. Consequently, improved treatment response and tolerability could be achieved by chronomodulated chemotherapy [95] and time-dependent radiotherapy scheduling [96]–[99].

1.4 Chronotherapy

In addition to the promotion of tumourigenesis, weak response to anticancer treatments and early mortality were reported in cancer patients with disturbed circadian rhythms, as compared to patients with a normal circadian phenotype [39]. Daily rhythms in cancer cell proliferation, drug metabolism, toxicity and treatment efficacy are the basis for the scheduled timing of drug administration over a 24 h period, the so-called chronotherapy [54]. Based on the current knowledge about the circadian clock and its role in cancer development and progression,

chronotherapy was established as a new treatment strategy which considers the patient's circadian clock and the timing for treatment. The administration of anticancer drugs in a defined circadian time window has been postulated to achieve optimal pharmacokinetic and therapeutic effects [100]. Chronopharmacology considers the dependency of drugs on circadian rhythms and investigates the circadian variation of chronotoxicity, chronopharmacokinetics and chronopharmacodynamics of a drug [101]. Time-dependent drug administration should improve the efficacy and tolerability of a drug, while toxicity and side effects should be decreased. These effects may be mostly due to the circadian control of metabolic processes, which strongly influence the pharmacokinetics and pharmacodynamics of anticancer drugs [11]. Due to the metabolic control, the circadian clock impacts the optimal dosing time of many drugs and oscillations in drug absorption, distribution, metabolism, and excretion (ADME) account for dosing-time dependent efficacy and safety of anticancer drugs [101]. Chronotherapy schedules were already applied in radiotherapy as well as in chemotherapy. A chronomodulated chemotherapy protocol prolonged the survival of men with colorectal cancer by 3.3 months [95]. However, this effect could not be observed in women, showing the need for patient and gender specific chronotherapeutic protocols [95]. Additionally, chronotherapy increased the survival time of children with acute lymphoblastic leukaemia (ALL) [102]. The timing of radiotherapy was tested in mouse experiments where morning radiation caused more hair loss than evening radiation [96]. Secondary effects of radiotherapy in humans seem to be day-time dependent as well, but only very few rather contradictory studies exist to date [97], [98].

Another approach that considers the patient's circadian clock is the determination of different circadian biomarkers such as melatonin and cortisol levels, body temperature and rest-activity rhythms. These are often disrupted in cancer patients and can have effects like fatigue, sleep problems and decreased overall survival [103]. Therapeutic approaches in this direction have the aim to stabilise the disrupted circadian timing system of the patient. These include the regulation of the sleep-wake cycle, physical activity, light therapy, timed meals and synchronisation through chronobiotic drugs [103]. Although some studies already exist, clear results regarding the effects of chronotherapy are still rare, probably because of the heterogeneity of different tumour types and the individual circadian profile of the patients. Studies in mice showed that tolerability and efficacy of a given drug are affected by the circadian time, therefore temporal coupling of drug administration and host circadian rhythm

may lead to best therapy results [39]. Chronotherapy is more beneficial for patients with an intact circadian clock, as can be seen by less drug toxicity, better tumour response and decreased frequency of tumour metastasis [39].

Most chemotherapeutics are toxic for all proliferating cells, independent of whether they are healthy cells or cancer cells. Optimal timing for anticancer treatment therefore considers differences in the circadian phase between normal and cancer cells in order to define the best treatment time. For a variety of anticancer drugs, including 5-fluorouracil, oxaliplatin and irinotecan time-dependent effects on treatment efficacy, tolerability and pharmacokinetics have been shown [101], [104]. It seems as though the clock can affect both the efficacy of cancer treatment by modulating the pharmacokinetics and pharmacodynamics of chemotherapeutic drugs as well as the activity of the DNA repair enzymes that repair the DNA damage caused by anticancer drugs [105]. A recent study on clock gene and circadian phenotype alterations in different human cancers revealed strong connections between clock genes and clinically actionable genes, highlighting the clinical value of circadian timing in cancer chronotherapy [106].

Besides the role of the circadian clock in treatment of cancer, anticancer drugs can likewise interfere with the circadian clock and may induce disruption of rest-activity cycles, body temperature or the circadian clock itself [104]. During the last years, effort has been made to identify small molecules that act as modulators of the circadian clock by affecting the period, phase or amplitude of circadian oscillations. Possible targets for these small-molecules are core-clock proteins, nuclear hormone receptors, and clock-related kinases [100]. Small molecules are either identified by phenotype-based circadian screenings or they are developed against known clock proteins [107]. The use of small molecules can modify circadian drug metabolism and the response to existing therapeutics and might potentially be used in chronotherapy to modulate the patient´s circadian clock prior to anticancer treatment [100]. Although chronotherapy and the use of clock modulators represent a new generation of anticancer treatment, the research field of chronotherapy is still at its beginning and needs further improvement, partly shown by the fact that long-term survival is not increased in patients with metastasising cancer [39]. Detailed insights into the mechanisms of chronotherapy and its effects on tumour biology and host physiology may contribute to improved chronotherapeutic anticancer treatment.

1.5 Aims of this thesis

Studies on the circadian regulation of metabolic and cancer-related pathways came into increased focus during the last years. Still, mechanisms by which the circadian clock regulates metabolism in cancer remain subject of ongoing research. The general aim of this project was to better understand the role of circadian clock in the control of tumour metabolism and drug response. SW480 and SW620 cells, derived from a primary tumour and a metastasis of the same patient, were used as a cellular model for colorectal cancer progression. The disruption of a core-clock gene should help to investigate time-dependent metabolic phenotype rewiring in both cell lines, as well as changes in treatment response. Results of this project should contribute to elucidate the interplay between metabolic genes and the circadian clock and identify novel connections between both systems that may play a pivotal role in colorectal cancer progression and response to therapy. The hypothesis underlying this project was that tumour stage-specific alterations of the circadian clock exist, leading to a more metastatic phenotype, and that these alterations have impact on cancer cell metabolism and treatment response. An overview of the workflow of this study is represented in **Figure 7**.

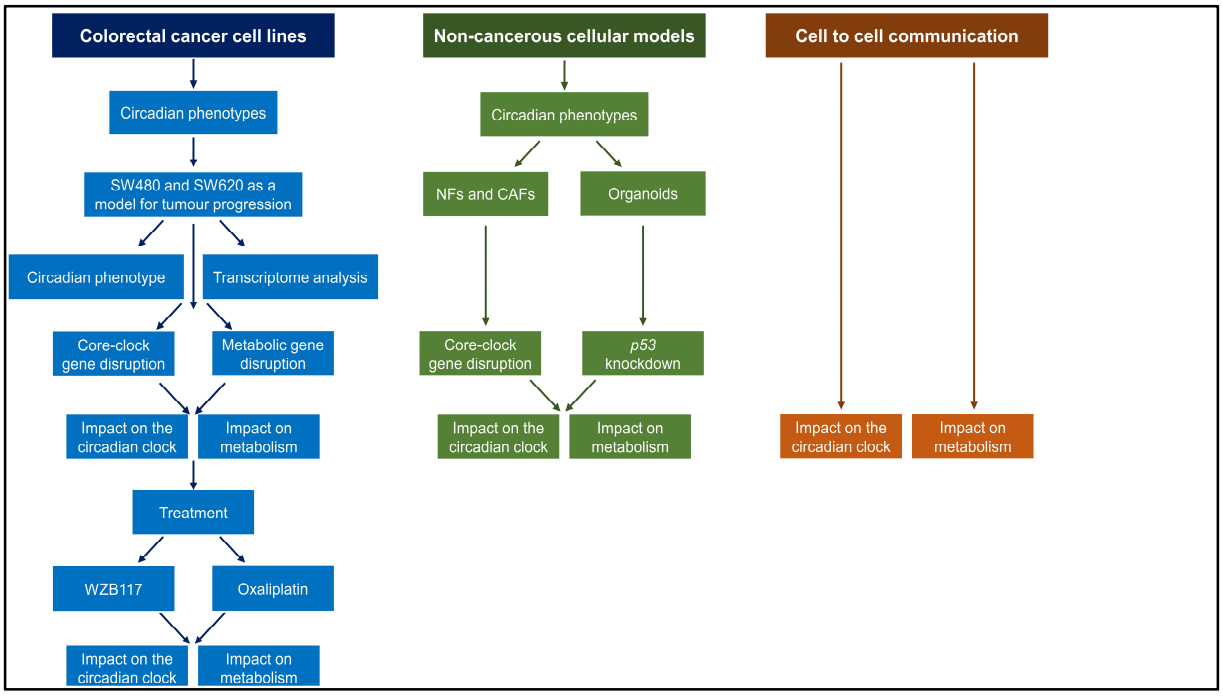

Figure 7: Experimental workflow

The specific aims of this project were:

1. Evaluation of the diversity of clock phenotypes in cancer cell lines and primary cell models by using several colorectal cancer cell lines as well as primary fibroblasts isolated from normal colon and colon adenocarcinoma of the same patient and non-cancerous human fallopian tube organoids
2. Analysis of the consequences of a deregulated clock on the transcriptome level by using SW480 and SW620 cells as a model of colorectal cancer progression. Based on the results, circadian-regulated metabolic pathways and putative clock-regulated metabolic candidate genes should be identified and used for further experiments.
3. Investigation of the effects of a deregulated clock on tumour metabolism by introducing a knockdown of the core-clock gene *Bmal1* in SW480 and SW620 cells. Additionally, NFs, CAFs and organoids should be used for supporting experiments.
4. Analysis of the effect of metabolic changes on the circadian clock by introducing a knockdown of the glycolytic gene *Hkdc1* in SW480 and SW620 cells.
5. Evaluation of the consequences of a deregulated clock on treatment response by treating SW480 and SW620 control and *shBmal1* cells with the glycolysis inhibitor WZB117.

2. Materials and methods

2.1 Materials

Table 2: Reagents, chemicals and media

Reagent	Company
100% ethanol absolute pure	Applichem
2-Mercaptoethanol	Sigma-Aldrich
2-Propanol	VWR
Activated charcoal	Sigma-Aldrich
Agarose	Thermo Fisher scientific
Ampicillin	Carl Roth
Antibiotic-Antimycotic (100x)	Gibco
Aquabator clean	Applichem
Blasticidin S HCL, powder	Life technologies
Bromopyruvic acid	Sigma-Aldrich
Calciumchlorid Dihydrat	Carl Roth
Carbenicillin	Applichem
CellMask Orange Plasma Membrane Stain	Thermo Fisher
D-(+)-Glucose	Sigma
Dexamethasone	Sigma-Aldrich
D-Luciferin	PJK
DMEM high glucose with L-Glutamine	Life technologies
DMEM high glucose, no phenol red	Gibco/Life technologies
DMEM low glucose without L-Glutamine	Lonza
DMEM/F12	Invitrogen
DMSO	Applichem
dNTP mix 10mM	Thermo scientific
FBS standard	Life technologies
Forskolin	Sigma
G418 (Geneticin)	Gibco
Gelatin	Sigma-Aldrich
GelRed Nucleic Acid Gel Stain, 10,000X in water	Biotium
Glucose	Carl Roth
GlutaMAX	Invitrogen
Glycerol	Applichem
HEPES, 1M, pH 7.2-7.5	Life technologies

HiPerFect transfection reagent	Qiagen
Human EGF	Invitrogen
Human FGF-10	Reprotech
Human noggin	Reprotech
Hyclone FBS	GE Healthcare
Hydrochloric acid solution	Sigma
Hygromycin B	Gibco
LB Agar	Carl Roth
LB Medium	Carl Roth
L-Glutamine (200mM)	Thermo Fisher scientific
Lipofectamine R 2000 Transfection Reagent	Thermo Fisher scientific
Matrigel	Corning
MEM Non-Essential Amino Acids Solution	Gibco
MEM α without nucleosides	Gibco
MEM α, nucleosides, no phenol red	Gibco
M-MLV reverse transcriptase	Life technologies
M-MLV reverse transcriptase buffer	Life technologies
MycoAlert Plus buffer	Lonza
N2	Invitrogen
Nicotinamide	Sigma
Opti-MEM R I reduced serum medium	Gibco
Oxaliplatin	Cayman Chemical
PBS 10x	Life technologies
Penicillin-Streptomycin 100x	Life technologies
Polybrene (Hexadimethrine bromide)	Sigma
Potassium cyanide	Sigma-Aldrich
Propidium iodide	Sigma
Protamine sulfate salt from salmon	Sigma
Puromycin Dihydrochloride	Gibco
Random hexamers	Eurofins MWG Operon
RiboLock RNase Inhibitor (40 U/µL)	Thermo Fisher scientific
Ribonuclease A from bovine pancreas	Sigma
ROCK inhibitor	Sigma
RPMI without L-Glutamine	Biochrom
RPMI, no phenol red	Gibco
RSPO1	Housemade stocks
Seahorse XF Base Medium	Agilent
SiR-DNA labeling	Spirochrome

Sodium pyruvate 100mM	Gibco
SsoAdvanced Universal SYBR Green	Bio-Rad
ssRNA Ladder	NEB
TE Buffer, 1X, Molecular Biology Grade	Promega
Technical ethanol	Carl Roth
TGF-β RI Kinase Inhibitor IV	Calbiochem
Triton X-100	Sigma
Trizol	Thermo Fisher scientific
Trypan blue 0.4% solution	Biozym
Tryple Express	Gibco
Ultraglutamine I 200mM	Lonza
Wnt3a	Housemade stocks
WZB-117	Sigma-Aldrich
X-tremeGENE TM HP DNA Transfection Reagent	Roche
Yeast extract	Carl Roth

Table 3: Instruments and software

Instrument/software	**Company**
CFX connect Real-time PCR detection system	Biorad
CFX manager	Biorad
Chronostar	[108]
ConsensusPathDB	http://cpdb.molgen.mpg.de
CSU-X spinning disc confocal microscope	Nikon
GraphPad Prism 6	GraphPad software
ImageJ Fiji	https://imagej.net
Lumicycle 32	Actimetrics
Lumicycle analysis	Actimetrics
LUNA automated cell counter	Logos Biosystems
NanoDrop 1000	Thermo Fisher scientific
R	https://www.r-project.org/
Seahorse wave software	Agilent
Seahorse XFe96 analyser	Agilent
Victor multilabel plate reader	PerkinElmer

Table 4: Consumables

Consumable	Company
µ-Slide 8 Well Glass Bottom	ibidi
0.1ml combitips advanced	Eppendorf
0.2µm filter	Sarstedt
0.2ml PCR tubes, individual attached caps	Kisker
0.45µm filter	Sarstedt
0.5ml combitips advanced	Eppendorf
0.5ml tubes	Sarstedt
1.5ml tubes	Eppendorf
10µl filter tips	Sarstedt
100µl filter tips	Sarstedt
1000µl filter tips	Sarstedt
10ml combitips advanced	Eppendorf
10ml serological pipettes	Sarstedt
10mm tissue culture dishes	Falcon
12 well plates	Sarstedt
15ml tubes	Kisker
175cm^2 cell culture flasks	Sarstedt
20µl filter tips	Sarstedt
200µl filter tips	Sarstedt
22mm TC coverslips	Sarstedt
24 well plates	Sarstedt
25cm^2 cell culture flasks	Sarstedt
25ml combitips advanced	Eppendorf
25ml serological pipettes	Sarstedt
2ml cryo tubes	Corning
2ml tubes	Eppendorf
35mm cell culture dishes	Falcon
35mm nunclon delta surface dishes	Thermo scientific
50ml serological pipettes	Sarstedt
50ml syringe	BD
50ml tubes	Kisker
5ml combitips advanced	Eppendorf
5ml cryo tubes	Thermo scientific
5ml serological pipettes	Sarstedt
6 well plates	Sarstedt
75cm^2 cell culture flasks	Sarstedt
96 well plates half area clear bottom black	Corning
Cell counting slides	Biozym
Hard-Shell® 96-Well PCR plates	Bio-Rad
Microseal® PCR Plate Sealing Film, adhesive, optical	Bio-Rad
Mr Frosty freezing container	Sigma Aldrich
Reagent reservoirs	Carl Roth
TC Coverslips 22mm	Sarstedt

Table 5: Cell lines, primary cells and bacteria

Cell line	Company
CaCo2	ATCC
Cancer-associated primary fibroblasts	Derived from patient material and kindly provided by Dr. Mikko Laukkanen, IRCCS SDN, Naples, Italy. (see section 2.2.1.3)
Colo678	ATCC
DH5a bacteria	ATCC
DLD1	ATCC
HCT116	ATCC
Hek293T	ATCC
HepG2	ATCC
HT29	ATCC
Human fallopian tube organoids	Derived from patient material and kindly provided by Prof. Thomas F. Meyer, Department of Molecular Biology, Max Planck Institute for Infection Biology Berlin, Germany (see section 2.2.1.2)
LIM1215	ATCC
Normal primary fibroblasts	Derived from patient material and kindly provided by Dr. Mikko Laukkanen, IRCCS SDN, Naples, Italy. (see section 2.2.1.3)
RKO	ATCC
SW480	ATCC
SW620	ATCC
U2OS	ATCC

Table 6: Constructs and plasmids

Construct	Company
REV-ERBα-VNP plasmid	Kindly provided by Ueli Schibler, Department of Molecular Biology, Sciences III, University of Geneva, iGE3, 1211 Geneva, Switzerland [109].
TRC Lentiviral pLKO.1 empty vector	Dharmacon (Catalogue no: RHS4080)
TRC-ARNTL shRNA, glycerol set	Dharmacon (Catalogue no: RHS3979-201750301)
TRC-HKDC1 shRNA, glycerol set	Dharmacon (Catalogue no: RHS4533-EG80201)
pMD2G (envelope plasmid)	Kindly provided by Prof. Achim Kramer, Laboratory of Chronobiology, Institute for Medical Immunology, Charité University of Medicine, Berlin, Germany.
BLH (*Bmal1*-promoter-Luciferase-Hygromycin)	Kindly provided by Prof. Achim Kramer, Laboratory of Chronobiology, Institute for Medical Immunology, Charité University of Medicine, Berlin, Germany [108], [110].
PLB (*Per2*-promoter-Luciferase-Blasticidin)	Kindly provided by Prof. Achim Kramer, Laboratory of Chronobiology, Institute for Medical Immunology, Charité University of Medicine, Berlin, Germany [108], [110].
psPAX (packing plasmid)	Kindly provided by Prof. Achim Kramer, Laboratory of Chronobiology, Institute for Medical Immunology, Charité University of Medicine, Berlin, Germany.

Table 7: Kits

Kit	Company
AllPrep RNA/Protein Kit	Qiagen
ApoTox-Glo TM Triplex Assay	Promega
CalPhos mammalian transfection kit	Clontech
CyQUANT Cell Proliferation Assay Kit	Thermo Fisher scientific
CytoTox-Glo Cytotoxicity Assay	Promega
GeneChip® Human Transcriptome Array 2.0	Affymetrix (Catalogue no: 902662)
MycoAlert Assay Control Set	Lonza
MycoAlert Mycoplasma Detection Kit	Lonza
PureLink HiPure Plasmid Midiprep Kit	Invitrogen
RNase free Dnase set	Qiagen
RNeasy 96 kit	Qiagen
RNeasy Mini kit	Qiagen
Seahorse XF Cell Mito Stress Test Kit	Agilent
Seahorse XF Glycolysis Stress Test Kit	Agilent
Seahorse XFe96 FluxPak mini	Agilent

Table 8: Buffers and solutions

Buffer/solution	Ingredients
SOB solution	0.5% yeast extract
	2% tryptone
	10mM NaCl
	2.5mM KCl
	10mM MgCl2
	10mM MgSO4
SOC solution	SOB solution + 20mM glucose
TB solution	10mM PIPES
	15mM CaCl2
	250mM KCl
	55mM $MnCl_2$

Table 9: Primer

Primer	Company/sequence
Hs_ALDH3A2_1_SG QuantiTect Primer Assay	Qiagen
Hs_ALDOC_1_SG QuantiTect Primer Assay	Qiagen
Hs_ARNTL_1_SG QuantiTect Primer Assay	Qiagen
Hs_CRY1_1_SG QuantiTect Primer Assay	Qiagen
Hs_CRY2_1_SG QuantiTect Primer Assay	Qiagen
Hs_GAPDH_1_SG QuantiTect Primer Assay	Qiagen
Hs_HKDC1_1_SG QuantiTect Primer Assay	Qiagen
Hs_NR1D1_1_SG QuantiTect Primer Assay	Qiagen
Hs_NR1D2_1_SG QuantiTect Primer Assay	Qiagen
Hs_PCK2_1_SG QuantiTect Primer Assay	Qiagen
Hs_PDHB_1_SG QuantiTect Primer Assay	Qiagen
Hs_PER1_1_SG QuantiTect Primer Assay	Qiagen
Hs_PER2_1_SG QuantiTect Primer Assay	Qiagen
Hs_PER3_1_SG QuantiTect Primer Assay	Qiagen
Hs_RORA_1_SG QuantiTect Primer Assay	Qiagen
Hs_RORB_1_SG QuantiTect Primer Assay	Qiagen
Hs_RORC_1_SG QuantiTect Primer Assay	Qiagen
Hs_TBP_1_SG QuantiTect Primer Assay	Qiagen
Hs_TP53_1_SG QuantiTect Primer Assay	Qiagen

2.2 Methods

2.2.1 Cell culture methods

2.2.1.1 Cultivation and subcultivation of cell lines

Cells were stored in liquid nitrogen until use. To take cells in culture, the vial was quickly thawed, and cells were transferred into falcon tubes containing complete growth medium. Cells were then centrifuged at 300 rpm for 5 minutes. The supernatant was discarded, and the cell pellet was resolved in complete growth medium. Afterwards, the cell suspension was transferred into a cell culture flask containing complete growth medium. Cells were incubated in an incubator at 37 °C and 5 % CO_2. Fresh medium was added the next day.

Table 10: Cell lines and growth medium

Cell line	Medium composition
CaCo2	DMEM low glucose without L-Glutamine, 10 % FBS, 1 % penicillin-streptomycin, 2 mM Ultraglutamine
Colo678	RPMI, 10 % FBS, 1 % penicillin-streptomycin, 1 mM sodium pyruvate, 2 mM Ultraglutamine
DLD1	RPMI, 10 % FBS, 2 mM Ultraglutamine, 1 % penicillin-streptomycin
HCT116	DMEM low glucose without L-Glutamine, 10 % FBS, 1 % penicillin-streptomycin, 2 mM Ultraglutamine
Hek293T	DMEM, 10 % FBS, 1 % penicillin-streptomycin, 25 mM HEPES
HT29	DMEM low glucose without L-Glutamine, 10 % FBS, 1 % penicillin-streptomycin, 2 mM Ultraglutamine
LIM1215	DMEM low glucose without L-Glutamine, 10 % FBS, 1 % penicillin-streptomycin, 2 mM Ultraglutamine
RKO	DMEM low glucose without L-Glutamine, 10 % FBS, 1 % penicillin-streptomycin, 2 mM Ultraglutamine
SW480	DMEM low glucose without L-Glutamine, 10 % FBS, 1 % penicillin-streptomycin, 2 mM Ultraglutamine
SW620	DMEM low glucose without L-Glutamine, 10 % FBS, 1 % penicillin-streptomycin, 2 mM Ultraglutamine
U2OS	DMEM, 10 % FBS, 1 % penicillin-streptomycin, 25 mM HEPES

Cells were cultured in complete growth medium as indicated in **Table 10** and incubated at 37 °C and 5 % CO_2. Cells were subcultivated before they reached complete confluence (about 80 %). Therefore, the culture medium was removed, and the cells were washed once with PBS and detached from the flask bottom by using TrypLE Express (2 ml for T75) and an incubation at 37 °C for 5-10 minutes, depending on the cell line. After detachment of the cells, the reaction was stopped by adding culture medium (8 ml for T75). The suspension was then transferred to

a falcon tube and centrifuged for 5 minutes at 300 rpm, RT. The supernatant was discarded, and the pellet was resolved in fresh medium. According to the subcultivation ratio, a proportion of resuspended cells was transferred into a new cell culture flask. Cells were counted, and cell viability was checked using a luna automated cell counter (Biozym) in a 1:1 trypan blue dilution. All cells were incubated at 37 °C in a humidified atmosphere with 5 % CO_2.

2.2.1.2 Cultivation of human fallopian tube organoids

Human fallopian tube samples were provided by the department of Gynaecology, Charité Medical University of Berlin, Germany. Scientific usage of the samples for experimental purposes was approved by the ethics commission of the Charité (EA1/002/07) and all subjects gave informed consent to their tissues being used in scientific research. Fragments were sourced from standard surgical procedures for benign gynaecological disease. Only anatomically normal fallopian tubes were used. Tubes were transported and dissected within 2–3 h of removal. Human fallopian tube organoids prepared for cell culture and all media and supplements needed for organoid culture as well as technical supervision were provided by the Group of Prof. Thomas F. Meyer, Department of Molecular Biology, Max Planck Institute for Infection Biology Berlin, Germany. Human fallopian tube organoids were maintained in Advanced DMEM/F12 supplemented with 12 mM HEPES, 1 % GlutaMAX, 2 % B27, 1 % N2, 10 ng/ml human EGF, 100 ng/ml human noggin, 100 ng/ml human FGF-10, 1 mM nicotinamide, 9 µM ROCK inhibitor and 0.5 µM TGF-β RI Kinase Inhibitor IV, Wnt3a and RSPO1 conditioned medium (housemade stocks) in Matrigel. Cells were isolated, maintained and cultured as previously described [111]. Organoids were incubated at 37 °C in a humidified atmosphere with 5 % CO_2.

2.2.1.3 Cultivation and subcultivation of primary fibroblasts

Normal (NF) and cancer-associated (CAF) human primary fibroblasts were isolated, prepared for cell culture and provided by the department of General, Laparoscopic and Robotic Surgery, Azienda Ospedaliera Specialistica dei Colli, Monaldi Hospital, Via Leonardo Bianchi, 80131 Naples, Italy. Fibroblasts were derived from colorectal cancer patients. The protocol and the scientific usage of the samples for experimental purposes was approved by IRCCS SDN (Comitato Etico per la Sperimentazione Clinica Progetto N:ro 2013_01_02) and Monaldi

Hospital ethical committees (Deliberazione del Direttore Generale n:o 1239). NFs were isolated from a normal colon segment with a distance of approximately 20 cm from the tumour and CAFs were isolated from the tumour of the same patient with moderately differentiated adenocarcinoma and lymph node metastasis. Fibroblasts prepared for cultivation were provided by Dr. Mikko Laukkanen, IRCCS SDN, Naples, Italy. Isolated fibroblasts were plated on gelatin (1 g/l) pre-treated dishes in αMEM supplemented with 10% Hyclone FBS, 1× antibiotic-antimycotic and 1× MEM Non-Essential Amino Acids Solution. The subcultivation protocol is described in detail in chapter 2.2.1.1.

2.2.1.4 Freezing cells

Cells were frozen before they reached complete confluence (about 80 %). Therefore, the culture medium was removed, and the cells were washed once with PBS and detached from the flask bottom by using TrypLE Express (2 ml for T75) and an incubation at 37 °C for 5-10 minutes, depending on the cell line. After detachment of the cells, the reaction was stopped by adding culture medium (8 ml for T75). The suspension was then transferred to a falcon tube and centrifuged for 5 minutes at 300 rpm, RT. The supernatant was discarded, and the pellet was resolved in freezing medium (complete growth medium supplemented with 10% DMSO) depending on the required concentration (normally $2x10^6$ cells/ml). Cell suspension was divided into cryovials. These were placed into a Mr. frosty freezing container at -80 °C overnight and then transferred to liquid nitrogen for long-term storage.

2.2.2 Cell synchronisation

For the time-dependent analysis of glycolysis, mitochondrial respiration, cell viability, cytotoxicity and apoptosis, cells were synchronised at three different timepoints prior to the treatment. Synchronisation timepoints were 24 h, 21 h and 18 h before treatment. Timepoint 0 h was defined as the timepoint of treatment at which all cells were treated simultaneously (**Figure 8**). Untreated control cells were treated in the same way, but with a vehicle control. For bioluminescence measurements after time-dependent treatment, cells were synchronised as described above in phenol-red free medium and the treatment was directly added to the dishes at timepoint 0 h immediately before bioluminescence measurements were started.

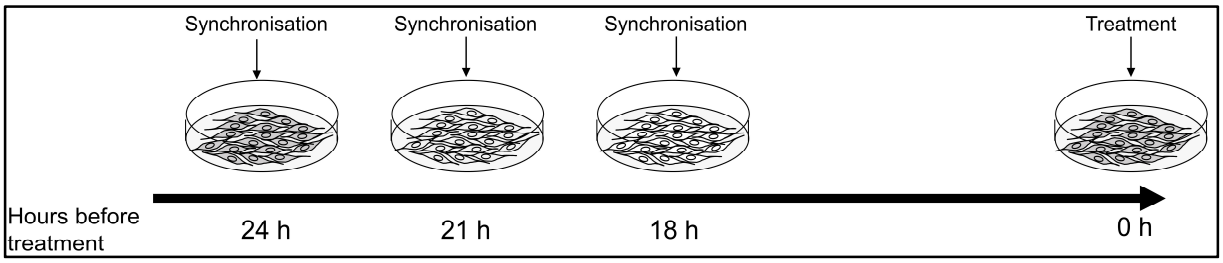

Figure 8: Treatment schedule for time-dependent treatment
Cells were synchronised 24 h, 21 h or 18 h before treatment. All cells were treated simultaneously at timepoint 0 h.

2.2.3 Proliferation curves

Cells were seeded at the same density and counted for four consecutive days 72 h – 144 h after seeding. Cells were counted, and cell viability was checked using an automated cell counter in a 1:1 trypan blue dilution.

2.2.4 Gene expression analysis

2.2.4.1 RNA purification

Total RNA was isolated using the RNeasy Mini kit (Qiagen) according to the manufacturer`s manual. Prior to the purification procedure, medium was discarded, and cells were washed twice with PBS and lysed in RLT buffer (Qiagen). To digest genomic DNA, an optional on column DNase digestion was performed, using the RNase-free DNase Set (Qiagen). RNA was eluted in 30-50 µl RNase-free water. The final RNA concentration was measured using the Nanodrop 1000. RNA was then stored at -80 °C until use.

2.2.4.2 Reverse transcription

For qPCR analysis, the extracted RNA was reverse transcribed into cDNA using random hexamers (Eurofins MWG Operon) and Reverse Transcriptase (Life technologies).

2.2.4.3 Quantitative real-time PCR

qPCR was performed using human QuantiTect Primer assays (Qiagen) and SsoAdvanced Universal SYBR Green Supermix (Biorad) in 96-well plates. The qPCR reaction and the subsequent melting curve were performed using a CFX Connect Real-Time PCR Detection System (Biorad). Briefly, after an initial denaturation at 95 °C for 10 min, the cDNA was amplified by 40 cycles of PCR (95 °C, 15 s; 60 °C, 60 s). Subsequently, a melting curve analysis was performed to detect potential unspecific amplification products. Relative gene expression levels were normalised using *Tbp* or *Gapdh* as housekeeping gene and quantified by the $2^{-\Delta\Delta Ct}$ method [112].

2.2.5 Microbiological methods

2.2.5.1 Streaking and isolating bacteria on LB agar plates

Bacteria were plated on LB-agar plates containing the appropriate antibiotic (100 µg/ml ampicillin). Using a sterile pipette tip, bacteria growing on top of a glycerol stock were touched and bacteria were gently spread on the LB-agar plate in three different dilutions. Plates were incubated overnight (12 – 18 h) at 37 °C. On the next day, single colonies could be used for further experiments.

2.2.5.2 Bacterial transformation

For bacterial transformation, a standard heat-shock transformation protocol of chemically component bacteria was used. Competent bacteria were taken out of -80 °C and thawed on ice for 20 – 30 min. 1 - 5 µl of DNA (10 pg - 100 ng) were mixed into 50 µl of competent cells in a microcentrifuge tube and gently mixed. The mixture was incubated on ice for 20 – 30 minutes. Heat shock of the transformation mixture was performed by placing the bottom of the tube 1/2 to 2/3 into a 42 °C water bath for 45 seconds. Then tubes were put back on ice for 2 minutes. 500 µl LB medium without antibiotic was added to the bacteria and bacteria were grown in a 37 °C shaking incubator for 45 minutes. Transformation mixture was plated on LB-agar plates containing the appropriate antibiotic and incubated overnight at 37 °C

2.2.5.3 Inoculating liquid bacterial culture

25 ml LB-medium containing 100 µg/ml ampicillin/carbenicillin was prepared in a flask. Using a sterile pipette tip, a single colony from the LB-agar plate was selected and the pipette tip was directly dropped into the LB-medium. The flask was covered with sterile aluminium foil and bacteria were incubated at 37 °C overnight in a shaking incubator at 180 rpm. After incubation time, plasmid DNA from the bacterial culture was isolated by using the PureLink HiPure Plasmid Midiprep Kit (Invitrogen).

2.2.5.4 Creating bacterial glycerol stocks

Bacterial glycerol stocks were prepared from liquid overnight cultures. 500 µl overnight culture was added to 500 µl 50 % glycerol in a 2 ml cryovial and gently mixed. Glycerol stocks were stored at -80 °C.

2.2.5.5 Preparing LB agar plates

LB-agar was autoclaved, and plates were labelled. Appropriate antibiotic was added to LB-agar at around 60 °C and gently mixed. LB-agar was poured into plates air bubble-free. When LB-agar in the plates was solidified, the plates were stored at 4 °C.

2.2.5.6 Preparation of ultra-competent *E. coli* for transformation

E. coli DH5a were cultured overnight at 37 °C and SOB-medium was prepared. Isolated bacteria colonies were picked with a sterile pipette tip and cultured in 250 ml SOC-medium in 1 l flasks at 19 °C and vigorous shaking to an OD of 0.5 (24-36 hours). On the next day, the flask was placed on ice for 10 minutes. Afterwards cells were pelleted by spinning at 4000 rpm for 10 minutes at 4 °C. The pellet was gently resuspended in 80 ml ice-cold TB and stored on ice for 10 minutes and again centrifuged at 4000 rpm for 10 minutes at 4 °C. The pellet was gently resuspended in 20 ml ice-cold TB and 1.4 ml DMSO. The bacterial suspension was aliquoted and stored at -80°C.

2.2.6 Measurement of metabolic activity

2.2.6.1 Measurement of basal respiration

Basal respiration was measured in a Seahorse XFe96 Analyzer (Agilent). Cells were seeded in seahorse assay plates one day prior to treatment. On the next day, cells were treated with the appropriate compound or a vehicle control and incubated for 24 hours. After 24 hours, cells were prepared according to the manual. The following medium composition was used: Seahorse XF base medium supplemented with 2 mM Glutamine, 5.5 mM glucose and 1 mM sodium pyruvate (for SW480 and SW620 cells). Extracellular acidification rate and oxygen consumption rate were measured every 30 minutes for 12 hours.

2.2.6.2 Measurement of glycolytic activity

Glycolytic activity was determined using a Seahorse XFe96 Analyzer (Agilent) and the Seahorse XF Glycolysis Stress Test Kit (Agilent). Glycolysis is, besides oxidative phosphorylation the major energy-producing pathway in the cell. The ability to switch between these two pathways, allows cells to adapt to their environment. During glycolysis, glucose is converted to pyruvate, and then converted to lactate in the cytoplasm, or CO_2 and water in the mitochondria. The conversion of glucose to pyruvate, and subsequently lactate, results in a net production and extrusion of protons into the extracellular medium, leading to an acidification of the medium. The seahorse machine measures the extracellular acidification rate (ECAR).

When using the glycolysis stress test kit, the assay procedure is as follows. First, cells are incubated in glycolysis stress test medium without glucose or pyruvate and the ECAR is measured. Subsequently, three successive chemical injections are carried out (**Figure 9**).

1. Injection of a saturating concentration of glucose. Glucose is catabolised through the glycolytic pathway to pyruvate, producing ATP, NADH, water, and protons. The ECAR increases due to proton extrusion. This glucose-induced response is reported as the rate of **glycolysis** under basal conditions.

2. The ATP synthase inhibitor oligomycin is injected and inhibits mitochondrial ATP production, and shifts the energy production to glycolysis. The increase in ECAR reveals the cellular maximum **glycolytic capacity**.

3. The last injection is 2-deoxy-glucose (2-DG), a glucose analogue, that inhibits glycolysis through competitive binding to hexokinase, the first enzyme in the glycolytic pathway. The resulting decrease in ECAR confirms that the ECAR produced in the experiment is due to glycolysis. The difference between glycolytic capacity and glycolysis rate defines glycolytic reserve. ECAR, prior to glucose injection, is referred to as non-glycolytic acidification which is caused by processes in the cell other than glycolysis.

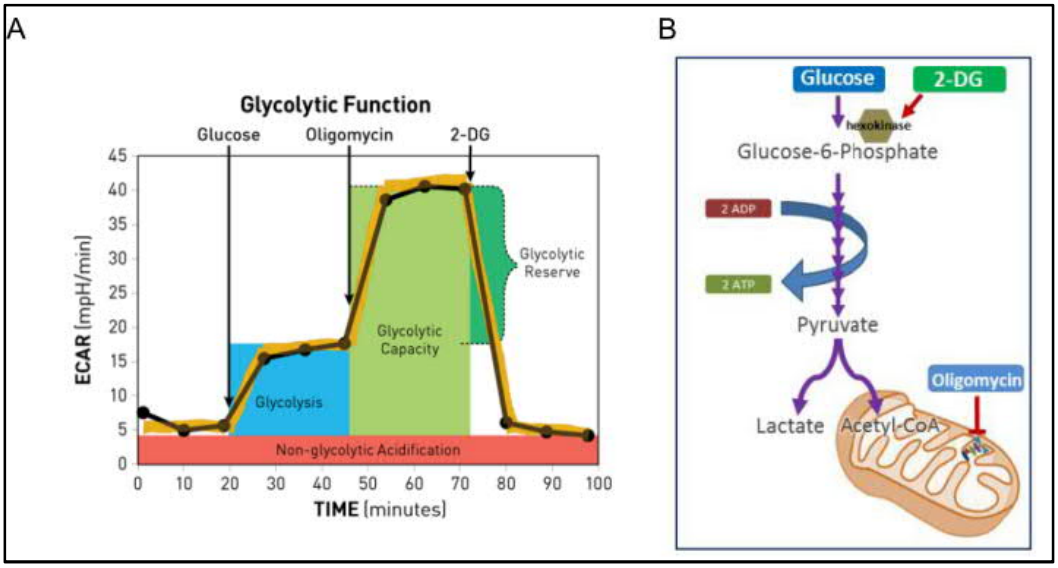

Figure 9: Glycolysis Stress Test
(**A**) Agilent Seahorse XF Glycolysis Stress Test profile of the key parameters of glycolytic function. Successive compound injections measure glycolysis and glycolytic capacity. Based on these parameters glycolytic reserve and non-glycolytic acidification can be calculated. (**B**) Schematic representation of the glycolytic pathway and the sites of action of the kit components. Glucose fuels glycolysis. Oligomycin inhibits ATP synthase in the mitochondria resulting in an increased dependence on glycolysis. 2-DG is a competitive inhibitor of glucose, and functions to shut down glycolysis. Adapted from Agilent (www.agilent.com).

Cells were seeded one day prior to the assay in 96-well seahorse plates. The assay was performed according to the manufacturer`s instructions. For the Glycolysis stress test seahorse XF base medium (Agilent) supplemented with 2 mM L-Glutamine was used and 10 mM glucose, 1 µM oligomycin and 50 mM 2-DG was used for the injections. Subsequently, plates were normalised based on the DNA content using the CyQuant kit (Thermo Fisher scientific) according to the manufacturer`s instructions. Data was analysed using the wave software (Agilent).

2.2.6.3 Measurement of mitochondrial respiration

Mitochondrial respiration was determined using a Seahorse XFe96 Analyzer (Agilent) and the Seahorse XF Cell Mito Stress Test Kit (Agilent). The kit measures key parameters of mitochondrial function by directly measuring the oxygen consumption rate (OCR) of cells. Different modulators of cellular respiration (oligomycin, FCCP, and a mix of rotenone and antimycin A) are serially injected into the medium to target components of the electron transport chain (ETC) in mitochondria. ATP production, maximal respiration, and non-mitochondrial respiration are measured. Each compound targets a specific component of the ETC (**Figure 10**).

1. Oligomycin inhibits ATP synthase (complex V) and the decrease in OCR following injection of oligomycin correlates with the mitochondrial respiration associated with cellular **ATP production**.

2. FCCP is an uncoupling agent that collapses the proton gradient and disrupts the mitochondrial membrane potential. As a result, electron flow through the ETC is uninhibited and oxygen is maximally consumed by complex IV (**maximal respiration**).

3. The third injection is a mix of rotenone, a complex I inhibitor, and antimycin A, a complex III inhibitor. This combination shuts down mitochondrial respiration and enables the calculation of non-mitochondrial respiration driven by processes outside the mitochondria.

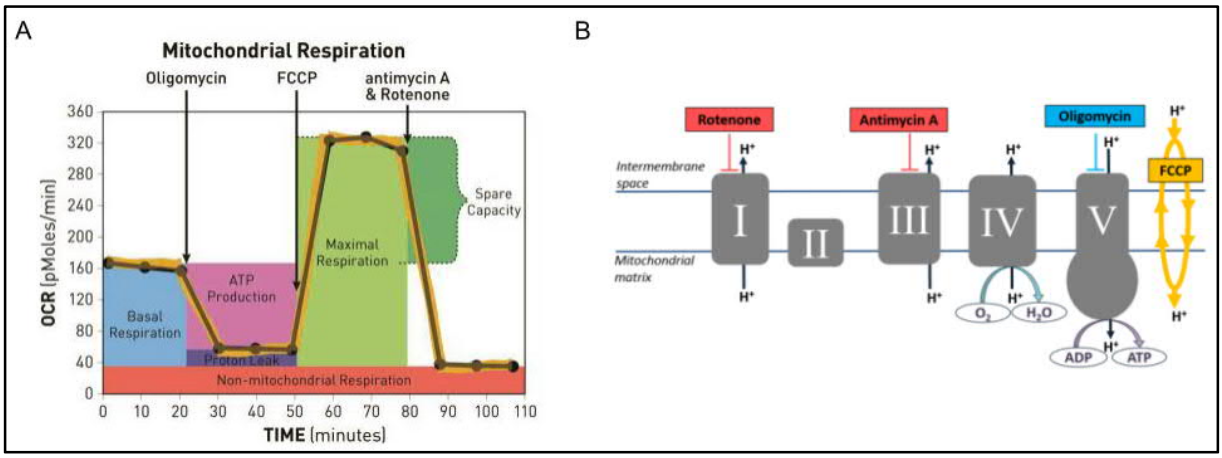

Figure 10: Cell Mito Stress Test
(**A**) Test profile of the key parameters of mitochondrial respiration. Consecutive compound injections measure basal respiration, ATP production, proton leak, maximal respiration, spare respiratory capacity, and non-mitochondrial respiration. (**B**) Schematic representation of the complexes of the ETC and the target of action of all test compounds. Oligomycin inhibits ATP synthase (complex V), FCCP uncouples oxygen consumption from ATP production, and rotenone and antimycin A inhibit complexes I and III, respectively. Adapted from Agilent (www.agilent.com).

Cells were seeded one day prior to the assay in 96-well seahorse plates. The assay was performed according to the manufacturer`s instructions. For the cell mito stress test, seahorse XF base medium (Agilent) supplemented with 2 mM L-Glutamine, 5.5 mM glucose and 1 mM sodium pyruvate was used and 2 µM oligomycin, 0.5 µM FCCP and 0.5 µM rotenone/antimycin A were used for the injections. Subsequently, plates were normalised based on the DNA content using the CyQuant kit (Thermo Fisher scientific) according to the manufacturer`s instructions. Data was analysed using the wave software (Agilent).

2.2.7 Lentiviral methods

2.2.7.1 Lentivirus production

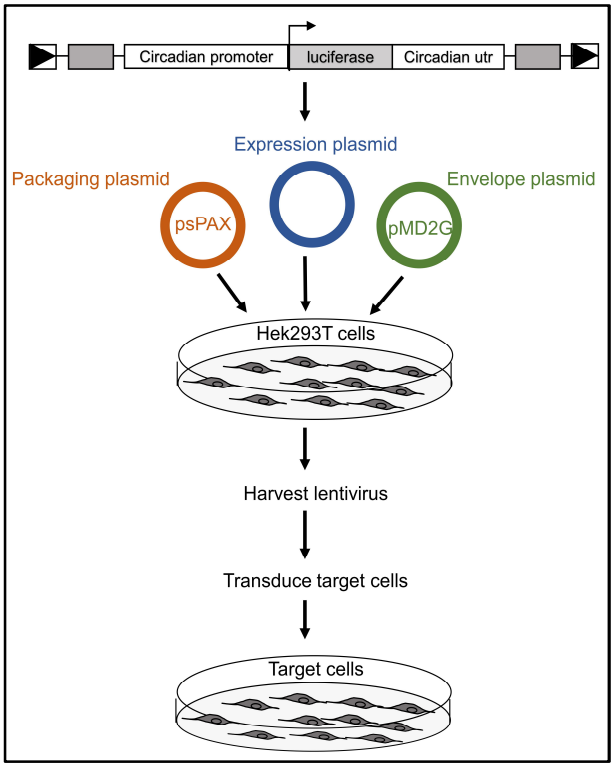

Figure 11: Lentivirus production and transduction of target cells
Hek293T cells were co-transfected with the packaging plasmid psPAX, the envelope plasmid pMD2G and the expression plasmid. Harvested lentiviral particles were used to transduce target cells.

Lentiviral elements containing either a *Bmal1*-promoter-driven luciferase (BLH) or a *Per2*-promoter-driven luciferase (PLB) were generated as previously described [110]. The vector maps can be found in the supplements (**Figure S 1** and **Figure S 2**). HEK293T cells were seeded in 175 cm^2 culture flasks and co-transfected with 12.5 µg packaging plasmid psPAX (**Figure S 3**) 7.5 µg envelope plasmid pMD2G (**Figure S 4**) and 17.5 µg expression plasmid using the CalPhos mammalian transfection kit (Clontech) according to the manufacturer's instruction (**Figure 11**). To harvest the lentiviral particles, the supernatant was centrifuged at 4100 x g for 15 min to remove cell debris and passed through a 45 µm filter. The lentiviral particles were stored at -80 °C until use.

2.2.7.2 Transduction with lentiviral vectors

For lentiviral transduction cells were seeded in 6-well plates. On the day of transduction, 1 ml medium and 1 ml of lentiviral particles were added. 8 µg/ml protamine sulphate and 4 µg/ml polybrene were used to enhance transduction efficiency. On the next day, the medium was replaced, and selection medium was added one day later (complete growth medium containing appropriate antibiotic) to obtain stable transduced cells and incubated at 37 °C with 5 % CO_2 atmosphere. Untransduced cells treated with the same antibiotic concentration were used as selection controls.

2.2.8 Bioluminescence measurements

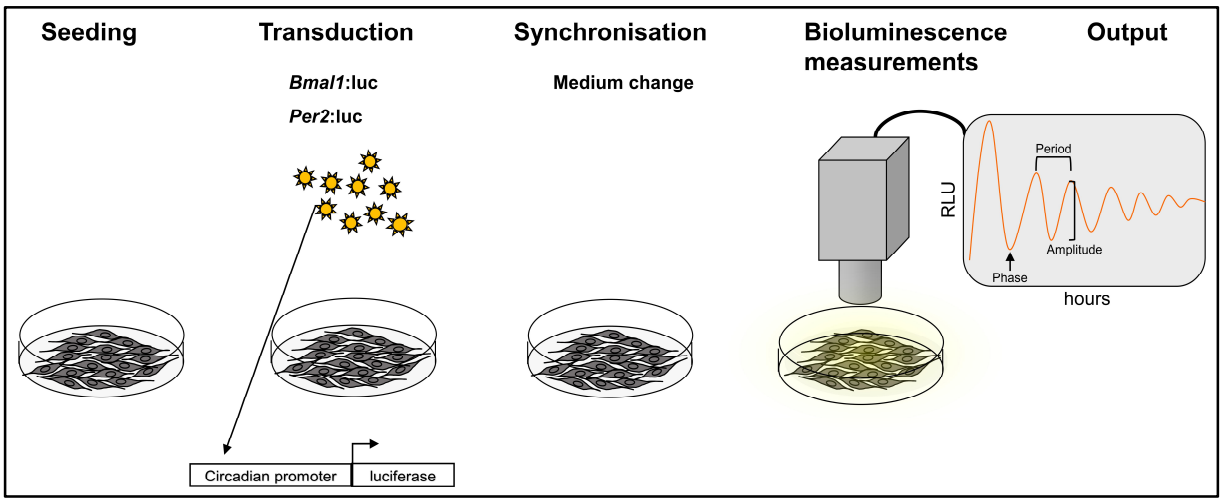

Figure 12: Workflow for live-cell bioluminescence measurements
Cells were seeded and transduced with *Bmal1*:luc or *Per2*:luc reporter constructs. After selection, cells were synchronised by medium change and live-cell bioluminescence was measured using a photomultiplier. Period = the time for one cycle. Phase = the timing of each cycle relative to an external zeitgeber. Amplitude = the ratio of max to min expression.

For live-cell bioluminescence recordings, cells were maintained in phenol red-free DMEM or RPMI containing 10 % FBS, 1 % penicillin-streptomycin and 250 µM D-Luciferin. NFs and CAFs were maintained in phenol red-free MEM-α medium supplemented with 10 % Hyclone FBS, 1 x antibiotic-antimycotic and 1 x MEM Non-Essential Amino Acids Solution and 250 µM D-Luciferin. Human fallopian tube organoids were maintained in normal growth medium supplemented with 250 µM D-Luciferin. Cells were synchronised by medium change prior to measurement. *Bmal1*-promoter-(BLH)-reporter activity or *Per2*-promoter (PLB)-reporter activity was measured using a LumiCycle instrument (Actimetrics) for five

consecutive days (**Figure 12**). Bioluminescence data was analysed using the Chronostar software [108]. Raw bioluminescence data was de-trended by the 24 hours running average and a sine fit was fitted to the data. Based on the sine fit, circadian parameters were calculated.

2.2.9 Single live-cell microscopy

For single live-cell microscopy, SW480 and SW620 cells were transfected with a REV-ERBα-VNP plasmid using the X-tremeGENE HP DNA Transfection reagent (Sigma-Aldrich) according to the manufacturer's instructions. REV-ERBα-VNP positive cells were sorted via fluorescence-activated cell sorting and cultured under normal growth conditions until use. For the experiment, cells were plated in µ-Slide 8 Well Glass Bottom dishes (ibidi). Time course live-cell microscopy was performed using a CSU-X spinning disc confocal microscope (Nikon). Pictures were taken and fluorescence intensity was determined every 30 min for 38 h. Data processing was done using ImageJ Fiji [113], [114].

2.2.10 Measurement of cell viability, cytotoxicity and apoptosis

To determine cell viability, cytotoxicity and apoptosis, the ApoTox-Glo Triplex Assay (Promega) was used. The test measures live-cell protease activity using a fluorogenic, cell-permeant peptide substrate (GF-AFC Substrate), dead-cell protease activity using a cell-impermeant, fluorogenic peptide substrate (bis-AAF-R110 Substrate) and caspase-3/7 activation as a key indicator of apoptosis. Cells were seeded in black 96-well half-area plates with clear bottom. The assay was performed according to the manufacturer`s instructions. Subsequently, plates were normalised based on the DNA content using the CyQuant kit (Thermo Fisher scientific) according to the manufacturer`s instructions.

2.2.11 shRNA-mediated knockdown

For the knockdown of *Bmal1* and *Hkdc1*, a TRC lentiviral shRNA glycerol set (Dharmacon) specific for each gene was used consisting of five individual shRNAs. The construct that gave best knockdown efficiency was determined by gene expression analysis and used for further experiments. The empty pLKO.1 vector was used as a control (**Figure S 5**). The transduction was performed as described in chapter 2.2.7.2.

2.2.12 Treatment with WZB117 and oxaliplatin

Treatment concentrations were determined based on the experimentally determined IC50 value (**Figure 43**) or based on literature search [115]. For the experimental determination of WZB117 treatment concentration, cells were seeded in 96 well plates one day prior to treatment. Cells were treated with 1.25 µM, 2.5 µM, 5 µM, 10 µM, 20 µM, 40 µM, 80 µM, 160 µM, 320 µM or 640 µM WZB117 for 48 h. The cytotoxicity was determined using the CytoTox-Glo Cytotoxicity Assay (Promega) following the manufacturer's manual. The following treatment concentrations were used: WZB117: 80 µM, oxaliplatin: 5 µM. Treatment duration was 24 h. The structure of WZB117 (CAS number 1223397–11-2) as well as oxaliplatin (CAS number 61825–94-3) is already published.

2.2.13 Sample preparation for 24 h time course microarray studies

Cells were seeded in triplicates in 6-well plates one day prior to the experiment. On the next day, cells were synchronised by medium change and samples were taken every 3 h for 24 h and prepared for RNA extraction. RNA extraction was carried out as described above (2.2.4.1). Microarray hybridisation was carried out by the *Labor für funktionelle Genomforschung* (LFGC, Charité - Universitätsmedizin Berlin) using Affymetrix GeneChip Human Transcriptome Array 2.0. The microarray dataset has been deposited in the ArrayExpress database at EMBL-EBI (www.ebi.ac.uk/arrayexpress) under accession number E-MTAB-5876.

2.2.14 Co-culture

One day prior to start of the co-culture, cells were seeded at the appropriate density dependent on the cells used. Untransduced cells were seeded in 35 mm dishes and transduced cells (*Bmal1*-promoter-(BLH)-reporter) were seeded on 22 mm coverslips. The next day, cells on coverslips were added to the appropriate untransduced cells. From this timepoint on, all cells were maintained in MEMα complete growth medium. Co-culture was maintained for 48 hours. For bioluminescence measurements, cells were synchronised by serum shock with medium containing 50 % FBS for 2 hours. Next, cells were washed once with 1x PBS and phenol-red-free MEMα supplemented with 250 µM D-Luciferin was added. Bioluminescence measurements and data analysis were performed as described above (2.2.8).

2.2.15 Bioinformatics methods

2.2.15.1 Microarray analysis

The microarray analysis was conducted in R version 3.4.1 [116] using the oligo package [117]. Gene expression data was pre-processed for all samples as one batch using the Robust Multichip Average (RMA) methodology [118], [119]. The R package arrayQualityMetrics [120] was used for quality control and statistical testing of the array data. Top differentially expressed genes with a log fold change (lfc) > 2 and $p < 0.001$ were identified using the limma package in R [121]. To detect genes exhibiting rhythmic behaviour with a period of 24 h in their expression intensities, the R package RAIN [122] and the R package Harmonic regression [123] were applied to identify robustly 24 h cycling transcripts with a p-value < 0.05. Since the algorithm works optimally with periods that are a multiple of the sampling interval, a period of 24 h was chosen which is the nearest approximation to the observed period of 24.59 h in SW480 cells. Expression heatmaps were created using the R package gplots [124]. The colours blue, white and red were assigned to the colourpanel (low, mid, high), meaning blue indicates low expression, white indicates middle expression and red indicates high expression.

2.2.15.2 Over-representation analysis

For the over-representation analysis of 24 h oscillating genes, genes were grouped into three sets: genes oscillating in both cell lines, genes oscillating only in SW480 cells and genes oscillating only in SW620 cells. Over-representation analysis was performed using ConsensusPathDB (http://cpdb.molgen.mpg.de/). *p*-values were computed by ConsensusPathDB according to the hypergeometric test based on the number of physical entities present in both the predefined set and user-specified list of physical entities. The *p*-values were corrected for multiple testing using the false discovery rate method. All pathways with a *p*-value < 0.01 and containing at least two overlapping members of the defined sets (genes oscillating in both cell lines, genes oscillating only in SW480 cells, genes oscillating only in SW620 cells) were taken into consideration for further analyses.

2.2.16 Statistical Analysis

The experiments were carried out with at least three biological replicates for each condition. All results are represented as mean ± SEM. Statistical analysis of the results was performed using either one-way ANOVA followed by Tukey`s multiple comparisons test or by two-tailed unpaired t-test, based on the experimental design. A p-value < 0.05 was considered as statistically significant. (* = $p < 0.05$; ** = $p < 0.01$; *** = $p < 0.001$).

3. Results

3.1 Colorectal cancer cell lines exhibit diverse circadian phenotypes

Cancer cell lines show a huge variety of circadian phenotypes [10]. Therefore, in a first step the circadian phenotype of different colorectal cancer cell lines was evaluated. To measure the circadian clock in living cells, cells were lentivirally transduced with a construct harbouring a luciferase under the control of the *Bmal1* or *Per2* promoter. Bioluminescence was measured in live cells over five consecutive days in a photomultiplier.

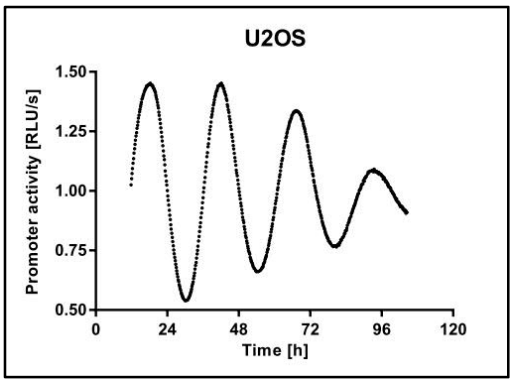

Figure 13: *Bmal1*-promoter activity in U2OS cells
Cells were lentivirally transduced with a *Bmal1*-luciferase construct (BLH) and synchronised with 1µM dexamethasone for 30 minutes. Bioluminescence was measured over five days. Displayed is one representative replicate.

The osteosarcoma cell line U2OS was used as a reference cell line as it is a commonly used cellular model for circadian research with stable and robust oscillations of about 24 h. **Figure 13** shows bioluminescence measurements of U2OS cells over five consecutive days. As expected, U2OS cells had a period of 24.7 h (SEM = 0.13, n = 3) and exhibited robust oscillations in *Bmal1*-promoter activity.

It has already been shown before that human colorectal cancer cell lines exhibit large phenotypic variations in circadian rhythms [10]. These differences in clock phenotypes were confirmed as well as extended for more cell lines. Overall, nine colorectal cancer cell lines were tested for their clock phenotype (CaCo2, Colo678, HCT116, HT29, LIM1215, RKO, SW480 and SW620).

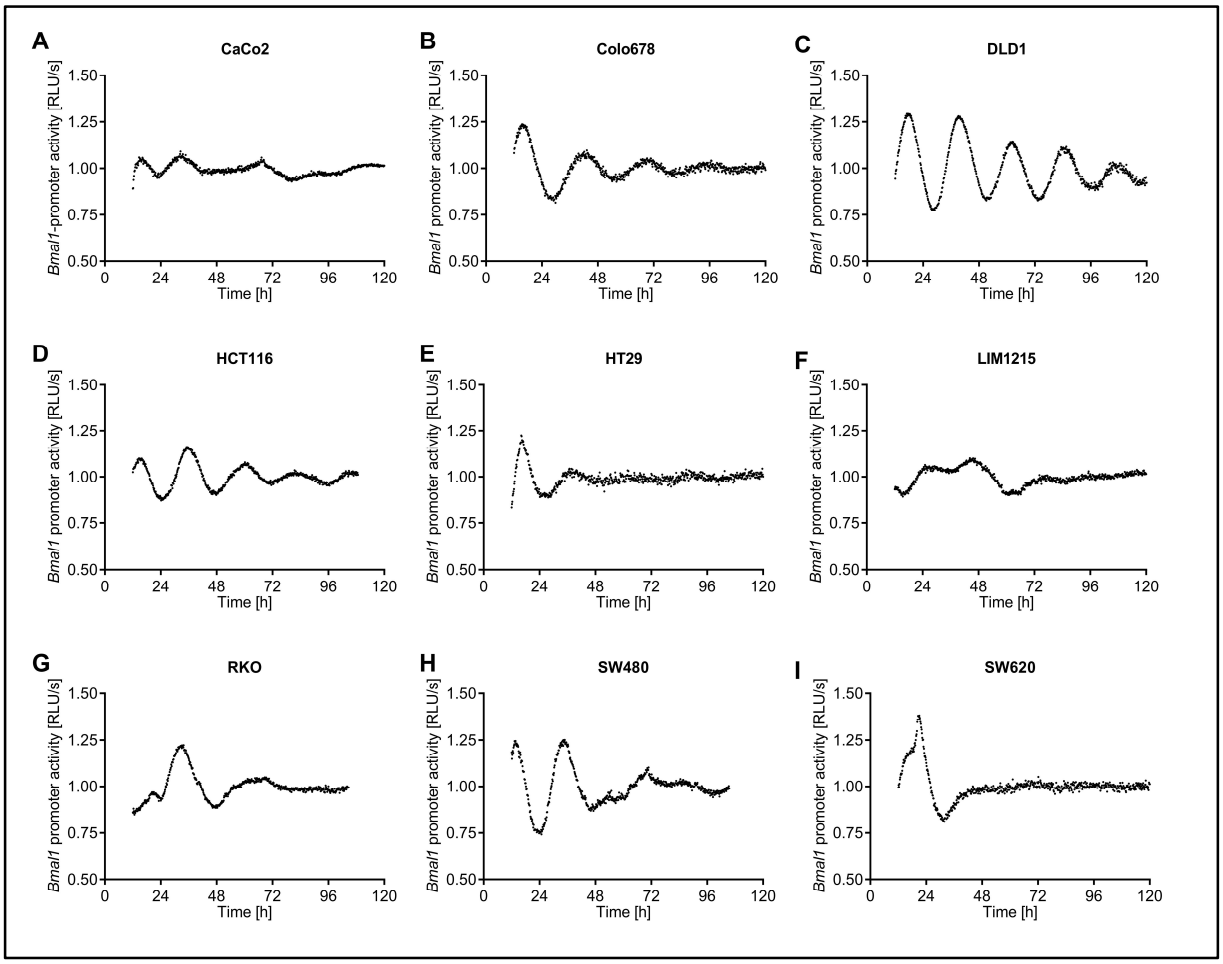

Figure 14: Clock phenotypes of different colorectal cancer cell lines
Bioluminescence measurements of Caco2 (**A**), Colo678 (**B**), DLD1 (**C**), HCT116 (**D**), HT29 (**E**), LIM1215 (**F**), RKO (**G**), SW480 (**H**) and SW620 (**I**) cells. Cells were lentivirally transduced with a *Bmal1*-luciferase construct (BLH) and synchronised with 1µM dexamethasone for 30 minutes. Bioluminescence was measured over five days. Displayed is one representative replicate per cell line.

A comparison of the oscillatory profile of all tested cell lines revealed differences between the tested cell lines with respect to their *Bmal1*-promoter activity (**Figure 14)**. While DLD1, HCT116, and SW480 showed robust oscillations, CaCo2, HT29, LIM1215, RKO and SW620 cells showed only very weak or no oscillations at all. The calculated periods of all cell lines, independent from their observed clock phenotype are displayed in **Table S 1**. These results once more demonstrate that colorectal cancer cell lines show diverse and distinct clock phenotypes. However, due to the lack of information about the cancer stage for many cell lines, it was not possible to correlate the tumour stage and the clock phenotype.

3.2 Determination of a synchronisation method

To study the circadian clock in a cell population, it is necessary to synchronise the cells so that they are in the same circadian phase. For cell synchronisation, different methods exist, including the glucocorticoid dexamethasone, forskolin that elevates cAMP levels and a simple serum-containing medium change [87], [125], [126].

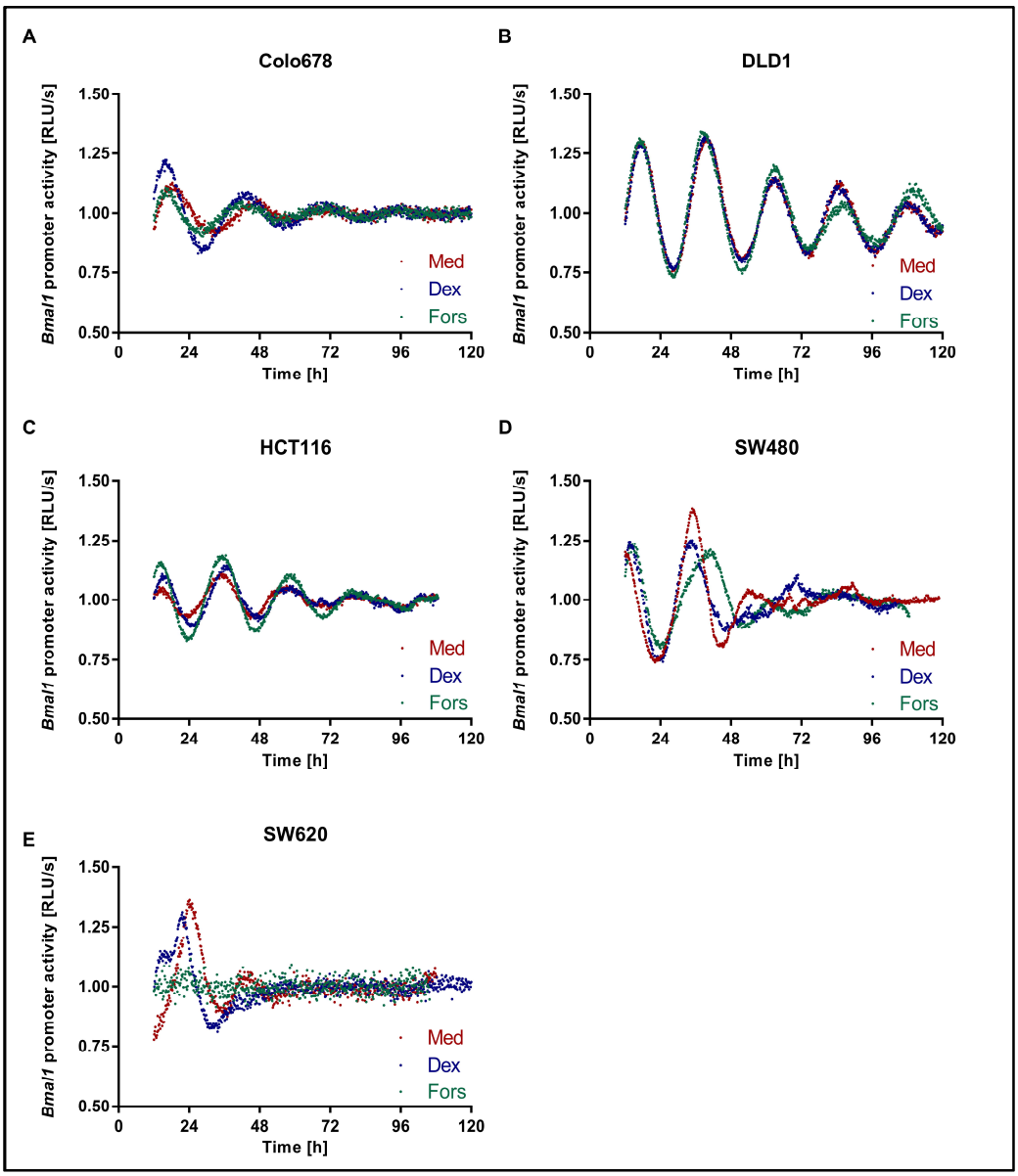

Figure 15: Comparison of different synchronisation methods in selected colorectal cancer cell lines
Bioluminescence measurements of Colo678 (**A**), DLD1 (**B**), HCT116 (**C**), SW480 (**D**) and SW620 (**E**) cells after synchronisation with forskolin, dexamethasone or medium change. Cells were lentivirally transduced with a *Bmal1*-luciferase construct (BLH) and synchronised with 1µM dexamethasone (Dex), 40µM forskolin (Fors) or medium (Med) for 30 minutes. Bioluminescence was measured over five days. Displayed is one representative replicate for each synchronisation method and cell line.

All beforementioned synchronisation methods reset the circadian clock by inducing circadian gene expression. The abovementioned chemicals dexamethasone and forskolin as well as a normal medium change were tested for their capability to synchronise cells and generate robust oscillations. **Figure 15** shows bioluminescence measurements in different colorectal cancer cell lines after synchronisation with dexamethasone, forskolin or medium change. In SW480 cells, forskolin synchronisation led to a significantly longer period when compared to medium change and dexamethasone treatment. Apart from that, no significant changes regarding the period length were observed and oscillations were very similar, independent from the synchronisation method used. Overall the results indicate that the synchronisation method only has minor effects on cell oscillations. Based on these results, cells were synchronised by a simple medium change for further experiments as this method does not include the use of additional chemicals that might influence the results.

3.3 SW480 and SW620 cells as a model for tumour progression

3.3.1 Detailed analysis of the core-clock in SW480 and SW620 cells

For further experiments, a pair of cell lines was selected that can be used as a model for circadian studies in the context of colorectal cancer progression. Based on the comparison of different colorectal cancer cell lines, SW480 and SW620 cells were chosen as an experimental model to investigate the interplay of a dysregulated circadian clock and the resultant metabolic output in colorectal cancer progression. Both cell lines are originally derived from the same patient but from different sites and at different times, representing two stages of cancer progression. The SW480 cell line is derived from a primary Duke's stage B colorectal adenocarcinoma, and the SW620 cell line is derived from a mesenteric lymph node metastasis. In a first attempt the circadian phenotype of both cell lines was evaluated in greater detail by measuring the circadian clock on the population level via bioluminescence measurements, on the single cell level by the use of live-cell microscopy and on the gene expression level via qPCR.

3.3.1.1 Bioluminescence measurements

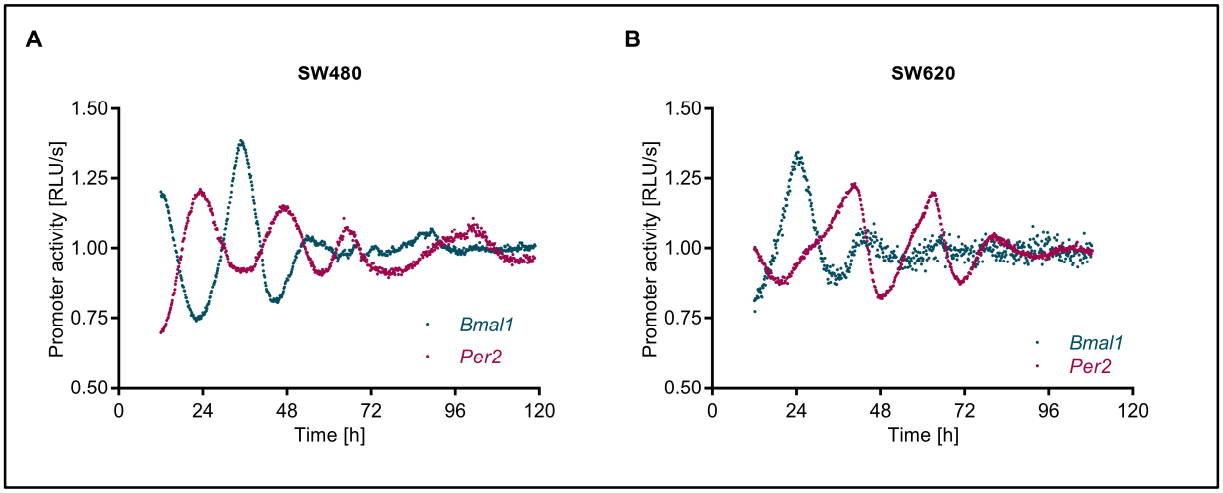

Figure 16: Bioluminescence measurements of *Bmal1*- and *Per2*-promoter activity in SW480 and SW620 cells
To investigate circadian clock activity, SW480 (**A**) and SW620 (**B**) cells were lentivirally transduced with a *Bmal1*-promoter (blue) or *Per2*-promoter (pink) driven luciferase construct. Bioluminescence was measured for five consecutive days. Shown is one representative replicate for each condition. Adapted from **Fuhr** *et al.*, 2018 [1].

Bioluminescence measurements of *Bmal1*- and *Per2*-promoter activity in SW480 and SW620 cells revealed that both cell lines exhibit different clock phenotypes (**Figure 16**). SW480 cells showed robust oscillations (T= 24.59 h ± 0.34, n = 3) with *Bmal1* and *Per2* oscillating in antiphase, as expected [127], [128]. In contrast, the oscillations in SW620 cells were less robust and had a delayed phase of around 12 h for both *Bmal1* and *Per2*, as compared to SW480 cells.

3.3.1.2 Single-cell clock measurements

Bioluminescence measurements in live cells using a photomultiplier always display the behaviour of a bulk of synchronised cells. To find out whether different clock phenotypes in SW480 and SW620 cells are truly based on differences in the molecular clock on the single cell level and do not only occur because of synchronisation problems of SW620 cell populations, the circadian clock on the single cell level was evaluated. Thus, cells were transfected with a REV-ERBα-VNP fluorescence fusion protein and time course single live-cell fluorescence microscopy was performed to determine the clock phenotype on the single cell level.

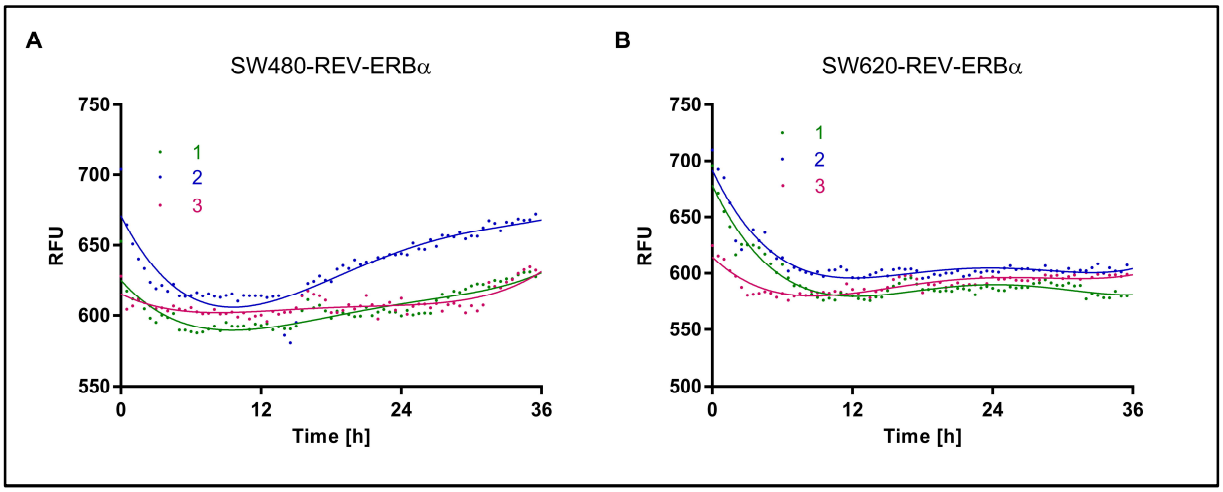

Figure 17: Time course single-cell microscopy
Single-cell time-series measurements of REV-ERBα protein abundance in SW480 and SW620 cells. The fluorescence intensity of a REV-ERBα-VNP fusion protein was measured for 36 h in SW480 (**A**) and SW620 (**B**) single live-cells. A fourth-grade polynomial fit was applied. Adapted from El-Athman, **Fuhr**, *et al.*, 2018 [2].

The analysis of time course microscopy for 36 h revealed different oscillation patterns in SW480 and SW620 cells in (**Figure 17**). The oscillations in SW620 cells seemed to be weaker, as the curve was rather flat, as compared to SW480 cells. These results confirm the assumption, that the differences in the circadian clock of both cell lines are due to changes within the molecular clock rather than due to a different ability of cell synchronisation within the population.

3.3.1.3 qPCR

The lumicycle analysis as well as the live-cell microscopy revealed profound changes in the core-clock between SW480 and SW620 cells. To confirm and extend these observations, a 45 h time course qPCR experiment was carried out and the expression of selected core-clock genes was analysed. The analysis of 45 h time course qPCR data confirmed the results gained from the bioluminescence measurements. In particular, the observed phase shift in *Bmal1* expression between SW480 and SW620 cells was confirmed via qPCR (**Figure 18**). Furthermore, the analysis of oscillating genes approved that the oscillations of *Bmal1* and *Per2* expression were more robust in SW480 cells as compared to SW620, as indicated by lower p-values in the RAIN analysis (**Table S 2**). Minor discrepancies regarding the circadian parameters between bioluminescence measurements and qPCR experiments occur due to the different methods used and different sampling intervals. While bioluminescence measurements in live cells measure

the promoter activity of *Bmal1* and *Per2* every 10 minutes, mRNA levels of *Bmal1* and *Per2* (as well as other clock genes) were determined every three hours via qPCR.

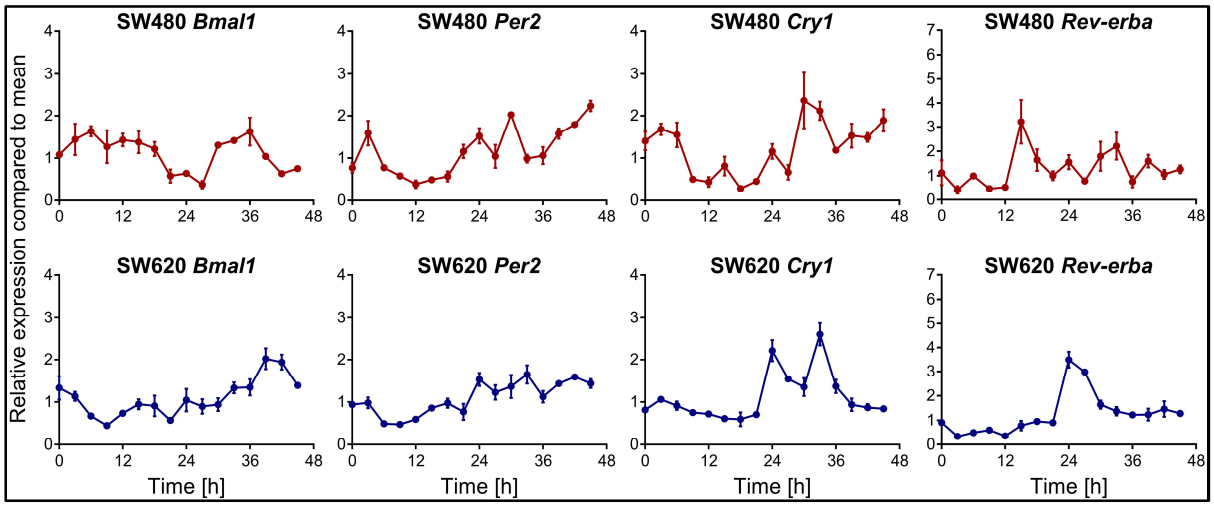

Figure 18: Time course gene expression analysis of core-clock genes in SW480 and SW620 cells
45 h time course qPCR measurements of selected core-clock genes (*Bmal1, Per2, Cry1 and Rev-erbα*) in SW480 (dark red) and SW620 (dark blue) cells. Data are expressed as mean ± SEM, n = 3. See also Table S 2. Adapted from **Fuhr** *et al.*, 2018 [1].

A detailed analysis of clock phenotypes in SW480 and SW620 cells revealed changes in the core-clock between both cell lines that are likely to affect genome-wide circadian expression of clock-regulated genes. Hence, in a next step, the consequences of different clock phenotypes on the transcriptome level were investigated. For this purpose, a 24 h time course microarray analysis for both cell lines was performed with a sampling interval of 3 h. This set of data represents the first 24 h time course microarray study for SW480 and SW620 cells and can be found in the ArrayExpress database at EMBL-EBI (www.ebi.ac.uk/arrayexpress) under accession number E-MTAB-5876.

3.3.2 Changes in the core-clock have consequences on the transcriptome level

In a first step, the expression profiles of 14 core-clock genes were evaluated to further analyse differences in the core-clock between SW480 and SW620 cells. Furthermore, these genes were tested for oscillations in gene expression.

The time course analysis of 14 core-clock genes revealed different expression patterns of core-clock genes between both cell lines, as can be seen in the phase-ordered heatmap of core-clock genes in **Figure 19**. The ordering of the genes was based on their peak phases of

expression in SW480 cells and the same ordering was used to represent the temporal expression profiles of the same set of genes in SW620 cells. Furthermore, a RAIN analysis was performed to define 24 h oscillating genes. Out of 14 tested core-clock genes, 8 were identified to be oscillating in SW480 cells with a period of around 24 h ($p < 0.05$), but only 4 in SW620 cells (**Table S 3**). These results are in line with the observations made from bioluminescence measurements, single live-cell microscopy and time course qPCR of SW480 and SW620 cells.

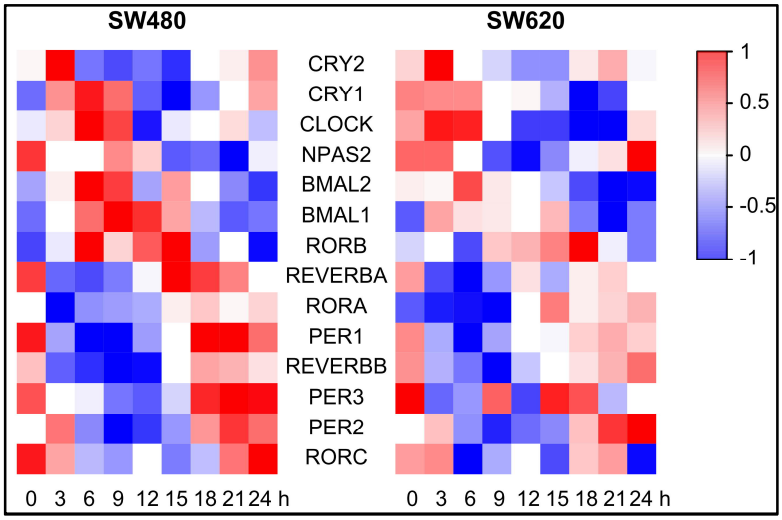

Figure 19: Heatmap of core-clock genes in SW480 and SW620 cells
Phase-ordered, median-normalised heatmap of core-clock genes in SW480 and SW620 cells. Phase-ordering was performed based on SW480 expression data and the same ordering of genes was used for SW620 cells. See also Table S 3. Adapted from **Fuhr** *et al.*, 2018 [1].

These results showed that SW480 and SW620 cells display very diverse phenotypes, which could be confirmed on different levels of gene expression and promoter activity. To analyse changes in gene expression between both cell lines on the transcriptome level, an analysis of the top differentially expressed genes was performed.

Figure 20 shows a heatmap of differentially expressed genes in SW480 and SW620 cells. A subsequent over-representation analysis of this set of genes revealed different cancer-associated pathways to be over-represented. These included, among others, the KEGG pathways pathways in cancer ($p = 0.001$) and p53 signalling pathway ($p = 0.0005$) as well as the GO terms apoptotic process ($p = 4.73E-07$), positive regulation of cellular metabolic process ($p = 4.29E-06$) and positive regulation of cell death ($p = 1.80E-06$). These results show that the different cancer stages of the two tested cell lines are represented by transcriptomic changes especially with respect to cancer-associated gene expression.

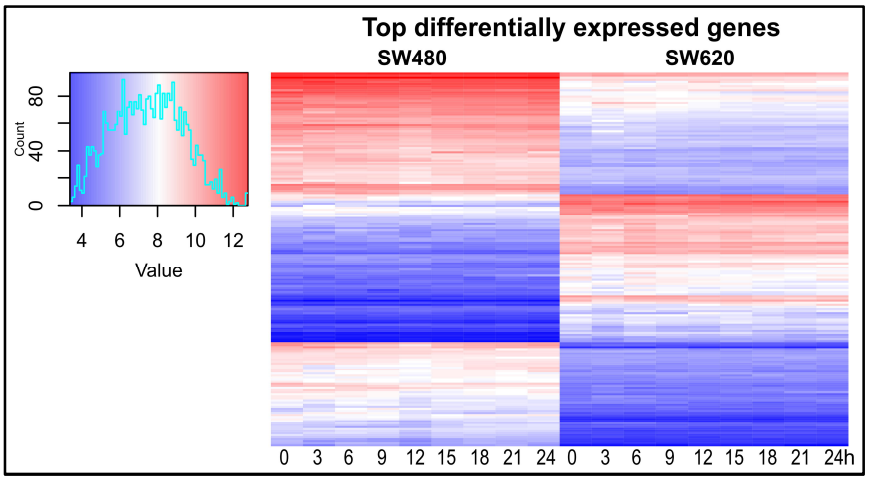

Figure 20:Top differentially expressed genes between SW480 and SW620 cells
Top differentially expressed genes with a lfc > 2 and p < 0.001 were defined using the limma package in R.

3.3.2.1 A deregulated clock induces a shift in oscillating gene expression

As the circadian clock regulates a huge number of target genes, a deregulated clock is very likely to induce changes in the oscillations of target gene expression. Consequently, in a next step, all oscillating genes with a period of 24 h were determined and compared between both cell lines to see whether changes in the core-clock induce global changes in oscillating gene expression.

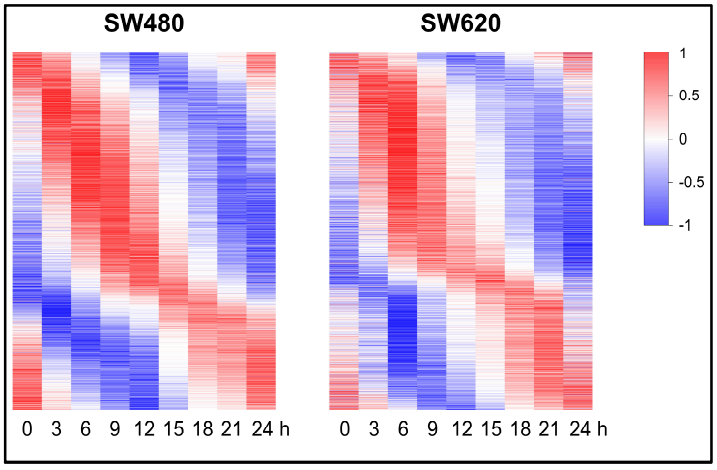

Figure 21: Phase-ordered heatmap of 24 h oscillating genes in SW480 and SW620 cells
Phase-ordered heatmap of all oscillating genes in SW480 (left panel) and SW620 cells (right panel). P < 0.05. Adapted from El-Athman, **Fuhr**, *et al.*, 2018 [2].

The analysis of all 24 h oscillating genes revealed a slight phase-shift between both cell lines (**Figure 21**). In total, a similar number of oscillating genes was found in both cell lines when

analysing the oscillations independently in each cell line. Namely 16.0% (3998) of all genes were oscillating in SW480 cells and 14.8% (3693) were oscillating in SW620 cells. However, only 5.5% (1385) of all genes were oscillating in both cell lines, which points to a reprogramming in the 24 h oscillating genetic landscape of these cells. When analysing only genes that oscillate in at least one of the two cell lines, 22 % (1385) of these genes were found to be oscillating in both cell lines, 41.4 % (2613) were oscillating only in SW480 cells and 36.6 % (2308) were only oscillating in SW620 cells (**Figure 22**).

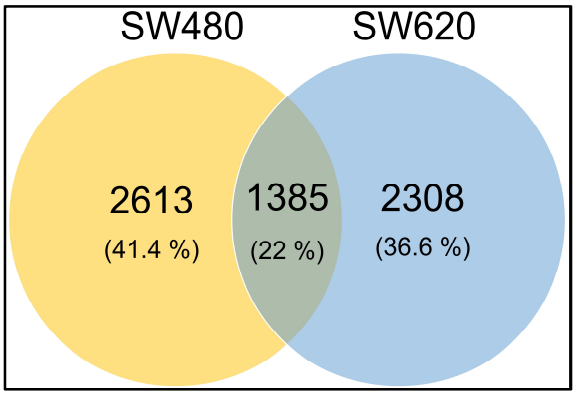

Figure 22: Venn diagram of 24 h oscillating genes in SW480 and SW620 cells
In total 3998 genes were oscillating in SW480 cells and 3693 genes were oscillating in SW620 cells. An intersect of 1385 genes was oscillating in both cell lines with a period of 24 h.

3.3.2.2 Metabolic pathways are over-represented in distinct sets of oscillating genes

To analyse the sets of oscillating genes in greater detail, an over-representation analysis of these genes was performed. For this purpose, all 24 h oscillating genes were grouped into three sets of genes: Genes oscillating only in SW480 cells, genes oscillating only in SW620 cells and genes oscillating in both cell lines. Interestingly, the over-representation analysis revealed several metabolic pathways to be overrepresented (**Figure 23**). The KEGG pathways glucose metabolism (p = 1.06E-05) and glycolysis (p = 3E-03) were over-represented in the set of genes oscillating in both cell lines. Genes oscillating only in SW620 cells showed over-represented pathways involved in mitochondrial respiration, including the tricarboxylic acid (TCA) cycle (p = 5.85E-04), mitochondrial electron transport chain (p = 7.66E-05), and the Warburg effect (p = 1.04E-06).

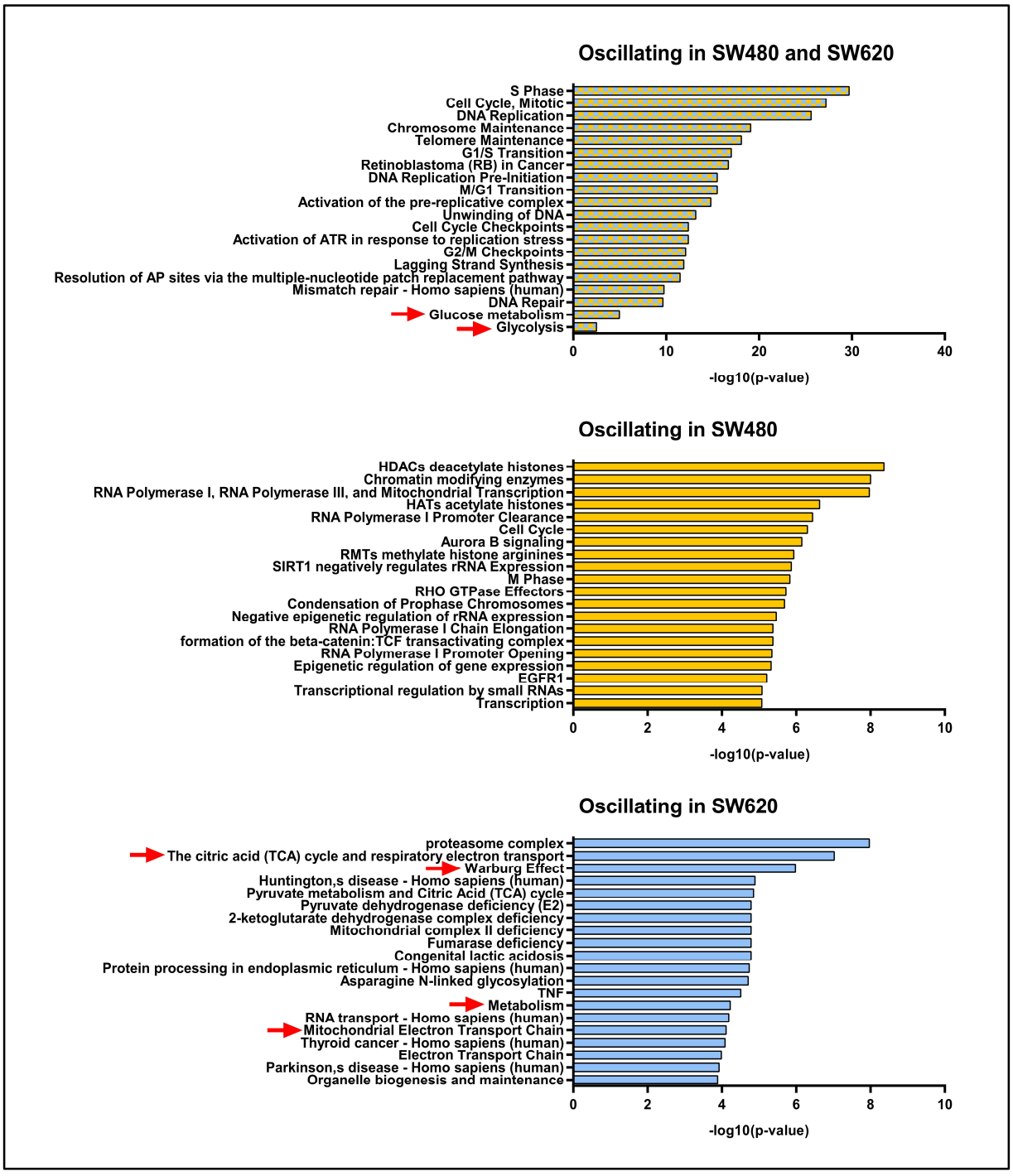

Figure 23: Over-representation analysis of 24 h oscillating genes
All 24 h oscillating genes were divided into sets of genes oscillating in both cell lines, oscillating only in SW480 cells and oscillating only in SW620 cells and an over-representation analysis was performed. The figure displays a curated list of KEGG pathways. Relevant metabolic pathways are marked with a red arrow. See also Table S 4 - S 8.

The expression patterns of 24 h oscillating genes involved in the pathways glycolysis, oxidative phosphorylation and Warburg effect are displayed as heatmaps in **Figure 24**. Genes were ordered based on their phase in SW480 cells and the same ordering was used for SW620 cells.

A comparison of the heatmaps between both cell lines revealed visible differences regarding the temporal expression patterns in all three pathways, further supporting the metabolic differences between both cell lines, especially with respect to oscillating genes in metabolic pathways.

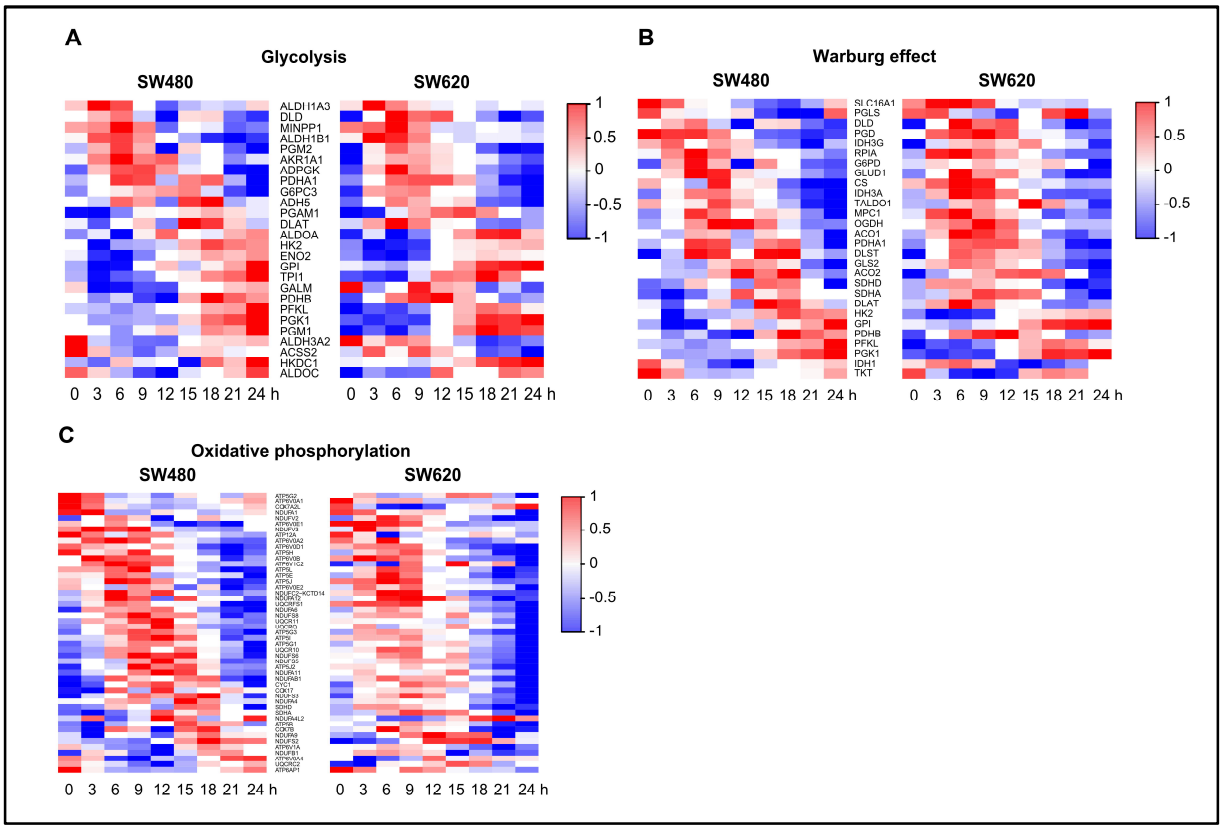

Figure 24: 24 h oscillating genes belonging to different metabolic pathways in SW480 and SW620 cells
Phase-ordered, median-normalised heatmaps of the pathways glycolysis (**A**), Warburg effect (**B**) and oxidative phosphorylation (**C**). Only genes are displayed that oscillate with a 24 h period in at least one of the two tested cell lines. Phase-ordering was performed based on SW480 expression data and the same ordering of genes was used for SW620 cells. Adapted from **Fuhr** *et al*., 2018 [1].

3.3.2.3 Metabolic candidate genes show different time-dependent expression patterns

Based on the results gained from the analysis of oscillating genes and the over-representation analysis, metabolic candidate genes were defined within over-represented metabolic pathways for further experiments. Therefore, the 24 h microarray expression data of all genes included in the pathways glycolysis, oxidative phosphorylation and Warburg effect were evaluated and five putatively clock-controlled candidate genes were selected based on differences in the temporal mRNA expression profiles of these genes between both cell lines (**Figure S 6**).

Five genes were selected that all belong to the KEGG pathway glycolysis and gluconeogenesis. *Aldh3a2* is involved in oxidative stress response [129], *Aldoc* catalyses the conversion of fructose-1,6-bisphosphate to glyceraldehyde-3-phosphate and dihydroxyacetone phosphate [130], *Hkdc1* catalyses the phosphorylation of glucose [131], *Pck2* catalyses the conversion of oxaloacetate to phosphoenolpyruvate [132] and *Pdhb* catalyses the overall conversion of pyruvate to acetyl-CoA and carbon dioxide and provides the primary link between glycolysis and the TCA cycle [133].

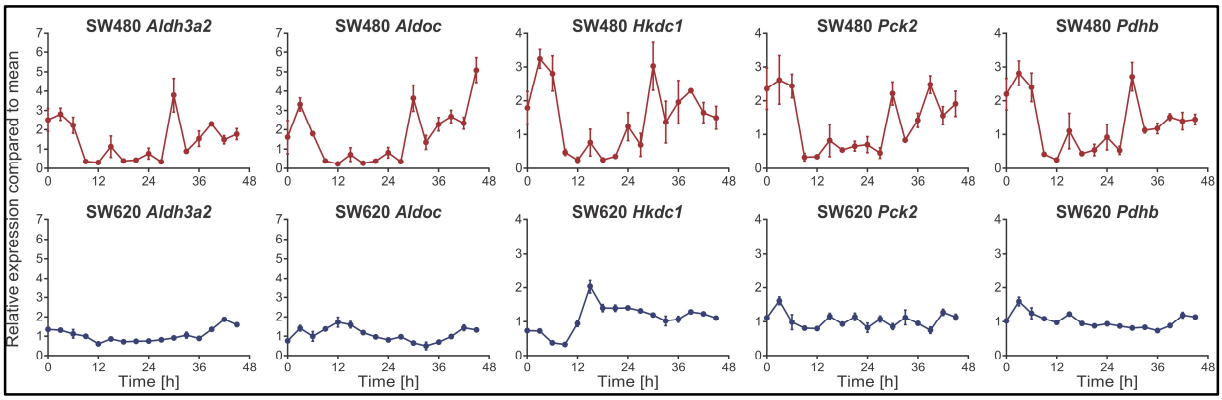

Figure 25: Time course gene expression analysis of metabolic genes in SW480 and SW620 cells
45 h time course qPCR measurements of selected metabolic genes (*Aldh3a2*, *Aldoc*, *Hkdc1*, *Pck2*, *Pdhb*) in SW480 (dark red) and SW620 (dark blue) cells. Data are expressed as mean ± SEM, n = 3. See also Figure S 6. Adapted from **Fuhr** *et al.*, 2018 [1].

The expression profiles of the five candidate genes *Aldh3a2*, *Aldoc*, *Hkdc1*, *Pck2* and *Pdhb* were evaluated via qPCR (**Figure 25**). Based on 45 h time course qPCR data, all candidate genes had higher fold changes over time in SW480 cells. Especially *Hkdc1* showed a phase-shift of around 13 h in its peak expression between both cell lines. This is consistent with the observed phase shift in *Bmal1* expression between SW480 and SW620 cells (**Figure 16**) and might be a hint for a circadian regulation of *Hkdc1* expression via *Bmal1*, though further targeted studies will be needed to test this hypothesis in future work. Among the top candidates, *Hkdc1* showed 24 h oscillations with the lowest p-value (p = 5.7E-04, SW480; p = 1.6E-05, SW620) and the highest relative amplitude (0.562 in SW480; 0.353 in SW620) for both cell lines, as estimated by harmonic regression analysis and was thus chosen for further investigation (**Table S 2**). Furthermore, an inhibitory effect of intracellular glucose on the expression of the core-clock genes *Bmal1*, *Per1* and *Per2* was reported before, pointing to an interplay between glycolysis and the circadian clock [83]. As *Hkdc1* is a central gene in the glycolytic pathway, it seemed to be an appropriate candidate gene for further experiments.

A detailed analysis of SW480 and SW620 cells with respect to their clock phenotypes and metabolic gene expression confirmed that these two cell lines are a good model for circadian studies in tumour progression. Particularly metabolic changes between both cell lines could be observed on the transcriptome level and a detailed analysis of metabolic genes expression revealed *Hkdc1* as a potential clock-regulated metabolic candidate gene that drives metabolic alterations between the tumour stages of both cell line.

Before the consequences of a deregulated clock on metabolic changes during tumour progression were analysed by introducing a knockdown of the core-clock gene *Bmal1*, the circadian clock was evaluated in primary cellular models.

3.4 The circadian clock in non-cancerous cellular models

Apart from the investigation of circadian phenotypes in colorectal cancer cell lines, the circadian clock was also evaluated in primary cellular models that served as a comparison for the results gained in cell lines. For this purpose, human normal and cancer-associated fibroblasts isolated from colorectal cancer patients were used as well as non-cancerous human fallopian tube organoids.

3.4.1 Human normal and cancer-associated fibroblasts

Cancer cells are under continuous bidirectional communication with tumour stroma that nurtures and supports tumour progression. Stroma modifies proliferation, local migration, metastasis, metabolism, and drug resistance responding to the needs of cancer cells [134]. To compare the results gained from the colorectal cancer cell lines SW480 and SW620 with a pair of patient-derived primary stromal cells, normal fibroblasts (NFs) and cancer-associated fibroblasts (CAFs) derived from the same colorectal cancer patient were used. In total NFs and CAFs from three patients were evaluated with respect to their circadian phenotype.

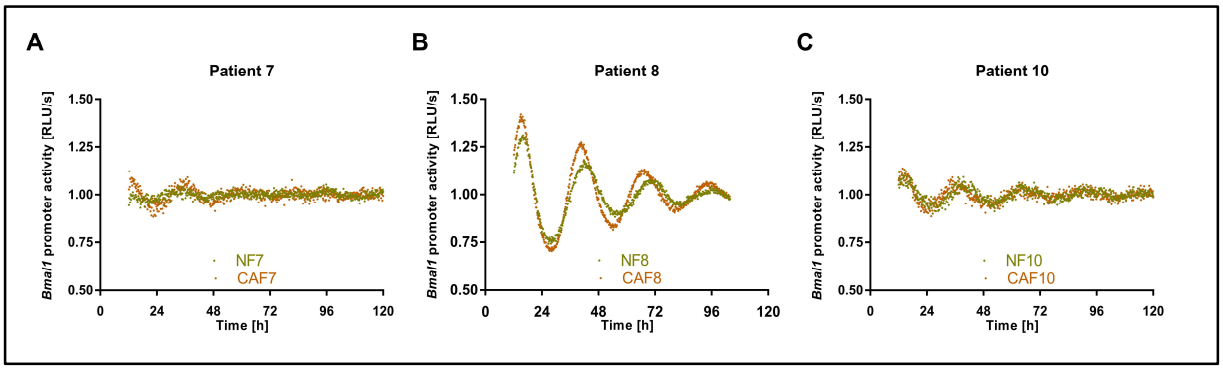

Figure 26: Bioluminescence measurements of NFs and CAFs from individual patients
NFs and CAFs from three patients were lentivirally transduced and the *Bmal1*-promoter activity was measured over five consecutive days. Shown is one representative replicate for each cell type.

Bioluminescence measurements of NFs and CAFs derived from three different patients revealed that NFs as well as CAFs showed robust oscillations even though the amplitudes were low for patient 10 and patient 7, most likely due to relatively low cell numbers (**Figure 26**). Periods ranged between 24.74 h and 27.31 h, but no significant differences were observed between NFs and CAFs or between different patients. Regarding the period and the oscillation profile, the clock phenotype, especially in patient 8 seemed to be very similar to the circadian model cell line U2OS.

3.4.2 Human fallopian tube organoids

As a second non-cancerous model system, human fallopian tube organoids derived from females without cancer were used to study the circadian clock in normal tissue in comparison to cancer cell lines. These cells form an organ-like 3D structure consisting of different cell types and therefore represent the structure of normal tissue quite well. Organoids mimic the physiology and anatomy of the donor-tissue very closely [111], [135]. Hence, this cellular model system allows for the analysis of the circadian clock in healthy cells in an organ-like context.

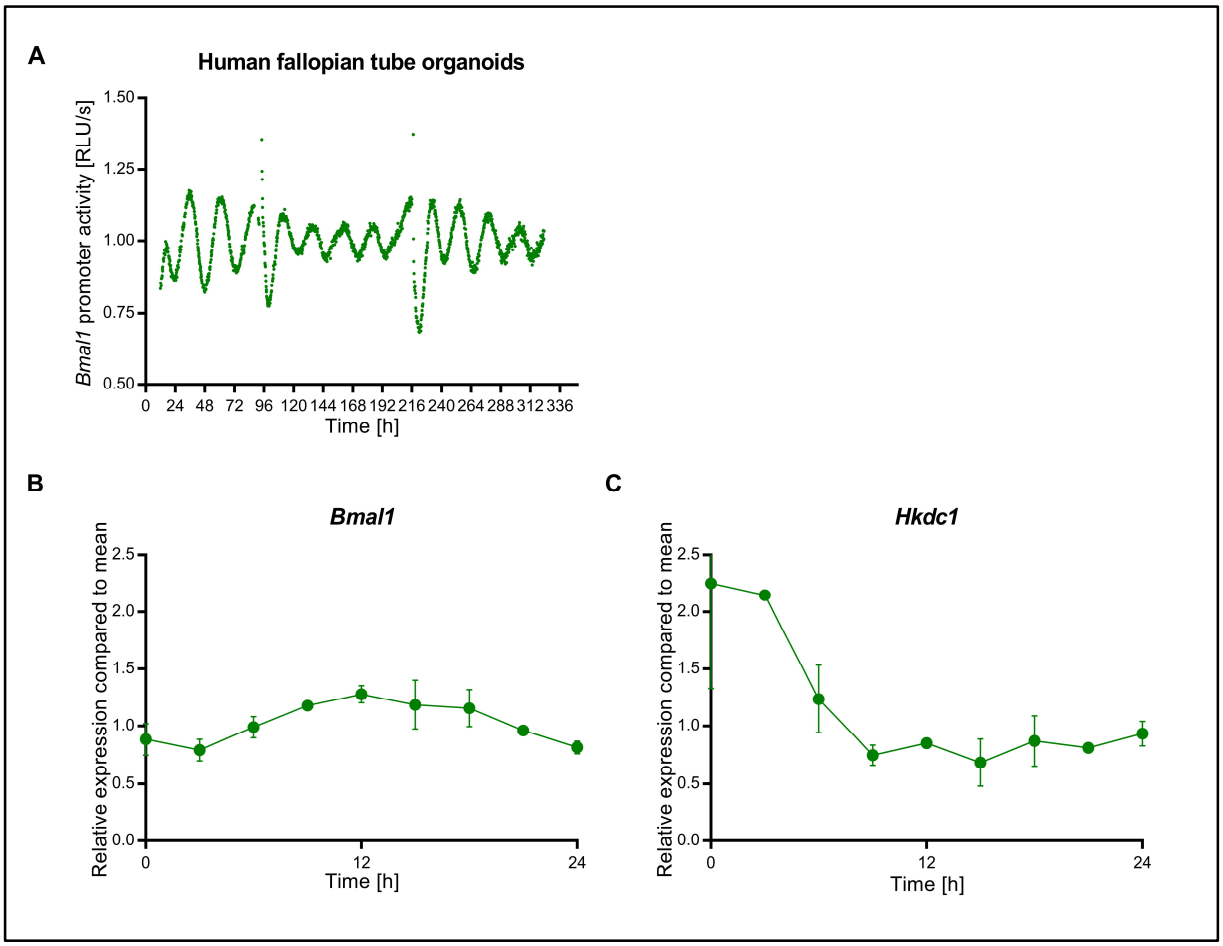

Figure 27: The circadian clock in human fallopian tube organoids
(**A**) Bioluminescence measurements of human fallopian tube organoids transduced with a *Bmal1*-promoter driven luciferase construct. Bioluminescence was measured for 14 consecutive days. High peaks indicate medium changes. Shown is one representative replicate. 24 h time course qPCR measurements of *Bmal1* (**B**) and *Hkdc1* (**C**) in human fallopian tube organoids. Data are expressed as mean ± SEM, n = 3. Adapted from **Fuhr** *et al.*, 2018 [1].

Figure 27 shows bioluminescence measurements of fallopian tube organoids over 14 consecutive days. Human fallopian tube organoids showed very robust oscillations even for longer time frames with a period of 24.64 ± 0.10 h which was similar to the period measured in SW480 cells (T = 24.59 h ± 0.34, n = 3, **Figure 16**). In contrast to all tested colorectal cancer cell lines, no typical damping of oscillations was observed over time, probably due to the communication between different cell types within the organoids.

The metabolic gene *Hkdc1* was identified as a potential clock-regulated candidate gene in the CRC cell line model. *Hkdc1* is known to catalyse the phosphorylation of glucose in the glycolytic pathway, but its role in cancer remains largely unknown [131]. In the cellular model system of colorectal cancer progression, *Hkdc1* showed time-dependent changes in its mRNA

expression levels that differed between SW480 and SW620 cells. In order to compare the expression of the core-clock gene *Bmal1* and *Hkdc1* in a normal scenario, a 24 h time course gene expression analysis was performed in human organoids derived from normal fallopian tubes. The comparison of SW480 and SW620 cells with organoids derived from non-cancer tissues was used to evaluate the relative similarity of both cell lines to a normal tissue. In the fallopian tube organoids, *Bmal1* showed circadian oscillations with a phase at 8-12 h after synchronisation, as also observed in SW480 cells (**Figure 27 B** and **Figure 18**). Therefore, the time-dependent expression pattern of *Bmal1* seems to be a characteristic that is shared between normal cells and non-metastatic cancer cells. Moreover, the changes of *Hkdc1* mRNA expression over time in human fallopian tube organoids followed a very similar pattern to that observed in SW480 cells with a trough of expression at around 12 h after synchronisation, in antiphase to *Bmal1* (**Figure 27 B** and **Figure 25**). Thus, it seems that the hypothesised interplay between *Bmal1* and *Hkdc1* expression in SW480 cells is different from that of the metastatic cell line SW620, despite their common genetic origin, and instead resembles more closely the phenotype observed in organoids derived from non-cancerous tissue.

3.5 Core-clock gene disruption induces a metastatic phenotype in SW480 cells

The global analysis of different clock phenotypes on the transcriptomic level revealed metabolic changes between SW480 and SW620 cells. To further investigate the connection between altered circadian rhythms and possible effects on cell metabolism, a stable knockdown of the core-clock gene *Bmal1* was performed using lentivirus-based shRNA constructs (see 2.2.11) and the output on gene expression and metabolic activity was evaluated. Although the knockdown was carried out at a specific time-point in synchronised cells, the gene is from then on constantly lower expressed in KD-cells than in control cells.

3.5.1 *Bmal1*-knockdown in SW480 and SW620

The knockdown efficiency of different shRNA-constructs was tested via qPCR and the construct that gave the best knockdown efficiency was used for further experiments.

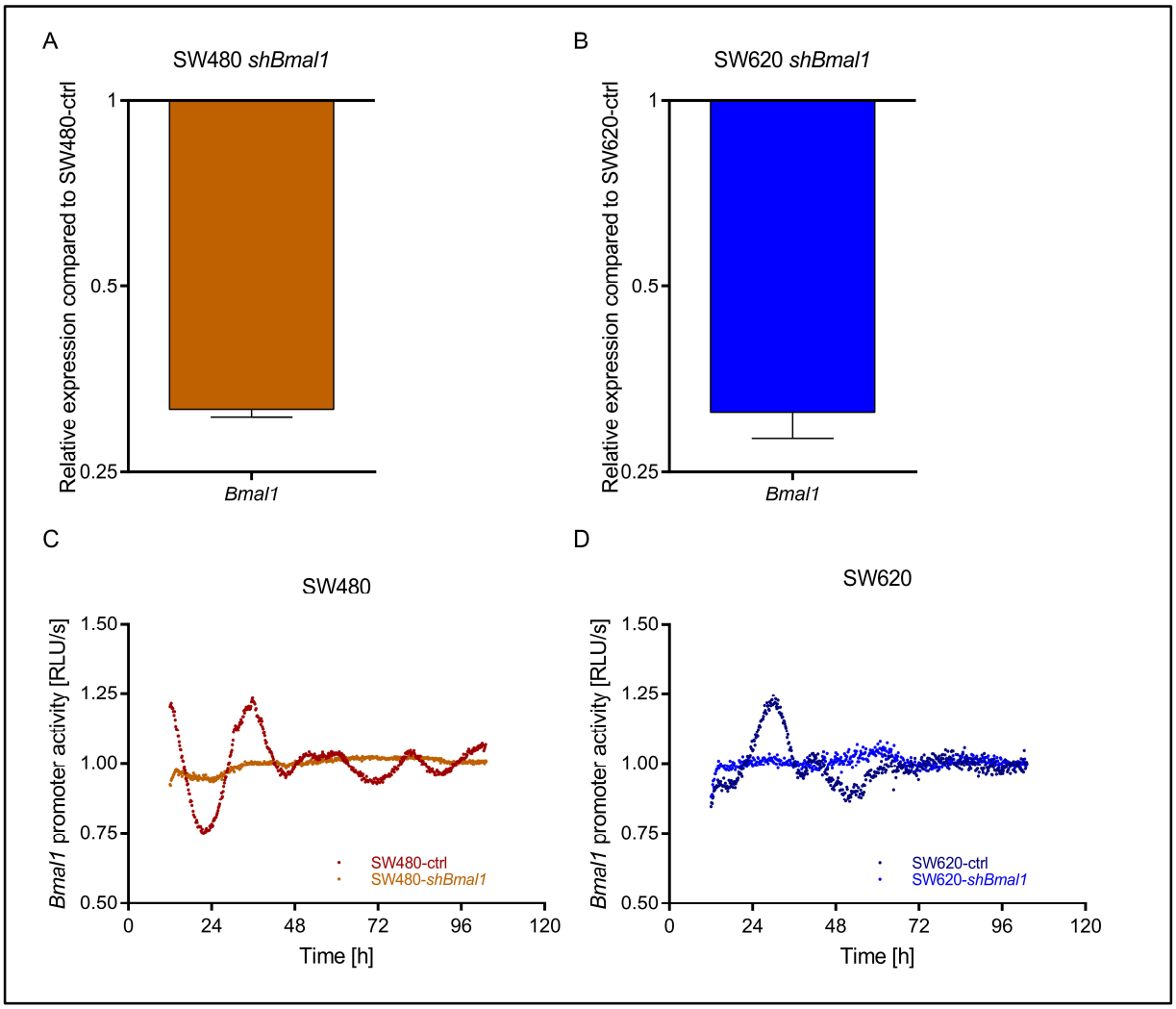

Figure 28: Knockdown efficiency after shRNA-mediated KD of *Bmal1*
Gene expression analysis of *Bmal1* in SW480 (**A**) and SW620 (**B**) cells after shRNA-mediated *Bmal1*-KD. Gene expression is shown compared to the corresponding control gene. Mean ± SEM, n = 3. KD efficiency in SW480-*shBmal1* cells: 0.317 ± 0.009 (68.3%). KD efficiency in SW620-*shBmal1* cells: 0.313 ± 0.03 (68.7%). Bioluminescence measurements in SW480 (**C**) and SW620 (**D**) cells. Cells were lentivirally transduced either with an empty vector (ctrl) or with a *shBmal1*-construct. Additionally, cells were lentivirally transduced with a *Bmal1*-promoter driven luciferase construct. Bioluminescence was measured for five consecutive days. Shown is one representative replicate for each condition. Adapted from **Fuhr** *et al*., 2018 [1].

Figure 28 shows the expression of *Bmal1* in SW480 (**A**) and SW620 (**B**) cells after shRNA-mediated *Bmal1*-KD. The knockdown efficiency was very similar in both cell lines, with 68.3 % in SW480 cells and 68.7 % in SW620 cells. Additionally, the effect of *Bmal1*-KD on *Bmal1*-promoter activity was tested via bioluminescence measurements (**Figure 28 C** and **D**). The knockdown led to a complete loss of oscillations in *Bmal1*-promoter activity, further confirming the temporal stability of the knockdown.

Additionally, a 24 h time course qPCR analysis was carried out to examine the effect of *Bmal1*-KD on temporal *Hkdc1* expression (**Figure 29**, **Figure 18** and **Figure 25**), as a possible interplay between both genes was supposed based on the results gained so far. In both cell lines, the *Hkdc1* expression profile changed upon *Bmal1*-KD, further supporting the assumption that *Bmal1* and *Hkdc1* expression are correlated. These results further reinforce a connection between the core-clock and clock-controlled metabolic genes with possible consequences on metabolic activity.

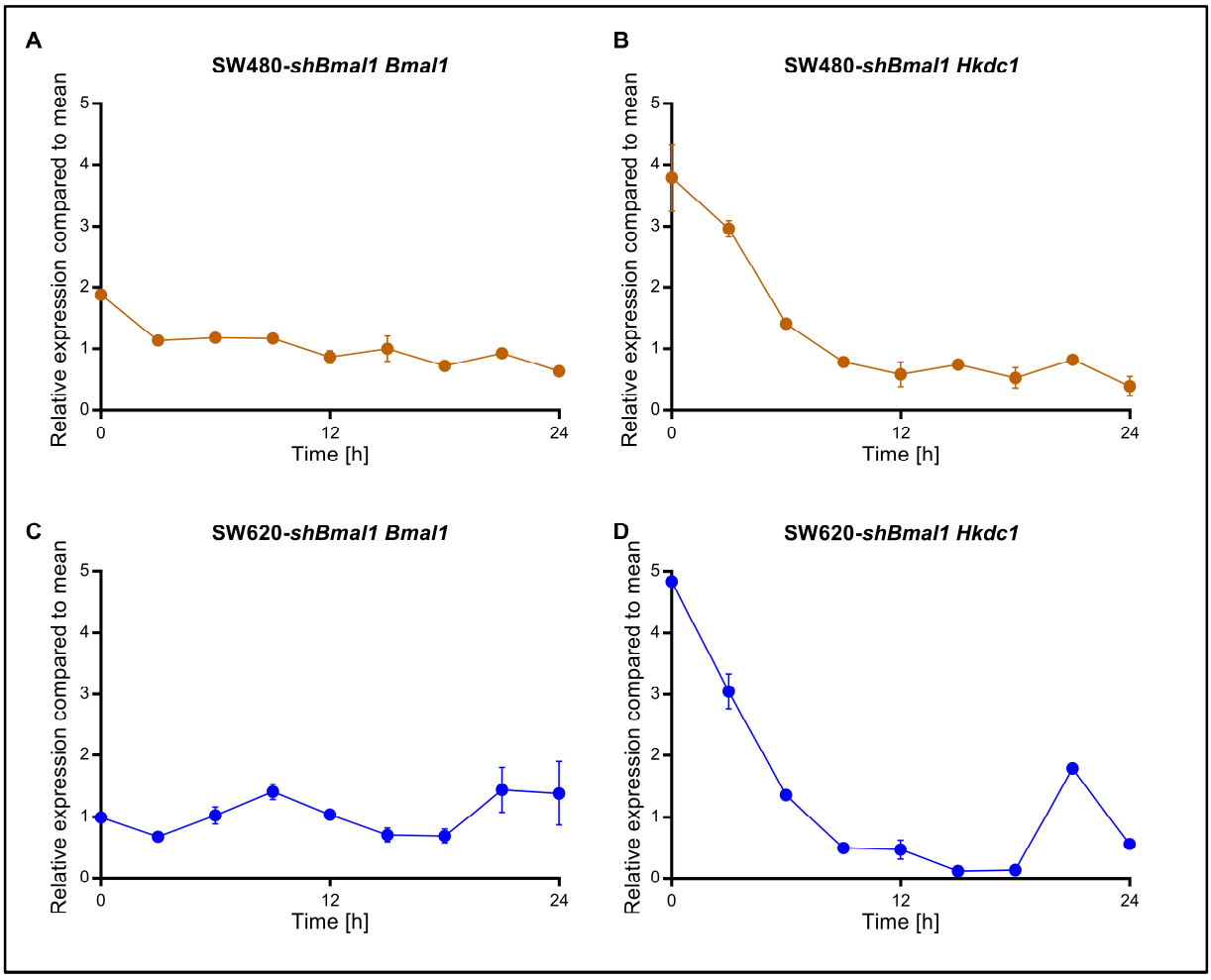

Figure 29: Time-dependent gene expression after *Bmal1*-KD in SW480 and SW620 cells
24 h qPCR measurements of *Bmal1* and *Hkdc1* in SW480-*shBmal1* (**A** and **B**) and SW620-*shBmal1* (**C** and **D**) cells. Data are shown compared to the mean expression. Mean ± SEM, n = 3. Adapted from **Fuhr** *et al.*, 2018 [1].

3.5.2 *Bmal1*-KD induces alterations in core-clock and metabolic gene expression

After having confirmed the efficiency and stability of *Bmal1*-KD, the consequences of *Bmal1*-KD on the expression of other core-clock genes as well as on the previously selected metabolic candidate genes were tested via qPCR (**Figure 30**).

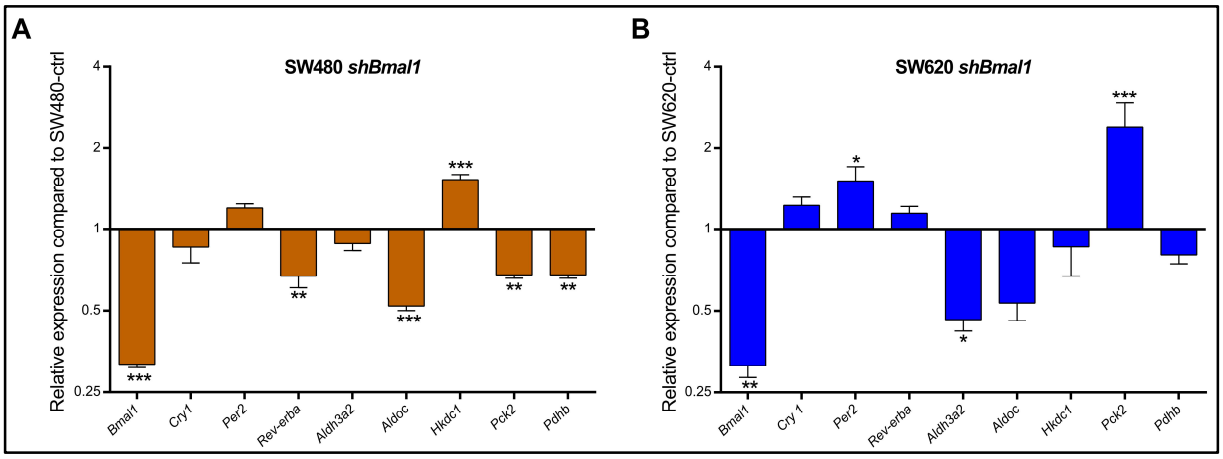

Figure 30: Gene expression analysis of selected core-clock and metabolic genes
Gene expression of selected core-clock (*Bmal1*, *Cry1*, *Rev-erbα*, *Per2*) and metabolic genes (*Aldoc*, *Aldh3a2*, *Hkdc1*, *Pck2* and *Pdhb*) was measured in (**A**) SW480 and (**B**) SW620 cells after *Bmal1*-KD. Gene expression is shown compared to the corresponding control-gene. Mean ± SEM, n = 3. * = $p < 0.05$, ** = $p < 0.01$, *** = $p < 0.001$. Adapted from **Fuhr** *et al.*, 2018 [1].

In SW480 cells, *Hkdc1* expression was significantly upregulated after *Bmal1*-KD ($p < 0.001$), whereas *Rev-erbα* ($p < 0.01$), *Aldoc* ($p < 0.001$), *Pck2* ($p < 0.01$) and *Pdhb* ($p < 0.01$) were significantly downregulated (**Figure 30 A**). Interestingly, *Bmal1*-KD led to different effects in SW620 cells. While *Per2* ($p < 0.05$) and *Pck2* ($p < 0.001$) were significantly upregulated, *Aldh3a2* ($p < 0.05$) was significantly downregulated (**Figure 30 B**). These results show that the knockdown of the core-clock gene *Bmal1* does not only affect other core-clock genes, but also influences the expression of metabolic genes in both cell lines. However, the effect on metabolic gene expression was stronger in SW480 cells. Especially the effect of *Bmal1*-KD on *Hkdc1* expression in SW480 cells further supports the hypothesised interplay between both genes.

SW620 cells represent the metastatic counterpart to primary tumour-derived SW480 cells. Additionally, the circadian clock in SW620 cells is deregulated when compared to SW480 cells. Consequently, in a next step it was tested whether *Bmal1*-KD in SW480 cells resembles the metastatic phenotype of SW620 cells. Therefore, relative expression changes of SW480-*shBmal1* and SW620-ctrl cells were compared to SW480-ctrl cells and analysed for

their similarity. Remarkably, the expression profile of SW620-ctrl cells closely resembled the expression profile of SW480-*shBmal1* cells (**Figure 31**). Namely *Hkdc1* was also significantly upregulated and *Aldoc* and *Pck2* also significantly downregulated (comparison of **Figure 30 A** and **Figure 31**). These results support the hypothesis that SW480-*shBmal1* cells have a phenotype similar to SW620-ctrl cells and therefore resemble a phenotype of tumour progression or metastasis.

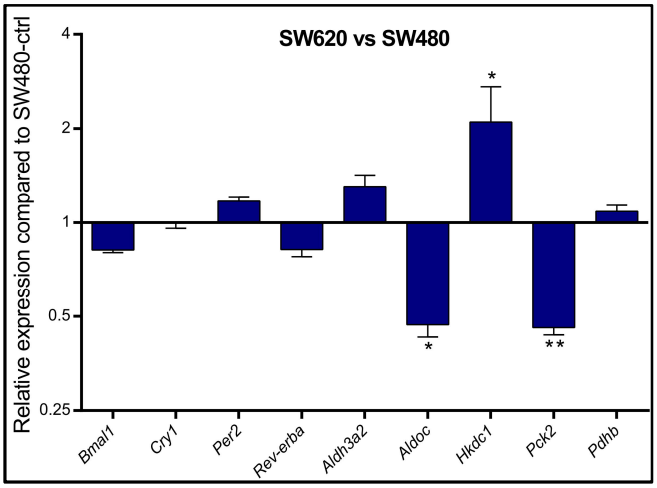

Figure 31: Gene expression analysis of selected genes in SW620 cells compared to SW480 cells
Gene expression analysis of selected core-clock (*Bmal1*, *Cry1*, *Rev-erbα*, *Per2*) and metabolic genes (*Aldoc*, *Aldh3a2*, *Hkdc1*, *Pck2* and *Pdhb*) in SW620 cells compared to SW480 cells. Gene expression is shown compared to SW480 cells. Mean ± SEM, n = 3. * = $p < 0.05$, ** = $p < 0.01$. Adapted from **Fuhr** *et al*., 2018 [1].

3.5.3 *Bmal1*-KD induces changes in cell proliferation and apoptosis

A knockdown of the core-clock gene *Bmal1* induced expression changes in other core-clock and metabolic genes. In SW480 cells, *Bmal1*-KD induced a gene expression phenotype similar to the metastatic cell line SW620. Consequently, the effects of *Bmal1*-KD were further evaluated and the consequences on proliferation, viability, cytotoxicity and apoptosis were evaluated in SW480 and SW620 cells.

As shown in **Figure 32**, SW480-*shBmal1* cells proliferated faster than SW480-ctrl cells ($p < 0.05$ for all timepoints), and their proliferation profile resembled that of metastatic SW620 ctrl cells ($p < 0.05$ for the last two timepoints). These findings support published data regarding the role of the biological clock as a tumour suppressor [22], [56], [136]–[141] and support the assumption that a deregulated clock promotes a more metastatic phenotype.

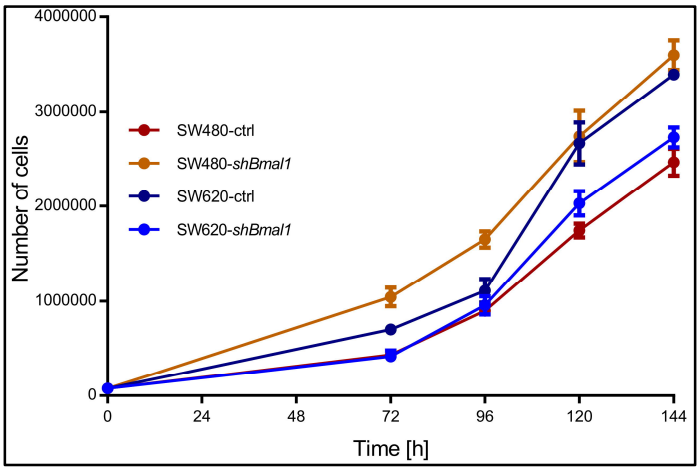

Figure 32: Proliferation curves of SW480 and SW620 cells
The proliferation of SW480-ctrl, SW480-*shBmal1*, SW620-ctrl and SW620-*shBmal1* cells was measured for four days. Adapted from **Fuhr** *et al*., 2018 [1].

Furthermore, the impact of *Bmal1*-KD on cell viability, cytotoxicity and apoptosis was evaluated at three different timepoints after cell synchronisation (18 h, 21 h and 24 h) (**Figure 33**). Cell viability and cytotoxicity tendentially decreased with later synchronisation timepoints in SW480-ctrl and SW620-ctrl cells. After *Bmal1*-KD, the time-dependent profile was inverted as compared to the normal scenario in both cell lines and viability and cytotoxicity increased with time. The apoptotic profile of the cells was not dependent on the synchronisation timepoint. However, *Bmal1*-KD led to significantly lower apoptosis rates in SW480 ($p < 0.001$) as well as in SW620 ($p < 0.001$) cells. Therefore, *Bmal1*-KD may protect cells from apoptosis and support cell survival and consequently progression towards malignant phenotypes. These results are in agreement with recent findings in a model system of mouse embryonic fibroblasts published by our group [52].

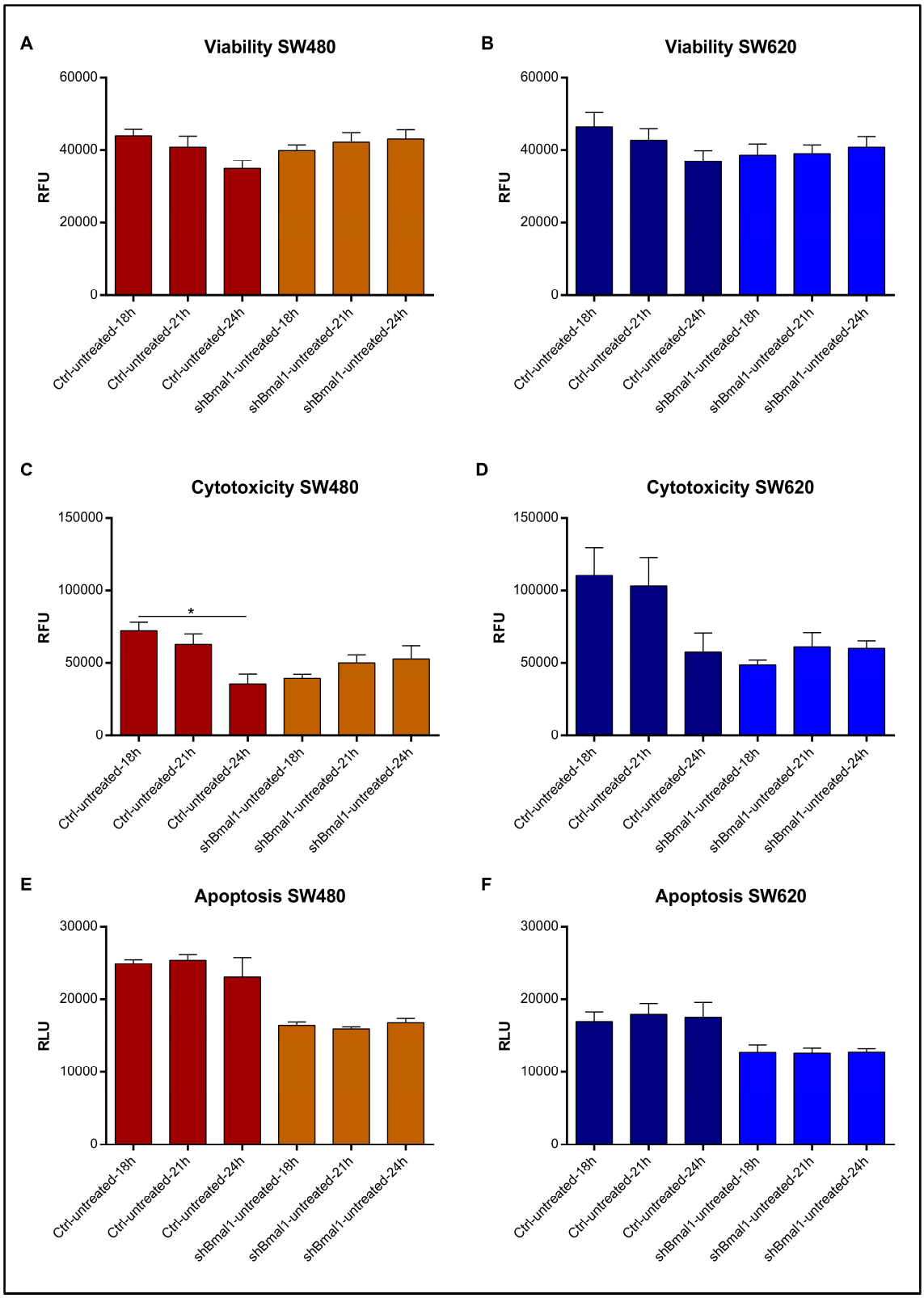

Figure 33: Viability, cytotoxicity and apoptosis in SW480 and SW620 cells
Viability (**A**, **B**), cytotoxicity (**C**, **D**) and apoptosis (**E**, **F**) in SW480 and SW620 control and *shBmal1* cells synchronised at different timepoints. Mean ± SEM, n = 3. Significant changes ($p < 0.05$) between different synchronisation timepoints of the same condition are marked with *. Adapted from **Fuhr** *et al.*, 2018 [1].

3.5.4 *Bmal1*-knockdown induces metabolic changes in SW480 and SW620 cells

The knockdown of *Bmal1* in SW480 and SW620 cells induced changes in metabolic gene expression. Hence, in a next step it was tested if these changes also lead to alterations in metabolic activity. The metabolic profiles were investigated in control cells as well as in *shBmal1* cells and an energy map was created based on the extracellular acidification rate (ECAR) and the oxygen consumption rate (OCR) of the cells.

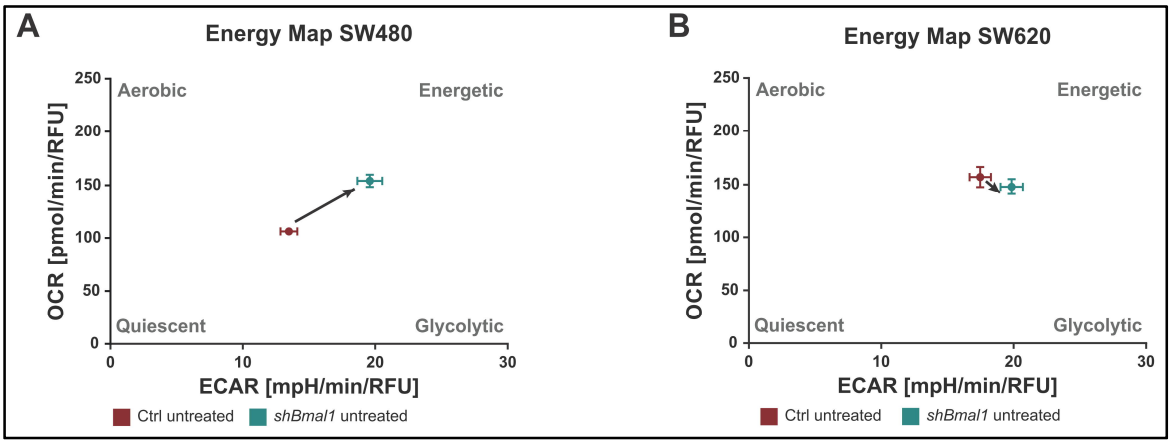

Figure 34: Energy map of SW480 and SW620 cells
Energy map of SW480 (**A**) and SW620 (**B**) control and *shBmal1* cells. The mean of three treatment timepoints after synchronisation is shown (18 h, 21 h, 24 h). Mean ± SEM, n = 16. Adapted from **Fuhr** *et al.*, 2018 [1].

The energy maps of SW480 and SW620 cells revealed that the knockdown of *Bmal1* induced a more energetic phenotype in SW480 cells (**Figure 34 A**), while for SW620 cells, no change upon *Bmal1*-KD was observed (**Figure 34 B**). Remarkably, the energy phenotype of SW480 *shBmal1* cells closely resembled the energy phenotype of SW620 cells. These findings further support the hypothesis that clock gene disruption leads to a more metastatic phenotype, reinforcing the role of the circadian clock as a tumour suppressor.

As a deregulated circadian clock changed the metabolic profile of SW480 cells and induced a more energetic metabolic phenotype, in a next step, it was tested whether a deregulated clock also changes the time-dependent metabolic profile of SW480 and SW620 cells. Therefore, ECAR and OCR were measured for 12 h in SW480 and SW620 control and *shBmal1* cells.

SW480-ctrl cells showed distinct time-dependent fluctuations in the ECAR rates, which were diminished upon *Bmal1*-KD (**Figure 35 A**). Remarkably, as already observed before for proliferation and energy phenotype, the time-dependent metabolic profile of SW480-*shBmal1*

cells resembled that of SW620 cells, again supporting the hypothesis that a deregulated clock induces a more metastatic phenotype. The time-dependent fluctuations in the OCR were also reduced in SW480 cells after *Bmal1*-KD but in the opposite direction as the ECAR (**Figure 35 B**). The OCR profile in SW620 cells did not change upon *Bmal1*-KD and was generally higher than in SW480 cells (**Figure 35 B**).

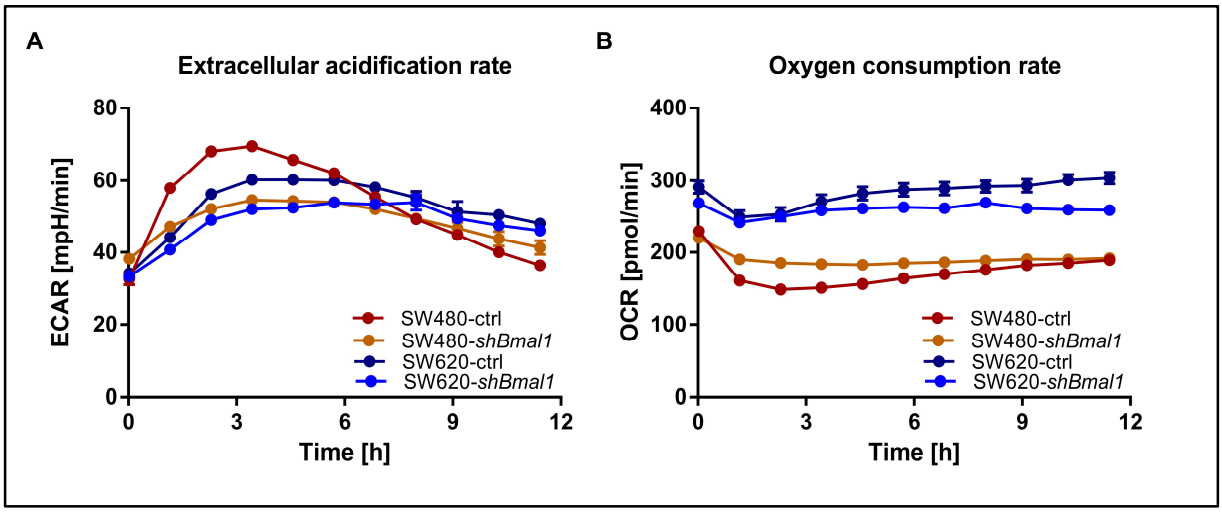

Figure 35: Time-dependent metabolic activity in SW480 and SW620 cells
Extracellular acidification rate (**A**) and oxygen consumption rate (**B**) of SW480 and SW620 control and *shBmal1* cells measured using a seahorse machine for 12 h. Mean ± SEM, n = 8.

In summary, a knockdown of the core-clock gene *Bmal1* leads to time-dependent metabolic changes in SW480 and SW620 cells and the results shown above again support the hypothesis that a deregulated clock may induce a more metastatic phenotype probably through metabolic phenotype rewiring.

3.6 *Hkdc1*-knockdown alters clock and metabolic gene expression

The results gained so far showed that a deregulated clock induces metabolic changes in tumour cells evoking a more metastatic phenotype. The glycolytic gene *Hkdc1* was identified as a possible mediator of clock-dependent metabolic changes. Especially in SW480 cells, the expression of *Bmal1* and *Hkdc1* seemed to be connected and *Hkdc1* was found to be upregulated in SW480-*shBmal1* cells. Furthermore, the expression of *Hkdc1* differed between SW480 and SW620 cells. Therefore, out of the five metabolic candidate genes, *Hkdc1* was chosen for further experiments. To gain further insights into the interplay between the circadian clock and

cellular metabolism, a knockdown of *Hkdc1* was carried out in SW480 and SW620 cells and the output on the circadian clock and metabolic activity were evaluated.

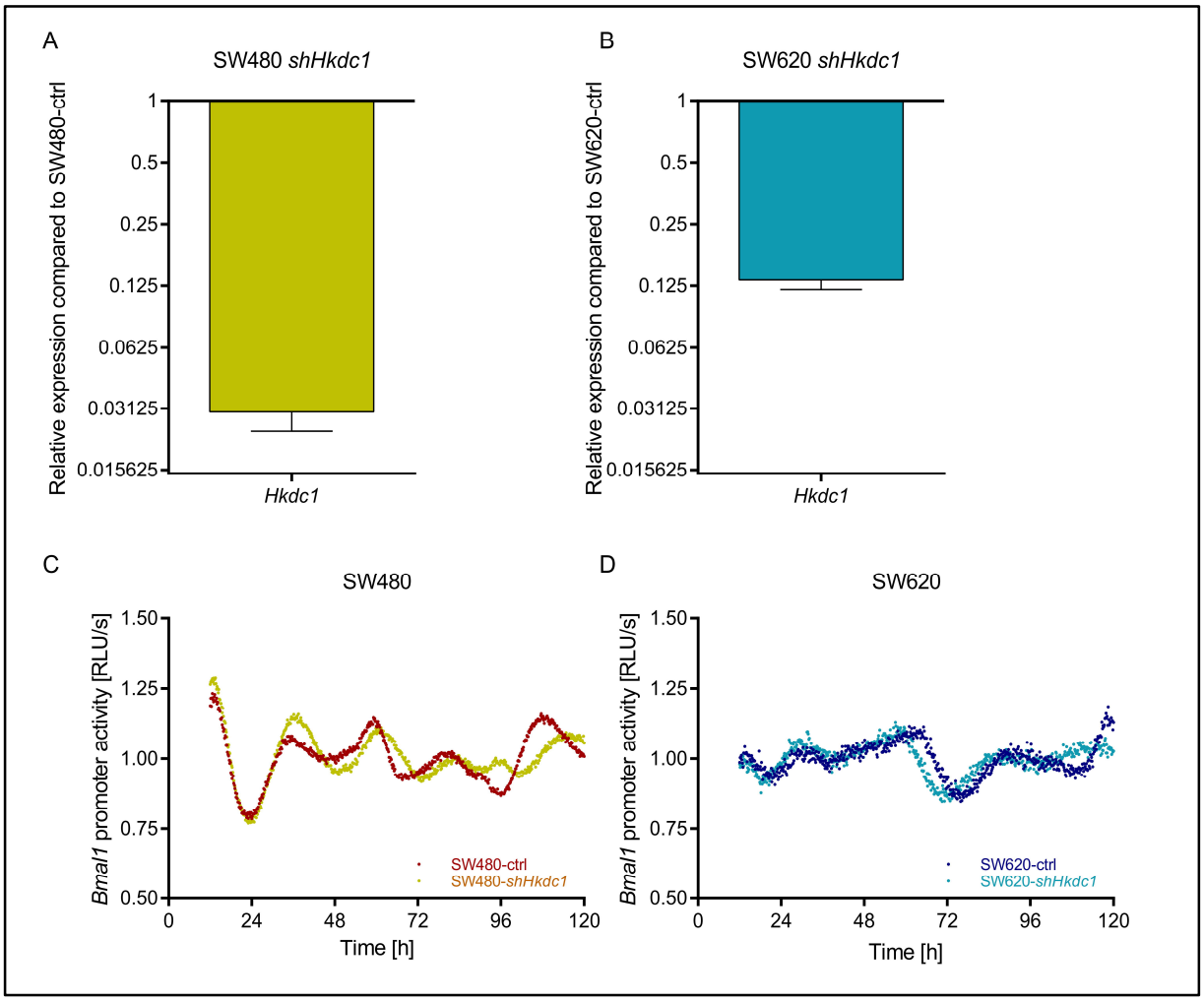

Figure 36: Knockdown efficiency after shRNA-mediated KD of *Hkdc1*
Gene expression analysis of *Hkdc1* in SW480 (**A**) and SW620 (**B**) cells after shRNA-mediated *Hkdc1*-KD. Gene expression is shown compared to the corresponding control gene. Mean ± SEM, n = 3. KD efficiency in SW480-*shHkdc1*: 0.03 ± 0.006 (97%). KD efficiency in SW620-*shHkdc1*: 0.13 ± 0.013 (87%). Bioluminescence measurements in SW480 (**C**) and SW620 (**D**) cells. Cells were lentivirally transduced either with an empty vector (ctrl) or with a *shHkdc1*-construct. Additionally, cells were lentivirally transduced with a *Bmal1*-promoter driven luciferase construct. Bioluminescence was measured for five consecutive days. Shown is one representative replicate for each condition.

A stable knockdown of *Hkdc1* was performed using lentivirus-based shRNA constructs (see 2.2.11) and the consequences on core-clock and metabolic gene expression were evaluated. The knockdown efficiency of different shRNA-constructs was tested via qPCR and the construct that gave the best knockdown efficiency was used for further experiments. **Figure 36** shows the expression of *Hkdc1* in SW480 (**A**) and SW620 (**B**) cells after shRNA-mediated *Hkdc1*-KD. The knockdown efficiency was high in both cell lines with 97 % in SW480 cells

and 87 % in SW620 cells. Bioluminescence measurements of the *Bmal1*-promoter activity after *Hkdc1*-KD showed that *Hkdc1*-KD had only minor effects on circadian oscillations in SW480 (**C**) and SW620 (**D**) cells.

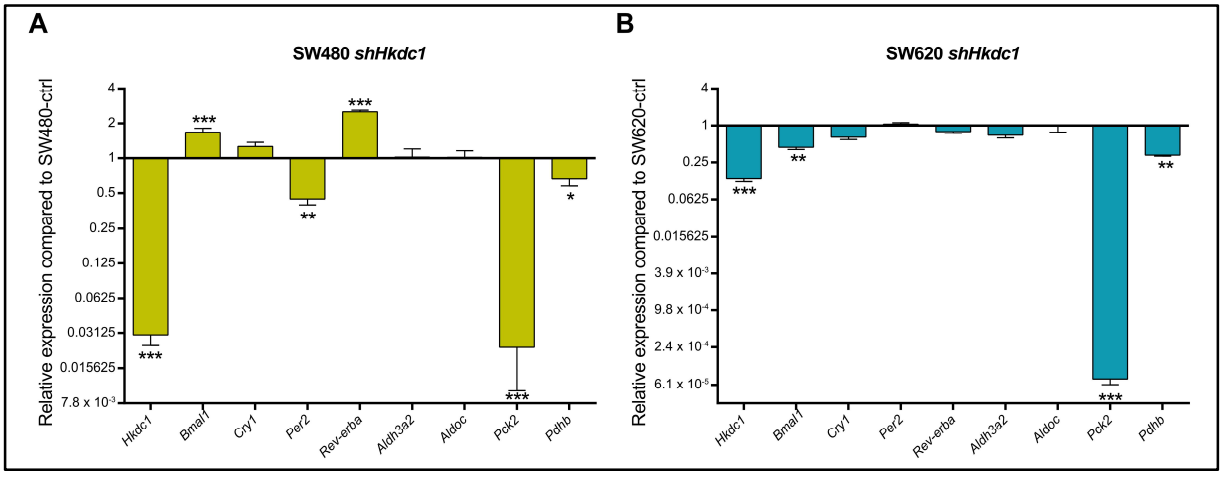

Figure 37: Gene expression analysis of selected core-clock and metabolic genes in SW480 and SW620 cells after *Hkdc1*-KD
The expression of core-clock (*Bmal1*, *Cry1*, *Rev-erbα*, *Per2*) and metabolic genes (*Aldoc*, *Aldh3a2*, *Hkdc1*, *Pck2* and *Pdhb*) was measured in (**A**) SW480 and (**B**) SW620 cells after *Hkdc1*-KD. Gene expression is shown compared to the corresponding control-gene. Mean ± SEM, n = 3. Significant changes ($p < 0.05$) are marked with *. * = $p < 0.05$, ** = $p < 0.01$, *** = $p < 0.001$. Adapted from **Fuhr** *et al.*, 2018 [1].

Subsequently, the effect of *Hkdc1*-KD on core-clock and metabolic gene expression was tested via qPCR. As also seen for the *Bmal1*-KD, the knockdown of *Hkdc1* had effects on the expression of several core-clock and clock-regulated metabolic candidate genes. In SW480 cells, *Hkdc1*-KD led to a significant upregulation of *Bmal1* ($p < 0.001$) and *Rev-erbα* ($p < 0.001$), whereas *Per2* ($p < 0.01$), *Pck2* ($p < 0.001$) and *Pdhb* ($p < 0.05$) were significantly downregulated (**Figure 37 A**). In SW620 cells, *Bmal1* ($p < 0.01$), *Pck2* ($p < 0.001$) and *Pdhb* ($p < 0.01$) were significantly downregulated upon *Hkdc1*-KD (**Figure 37 B**). Interestingly, in WT cells, the expression of *Hkdc1* in SW620 cells was higher as compared to SW480 cells, whereas *Bmal1* expression was lower (**Figure 31**).

Summarising, the results gained so far point to a reciprocal interplay between *Bmal1* and *Hkdc1*. A low expression of *Bmal1* leads to a higher expression of *Hkdc1*, as seen for SW620 vs SW480 cells and for SW480-*shBmal1* vs SW480-ctrl cells. On the other hand, low *Hkdc1* expression led to upregulated *Bmal1* expression, as seen for SW480-*shHkdc1* vs SW480-ctrl cells. However, this effect could not be observed in SW620 cells, most likely due to the initial gene expression levels of both genes in these cells.

3.7 *Bmal1*-KD and *Hkdc1*-KD alter metabolic activity in colorectal cancer cells

The results gained so far indicate an influence of *Bmal1* on metabolic activity most likely in coherence with *Hkdc1*. Consequently, the following step was to evaluate the effects of *Bmal1*- and *Hkdc1*-KD on the metabolic activity in SW480 and SW620 cells. The glycolytic and mitochondrial activity of the cells were compared between control, *shBmal1* and *shHkdc1* cells in a time-dependent manner at three different timepoints after synchronisation (18 h, 21 h and 24 h).

3.7.1 Effects of *Bmal1*- and *Hkdc1*-KD on glycolysis

The use of high rates if glycolysis even in the presence of oxygen, known as the Warburg effect, is a characteristic of many cancer cells. The altered glucose metabolism is required to fulfil the anabolic demands of tumour cells [65]. An elevated glucose metabolism was only very recently defined as one of the hallmarks of cancer [64].

To investigate the effects of *Bmal1*- and *Hkdc1*-KD on glycolytic activity, SW480 and SW620 cells were synchronised at three different timepoints (see 2.2.2) and the glycolytic activity was measured using the glycolysis stress test kit (Agilent) as described in chapter 2.2.6.2. Glycolysis and glycolytic capacity were compared between control, *shBmal1* and *shHkdc1* cells.

Figure 38 shows glycolysis (**A**, **B**) and glycolytic capacity (**C**, **D**) in SW480 and SW620 cells. Both, glycolysis and glycolytic capacity showed significant time-dependent alterations in SW480-ctrl cells. Remarkably, these time-dependent alterations were diminished in SW480-*shBmal1* cells. Although SW620-ctrl cells also showed time-dependent changes in glycolytic activity, these changes were not significant. When all timepoints were taken together as replicates, glycolysis was significantly increased ($p < 0.05$) after *Bmal1*-KD in SW480 cells whereas *Bmal1*-KD led to a significant decrease of glycolysis ($p < 0.05$) in SW620 cells. As expected, given its upstream role in the glycolytic pathway, a *Hkdc1*-KD led to a significant decrease of glycolysis in both cell lines ($p < 0.05$) (**Figure 38 A** and **B**), whereas only in SW480 cells, the glycolytic capacity increased after *Hkdc1*-KD (**Figure 38 C** and **D**). As also seen for *shBmal1* cells, no significant time-dependent changes between different synchronisation timepoints were observed after *Hkdc1*-KD.

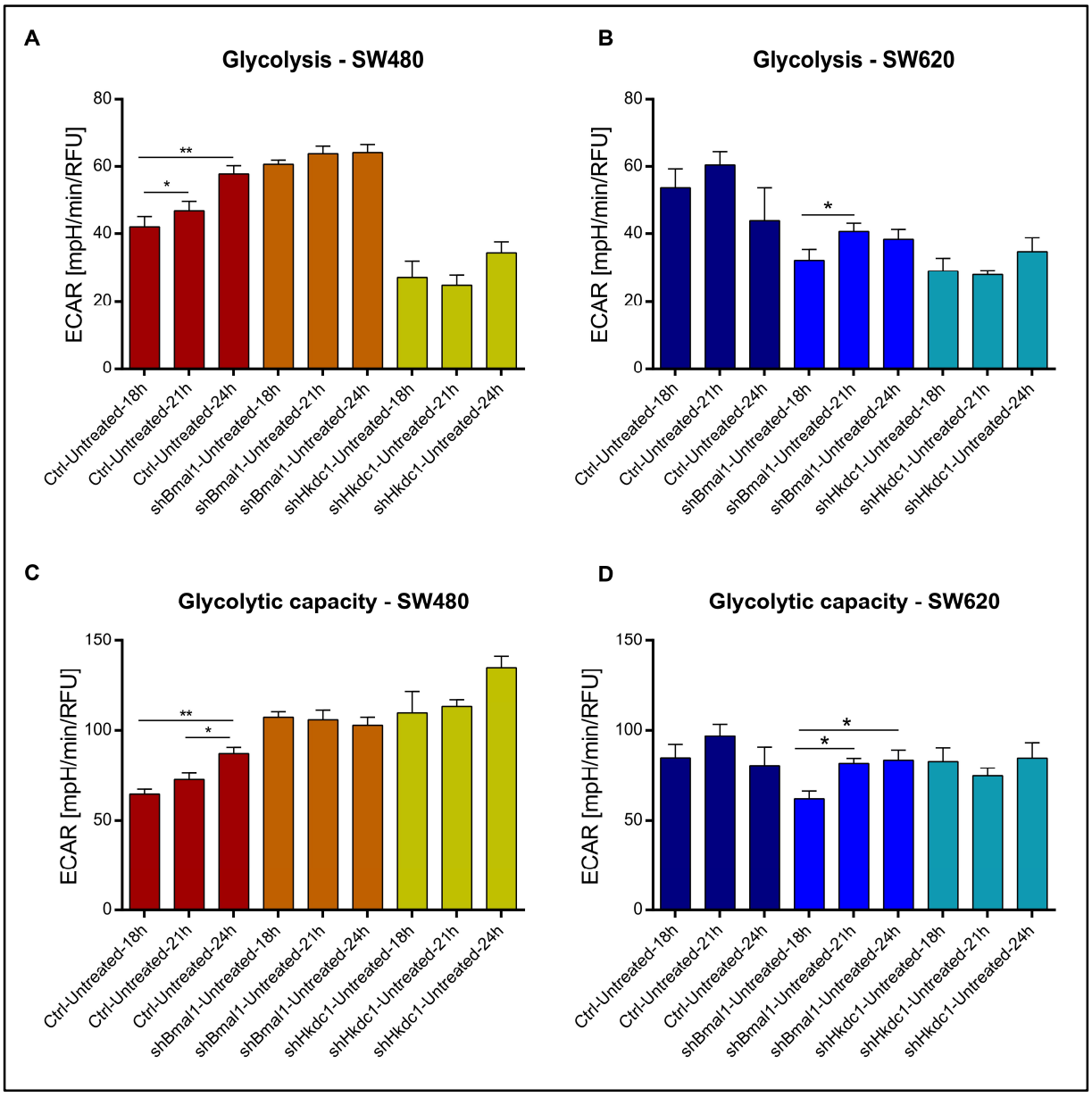

Figure 38: Glycolysis and glycolytic capacity in SW480 and SW620 cells
Glycolysis (**A, B**) and glycolytic capacity (**C, D**) in SW480 and SW620 control, *shBmal1* and *shHkdc1* cells at different timepoints after synchronisation. Mean ± SEM, n = 5. Significant changes ($p < 0.05$) between different timepoints of the same condition are marked with *. * = $p < 0.05$, ** = $p < 0.01$. Adapted from **Fuhr** *et al.*, 2018 [1].

Taken together, these results indicate a general control of glycolytic activity by the circadian clock. Additionally, the loss of time-dependent variations in glycolytic activity upon *Bmal1*-KD might be a hint for a circadian control of the timing of glycolytic activity in CRC cells.

3.7.2 Effect of *Bmal1*- and *Hkdc1*-KD on mitochondrial respiration

In addition to the glycolytic activity, the mitochondrial function plays an important role in tumour growth and metastasis as well [66]. Highly metastatic tumours increase mitochondrial NADPH and undergo further metabolic changes to fight stress caused by ROS [142]. To investigate the effects of *Bmal1* and *Hkdc1*-knockdown on mitochondrial respiration, SW480 and SW620 cells were synchronised at three different timepoints and the mitochondrial activity was measured using the cell mito stress test kit (Agilent) as described in chapter 2.2.6.3. Basal respiration, ATP production and maximum respiration were compared between control, *shBmal1* and *shHkdc1* cells.

Figure 39 shows the mitochondrial activity in SW480 and SW620 cells. In general, similar time-dependent effects on the mitochondrial activity were observed, although not as strong as for the glycolytic activity. Especially in SW480-*shHkdc1* cells, basal respiration, ATP production and maximum respiration showed time-dependent effects and increased in earlier timepoints after synchronisation, whereas no significant time-dependent changes were observed in SW480-ctrl and SW480-*shBmal1* cells. In SW620-*shHkdc1* cells, only maximum respiration showed synchronisation time-dependent effects, whereas ATP production and basal respiration remained unaffected in SW620 cells. As already observed for the glycolytic activity, *Bmal1*-KD led to a general increase of mitochondrial activity in SW480 cells, whereas in SW620 cells, the mitochondrial activity slightly decreased.

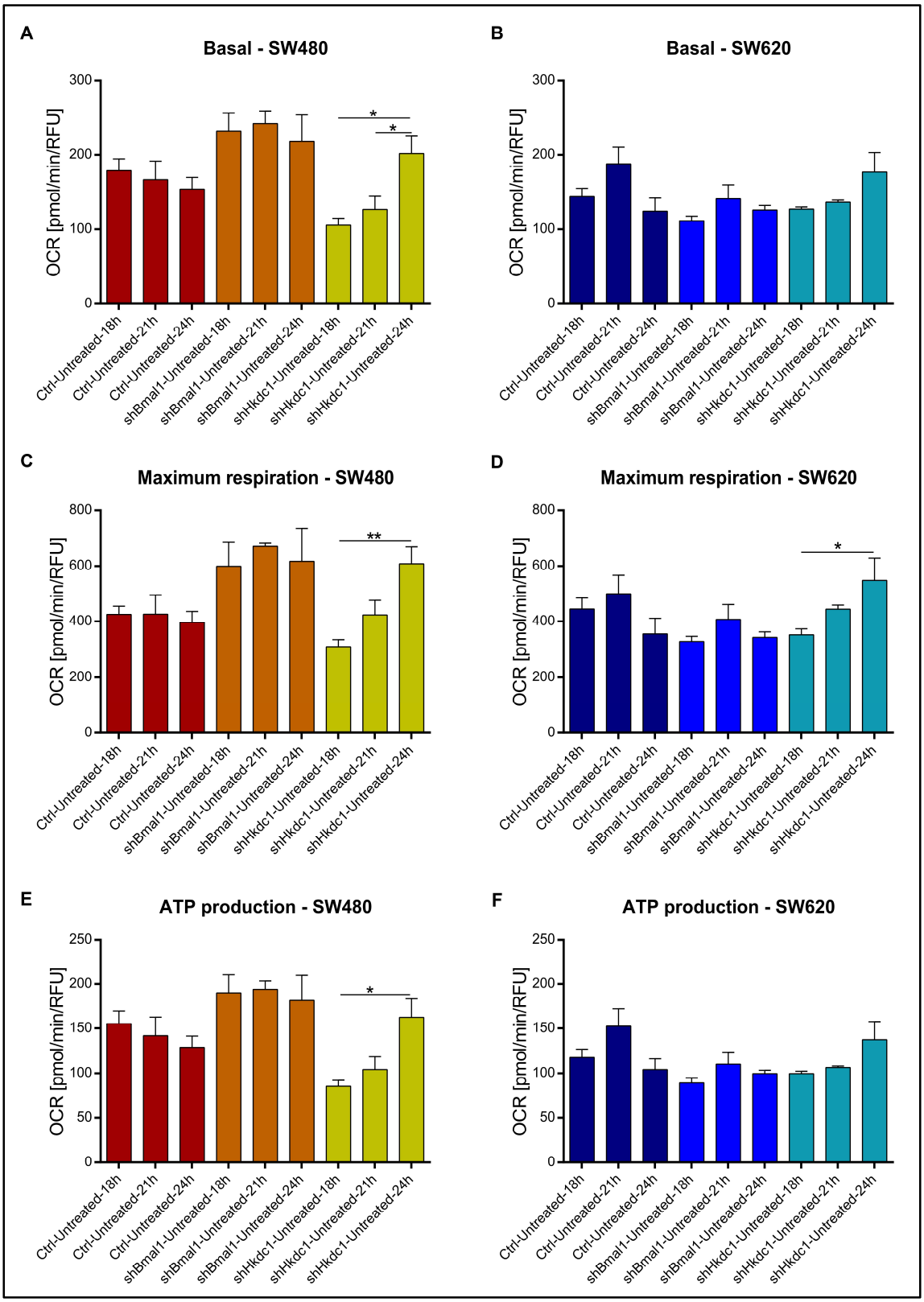

Figure 39: Basal respiration, maximum respiration and ATP production in SW480 and SW620 cells
Basal respiration (**A, B**), maximum respiration (**C, D**) and ATP production (**E, F**) in SW480 and SW620 control, *shBmal1* and *shHkdc1* cells at different timepoints after synchronisation. Mean ± SEM, n = 5. Significant changes ($p < 0.05$) between different timepoints of the same condition are marked with *. * = $p < 0.05$, ** = $p < 0.01$. Adapted from **Fuhr** *et al.*, 2018 [1].

Summarising, the results gained from knockdown studies in SW480 and SW620 cells point to an interplay between *Hkdc1* and the circadian clock, particularly in SW480 cells, since the KD of *Bmal1* led to a higher *Hkdc1* expression and consequently to a higher metabolic activity in these cells. Additionally, a KD of *Hkdc1* led to higher *Bmal1* expression and slightly lower glycolytic activity. In general, a KD of *Bmal1* led to a slight increase in metabolic activity in SW480 cells, but to the opposite change in SW620 cells. Upon *Bmal1*-KD, *Hkdc1* expression was upregulated in SW480 cells, but not in SW620 cells. This is likely a result of the overall increased metabolic activity of SW480-*shBmal1* cells. Thus, *Hkdc1* might be a mediator of time-dependent effects on energy producing metabolic pathways. Overall, the data shows that a deregulated biological clock leads to alterations in the expression of metabolic genes, as well as in metabolic activity that could be pivotal in colorectal cancer progression.

3.8 Clock gene knockdown in primary cell models

As already mentioned above, in addition to experiments carried out in colorectal cancer cell lines, primary cellular models were used to compare the results gained in cell lines, namely normal and cancer-associated primary fibroblasts and human fallopian tube organoids. To study the effects of a deregulated clock in a primary cell model, a *Bmal1*-KD was carried out in NFs and CAFs isolated from colorectal cancer patients. However, due to unresolved technical reasons, a *Bmal1*-KD could not be performed in organoids, as cells died upon transduction with *shBmal1*. As an alternative, a *p53*-KD was carried out in organoids and the effects on core-clock and metabolic gene expression were evaluated.

3.8.1 Clock gene knockdown in primary fibroblasts

To compare the results gained from cancer cell lines with patient-derived primary stromal cells, NFs and CAFs derived from the same colon cancer patient were used. Each pair of NFs and CAFs from one patient represents a single unique model system reflecting the status of the patient. The stromal cells were derived from a patient with lymph node metastasis, but without other distant organ metastasis observed. Therefore, this patient best represents the epithelial cancer cell model system used in this study (SW480 vs SW620). Bioluminescence measurements, gene expression analysis of selected core-clock and metabolic candidate genes and the glycolytic activity of WT and *shBmal1* NFs and CAFs were evaluated.

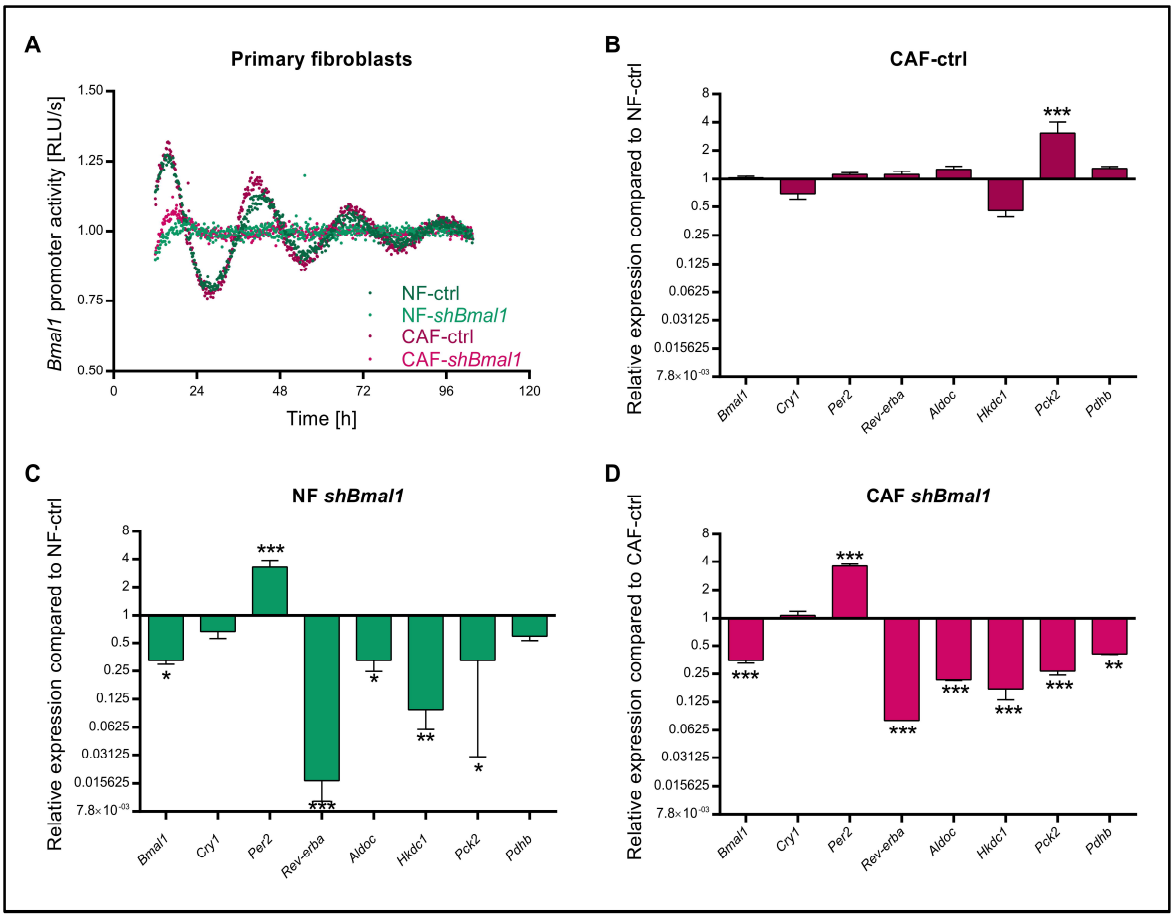

Figure 40: The circadian clock in primary fibroblasts
(**A**) Normal fibroblasts (NFs) and cancer associated fibroblasts (CAFs) were lentivirally transduced with either an empty vector (ctrl) or with a *shBmal1*-construct. Additionally, cells were lentivirally transduced with a *Bmal1*-promoter driven luciferase construct. Bioluminescence was measured for five consecutive days. Shown is one representative replicate for each condition. (**B**-**D**) Gene expression analysis of selected core-clock (*Bmal1*, *Cry1*, *Rev-erbα*, and *Per2*) and metabolic genes (*Aldoc*, *Hkdc1*, *Pck2* and *Pdhb*) in control (**B**) and *shBmal1* NFs (**C**) and CAFs (**D**). Gene expression is shown compared to the corresponding control-gene. KD efficiency in NF-*shBmal1* cells: 0.328 ± 0.028 (67.2 %). KD efficiency in CAF-*shBmal1* cells: 0.347 ± 0.022 (65.3 %). Mean ± SEM, n = 3. * = $p < 0.05$, ** = $p < 0.01$, *** = $p < 0.001$. Adapted from **Fuhr** *et al*., 2018 [1].

Bioluminescence measurements of NFs and CAFs revealed the same peak phase of rhythmic *Bmal1*-expression as already observed in SW480 cells (**Figure 40 A** and **Figure 28 C**). The oscillatory profile of NFs and CAFs was very similar and in both cell types a *Bmal1*-KD led to a complete loss of oscillations. An analysis of clock gene and metabolic gene expression in CAFs compared to NFs showed a significant upregulation of *Pck2* expression ($p < 0.001$) and a downregulation of *Hkdc1* (**Figure 40 B**). In a next step, the effect of *Bmal1*-KD on core-clock and metabolic gene expression was tested. In NFs as well as in CAFs, *Per2* was upregulated ($p < 0.001$) and *Rev-erbα* was downregulated ($p < 0.001$) upon *Bmal1*-KD (**Figure 40 C** and **D**). The same tendency was also observed in SW480-*shBmal* cells. Furthermore, *Bmal1*-KD led to the down- regulation of *Aldoc* (NF, $p < 0.05$; CAF, $p < 0.001$), *Hkdc1* (NF, $p < 0.05$;

CAF, $p < 0.001$) and *Pck2* (NF, $p < 0.01$; CAF, $p < 0.001$). In CAFs, *Bmal1*-KD additionally led to the downregulation of *Pdhb* ($p < 0.01$). These results gained in primary fibroblasts reinforce the observations made in CRC cell lines regarding the impact of *Bmal1* on the expression of metabolic genes.

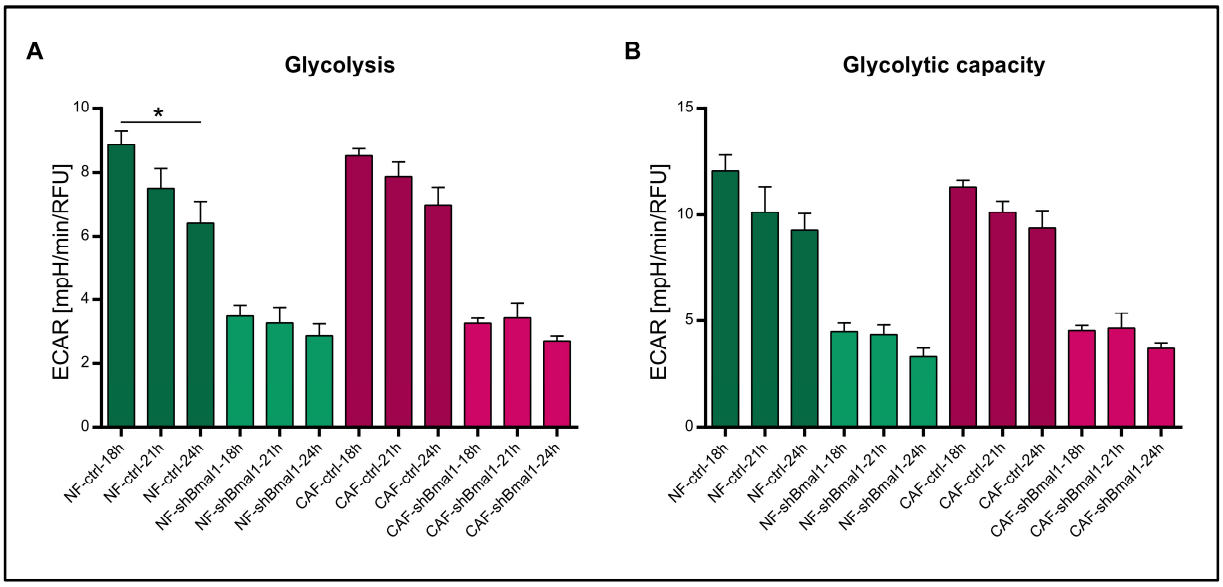

Figure 41: Glycolytic activity in primary fibroblasts
Glycolysis (**A**) and glycolytic capacity (**B**) of control and *shBmal1* NFs and CAFs at three different timepoints after synchronisation (18 h, 21h, 24h). Mean ± SEM, n = 5. Significant changes ($p < 0.05$) between different synchronisation timepoints of the same condition are marked with *. Adapted from **Fuhr** *et al.*, 2018 [1].

Figure 41 shows glycolysis and glycolytic capacity in WT NFs and CAFs and after *Bmal1*-KD. NFs showed time-dependent glycolytic activity, where glycolysis decreased at later synchronisation timepoints. The same tendency was observed in CAFs but with weaker time-dependent effects. The knockdown of *Bmal1* led to a decrease of glycolysis and glycolytic capacity in NFs, as well as in CAFs and an omission of time-dependent variations in glycolytic activity. These results support the hypothesis that the circadian clock influences the timing of metabolism and is able to reprogram metabolic activity in general. However, the specific effects of *Bmal1*-KD on metabolic activity seem to be dependent on the initial genetic conditions of a given cell, as *Bmal1*-KD induced higher glycolytic activity in SW480 cells, while glycolytic activity was decreased upon *Bmal1*-KD in primary fibroblasts.

3.8.2 *P53* knockdown in human fallopian tube organoids

As already mentioned above (see 3.4.2), human fallopian tube organoids were used as a model for non-cancerous tissue. In this case WT organoids and *p53*-knockdown (KD-efficiency: 96 %, **Figure S 7**) organoids were tested for their circadian phenotype. The knockdown of the tumour suppressor *p53* should serve as a simulation of a more cancerous stadium when compared to the WT organoids. Due to technical issues, a knockdown of *Bmal1* was not performed in organoids. During the time of this project, it was not possible to optimise the transduction and selection protocol for human organoids. In addition to bioluminescence measurements, gene expression analysis of selected core-clock and metabolic genes was performed, and the expression was compared between WT and *p53*-KD organoids.

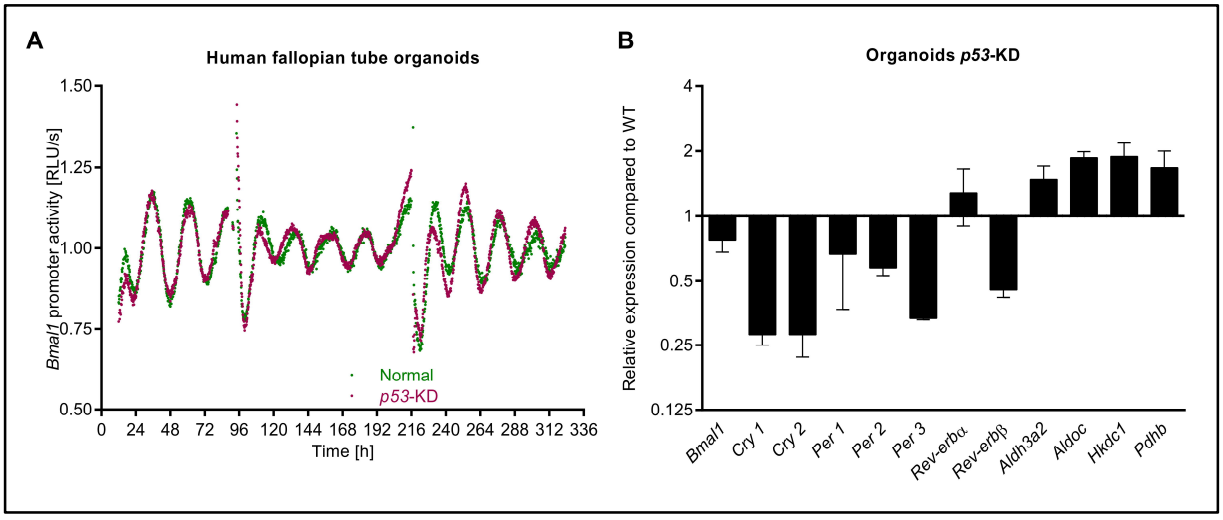

Figure 42: *Bmal1*-promoter analysis and gene expression analysis in WT and *p53*-KD organoids
(**A**) Cells were lentivirally transduced with a *Bmal1*-reporter construct and *Bmal1*-promoter activity was measured over 14 consecutive days. Shown is one representative replicate per condition. (**B**) The expression of selected core-clock and metabolic genes (*Bmal1*, *Cry1*, *Cry2*, *Per1*, *Per2*, *Per3*, *Rev-erbα*, *Rev-erbβ*, *Aldh3a2*, *Aldoc*, *Hkdc1*, *Pdhb*) was measured using qPCR in *p53*-KD organoids compared to WT organoids. Data are expressed as mean ± SEM, n = 2.

The *Bmal1*-promoter activity was measured over 14 consecutive days in WT and *p53*-KD organoids (**Figure 42**). WT as well as *p53*-KD organoids showed very robust circadian oscillations even for longer time frames. No significant difference in period length between both conditions was observed (WT: 24.64 ± 0.10, *p53*-KD: 24.34 ± 0.08). The gene expression analysis of several core-clock and metabolic genes in *p53*-KD organoids compared to WT organoids revealed strong effects of p53-KD on core-clock and metabolic gene expression. While core-clock genes were downregulated upon *p53*-KD, metabolic candidate genes were

upregulated after *p53*-KD (**Figure 42 B**). Although due to the lack of replicates, no assumptions about the statistical significance of the results could be made, the knockdown of the tumour suppressor *p53* seemed to induce metabolic gene expression and inhibited core-clock activity. These results support the assumptions made so far that a more cancerous phenotype is linked to a deregulated clock and enhanced metabolic activity.

3.9 A deregulated clock induces metabolic phenotype rewiring after treatment

By the experiments made so far, *Bmal1*- as well as *Hkdc1*-KD have been shown to induce metabolic changes in SW480 and SW620 cells. Consequently, in a next step, it was tested whether these metabolic changes also induce differential effects on treatment response. To answer this question, a metabolism-targeting anticancer treatment was applied to ctrl, *shBmal1* and *shHkdc1* cells. SW480 and SW620 cells were treated with WZB117, a glucose transporter (GLUT1) inhibitor, and its effect on gene expression, as well as on metabolic activity was evaluated.

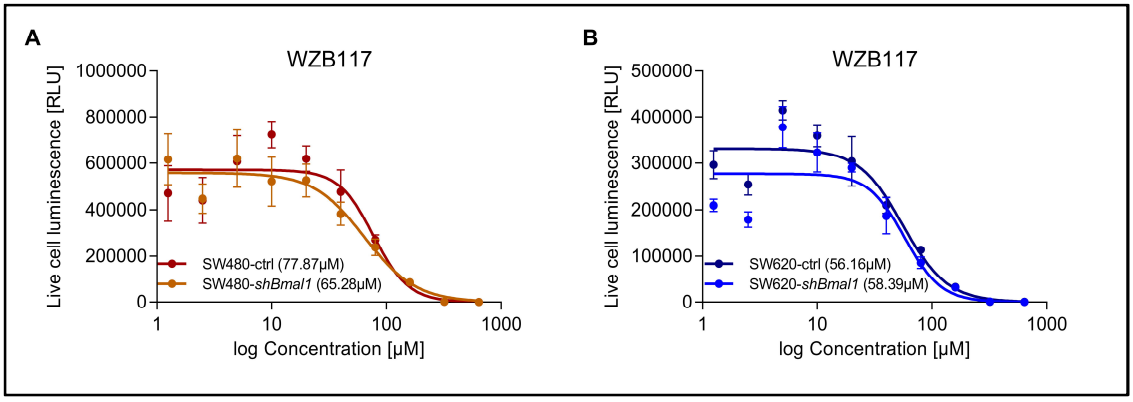

Figure 43: Determination of treatment concentration for WZB117 treatment.
To determine the appropriate treatment concentration, SW480-ctrl, SW480-*shBmal1*, SW620-ctrl and SW620-*shBmal1* cells were treated with different concentrations of WZB117 and the IC50 value was calculated based on the cytotoxicity. Adapted from **Fuhr** *et al.*, 2018 [1].

To determine the appropriate treatment concentration, cells were treated with different WZB117 concentrations and the cytotoxicity was measured (**Figure 43**). Based on the experimentally defined and calculated IC50 value, a treatment concentration of 80 µM was determined.

3.9.1 WZB117 treatment induces gene expression changes in SW480 and SW620 cells

In a first approach, SW480- and SW620-ctrl, *shBmal1* and *shHkdc1* cells were treated with WZB117 at a single timepoint and the effects on core-clock and metabolic gene expression were measured via qPCR.

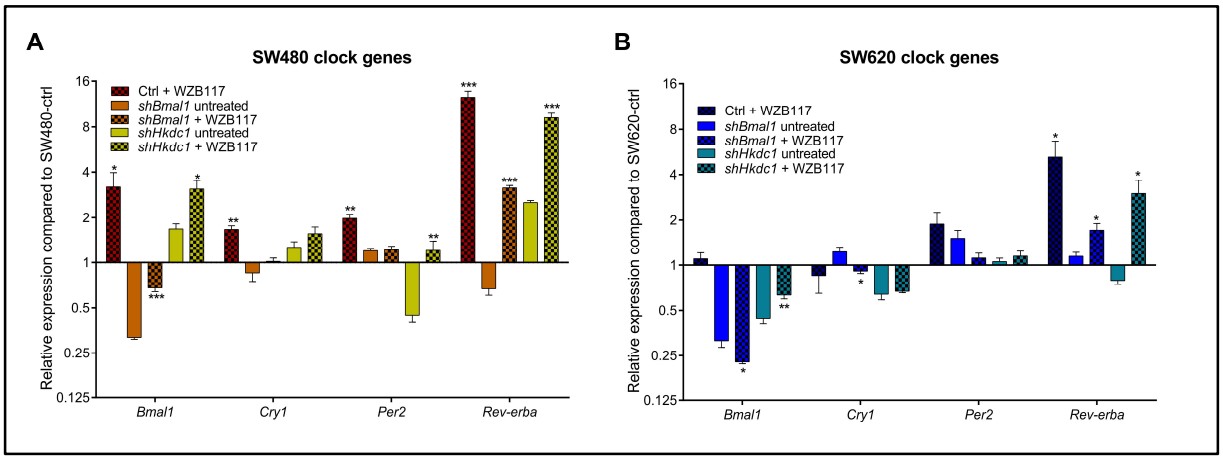

Figure 44: Consequences of *Bmal1*- and *Hkdc1*-KD on core-clock gene expression after WZB117 treatment
Gene expression analysis of selected core-clock genes (*Bmal1*, *Cry1*, *Per2* and *Rev-erbα*) in SW480 (**A**) and SW620 (**B**) control, *shBmal1* and *shHkdc1* cells after treatment with WZB117. Data are shown compared to untreated control cells. Mean ± SEM, n = 3. * = $p < 0.05$, ** = $p < 0.01$, *** = $p < 0.001$ compared to the corresponding untreated sample of the same condition (control, *shBmal1*, *shHkdc1*). Adapted from **Fuhr** *et al.*, 2018 [1].

Figure 44 shows the expression of selected core-clock genes in SW480 and SW620 cells after treatment with WZB117. In SW480-ctrl cells, WZB117 treatment led to a significant upregulation of all tested core-clock genes (*Bmal1* ($p < 0.05$), *Cry1* ($p < 0.01$), *Per2* ($p < 0.01$), *Rev-erbα* ($p < 0.001$)) (**Figure 44 A**). This result fits with the observed increase of glycolysis upon *Bmal1*-KD in untreated SW480 cells. Furthermore, these results are in concordance with the reported inhibitory effect of intracellular glucose on the expression of the core-clock genes *Bmal1*, *Per1* and *Per2* [83]. In SW480-*shBmal1* cells, *Bmal1* ($p < 0.001$) and *Rev-erbα* ($p < 0.001$) were upregulated after treatment with WZB117. This upregulation of core-clock genes was also observed for SW480-*shHkdc1* cells after WZB117 treatment where *Per2* was additionally upregulated ($p < 0.01$). In contrast to these observations, *Rev-erbα* was the only tested core-clock gene whose expression was significantly upregulated ($p < 0.05$) after treatment in SW620 cells in all conditions (**Figure 44 B**). Additionally, *Bmal1* ($p < 0.05$) and *Cry1* ($p < 0.05$) were downregulated in SW620-*shBmal1* cells, whereas *Bmal1* ($p < 0.01$) was upregulated in SW620-*shHKkdc1* cells upon treatment. Overall, the effect of WZB117

treatment on core-clock gene expression was weaker in SW620 cells when compared to SW480 cells.

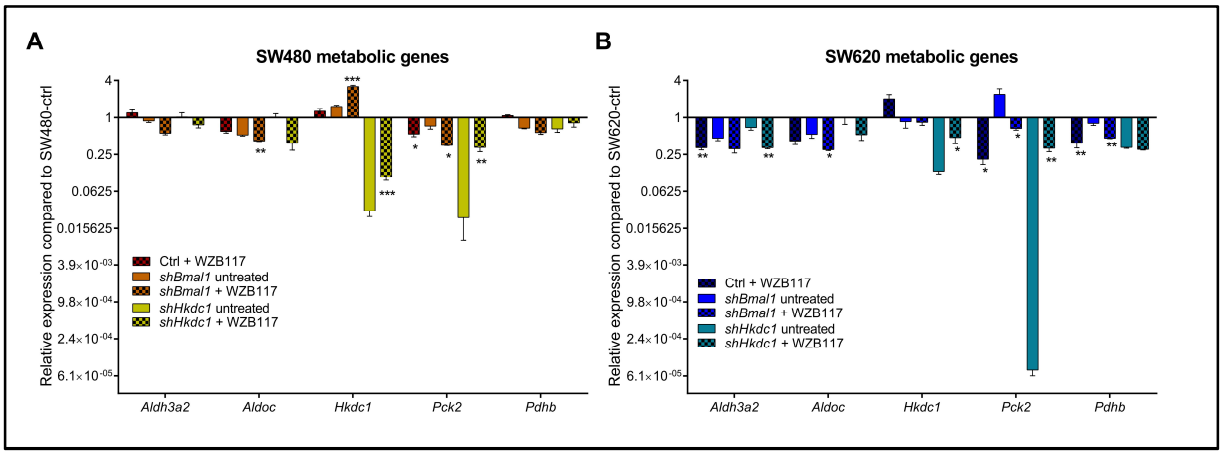

Figure 45: Consequences of *Bmal1*- and *Hkdc1*-KD on metabolic gene expression after WZB117 treatment
Gene expression analysis of selected metabolic genes (*Aldoc*, *Aldh3a2*, *Hkdc1*, *Pck2* and *Pdhb*) in SW480 (**A**) and SW620 (**B**) control, *shBmal1* and *shHkdc1* cells after treatment with WZB117. Data are shown compared to untreated control cells. Mean ± SEM, n = 3. * = $p < 0.05$, ** = $p < 0.01$, *** = $p < 0.001$ compared to the corresponding untreated sample of the same condition (control, *shBmal1*, *shHkdc1*). Adapted from **Fuhr** *et al.*, 2018 [1].

Moreover, the outcome of WZB117 treatment on the expression of metabolic genes was analysed. In this case, the effects were very diverse for the different ctrl and KD conditions (**Figure 45**). Upon WZB117 treatment, *Pck2* expression was significantly downregulated in SW480 and SW480-*shBmal1* cells ($p < 0.05$) but upregulated in SW480-*shHkdc1* cells ($p < 0.01$). The same effect could be observed in SW620 cells. While *Hkdc1* expression was not affected in SW480- and SW620-ctrl cells, it was upregulated in both cell lines after *Hkdc1*-KD, as well as in SW480-*shBmal1* cells ($p < 0.001$). Interestingly, no significant effect on *Pdhb* expression was observed in any of the SW480 conditions but a downregulation of *Pdhb* was measured after treatment in SW620 ctrl and -*shBmal1* cells ($p < 0.01$). Additionally, *Aldh3a2* expression was downregulated upon treatment in SW620-ctrl and SW620-*shHkdc1* cells and *Aldoc* was downregulated upon treatment in SW480-*shBmal1* and SW620-*shBmal1* cells. The diverse treatment effects on metabolic gene expression based on different cellular conditions led to the conclusion that the initial genetic status of the cell affects treatment response.

3.9.2 WZB117 treatment affects *Bmal1*-promoter activity

As WZB117 treatment induced changes in core-clock gene expression, live-cell bioluminescence measurements were carried out to evaluate if these changes can also be observed in the *Bmal1*-promoter activity. For this purpose, SW480-ctrl and SW480-*shBmal1* cells were synchronised at three different timepoints (18 h, 21 h, 24 h before treatment) and treated with 80 µM WZB117. Subsequently, *Bmal1*-promoter activity was measured for five consecutive days to evaluate the effects of WZB117 on the core-clock and to see if these effects are dependent on the time of treatment. Only SW480 and not SW620 cells were used for this experiment, as SW480 cells were previously defined as the more robust oscillators, allowing for a more reliable interpretation of the results.

In ctrl as well as in *Bmal1*-KD cells, WZB117 treatment induced changes in *Bmal1*-promoter activity until cells died after approximately 48 h (**Figure 46**). Interestingly, in SW480-ctrl cells, cells synchronised 24 h before treatment showed a different oscillatory profile when compared to the other synchronisation timepoints (**Figure 46 A**). In SW480-*shBmal1* cells however, cells synchronised 21 h before treatment showed a different oscillatory profile than cells synchronised 18 h and 24 h before treatment (**Figure 46 B**). These results indicate that WZB117 treatment has time-dependent effects on core-clock activity in SW480 cells.

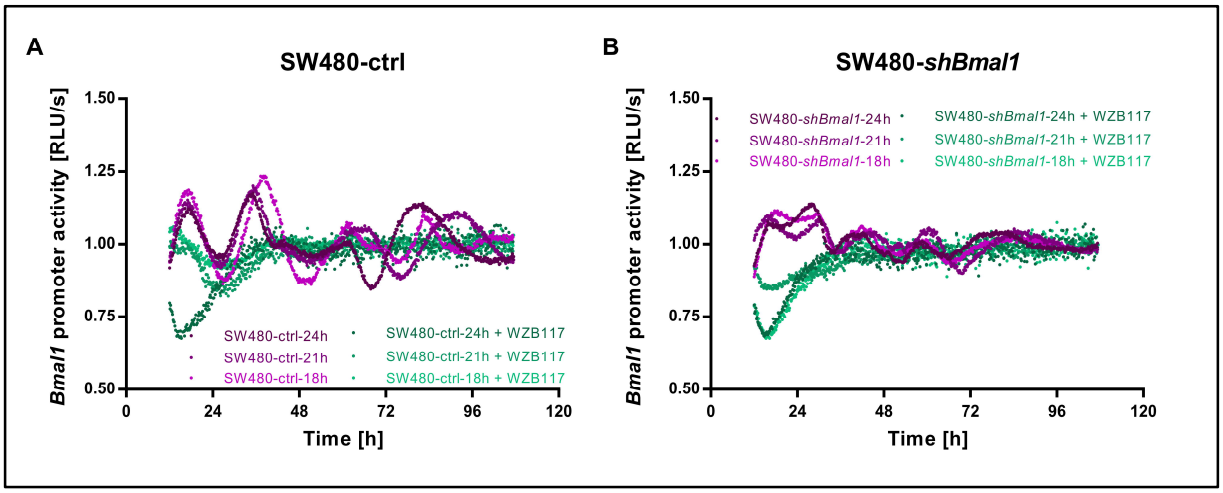

Figure 46: Bioluminescence measurements in SW480 cells after treatment with WZB117
SW480 cells were lentivirally transduced with an empty vector (ctrl) or with a *shBmal1*-construct. Additionally, cells were lentivirally transduced with a *Bmal1*-promoter driven luciferase construct. Cells were synchronised 18 h, 21 h or 24 h before treatment and then either untreated or treated with 80 µM WZB117. Bioluminescence was measured for five consecutive days. Shown is one representative replicate for each condition.

3.9.3 The energy phenotype is affected by WZB117 treatment

After having observed diverse effects after WZB117 treatment on gene expression and on the circadian phenotype, in a next step, the energy phenotype was evaluated in SW480 and SW620 cells after treatment with the glycolysis inhibitor WZB117.

The energy phenotypes in untreated cells have been described above (3.5.4). WZB117 treatment induced a shift from an energetic towards a more quiescent phenotype in ctrl as well as in *shBmal1* cells for both cell lines (**Figure 47**). However, untreated SW480-*shBmal1* cells exhibited a more energetic phenotype than SW480-ctrl cells and this difference was still present after WZB117 treatment (**Figure 47 A**). More precisely, the energy phenotype in SW480-*shBmal1* cells upon WZB117 treatment corresponded to the energy phenotype of untreated SW480-ctrl cells. Likewise, in SW620 cells, WZB117 treatment led to a shift from a more energetic to a more quiescent phenotype. In this case, untreated ctrl and *shBmal1* cells showed a very similar energy phenotype. Consequently, the shift upon WZB117 treatment regarding the energy phenotype was very similar in both conditions (**Figure 47 B**). Summarising, the energy phenotype after WZB117 treatment was dependent on the initial condition of the cells. Especially in highly energetic SW480-*shBmal1* cells, the resulting phenotype upon WZB117 treatment was still more energetic than in all other tested conditions.

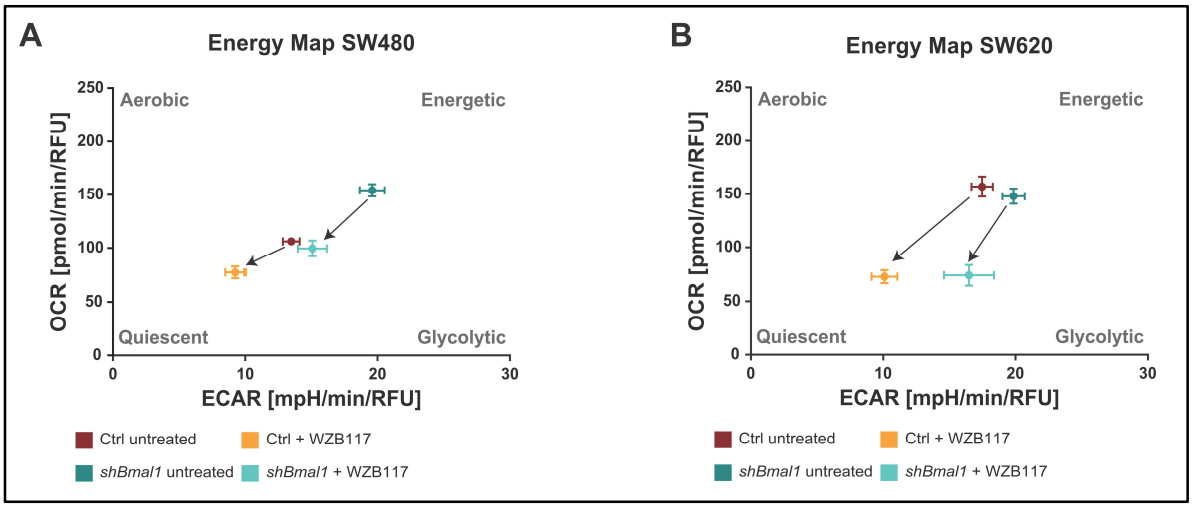

Figure 47: Energy map of SW480 and SW620 cells after WZB117 treatment
Energy map of SW480 (**A**) and SW620 (**B**) control and *shBmal1* cells untreated or after treatment with WZB117. The mean of three treatment timepoints after synchronisation is shown (18 h, 21 h, 24 h). Mean ± SEM, n = 16. Adapted from **Fuhr** *et al.*, 2018 [1].

3.9.4 A deregulated clock affects time-dependent treatment response

Following the evaluation of the energy phenotype, it was analysed if a deregulated clock influences the time-dependent effect of WZB117 treatment on metabolic activity in SW480 and SW620 cells. Therefore, ECAR and OCR were measured for 12 h in SW480 and SW620 ctrl and *shBmal1* cells either untreated or treated with WZB117.

The time-dependent metabolic activity of SW480 and SW620 ctrl cells was already described above and shown in **Figure 35**. WZB117 treatment induced changes in the distinct time-dependent ECAR profile in SW480 and SW620 cells (**Figure 48**). After a short increase in glycolytic activity, glycolysis rapidly decreased in ctrl as well as in *shBmal1* cells. The oxygen consumption rate also decreased after WZB117 treatment in all tested cells. Overall, the treatment with WZB117 affected the metabolic activity of SW480 and SW620 cells, but in the same direction for ctrl and *shBmal1* cells.

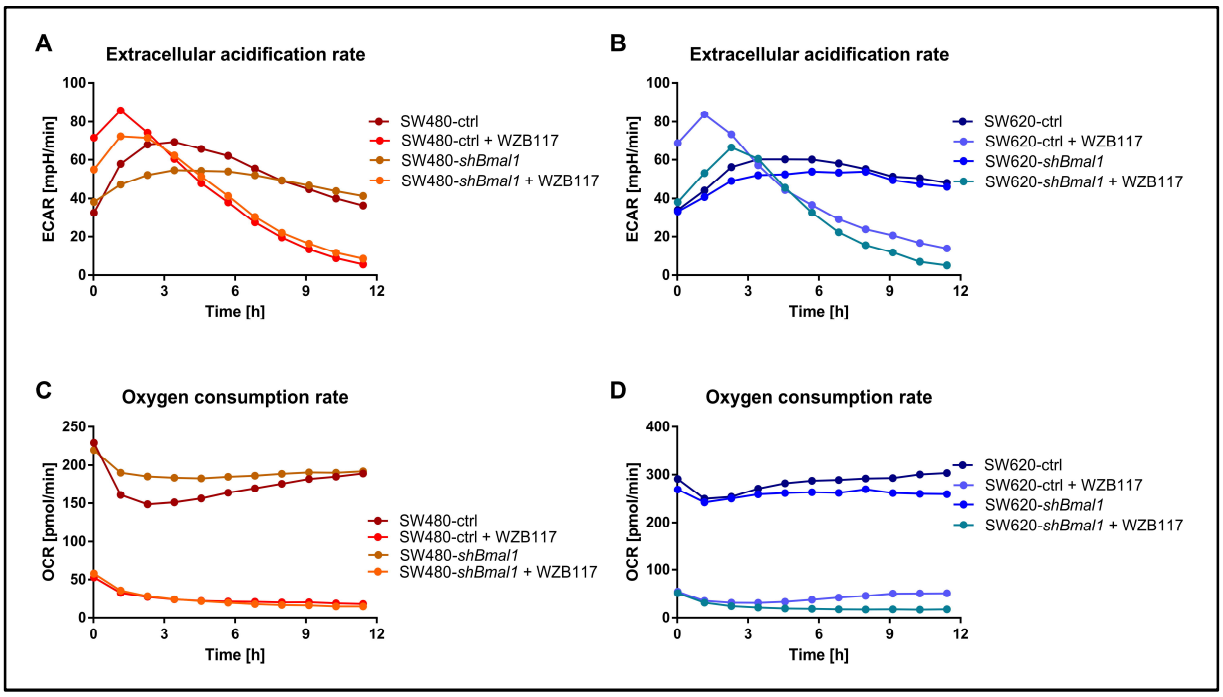

Figure 48: Time-dependent metabolic activity in SW480 and SW620 cells after WZB117 treatment
Extracellular acidification rate (**A, B**) and oxygen consumption rate (**C, D**) of SW480 and SW620 control and *shBmal1* cells untreated or after treatment with WZB117 measured using a seahorse machine for 12h. Mean ± SEM, n = 8.

As described above, the time-dependent pattern of glycolytic activity changed upon *Bmal1*-KD, especially in SW480 cells. To investigate the dependence of the time of treatment on subsequent

effects on metabolism in greater detail, ctrl, *shBmal1* and *shHkdc1* cells were synchronised 18 h, 21 h and 24 h before treatment. After treatment with WZB117, glycolytic and mitochondrial activity of the cells were determined.

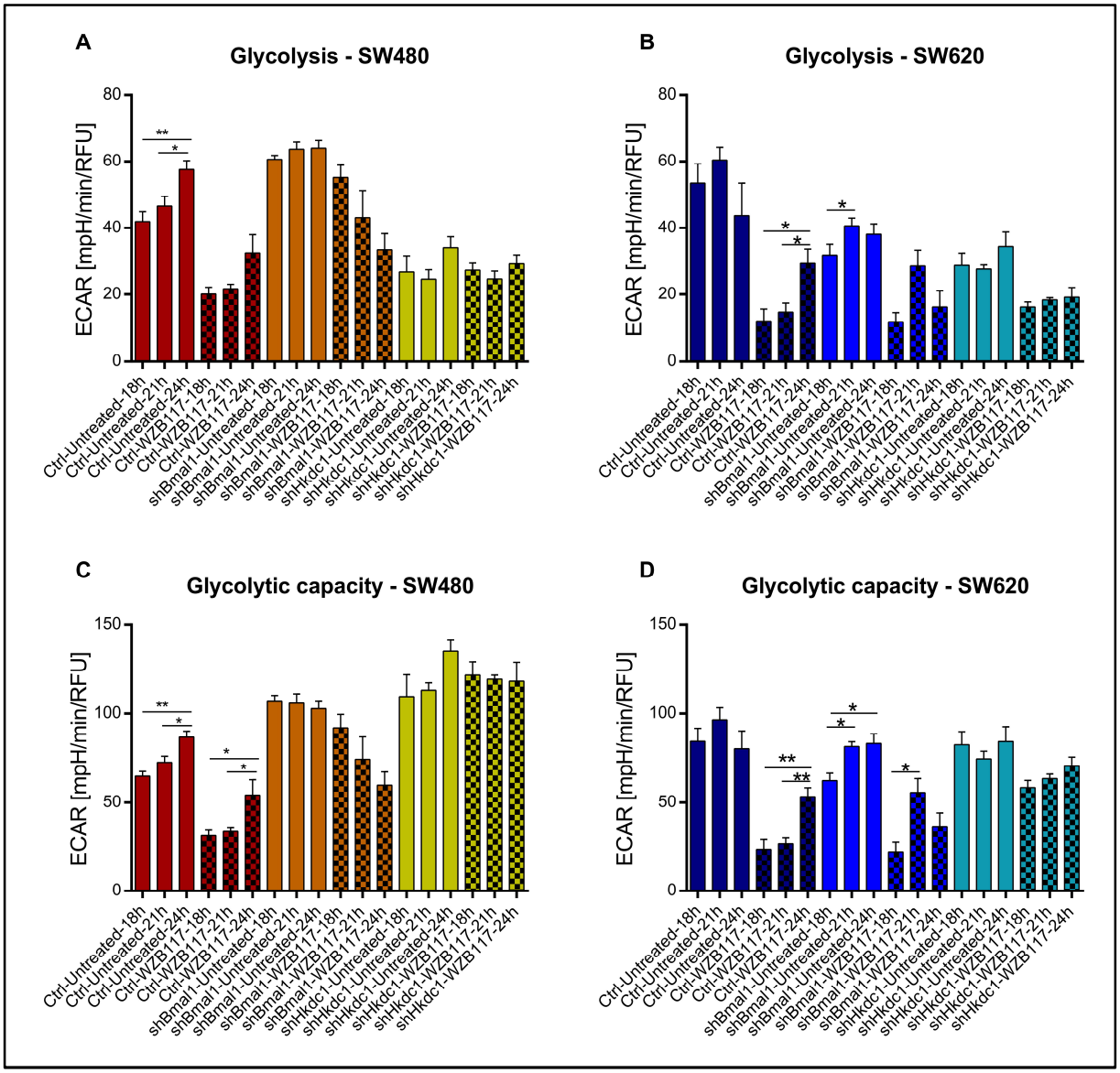

Figure 49: Glycolysis and glycolytic activity in SW480 and SW620 cells after WZB117 treatment
Glycolysis (**A, B**) and glycolytic activity (**C, D**) of SW480 and SW620 control, *shBmal1* and *shHkdc1* cells at three different timepoints after synchronisation. Cells were either untreated or treated with WZB117. Mean ± SEM, n = 5. Significant changes ($p < 0.05$) between different timepoints of the same condition are marked with *. * = $p < 0.05$, ** = $p < 0.01$. Adapted from **Fuhr** *et al*., 2018 [1].

Figure 49 shows glycolysis and glycolytic capacity in SW480 and SW620 ctrl, *shBmal1* and *shHkdc1* cells. Cells were either untreated or treated with WZB117. Untreated conditions were already described in chapter 3.7.1. Treatment with the GLUT1 inhibitor WZB117 led to the inhibition of glycolysis in SW480-ctrl, as well as in SW480-*shBmal1* cells, but with differential

time-dependent effects (**Figure 49 A** and **C**). In SW480-ctrl cells, WZB117 treatment induced a significant inhibition of glycolysis, as well as of glycolytic capacity independently of the treatment timepoint. In contrast to that, upon *Bmal1*-KD, glycolysis was only inhibited when cells were either synchronised 24 h or 21 h before treatment and glycolytic capacity was only found to be significantly lower for cells synchronised 24 h before treatment. Interestingly, when all synchronisation timepoints were taken together, the inhibiting effect of WZB117 treatment on glycolysis was stronger in SW480 and SW620 ctrl cells as compared to *shBmal1* cells. WZB117 treatment did neither lead to lower glycolysis, nor to lower glycolytic capacity in SW480-*shHkdc1* cells, independent from the time of treatment. In SW620 cells, the glycolysis rate was lower when treated at timepoint 21 h or 18 h after synchronisation, whereas glycolytic capacity was downregulated for all treatment timepoints (**Figure 49 B** and **D**). Comparable results were obtained after *Bmal1*-KD. In contrast to the observation in SW480 cells, WZB117 treatment led to a slight inhibition of glycolysis and glycolytic capacity in SW620-*shHkdc1* cells. These results led to the hypothesis that not only glycolysis itself is time-dependent but also the effect of glycolysis-targeting treatment.

The mitochondrial activity represented by basal respiration, maximum respiration and ATP production, was not affected upon WZB117 treatment in SW480-ctrl cells but in SW480-*shBmal1* cells, independent from the time of treatment (**Figure 50 A**, **C**, **E**). For *shHkdc1* cells, while basal respiration and ATP production were not affected, maximum respiration was inhibited independent from the time of treatment. This might result from a weaker input into the glycolytic pathway that subsequently impacts on the mitochondrial respiration pathway, leading to an overall inhibition of maximum respiration. WZB117 treatment in SW620 cells led to differing results when compared to the untreated scenario as compared to SW480 cells (**Figure 50 B**, **D**, **F**). In SW620 cells basal respiration, maximum respiration and ATP production were inhibited in ctrl cells after WZB117 treatment, independent from the treatment time. The results for *shBmal1* and *shHkdc1* cells, however, were the same in both cell lines. While basal respiration, ATP production and maximum respiration were affected in *shBmal1* cells, only maximum respiration was inhibited in *shHkdc1* cells. Interestingly, while the effect of WZB117 treatment on glycolysis was stronger in ctrl cells, mitochondrial respiration was affected to a higher extend in *shBmal1* cells.

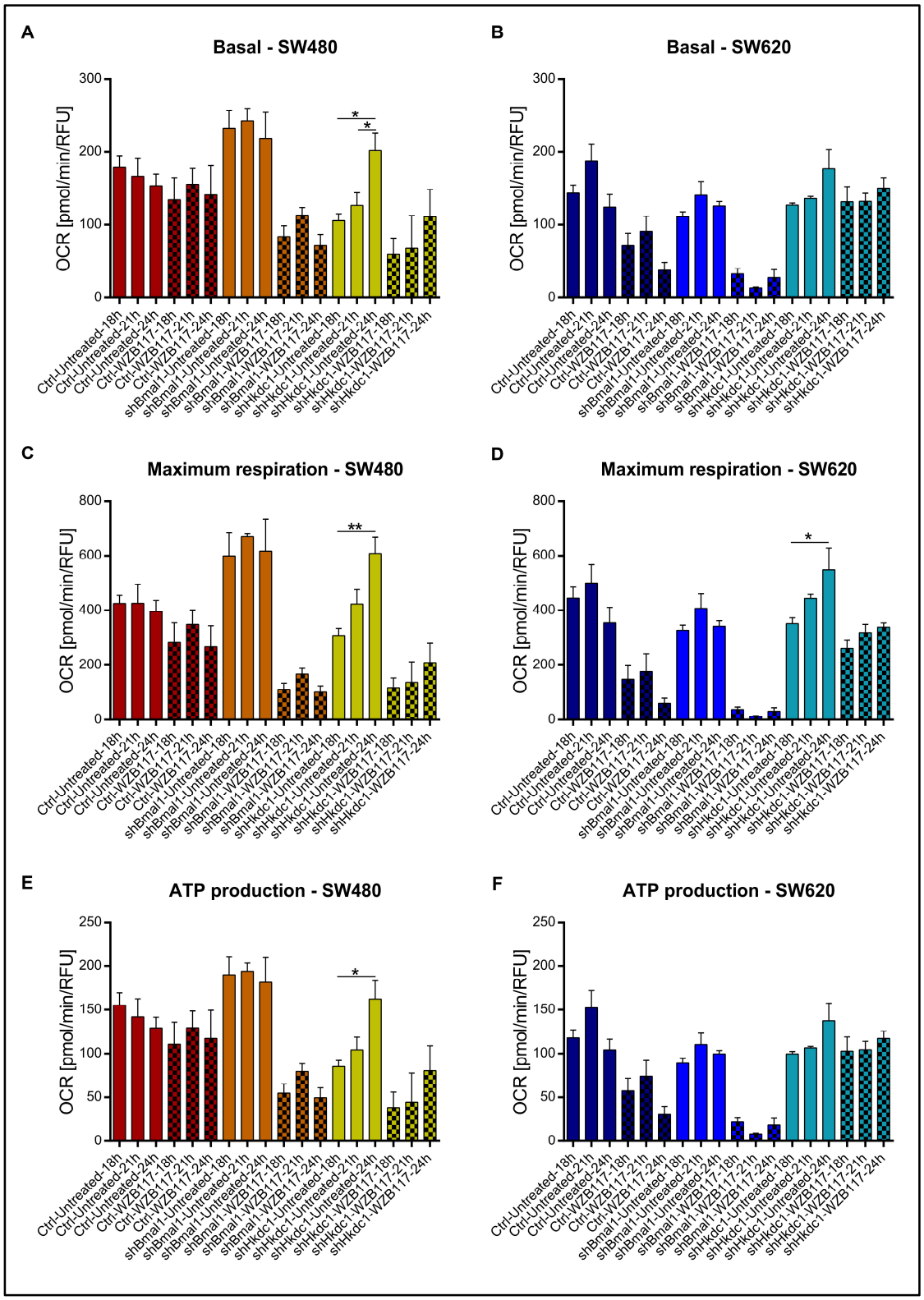

Figure 50: Basal respiration, maximum respiration and ATP production in SW480 and SW620 cells after WZB117 treatment

Basal respiration (**A, B**), maximum respiration (**C, D**) and ATP production (**E. F**) of SW480 and SW620 control, *shBmal1* and *shHkdc1* cells at different timepoints after synchronisation. Cells were either untreated or treated with WZB117. Mean ± SEM, n = 5. Significant changes ($p < 0.05$) between different timepoints of the same condition are marked with *. * = $p < 0.05$, ** = $p < 0.01$. Adapted from **Fuhr** *et al.*, 2018 [1].

Although the selection of a temporal window of six hours is too short to draw conclusions concerning detailed chronopharmacology profiles, the results show that the efficiency of WZB117 treatment on metabolic activity appears to change depending on the time of treatment. Furthermore, a deregulated clock, as represented by *shBmal1* cells influences response to treatment.

3.9.5 Effect of oxaliplatin treatment on metabolic activity

The observed effect of WZB117 treatment on metabolic activity in ctrl, *shBmal1* and *shHkdc1* cells was further compared to the effect after treatment with the classical chemotherapeutic oxaliplatin, a platinum complex that is used effectively for CRC treatment and exerts its cytotoxic effect mostly through DNA damage [94].

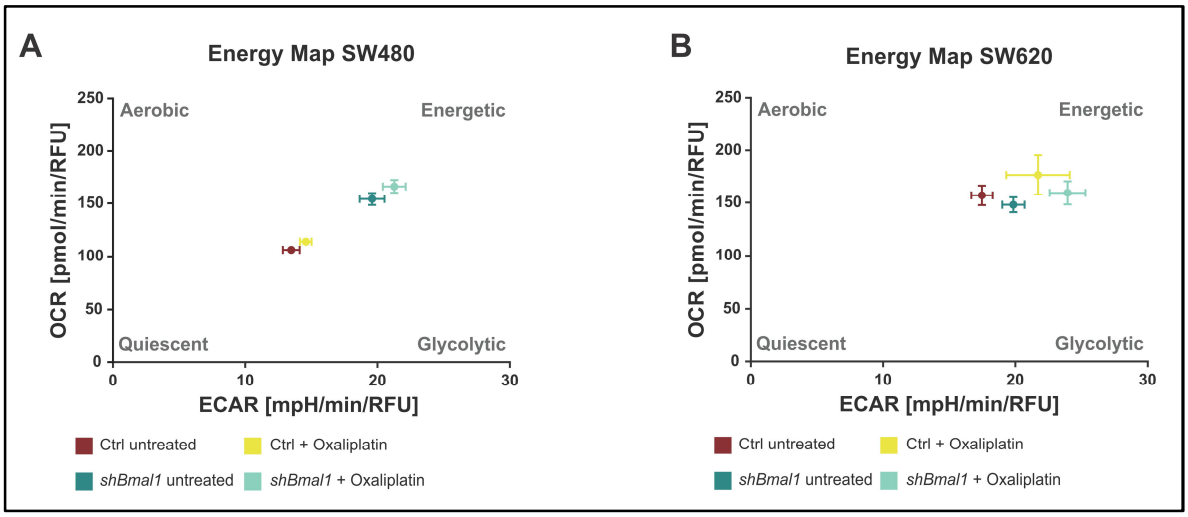

Figure 51: Energy map of SW480 and SW620 cells after oxaliplatin treatment
Energy map of SW480 (**A**) and SW620 (**B**) control and *shBmal1* cells untreated or after treatment with oxaliplatin. The mean of three treatment timepoints after synchronisation is shown (18 h, 21 h, 24 h). Mean ± SEM, n = 16.

The results gained from WZB117 and oxaliplatin treatment were used to evaluate whether the metabolic effects of WZB117 treatment are due to the treatment with a GLUT1 inhibitor itself or whether these effects on metabolism can be generally observed after anticancer treatment even when applying a drug with a different mechanism of action. Regarding the energy phenotype, oxaliplatin treatment did not induce any changes in SW480 and SW620 ctrl or *shBmal1* cells (**Figure 51**).

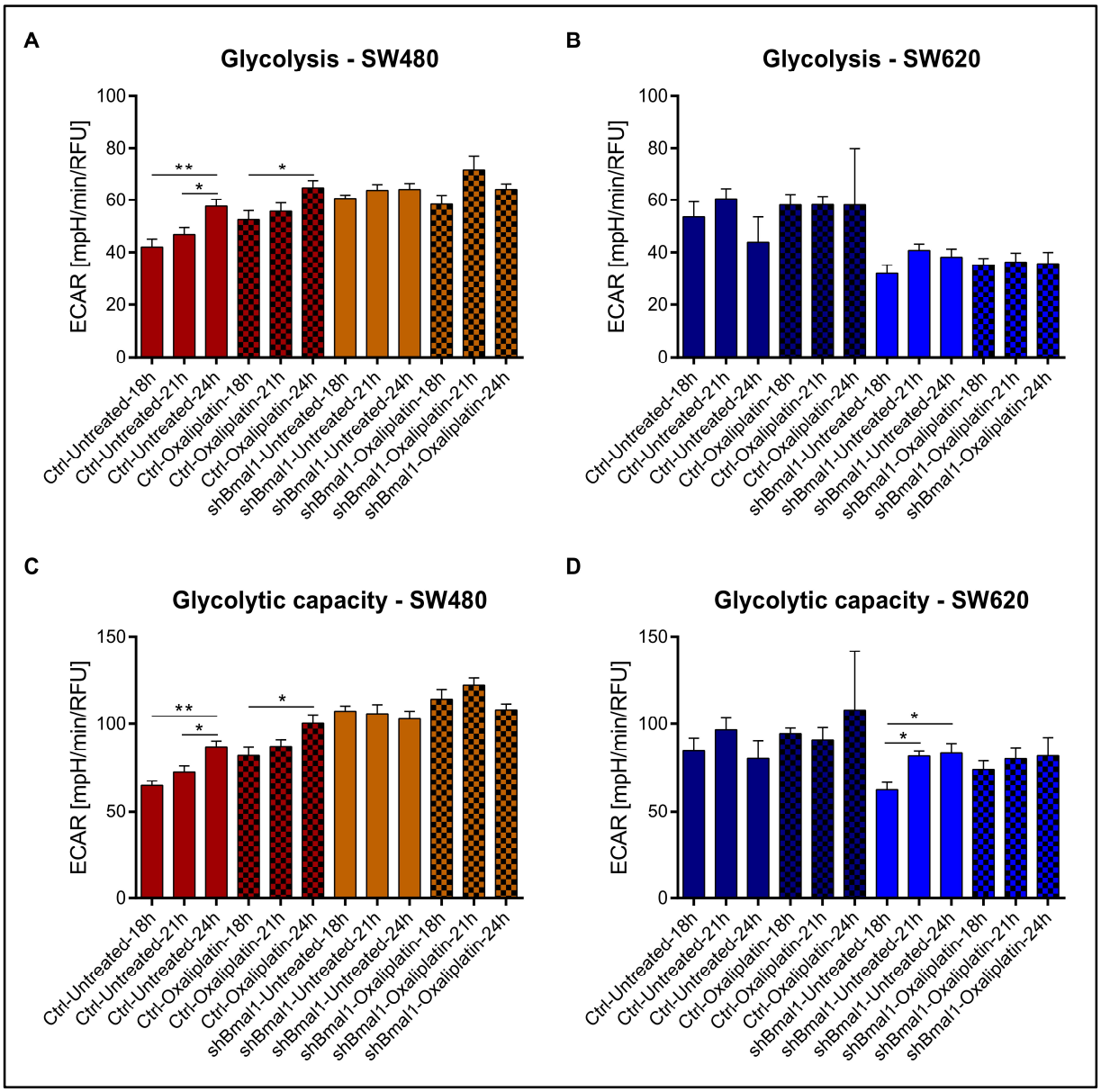

Figure 52: Glycolytic activity of SW480 and SW620 control and *shBmal1* cells after oxaliplatin treatment
Glycolysis of SW480 (**A**) and SW620 (**B**) control and *shBmal1* cells at three different timepoints after synchronisation (18 h, 21 h, 24 h). Cells were either untreated or treated with oxaliplatin. Mean ± SEM, n = 5. Glycolytic capacity of SW480 (**C**) and SW620 (**D**) control and *shBmal1* cells at different timepoints. Cells were either untreated or treated with oxaliplatin. Mean ± SEM, n = 5. Significant changes ($p < 0.05$) between different timepoints of the same condition are marked with *. * = $p < 0.05$, ** = $p < 0.01$. Adapted from **Fuhr** *et al.*, 2018 [1].

Regarding the glycolytic activity, oxaliplatin treatment did not induce changes in SW480 or SW620 cells, neither in ctrl nor in *shBmal1* cells (**Figure 52**). Although oxaliplatin treatment did induce slight changes in time-dependent mitochondrial activity especially in SW480-*shBmal1* cells, overall, no significant effects could be observed after oxaliplatin treatment (**Figure 53**).

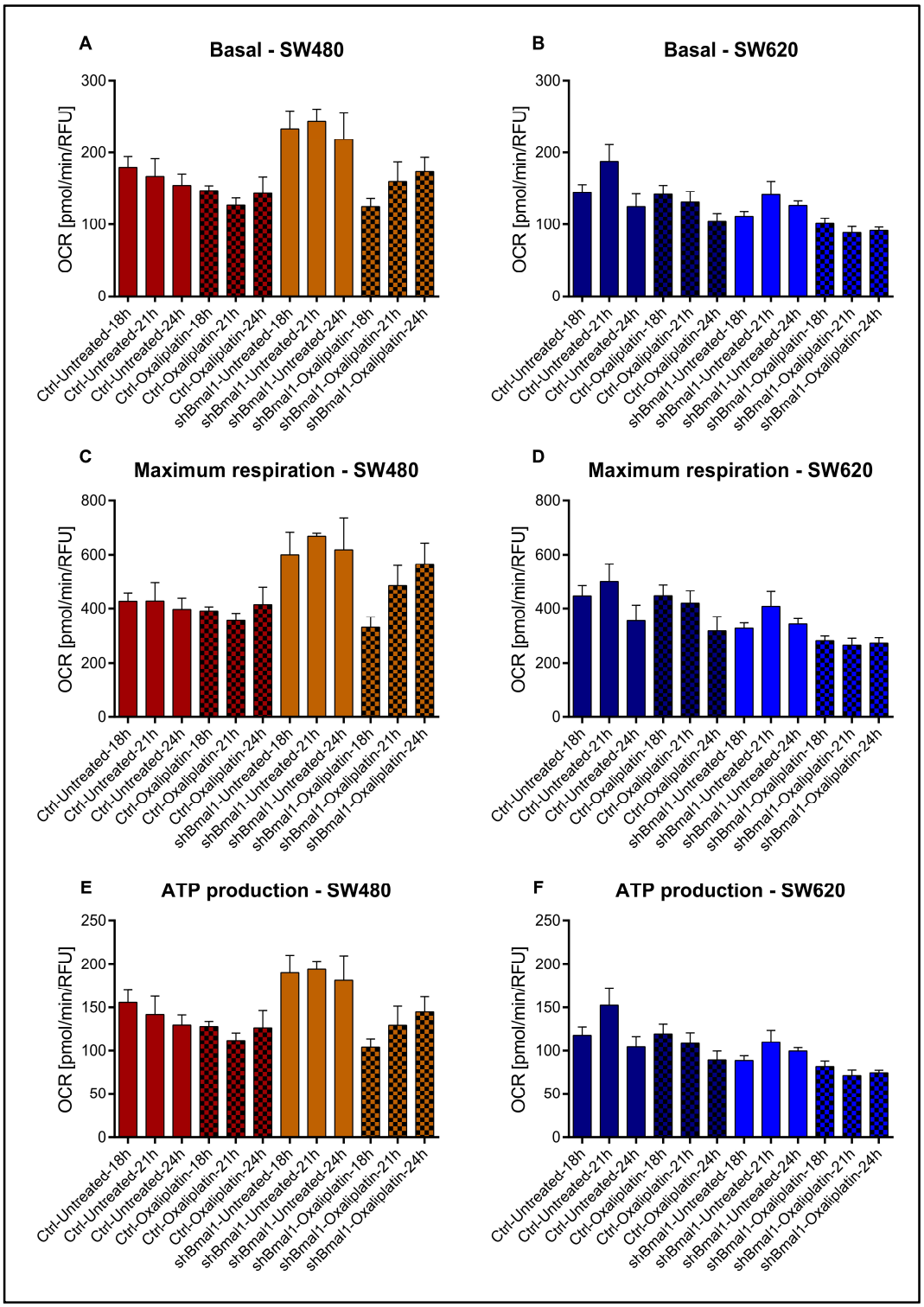

Figure 53: Basal respiration, maximum respiration and ATP production in SW480 and SW620 cells after oxaliplatin treatment
Basal respiration of SW480 (**A**) and SW620 (**B**) control and *shBmal1* cells at different timepoints (18 h, 21 h, 24 h). Cells were either untreated or treated with oxaliplatin. Mean ± SEM, n = 5. Maximum respiration of SW480 (**C**) and SW620 (**D**) control and *shBmal1* cells at three different timepoints. Cells were either untreated or treated with oxaliplatin. Mean ± SEM, n = 5. ATP production of SW480 (**E**) and SW620 (**F**) control and *shBmal1* cells at three different timepoints. Cells were either untreated or treated with oxaliplatin. Mean ± SEM, n = 5. Adapted from **Fuhr** *et al.*, 2018 [1].

In summary, oxaliplatin treatment did not induce significant metabolic changes in SW480 and SW620 cells. Hence, the metabolic alterations observed after WZB117 treatment seem to be specific to anticancer treatment aiming at the tumour`s metabolism.

3.9.6 Effect of WZB117 treatment on viability, cytotoxicity and apoptosis

Besides the effect of WZB117 treatment on metabolic activity, in a next step, its consequences on cell viability, cytotoxicity and apoptosis were evaluated in SW480 and SW620 ctrl, *shBmal1* and *shHkdc1* cells. For this purpose, WT and *shBmal1* as well as *shHkdc1* cells were synchronised at three different timepoints and treated with the glycolysis inhibitor WZB117 and as a comparison with the classical chemotherapeutic oxaliplatin.

Figure 54 shows cell viability, cytotoxicity and apoptosis in ctrl and *shBmal1* cells after treatment with either WZB117 or oxaliplatin. Viability and cytotoxicity were not affected by WZB117 treatment in SW480-ctrl and -*shBmal1* cells, as they still showed the same synchronisation time-dependent pattern as without treatment. Interestingly, after WZB117 treatment, a lower apoptosis rate was observed in SW480-ctrl as well as in -*shBmal1* cells. In SW620 cells, this effect was not present. Furthermore, oxaliplatin treatment did not affect viability, cytotoxicity or apoptosis. This might be due to the used treatment concentration or treatment duration that was adjusted for WZB117 treatment. Cytotoxicity, viability and apoptosis were also evaluated in *shHkdc1* cells after treatment with WZB117 or oxaliplatin but in both cases, no significant changes upon treatment were observed (**Figure S 8**).

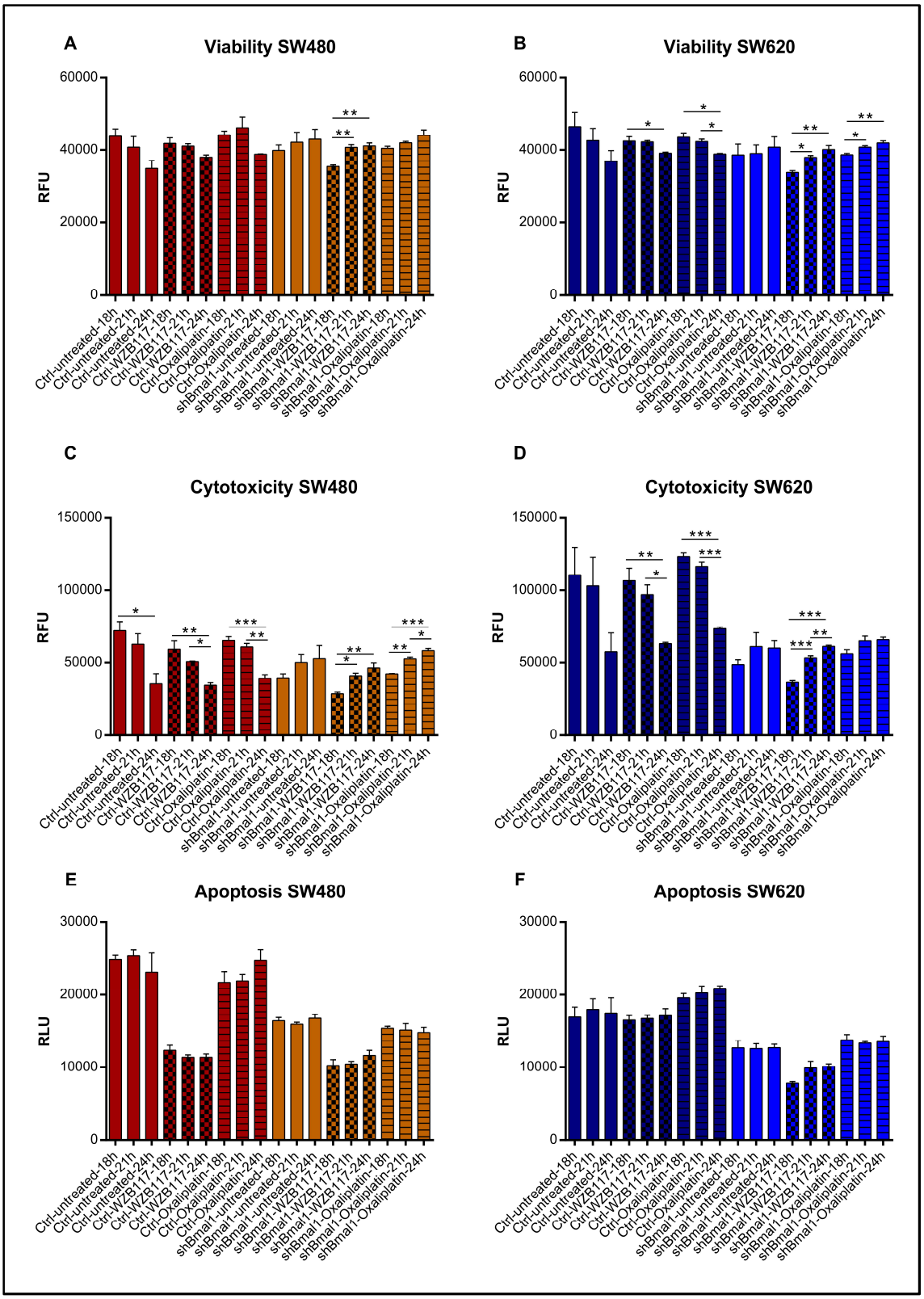

Figure 54: Viability, cytotoxicity and apoptosis in SW480 and SW620 cells after treatment
Viability (**A**, **B**), cytotoxicity (**C**, **D**) and apoptosis (**E**, **F**) in SW480 and SW620 control and *shBmal1* cells synchronised at different timepoints. Cells were either untreated or treated with WZB117 or oxaliplatin. Mean ± SEM, n = 3. Significant changes ($p < 0.05$) between different synchronisation timepoints of the same condition are marked with *. * = $p < 0.05$, ** = $p < 0.01$, *** = $p < 0.001$. Adapted from **Fuhr** *et al.*, 2018 [1].

3.10 Cell-to-cell communication impacts on the circadian phenotype

Apart from the use of human fallopian tube organoids, all experiments so far were carried out in a cell model containing only a single cell type. However, a tumour does not consist of homogenous cancer cells only but rather of a complex tissue that is composed of different cell types mainly derived from the neighbouring stroma, thus making up the tumour microenvironment. Interactions between these different cell types have positive as well as negative effects on tumourigenesis [143]. In normal colonic mucosa, the stromal population mainly consists of fibroblasts [144]. Through different pathways fibroblasts may differentiate into cancer-associated fibroblasts which are then the main cellular component of tumour stroma. [145]. CAFs secrete growth factors and support tumour growth and migration [134]. Because of the nowadays known importance of the tumour microenvironment and its constituents, especially CAFs, they might be used as diagnostic and prognostic biomarkers and should be considered as potential targets for anticancer therapy.

It is still unclear how the individual molecular clocks of different cell types influence each other, especially in a cell culture model system. To further evaluate this question, different human cell types were used for co-culture experiments and the effect on the clock phenotype was evaluated via bioluminescence measurements. In a first attempt, the colorectal cancer cell line HCT116 and the human intestinal fibroblast cell line HIF were used as a co-culture model. The clock phenotype was measured in cells without co-culture and in co-cultured cells, but with only one cell type being transduced and measured. In a second attempt, HCT116 cells were co-cultured with CAFs or NFs. In this case, all cells were measured individually and in co-culture, where the clock phenotype of HCT116 cells was determined and it was evaluated if co-culture with stromal cells changes the oscillation profile.

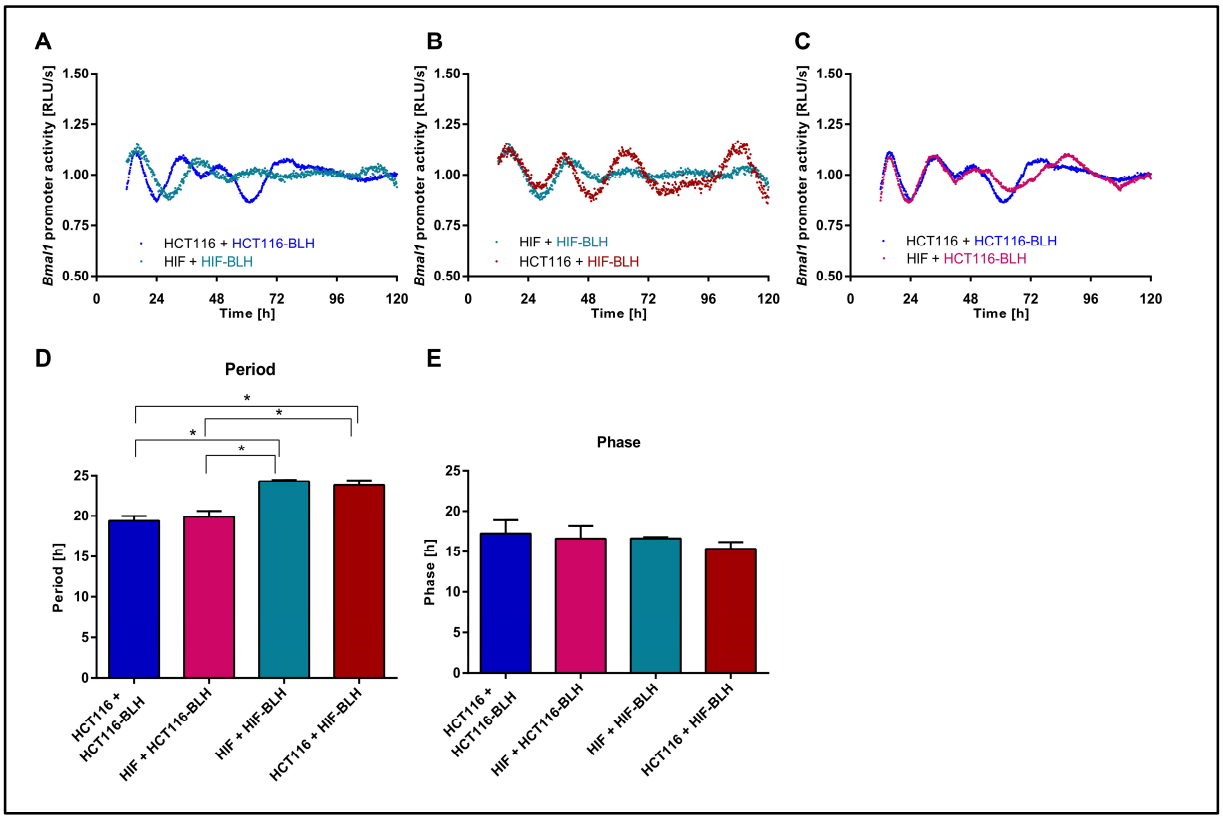

Figure 55: Effect of co-culture on circadian rhythms in HCT116 and HIF cells
Cells were lentivirally transduced and the *Bmal1*-promoter activity was measured over five consecutive days. Cells were either co-cultured with the same cell line (**A**) or with a different cell line (**B** and **C**). Shown is one representative replicate per condition. The sample written in coloured letters was the one that was measured. Period (**D**) und phase (**E**) were calculated in samples with and without co-culture. Data are expressed as mean ± SEM, n = 3. Significant changes ($p < 0.05$) between different conditions are marked with *. Unpublished data, paper in preparation.

Under control conditions, HCT116 and HIF cells showed significantly different periods ($p < 0.05$) (**Figure 55 A** and **D**). Although co-culture of both cell lines did not lead to significant changes in period length or phase, the oscillatory patterns changed in HIF cells upon co-culture with HCT116 cells. In particular, the oscillations were more robust when cells were measured in co-culture (**Figure 55 B**). This influence could not be observed the other way around, when HCT116 cells were measured in co-culture with HIF cells (**Figure 55 C**).

In a next step, HCT116 cells were co-cultured with NFs or CAFs from two patients and the effect on the circadian phenotype was evaluated. The results for patient 7 and patient 10 are displayed in **Figure 56** and **Figure 57**, respectively.

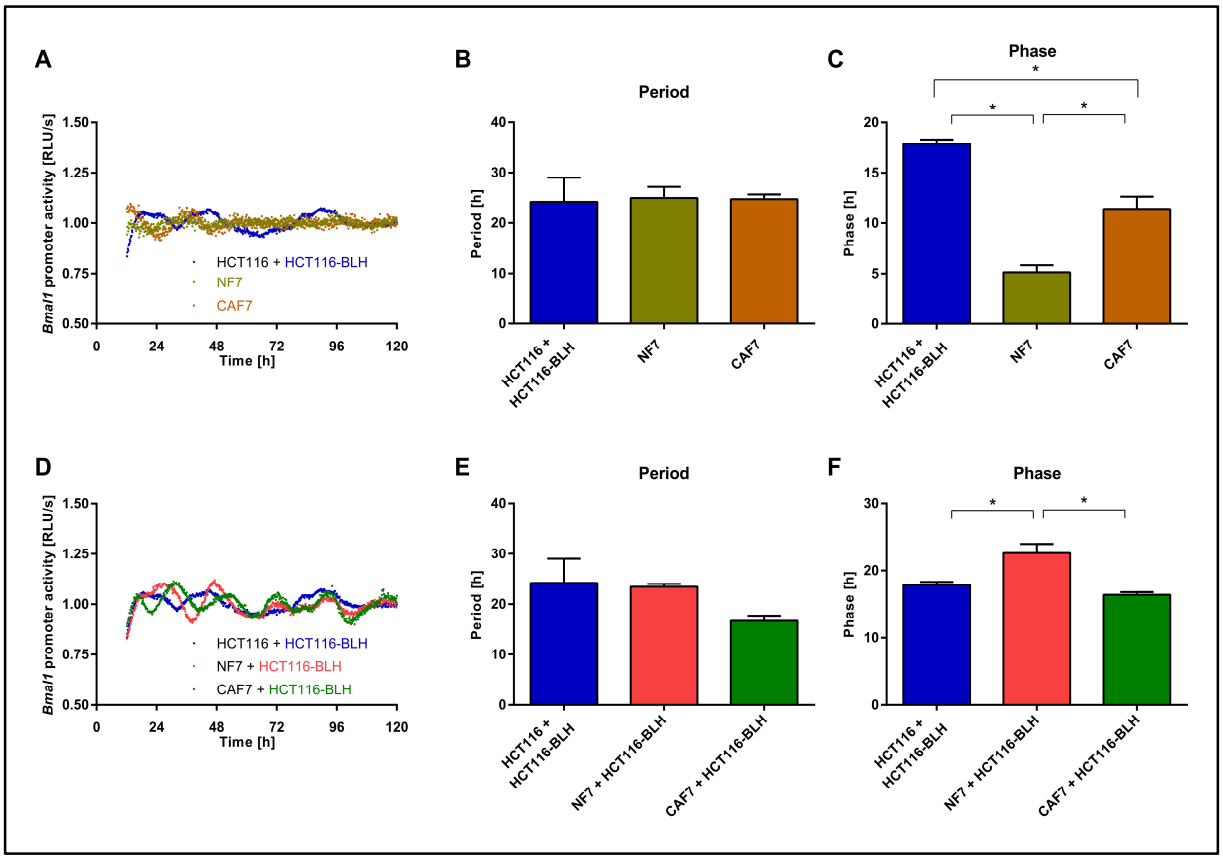

Figure 56: Effect of cell-to-cell communication on circadian rhythms
(**A**) HCT116, NF7 and CAF7 cells were lentivirally transduced and the *Bmal1*-promoter activity was measured over five consecutive days. Shown is one representative replicate per condition. Period (**B**) und phase (**C**) were calculated. Data are expressed as mean ± SEM, n = 3. Significant changes ($p < 0.05$) between different cells are marked with *. (**D**) HCT116, NF7 and CAF7 cells were lentivirally transduced and the *Bmal1*-promoter activity was measured over five consecutive days. HCT116 cells were either co-cultured with themselves or with NFs or CAFs. Shown is one representative replicate per condition. The sample written in coloured letters was the one that was measured. Period (**E**) und phase (**F**) were calculated. Data are expressed as mean ± SEM, n = 3. Significant changes ($p < 0.05$) between different conditions are marked with *. Unpublished data, paper in preparation.

The oscillatory profile and the circadian parameters period and phase were first determined without co-culture in all tested cells. While NFs and CAFs from patient 7 did not have a different period as compared to HCT116 cells (**Figure 56 A** and **B**), the period of NFs and CAFs from patient 10 was significantly longer. (**Figure 57 A** and **B**). The phase was significantly different in NFs and CAFs from both patients as compared to HCT116 cells. When HCT116 were co-cultured with primary NFs and CAFs, a phase shift was observed as compared to the normal HCT116 oscillatory profile without co-culture. For patient 10 this effect was present for NFs and CAFs (**Figure 57 D** and **F**), whereas in patient 7 this effect was only present when HCT116 cells were co-cultured with CAFs (**Figure 56 D** and **F**). Co-culture with primary fibroblasts also had effects on the period in HCT116 cells, especially with cells from patient 10,

where co-culture led to a significantly longer period in HCT116 cells (**Figure 57 E**). Interestingly, the longer period was very similar to the period observed for NFs and CAFs.

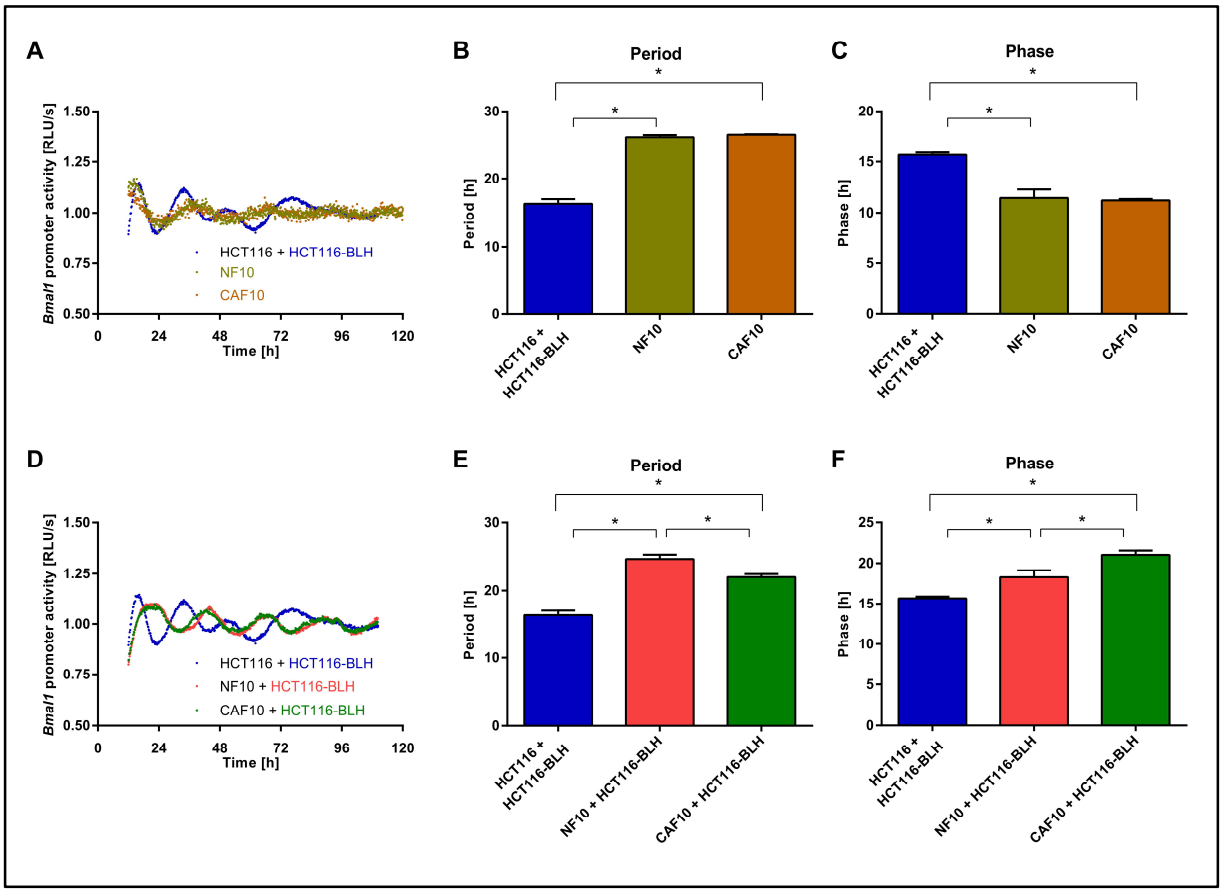

Figure 57: Cell-to-cell communication impacts on the circadian phenotype
(**A**) HCT116, NF10 and CAF10 cells were lentivirally transduced and the *Bmal1*-promoter activity was measured over five consecutive days. Shown is one representative replicate per condition. Period (**B**) und phase (**C**) were calculated. Data are expressed as mean ± SEM, n = 3. Significant changes ($p < 0.05$) between different cells are marked with *. (**D**) HCT116, NF10 and CAF10 cells were lentivirally transduced and the *Bmal1*-promoter activity was measured over five consecutive days. HCT116 cells were either co-cultured with themselves or with NFs or CAFs. Shown is one representative replicate per condition. The sample written in coloured letters was the one that was measured. Period (**E**) und phase (**F**) were calculated. Data are expressed as mean ± SEM, n = 3. Significant changes ($p < 0.05$) between different conditions are marked with *. Unpublished data, paper in preparation.

As co-culture with primary fibroblasts induced changes in the circadian phenotype of HCT116 cells, in a next step it was tested whether co-culture also influences metabolic activity as well as cell viability, cytotoxicity and apoptosis.

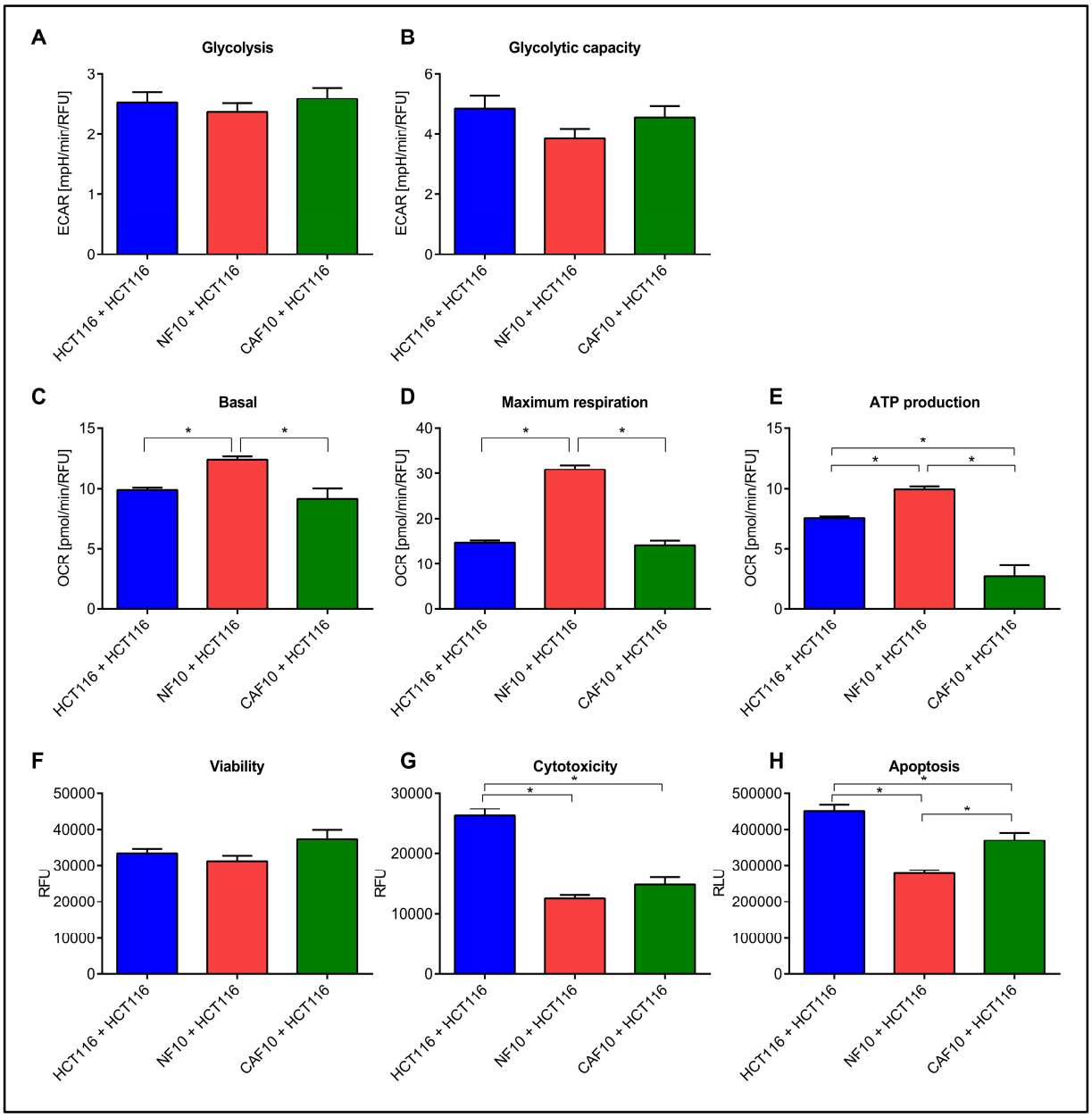

Figure 58: Cell-to-cell communication impacts on cell metabolism
(A) Glycolysis and (**B**) glycolytic capacity in HCT116 cells cultivated alone or after co-culture with NFs or CAFs. Only HCT116 cells were measured. Data are represented as mean ± SEM (n = 8). **(C)** Basal respiration, **(D)** maximum respiration and **(E)** ATP production in HCT116 cells cultivated alone or after co-culture with NF or CAF. Only HCT116 cells were measured. Data are represented as mean ± SEM (n = 8). (**F**) Viability, (**G**) cytotoxicity and (**H**) apoptosis in HCT116 cells cultivated alone or after co-culture wit NF or CAF. Only HCT116 cells were measured. Data are represented as mean ± SEM (n = 5). Statistically significant values ($p < 0.05$) are indicated with *. Unpublished data, paper in preparation.

Co-culture with NFs or CAFs did not induce changes regarding the glycolytic activity (**Figure 58 A** and **B**) in HCT116 cells, whereas the mitochondrial activity was altered. Basal respiration, maximum respiration and ATP production were significantly increased after co-culture with NFs in HCT116 cells (**Figure 58 C - E**). On the other hand, co-culture with CAFs

tendentially decreased the mitochondrial activity. While cell viability was not changed after co-culture, cytotoxicity and apoptosis were both significantly decreased in HCT116 cells when co-cultured with NFs or CAFs (**Figure 58 F and H**). Taken together the results gained from co-culture experiments showed that cell-to-cell communication of primary fibroblasts and HCT116 cells influences the circadian phenotype, changes mitochondrial respiration and prevents cells from apoptosis and decreases cell cytotoxicity.

4. Discussion

4.1 SW480 and SW620 cells - a model for circadian studies in tumour progression

Cancer cell lines show a wide diversity of circadian phenotypes, varying from robust 24 h oscillations of core-clock gene expression to a complete loss of oscillations in circadian gene expression [10]. These alterations in circadian clock function have impact on cell metabolism and proliferation that ultimately lead to different cancer phenotypes [37]. In the present project, the consequences of a deregulated clock on cancer progression were studied with a focus on the effects of clock disruption on cancer metabolism and the resulting effects on drug response in cancer cells. The diversity of clock phenotypes in cancer cell lines was confirmed in selected colorectal cancer cell lines. These cells displayed a range of oscillatory profiles, from robust to very weak oscillations and with different periods to no detectable oscillations in *Bmal1*-promoter activity at all. However, no correlation could be made between tumour stage and clock phenotype, indicating that deregulations of the core-clock in cancer cells are specific for a given cell line and might be associated to other factors such as the genetic and epigenetic signature of a cell as well as present mutations.

To study the consequences of a deregulated clock on tumour progression and tumour metabolism in greater detail, SW480 and SW620 cells were used as a cellular model for colorectal cancer progression in which the consequences of clock gene disruption were tested in a time-dependent manner. Both cell lines are derived from the same patient with SW480 cells originating from a primary tumour and SW620 cells from a lymph node metastasis. The chosen cell model is a commonly used model to study and compare the behaviour of primary and metastatic tumours [146], [147]. However, other causes for different phenotypes of both cell lines must be considered, apart from their primary and metastatic origin. For example, do these cell lines also represent two clones from the same cancer with different features, not necessarily pointing toward metastatic versus non-metastatic behaviour. Therefore, a thorough comparison between both cell lines using different experimental methods was carried out to confirm the usability of this pair of cells as a model for cancer progression. Bioluminescence measurements confirmed different clock phenotypes for both cell lines. SW480 cells showed robust

oscillations with a period of around 24 h while SW620 showed rather weak oscillations in the promoter activity of the core-clock genes *Bmal1* and *Per2*. The same tendency was observed in time course qPCR data of the same genes and other core-clock genes. In line with these observations, a recently published study identified a large number of differentially expressed clock genes among different tumour stages, supporting the hypothesised involvement of clock genes in tumour progression [106]. To exclude the possibility that variations in clock phenotypes only occur due to different capability to synchronise both cell lines, single-cell time course microscopy of the core-clock protein REV-ERBα was performed. Higher time-dependent expression changes in SW480 cells on the single cell level led to the assumption that different clock phenotypes between SW480 and SW620 cells are indeed based on differences in the molecular clock. Based on these results, SW480 and SW620 cells seem to be a suitable model for circadian research in tumour progression.

4.2 A deregulated clock induces alterations on the transcriptome level

To study the consequences of a disrupted clock on the transcriptome level, a 24 h time course microarray analysis was performed for both SW480 and SW620 cells. This study represents the first set of time course microarray data for both cell lines and might help to understand how a deregulated core-clock contributes to tumour progression and metastasis. The time course microarray study of SW480 and SW620 cells confirmed different time-dependent expression patterns of core-clock genes and revealed global gene expression changes between both cell lines. An analysis of differentially expressed genes revealed diverse cancer-associated pathways to be over-represented. Hence, it is very likely that differences between both cell lines occur due to their different cancer progression stages and possibly also due to a deregulated clock associated with different tumour stages. A global phase-shift of oscillating genes was observed between both cell lines and although the total number of 24 h oscillating genes was very similar, the intersect of genes that oscillate in both cell lines was rather small. This finding led to the assumption that a deregulated clock induces a switch in the genetic landscape of circadian-controlled genes, representing the progression from primary tumour to metastatic cells. These results are in line with recently analysed time course transcriptome data of the breast cancer cell line MCF7 and the non-tumourigenic epithelial cell line MCF10A [106]. The oscillation patterns of several clock genes were disrupted in the cancer cell line, supporting the

conclusion made in this thesis that core-clock alterations are a characteristic feature of cancer development and progression. Furthermore, the authors also observed a shift in circadian gene expression, in line with the results gained in this project, further supporting the hypothesis that disrupted and reprogrammed circadian rhythms contribute to cancer development. Gene expression changes on the transcriptome level induced by a deregulated core-clock and a global phase-shift in the expression of circadian-regulated genes might represent an important step in tumour progression from a primary tumour towards a metastatic cell line.

An over-representation analysis of all 24 h oscillating genes identified different metabolic pathways, including glycolysis, Warburg effect and mitochondrial respiration. While the pathway glycolysis was over-represented in the set of genes oscillating in both cell lines, metabolic pathways such as the TCA cycle and the Warburg effect were over-represented in the set of genes oscillating only in SW620 cells. Based on changes in the core-clock between both cell lines, these metabolic pathways showed different oscillation patterns. Thus, changes in the core-clock seem to induce a reprogramming of the circadian system in the metastatic cell line SW620 and appear to contribute to a shift in the metabolic gene expression profile between both cell lines which consequently leads to metabolic modifications during tumourigenesis and metastasis. The differential temporal expression between both cell lines led to the hypothesis that these pathways are differentially regulated by the circadian clock dependent on the tumour stage. A subsequent analysis of all metabolic genes from the over-represented pathways revealed differences in their temporal expression patterns between both cell lines. Based on these results, five putative clock-regulated metabolic candidate genes were identified. One of these genes was *Hkdc1* which encodes a recently identified member of the hexokinase family that plays a role in glucose metabolism [148]. Furthermore, several studies revealed a potential role for HKDC1 in tumourigenesis. A recent study points to HKDC1 as a potential therapeutic target for lung cancer [149] and a high expression of *Hkdc1* is associated with poor prognosis and aggressive phenotype in hepatocarcinoma [131]. Concomitant with these findings, metastatic SW620 cells showed higher *Hkdc1* expression compared to SW480 cells. However, the mechanisms by which HKDC1 influences cell proliferation and tumour progression are still unknown, especially in CRC.

The results gained from the analysis of SW480 and SW620 cell lines were compared with data from primary cells, including normal and cancer-associated human primary fibroblasts as well

as non-cancerous human fallopian tube organoids. The circadian phenotype of NFs and CAFs from three patients was evaluated. Although all tested NFs and CAFs exhibited robust oscillations with similar periods, especially the amplitudes varied between the tested patients. A time course analysis of *Hkdc1* and *Bmal1* in normal human fallopian tube organoids revealed a gene expression profile which rather resembled the profile observed in the primary tumour cell line SW480, indicating that SW480 cells are more similar to normal tissue than to their metastatic counterpart SW620.

4.3 A deregulated clock induces metabolic phenotype rewiring

Following the identification of differential expressed metabolic pathways in both cell lines, the impact of a deregulated clock on metabolic activity and drug response was further analysed. To get better insights into the interplay between the core-clock and cancer metabolism, a knockdown of the core-clock gene *Bmal1* was carried out in SW480 and SW620 cells. A time course gene expression analysis of *Bmal1* and *Hkdc1* confirmed a connection between both genes, as *Bmal1*-KD did not only induce changes in the time-dependent expression of *Bmal1*, but also of *Hkdc1*. The postulated connection between the circadian clock and cancer metabolism could be further clarified after a gene expression analysis in *shBmal1* cells. In addition to its effects on other core-clock genes, *Bmal1*-KD induced alterations in metabolic gene expression. Interestingly, in both cell lines most metabolic genes were tendentially downregulated except for *Hkdc1* in SW480-*shBmal1* cells, further supporting the hypothesis of an interplay between *Bmal1* and *Hkdc1*. A study that compared normal and tumour cells revealed *Hk* and *Aldoc* as upregulated, and *Pdh* as downregulated in most tumours [150]. In the present study, the same tendency regarding *Hkdc1* and *Pdhb* was observed, leading to the assumption that these changes are important for both tumour onset and progression. However, this tendency could not be observed after *Bmal1*-KD in metastatic SW620 cells, indicating that the effect of a deregulated clock in cancer cells is dependent on the initial genetic condition of the cell. Interestingly, the gene expression profile of SW480-*shBmal1* and metastatic SW620-ctrl cells was very similar, supporting the hypothesis that *Bmal1*-KD induces a metastatic phenotype in SW480 cells. In line with these findings, the proliferation profile of SW480-*shBmal1* cells resembled that of SW620 cells and both cell types proliferated faster than SW480 cells. These results support previous studies that point to a role of BMAL1 in

tumorigenesis, through influencing the cell cycle [52], [151]. Furthermore, lower apoptosis rates were observed in SW480 cells after *Bmal1*-KD, again resembling the apoptosis rate observed for metastatic SW620 cells. Taken together, the induced changes upon *Bmal1*-KD in SW480 cells closely resembled the phenotype of SW620 cells, leading to the assumption that a deregulated clock induces a more metastatic phenotype in cancer cells. Remarkably the induction of a more metastatic phenotype is also connected to metabolic phenotype rewiring as shown by the observation that *Bmal1*-KD induced a more energetic phenotype in SW480 cells and a change in time-dependent glycolytic activity, both resembling the energy phenotype of SW620 WT cells.

The results described so far support the hypothesis that perturbations of the core-clock lead to a more metastatic phenotype, measurable by fast proliferation and high metabolic activity. Because of the hypothesised role of HKDC1 and BMAL1 in tumour progression and therapy, the impact of *Hkdc1*-KD on gene expression and drug response in SW480 and SW620 cells was evaluated. *Bmal1*-KD induced upregulation of *Hkdc1* expression, while *Hkdc1*-KD induced *Bmal1* expression in SW480 cells, pointing to a reciprocal control between both genes. In both CRC cell lines, *Hkdc1*-KD led to a strong decrease of *Pck2* expression. PCK2 is a mitochondrial enzyme that catalyses the conversion of oxaloacetate to phosphoenolpyruvate (PEP). The functional role of the mitochondrial isoform PCK2 is likely linked to the provision of precursor intermediates for the biosynthesis of phospholipids, amino acids and purines thereby fulfilling the increased demand for biomass in rapidly proliferating cells [152]. This is particularly relevant in cancer cells under restricted glucose where glutamine-derived oxaloacetate is converted into PEP by PCK2. Additionally, *Hkdc1*-KD induced changes in core-clock gene expression, mainly in SW480 cells, suggesting, that the interplay between the core-clock and HKDC1 is stronger in SW480 cells than in SW620 cells. As mentioned above, the reciprocal interplay between *Bmal1* and *Hkdc1* seems to be dependent from the initial genetic condition of the particular cell line.

Cancer cells show a variety of metabolic alterations to fulfil the anabolic demands of tumour cells, including glycolysis [65]. High rates of aerobic glycolysis are maintained, known as the Warburg effect. Although enhanced aerobic glycolysis has been used as a marker to distinguish cancer cells from normal cells already decades ago, an elevated glucose metabolism was only very recently defined as one of the hallmarks of cancer [64]. Besides glycolytic activity,

mitochondrial function also plays a role in tumour growth and metastasis [66]. Published data show that highly metastatic tumours increase mitochondrial NADPH and undergo further metabolic changes to fight stress caused by ROS [142]. To further evaluate the role of a deregulated clock in metabolic phenotype rewiring during tumourigenesis, glycolysis and mitochondrial respiration were measured under different conditions. While the metabolic activity was similar in both WT cell lines, glycolysis as well as mitochondrial respiration were increased in SW480 cells after *Bmal1*-KD. These results are in line with a reported inhibitory effect of intracellular glucose on the expression of the core-clock genes *Bmal1*, *Per1* and *Per2*, pointing to an interplay between glycolysis and the circadian clock [83]. Furthermore, the higher *Hkdc1* expression observed in SW480-*shBmal1* cells and the subsequent increase of glycolytic activity agree with the reported reprogramming of metabolism in cancer cells [64], [142], [153], which allows them to fulfil the enhanced energy demands of fast growing and proliferating cells. However, the KD of *Bmal1* led to a decrease in metabolic activity in SW620 cells, again indicating that the effect of a deregulated clock on tumour metabolism is dependent on the initial genetic status of a cell. Remarkably, the time-dependent glycolytic activity observed in SW480-ctrl cells was disrupted upon *Bmal1*-KD. These observations point to a regulation of tumour metabolism by the circadian clock and a circadian regulation of temporal patterns in metabolic activity that are lost upon clock disruption through *Bmal1*-KD. Upon *Hkdc1*-KD, glycolysis decreased in both cell lines, while mitochondrial respiration was not affected. On the one hand, a decrease in glycolytic activity was expected, as HKDC1 is a central enzyme of the glycolytic pathway. On the other hand, other members of the HK family might have compensated the effects *Hkdc1*-KD.

Taken together, these results point to a reciprocal interplay between *Hkdc1* and the circadian clock, in particular in SW480 cells, since the KD of *Bmal1* led to a higher *Hkdc1* expression and consequently to a higher metabolic activity in these cells. Additionally, a KD of *Hkdc1* led to higher *Bmal1* expression and slightly lower glycolytic activity. In general, a KD of *Bmal1* led to a slight increase in metabolic activity in SW480 cells, but to the opposite change in SW620 cells. Upon *Bmal1*-KD, *Hkdc1* expression was upregulated in SW480 cells, but not in SW620 cells. This is likely a result from the overall increased metabolic activity of SW480-*shBmal1* cells. Thus, *Hkdc1* is a putative mediator of time-dependent effects on energy producing metabolic pathways. Overall, the data shows that a dysregulation of the biological

clock leads to alterations in expression of metabolic genes, as well as in metabolic activity that could be pivotal in colorectal cancer progression.

Findings from the CRC cell lines regarding the circadian regulation of metabolic genes were further validated in primary fibroblasts isolated from normal colon (NF) and colon adenocarcinoma (CAF) of the same patient. In NFs, *Bmal1*-KD led to a downregulation of *Hkdc1* and a subsequent inhibition of glycolytic activity. These results suggest that clock disruption via *Bmal1*-KD leads to changes in the expression levels of *Hkdc1* with subsequent effects on glycolysis. In normal cells, the inhibition of *Hkdc1* and glycolysis is favoured, while in primary tumour cells an upregulation of *Hkdc1* and glycolysis is preferred, resulting in a more cancerous phenotype. These results further support the above made conclusion, that the initial genetic composition of a cell determines the effect of *Bmal1*-KD. As a second non-cancerous cell model, human fallopian tube organoids were used. WT organoids and *p53*-KD organoids were tested for their circadian phenotype. The knockdown of the tumour suppressor *p53* should serve as a more cancerous stadium as compared to the WT organoids. *P53*-KD had strong effects on core-clock and metabolic gene expression. While core-clock genes were downregulated upon *p53*-KD, metabolic candidate genes were upregulated, supporting the assumptions made so far that a more cancerous phenotype is linked to a deregulated clock and enhanced metabolic activity.

The results from the present study point to a tumour suppressor role of BMAL1. This is in line with published data including recent work from our group [52], [154]. Furthermore, after *Bmal1*-KD, SW480 cells proliferate faster and their proliferation profile resembles that of the metastasis-derived SW620 cells. This leads to the assumption that a deregulated clock induces a more metastatic phenotype which is further supported by the observation that SW480-*shBmal1* cells develop an active energy phenotype that is similar to that of SW620-ctrl cells in order to fulfil the energetic demands of proliferating cells.

4.4 A deregulated clock impacts on response to anticancer treatment

The results discussed so far show that the circadian clock regulates tumour metabolism, partially in a time-dependent manner. As a logical consequence, the following experiments on the role of a deregulated clock on treatment response were not only performed at a single

timepoint but at three different timepoints after cell synchronisation. In recent years, cancer therapy approaches increasingly take the circadian timing of treatment administration into account to improve tolerability of anti-cancer drugs and treatment efficacy. Chronotherapy protocols have been used in chronomodulated chemotherapy [95] and time-dependent radiotherapy scheduling [96]–[99]. Based on the idea of chronotherapeutic treatment strategies SW480 and SW620 cells were treated with the GLUT1 inhibitor WZB117 at three different timepoints after synchronisation to analyse putative time-dependent treatment effects. The glucose transporter GLUT1 was shown to be upregulated in different cancer types and therefore is a potential target for cancer therapy [155], [156]. WZB117 inhibits GLUT1 by binding at the exofacial sugar binding site [157]. WZB117 was shown to inhibit cell growth in cancer cell lines as well as in a nude mouse model. WZB117 treatment decreased GLUT1 levels, intracellular ATP, and glycolytic enzymes finally resulting in cell-cycle arrest, senescence, and necrosis [72]. Furthermore, a study showed that 5-Fu resistance, a commonly used drug in colon cancer treatment, was associated with *Glut1* overexpression in colon cancer cells and that WZB117 treatment significantly increased the sensitivity of 5-Fu resistant cells to the drug, providing new treatment options for patients with 5-Fu resistance [73]. In the present study, WZB117 showed a strong impact on clock gene expression, in line with the described inhibitory effect of intracellular glucose on clock gene expression [83]. Interestingly, *Bmal1* and *Rev-erbα* were upregulated in SW480 cells after WZB117 treatment in all conditions (ctrl, *shBmal1*, *shHkdc1*). In SW620 cells, the effect of WZB117 on core-clock gene expression was weaker. WZB117 also induced expression changes of *Hkdc1*. While *Hkdc1* was upregulated upon treatment in SW480-*shBmal1* and SW480-*shHkdc1* cells, in SW620 cells *Hkdc1* was only upregulated upon treatment in *shHkdc1* cells. Taken together, the effects of WZB117 treatment on core-clock and metabolic gene expression support the above made conclusion that the initial genetic condition of a cell is responsible for the resulting treatment response. The effect of WZB117 treatment on the circadian phenotype was further evaluated by treating ctrl and *shBmal1* cells at three different timepoints after synchronisation and measuring the *Bmal1*-promoter activity. The effects of WZB117 treatment on the circadian phenotype differed depending on the time of treatment. These results indicate that the circadian clock is affected by anticancer treatment aiming at the cells metabolism and that the effect depends on the treatment time. A chronotherapeutic approach might therefore not only be reasonable because of the effect of a drug itself, but also because a certain treatment time might affect the clock to a lesser extent than another treatment timepoint. Regarding metabolic effects, WZB117

treatment induced a change towards a more quiescent energy phenotype in all conditions. However, as the initial energy phenotype in SW480-*shBmal1* cells was more energetic than in ctrl cells, the resulting energy phenotype after WZB117 treatment was still more energetic than in ctrl cells, meaning that the result of treatment is less effective in *shBmal1* cells. The same tendency could be observed regarding the glycolytic activity. Although WZB117 treatment decreased glycolysis in ctrl as well as in *shBmal1* cells, the effect was higher in ctrl than in *shBmal1* cells. In line with these results, high *Bmal1* expression was reported to increase sensitivity to cancer therapeutics in different cancer types [56], [136], [158]. A study using *Plasmodium*-infected erythrocytes treated with WZB117 showed that WZB117 inhibited glucose transporters and perturbed glycolysis. In consequence, glucose levels decreased, ROS levels increased and apoptosis was induced [159]. However, in the present study glycolysis was inhibited by WZB117 treatment while at the same time apoptosis was decreased, indicating a different mechanism of action in CRC cell lines. Alternatively, the temporal treatment window was too short to monitor the apoptotic effects of WZB117 treatment. Although WZB117 is a specific GLUT1 inhibitor, mitochondrial respiration was also affected upon WZB117 treatment. However, the results were different from those observed for glycolytic activity. The inhibitory effect of WZB117 treatment on mitochondrial respiration was much stronger in *shBmal1* cells. Taken together, in WT cells, WZB117 treatment has strong effects on glycolytic activity but minor effects on mitochondrial respiration. On the opposite, in *Bmal1*-KD and *Hkdc1*-KD cells, WZB117 treatment has only minor effects on glycolytic activity but stronger effects on mitochondrial respiration. In conclusion, after *Bmal1*-KD the efficacy of WZB117 treatment is changed from glycolysis inhibition towards inhibition of mitochondrial respiration. Possible reasons for the different effects might be due to a metabolic phenotype rewiring upon *Bmal1*-KD that induces the glycolytic pathway and protects cells from treatment aiming at this pathway but at the same time increases sensitivity at a different point of metabolism. The effects of *Bmal1*- and *Hkdc1*-KD on cancer metabolism and treatment response are schematically represented in **Figure 59**. Based on the results from this study, a deregulated clock might decrease treatment sensitivity of cancer cells and might consequently lead to poor prognosis. These results fit with published studies on the effect of clock gene expression on treatment sensitivity. In a study in tongue squamous cells, *Bmal1* inhibited tumourigenesis and increased sensitivity to paclitaxel [158]. Furthermore, in CRC cell lines, overexpression of *Bmal1* increased sensitivity to oxaliplatin treatment [56]. The results gained from WZB117 treatment were compared to oxaliplatin treatment, a platinum-based antineoplastic agent that is widely

used in chemotherapy for colorectal cancer [56], [160], [161]. Oxaliplatin exerts its cytotoxic effects mainly through DNA damage. Apoptosis of cancer cells can be caused by different mechanisms, including formation of DNA lesions, arrest of DNA synthesis and inhibition of RNA synthesis [162]. A comparison of the results after WZB117 treatment with oxaliplatin showed that oxaliplatin treatment did not have effects on cell metabolism measured by energy phenotype, glycolysis and mitochondrial respiration. Thus, the results gained from WZB117 treatment are specific for a metabolism-targeting anticancer treatment.

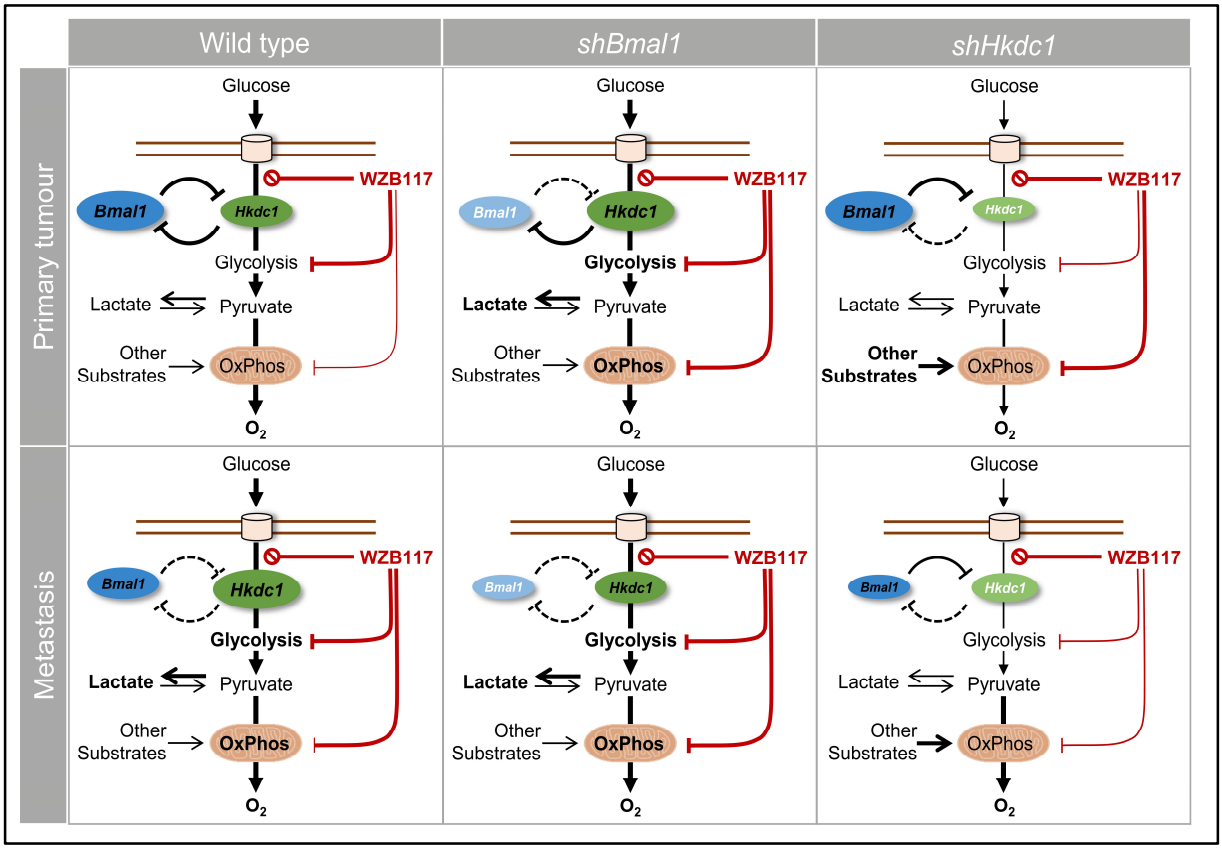

Figure 59: The interplay between the biological clock and metabolism in tumorigenesis
In the primary tumour cell line (SW480), clock gene disruption (*shBmal1*) leads to the upregulation of *Hkdc1* and subsequent activation of metabolic activity (glycolysis and mitochondrial respiration). The downregulation of *Hkdc1* (*shHkdc1*) leads to the upregulation of *Bmal1*. Upon treatment with WZB117, metabolic activity is inhibited in *shBmal1* cells, and glycolytic activity is inhibited to a lesser extent than in SW480-ctrl cells, partially explained by an increase of *Hkdc1* expression in *shBmal1* cells. In the metastatic cells (SW620) the effect of clock gene disruption (*shBmal1*) on *Hkdc1* expression is rather low and consequently *Bmal1*-KD leads to a slight inhibition of metabolic activity (glycolysis and mitochondrial respiration). After treatment with WZB117, the glycolytic activity is inhibited in *shBmal1* cells, and mitochondrial respiration is inhibited to a much larger extent. The effect

of WZB117 treatment is weaker in the *shHkdc1* cells. The size of the ellipses represents the relative RNA quantity, the width of the connecting lines represents the impact of the interaction. Adapted from **Fuhr** *et al*., 2018 [1].

Although the selection of a temporal window of six hours is too short to access detailed chronopharmacology profiles, the results indicate that the relative efficacy of treatment on the metabolic activity appears to change depending on the time of drug administration. This result provides insights into the scheduling of chronotherapeutic protocols targeting cancer cell metabolism and prompts to further deepen these studies in future work. The results further point to a role for the circadian clock in tumourigenesis, indicating that the disruption of the biological clock leads to a more metastatic phenotype. Metabolic alterations during tumorigenesis are a relevant factor to be considered for drug resistance [66]. While expression changes in some metabolic pathways including glycolysis are frequently observed during tumourigenesis, alterations in other pathways such as oxidative phosphorylation are very heterogeneous [150]. Glycolysis is an attractive target for cancer therapy with promising therapeutic potential, since many tumours increase glucose uptake and show elevated glycolysis rates. A possible glycolysis-related target might be the hexokinase HK2 which is upregulated in different tumour types and whose inhibition slows down tumour progression [66]. Although some isoforms of glycolytic enzymes are only present in cancer cells and not in normal cells, such as the hexokinase isoform HK2, the close similarity of different isoforms still makes them a difficult target, thus complicating the use of glycolysis as a potential therapeutic target [65]. An alternative candidate for targeting glycolysis might be the gene *Hkdc1* that was identified in this study as an important regulator via which the circadian clock influences metabolism in colorectal cancer cells. Importantly, the effect of *Bmal1* on metabolic function can be mediated in different ways. Either by influencing the clock machinery, and altering circadian rhythms, or by influencing the expression of genes that are direct targets of the CLOCK/BMAL1 complex. This could also be the result of other potential, non-circadian functions of BMAL1. As such, in order to differentiate between these two hypotheses and to better characterise the specific output results of *Bmal1*-KD phenotypes, further studies are necessary.

Altogether, the results from this project show that the circadian clock regulates metabolism in cancer cells with implications in metabolic phenotype rewiring observed during tumour progression. Additionally, the data suggests a role for the circadian clock in fine-tuning both drug efficiency and timing in cancer treatment, highlighting its crucial function as an elicitor of treatment response.

4.5 Cell-to-cell communication impacts on the circadian phenotype

It is common in oncological research to date to carry out experiments in human cancer cell lines, representing only one type of tumour cells. However, a tumour consists of a complex tissue, composed of different cell types mainly derived by the neighbouring stroma which make up the tumour microenvironment [143]. In normal colonic mucosa, the stromal population mainly consists of fibroblasts [144]. During tumourigenesis, fibroblasts may differentiate into cancer-associated fibroblasts which are then the main cellular component of tumour stroma. [145]. CAFs secrete growth factors and thereby support tumour growth and migration. They promote survival and proliferation in primary tumours as well as in metastasis [134]. Insights into the role of the tumour microenvironment show that cancer development is inseparably connected to it [144]. Based on this knowledge, CAFs and NFs were co-cultured with HCT116 cells and the impact of cell-to-cell communication on the circadian phenotype of HCT116 cells was evaluated. Co-culture induced both, a phase shift and a longer period in HCT116 cells. Interestingly, the longer period of HCT116 cells after co-culture closely resembled the period length of NFs and CAFs, suggesting that fibroblasts influence the cancer cell line`s period length into the direction of their own period length. The results are in line with existing findings that co-culture of fibroblasts and other cells has a profound impact on the expression of circadian genes [163]. Other co-culture experiments in the context of circadian research include experiments where the SCN was co-cultured with another cell type [164]. The observed effects on the circadian phenotype could be extended to the metabolic activity, cytotoxicity and apoptosis. While glycolysis was not affected in HCT116 cells upon co-culture, mitochondrial activity was altered. Basal respiration, maximum respiration and ATP production were significantly increased after co-culture with NFs in HCT116 cells. On the other hand, co-culture with CAFs tendentially decreased the mitochondrial activity. These results suggest that the surrounding stroma regulates metabolic activity in cancer cells and that the effects on cell metabolism may differ based on the type of surrounding cells. Furthermore, cytotoxicity and apoptosis were both significantly decreased in HCT116 cells when co-cultured with NFs or CAFs, leading to the assumption that the surrounding stroma protects cancer cells from cell death and promotes cell survival and growth. Taken together, the results gained from co-culture experiments show that cancer cells are highly affected by surrounding cells not only with respect to their circadian phenotype but also with respect to their metabolic activity and cell survival. Results from this study should be considered for future experiments and when

possible, co-culture experiments with different cell types should be preferred over experiments with one cell type only.

4.6 Conclusions and future perspectives

The circadian clock is a powerful endogenous timing system that regulates many aspects of human physiology. The role of the circadian clock in cancer and cancer-associated metabolic alterations has already been proposed by various studies. The results gained in this project further support the postulated interplay between the circadian clock and tumour metabolism and identify new connections between both systems. The role of the core-clock gene *Bmal1* as a tumour suppressor was further affirmed, as *Bmal1*-KD induced a more metastatic phenotype in SW480 cells. Moreover, *Bmal1*-KD induced metabolic phenotype rewiring by changing the overall metabolic activity as well as the time-dependent metabolic profile of the cells. Finally, *Bmal1*-KD led to changes in the response to treatment with the glycolysis inhibitor WZB117. The consequences of a deregulated clock on cancer metabolism and treatment response in colorectal cancer cell lines seem to be partly mediated by the glycolytic hexokinase HKDC1.

However, further experiments are necessary to overcome limitations and extend the insights gained from the present study. The time course microarray experiment performed during this project served as a starting point to identify over-represented pathways and candidate genes between SW480 and SW620 cells. Due to financial reasons, it was not possible to have replicates for each timepoint or to extend the timeframe to two full circadian cycles with smaller sampling intervals. Therefore, candidate genes were validated via 45 h time course qPCR. In future work, it will be beneficial to perform time course transcriptome studies with a longer timeframe. In the present project, time course transcriptome data were only available for SW480 and SW620 cells lines. In further studies, the additional use of a non-cancerous primary cell model as well as transcriptome data from SW480-*shBmal1* and SW620-*shBmal1* cells will be needed to generate a broader picture of the role of the circadian clock in tumourigenesis. To address the question whether *Bmal1* itself or the circadian clock in general is responsible for the effects on cancer metabolism and treatment response in this project, knockdown studies with another core-clock gene, for example *Per2*, will be needed. Due to time limits of this project, a repetition of the experiments with *Per2*-KD cells was not possible. Moreover, the timeframe of six hours used for time-dependent treatment in the present project gave hints that

the timing indeed plays a role in treatment response to metabolism-targeting drugs but is too short to generate reliable chronopharmacological profiles. Hence, in future work, a longer timeframe should be considered. Furthermore, animal studies will be needed to test whether the results gained from cell lines can be transferred to other model organisms *in vivo*. The treatment with the glycolysis inhibitor WZB117 showed that the circadian phenotype influences the effect of treatment on metabolic activity in colorectal cancer cells. To be able to make clear statements about the anti-cancer effects of metabolism-targeting drugs, further experiments are needed to investigate the effect on cell proliferation and cell survival. Furthermore, as described above, the treatment with drugs that target cell metabolism is difficult, as these drugs should ideally only target the metabolism of cancer cells and should not induce global metabolic effects. For this purpose, the identification of metabolic targets that are preferably only expressed in cancer cells is an important aim for future studies [67], [69], [70]. Although HK2 was identified as a possible metabolic target, the close similarity of different isoforms of glycolytic enzymes makes glycolysis still a difficult target in anti-cancer therapy [63], [65]. Likewise, antidiabetic drugs have been explored with respect to their anti-cancer activity [165] while other studies explored the Warburg effect as another potential target for anti-cancer therapy [71]. Furthermore, glutamine metabolism is an additional potential target for anticancer drugs. Although studies with inhibitors of glutamine metabolism have already been carried out, the toxicity of metabolism-targeting drugs remains an issue and the potential therapeutic resistance of cancer cells adds a new layer of complexity to this field of research [166]. Generally, different metabolism-targeting drugs may potentially be used in cancer therapy, based on the metabolic alterations a specific tumour has [167]. Another target that should be brought into focus is the circadian clock itself. Several attempts have been made to identify modulators of the circadian clock. These include small molecule clock modulators in general, REV-ERB agonists, ligand modulators of ROR, CRY stabilizers and circadian clock modulators from existing drugs, such as the period-shortening compound dehydroepiandrosterone (DHEA) [79], [168]–[172]. A study in mice showed that the clock-modulating compound L-methyl selenocysteine (MSC) elevates *Bmal1* transcription and protects mice against toxicity induced by the chemotherapeutic agent cyclophosphamide [173]. Although to date studies on this topic are rare, modulators that target the circadian clock offer a new possibility to existing chronotherapeutic approaches to cancer by providing pharmacological tools to actively adjust the molecular clock and thereby improving treatment efficiency and tolerability of a given anti-cancer agent.

Taken together, the results gained in this study elucidate new ways by which the circadian clock regulates metabolic phenotype rewiring during tumourigenesis and support the hypothesised role of the circadian clock as a tumour suppressor. The study gives new insights into the circadian regulation of cancer metabolism that may have implications on the development of new drug targets for cancer therapy and the timing of chronotherapeutic treatment protocols.

5. References

[1] L. Fuhr *et al.*, "The Circadian Clock Regulates Metabolic Phenotype Rewiring Via HKDC1 and Modulates Tumor Progression and Drug Response in Colorectal Cancer," *EBioMedicine*, vol. 33, pp. 105–121, Jul. 2018.

[2] R. El-Athman, L. Fuhr, and A. Relógio, "A Systems-Level Analysis Reveals Circadian Regulation of Splicing in Colorectal Cancer," *EBioMedicine*, vol. 33, pp. 68–81, Jul. 2018.

[3] T. Bollinger and U. Schibler, "Circadian rhythms - from genes to physiology and disease.," *Swiss Med. Wkly.*, vol. 144, no. July, p. w13984, Jan. 2014.

[4] U. Albrecht, "Timing to Perfection: The Biology of Central and Peripheral Circadian Clocks," *Neuron*, vol. 74, no. 2, pp. 246–260, 2012.

[5] J. Arendt, "Shift work: Coping with the biological clock," *Occup. Med. (Chic. Ill).*, vol. 60, no. 1, pp. 10–20, 2010.

[6] C. Dibner, U. Schibler, and U. Albrecht, *The mammalian circadian timing system: organization and coordination of central and peripheral clocks.*, vol. 72. 2010.

[7] M. K. Chandrashekaran, "Biological rhythms research: A personal account," no. 5, pp. 545–555, 1998.

[8] R. J. Konopka and S. Benzer, "Clock mutants of Drosophila melanogaster.," *Proc. Natl. Acad. Sci. U. S. A.*, vol. 68, no. 9, pp. 2112–2116, 1971.

[9] M. R. Ralph, R. G. Foster, F. C. Davis, and M. Menaker, "Transplanted suprachiasmatic nucleus determines circadian period.," *Science*, vol. 247, no. 4945, pp. 975–978, 1990.

[10] A. Relógio *et al.*, "Ras-mediated deregulation of the circadian clock in cancer.," *PLoS Genet.*, vol. 10, no. 5, p. e1004338, May 2014.

[11] L. Fuhr, M. Abreu, P. Pett, and A. Relógio, "Circadian systems biology: When time matters," *Comput. Struct. Biotechnol. J.*, vol. 13, pp. 417–426, 2015.

[12] P. L. Lowrey and J. S. Takahashi, *Genetics of circadian rhythms in Mammalian model organisms.*, 1st ed., vol. 74. Elsevier Inc., 2011.

[13] M. Astiz, I. Heyde, and H. Oster, "Mechanisms of Communication in the Mammalian Circadian Timing System," *Int. J. Mol. Sci.*, vol. 20, no. 2, p. 343, 2019.

[14] M. H. Hastings, E. S. Maywood, and M. Brancaccio, "The Mammalian Circadian Timing System and the Suprachiasmatic Nucleus as Its Pacemaker," *Biology (Basel).*, vol. 8, no. 1, p. 13, Mar. 2019.

[15] J. H. Meijer and W. J. Schwartz, "In Search of the Pathways for Light-Induced Pacemaker Resetting in the Suprachiasmatic Nucleus," *J. Biol. Rhythms*, vol. 18, no. 3, pp. 235–249, 2003.

[16] L. Curnicova and S. A. Brown, "Peripheral Circadian Oscillators Interesting Mechanisms and Powerful Tools," *Ann. N. Y. Acad. Sci.*, vol. 370, pp. 358–370, 2008.

[17] E. S. Maywood, *Synchronization and maintenance of circadian timing in the mammalian clockwork*. 2018.

[18] A. Relógio, P. O. Westermark, T. Wallach, K. Schellenberg, A. Kramer, and H. Herzel, "Tuning the mammalian circadian clock: robust synergy of two loops.," *PLoS Comput. Biol.*, vol. 7, no. 12, p. e1002309, Dec. 2011.

[19] U. Albrecht and J. A. Ripperger, "Clock Genes," in *Encyclopedia of Neuroscience*, U. Binder, M.D, Hirokawa, N, Windhorst, Ed. Springer, Berlin Heidelberg New York, 2008, pp. 1–5.

[20] E. E. Zhang and S. a Kay, "Clocks not winding down: unravelling circadian networks.," *Nat. Rev. Mol. Cell Biol.*, vol. 11, no. 11, pp. 764–776, 2010.

[21] R. Lehmann *et al.*, "Assembly of a Comprehensive Regulatory Network for the Mammalian Circadian Clock: A Bioinformatics Approach," *PLoS One*, vol. 10, no. 5, p. e0126283, May 2015.

[22] C. Savvidis and M. Koutsilieris, "Circadian rhythm disruption in cancer biology.," *Mol. Med.*, vol. 18, pp. 1249–60, 2012.

[23] R. Zhang, N. F. Lahens, H. I. Ballance, M. E. Hughes, and J. B. Hogenesch, “A circadian gene expression atlas in mammals: Implications for biology and medicine,” *Proc. Natl. Acad. Sci.*, vol. 111, no. 45, pp. 16219–16224, 2014.

[24] C. Scheiermann, Y. Kunisaki, and P. S. Frenette, “Circadian control of the immune system.,” *Nat. Rev. Immunol.*, vol. 13, no. 3, pp. 190–8, Mar. 2013.

[25] G. Mazzoccoli, V. Pazienza, and M. Vinciguerra, “Clock Genes and Clock-Controlled Genes in the Regulation of Metabolic Rhythms,” *Chronobiol. Int.*, vol. 29, no. 3, pp. 227–251, Apr. 2012.

[26] E. Maronde *et al.*, “The Clock Genes Period 2 and Cryptochrome 2 Differentially Balance Bone Formation,” *PLoS One*, vol. 5, no. 7, pp. 1–8, 2010.

[27] K. Vanselow *et al.*, “Differential effects of PER2 phosphorylation: Molecular basis for the human familial advanced sleep phase syndrome (FASPS),” *Genes Dev.*, vol. 20, no. 19, pp. 2660–2672, 2006.

[28] E. Borrelli, E. J. Nestler, C. D. Allis, and P. Sassone-corsi, “Decoding the Epigenetic Landscape of Neuronal Plasticity,” *Neuron*, vol. 60, no. 6, pp. 961–974, 2009.

[29] M. W. Young, “The Tick-Tock of the Biological Clock,” *Sci. Am.*, no. March, 2000.

[30] M. Keller *et al.*, “A circadian clock in macrophages controls inflammatory immune responses,” vol. 106, no. 50, pp. 21407–21412, 2009.

[31] S. S. Fonseca Costa and J. a. Ripperger, “Impact of the Circadian Clock on the Aging Process,” *Front. Neurol.*, vol. 6, no. March, pp. 1–5, 2015.

[32] V. Shanmugam, A. Wafi, N. Al-Taweel, and D. Büsselberg, “Disruption of circadian rhythm increases the risk of cancer, metabolic syndrome and cardiovascular disease,” *J. Local Glob. Heal. Sci.*, p. 3, 2013.

[33] J. B. Hogenesch and H. R. Ueda, “Understanding systems-level properties: timely stories from the study of clocks.,” *Nat. Rev. Genet.*, vol. 12, no. 6, pp. 407–416, 2011.

[34] E. E. Zhang *et al.*, “A Genome-wide RNAi Screen for Modifiers of the Circadian Clock

in Human Cells," *Cell*, vol. 139, no. 1, pp. 199–210, Oct. 2009.

[35] B. Marcheva *et al.*, "Disruption of the clock components CLOCK and BMAL1 leads to hypoinsulinaemia and diabetes.," *Nature*, vol. 466, no. 7306, pp. 627–631, 2010.

[36] F. Picard *et al.*, "Sirt1 promotes fat mobilization in white adipocytes by repressing PPAR-gamma.," *Nature*, vol. 429, no. 6993, pp. 771–776, 2004.

[37] S. Sahar and P. Sassone-Corsi, "Metabolism and cancer: the circadian clock connection.," *Nat. Rev. Cancer*, vol. 9, no. 12, pp. 886–96, Dec. 2009.

[38] F. C. Kelleher, A. Rao, and A. Maguire, "Circadian molecular clocks and cancer," *Cancer Lett.*, vol. 342, no. 1, pp. 9–18, 2014.

[39] L. Fu and N. M. Kettner, "The circadian clock in cancer development and therapy," *Prog. Mol. Biol. Transl. Sci.*, vol. 119, pp. 221–282, Jan. 2013.

[40] E. S. Schernhammer *et al.*, "Night-shift work and risk of colorectal cancer in the nurses' health study," *J Natl.Cancer Inst.*, vol. 95, no. 11, pp. 825–828, 2003.

[41] S. P. Megdal, C. H. Kroenke, F. Laden, E. Pukkala, and E. S. Schernhammer, "Night work and breast cancer risk: A systematic review and meta-analysis," *Eur. J. Cancer*, vol. 41, no. 13, pp. 2023–2032, 2005.

[42] M. Conlon, N. Lightfoot, and N. Kreiger, "Rotating shift work and risk of prostate cancer.," *Epidemiology*, vol. 18, no. 1, pp. 182–183, 2007.

[43] A. N. Viswanathan, S. E. Hankinson, and E. S. Schernhammer, "Night shift work and the risk of endometrial cancer," *Cancer Res.*, vol. 67, no. 21, pp. 10618–10622, 2007.

[44] T. a. Lahti, T. Partonen, P. Kyyrönen, T. Kauppinen, and E. Pukkala, "Night-time work predisposes to non-Hodgkin lymphoma," *Int. J. Cancer*, vol. 123, no. 9, pp. 2148–2151, 2008.

[45] S. T. Chen, K. B. Choo, M. F. Hou, K. T. Yeh, S. J. Kuo, and J. G. Chang, "Deregulated expression of the PER1, PER2 and PER3 genes in breast cancers," *Carcinogenesis*, vol. 26, no. 7, pp. 1241–1246, 2005.

[46] S. Gery, N. Komatsu, L. Baldjyan, A. Yu, D. Koo, and H. P. Koeffler, "The Circadian Gene Per1 Plays an Important Role in Cell Growth and DNA Damage Control in Human Cancer Cells," *Mol. Cell*, vol. 22, no. 3, pp. 375–382, 2006.

[47] S. Gery, R. K. Virk, K. Chumakov, a Yu, and H. P. Koeffler, "The clock gene Per2 links the circadian system to the estrogen receptor.," *Oncogene*, vol. 26, no. 57, pp. 7916–7920, 2007.

[48] C. Qi *et al.*, "A role for the clock gene Per1 in prostate cancer," *Cancer Res.*, vol. 69, no. 19, pp. 7619–7625, 2009.

[49] S. Gery *et al.*, "Transcription profiling of C / EBP targets identifies Per2 as a gene implicated in myeloid leukemia Transcription profiling of C / EBP targets identifies Per2 as a gene implicated in myeloid leukemia," *October*, vol. 106, no. 8, pp. 2827–2836, 2011.

[50] S. Masri, K. Kinouchi, and P. Sassone-Corsi, "Circadian clocks, epigenetics, and cancer," *Curr. Opin. Oncol.*, vol. 27, no. 1, pp. 50–56, Jan. 2015.

[51] S. Lee, L. A. Donehower, A. J. Herron, D. D. Moore, and L. Fu, "Disrupting Circadian Homeostasis of Sympathetic Signaling Promotes Tumor Development in Mice," *PLoS One*, vol. 5, no. 6, p. e10995, Jun. 2010.

[52] R. El-Athman *et al.*, "The Ink4a/Arf locus operates as a regulator of the circadian clock modulating RAS activity," *PLOS Biol.*, vol. 15, no. 12, p. e2002940, Dec. 2017.

[53] K. Davis, L. C. Roden, and P. J. Van, "Critical Review The Tumour Suppressing Role of the Circadian Clock," pp. 1–10.

[54] G. Mazzoccoli, M. Vinciguerra, G. Papa, and A. Piepoli, "Circadian clock circuitry in colorectal cancer.," *World J. Gastroenterol.*, vol. 20, no. 15, pp. 4197–207, 2014.

[55] J. Tommelein, L. Verset, T. Boterberg, P. Demetter, M. Bracke, and O. De Wever, "Cancer-associated fibroblasts connect metastasis-promoting communication in colorectal cancer.," *Front. Oncol.*, vol. 5, no. March, p. 63, Mar. 2015.

[56] Z. -l. Zeng *et al.*, "Overexpression of the Circadian Clock Gene Bmal1 Increases

Sensitivity to Oxaliplatin in Colorectal Cancer," *Clin. Cancer Res.*, vol. 20, no. 4, pp. 1042–1052, Feb. 2014.

[57] M. Soták, L. Polidarová, P. Ergang, A. Sumová, and J. Pácha, "An association between clock genes and clock-controlled cell cycle genes in murine colorectal tumors," *Int. J. Cancer*, vol. 132, no. 5, pp. 1032–1041, Mar. 2013.

[58] G. Mazzoccoli *et al.*, "Clock Gene Expression Levels and Relationship With Clinical and Pathological Features in Colorectal Cancer Patients," *Chronobiol. Int.*, vol. 28, no. 10, pp. 841–851, Dec. 2011.

[59] T. Orhan, P. B. Nielsen, T. V. F. Hviid, A. W. Rosen, and I. Gögenür, "Expression of Circadian Clock Genes in Human Colorectal Cancer Tissues Using Droplet Digital PCR," *Cancer Invest.*, vol. 0, no. 0, pp. 1–9, Feb. 2019.

[60] T. Karantanos, G. Theodoropoulos, D. Pektasides, and M. Gazouli, "Clock genes: Their role in colorectal cancer," *World J. Gastroenterol.*, vol. 20, no. 8, pp. 1986–1992, 2014.

[61] H. Reinke and G. Asher, "Crosstalk between metabolism and circadian clocks," *Nat. Rev. Mol. Cell Biol.*, Jan. 2019.

[62] D. Hanahan and R. A. Weinberg, "The Hallmarks of Cancer," *Cell*, vol. 100, no. 1, pp. 57–70, Jan. 2000.

[63] R. A. Cairns and T. W. Mak, "The current state of cancer metabolism," *Nat. Rev. Cancer*, vol. 16, no. 10, pp. 613–614, 2016.

[64] N. N. Pavlova and C. B. Thompson, "The Emerging Hallmarks of Cancer Metabolism," *Cell Metab.*, vol. 23, no. 1, pp. 27–47, 2016.

[65] N. Hay, "Reprogramming glucose metabolism in cancer: can it be exploited for cancer therapy?," *Nat. Rev. Cancer*, vol. 16, no. 10, pp. 635–649, Sep. 2016.

[66] R. J. DeBerardinis and N. S. Chandel, "Fundamentals of cancer metabolism," *Sci. Adv.*, vol. 2, no. 5, p. e1600200, May 2016.

[67] N. P. Jones and A. Schulze, "Targeting cancer metabolism - Aiming at a tumour's sweet-

spot," *Drug Discov. Today*, vol. 17, no. 5–6, pp. 232–241, 2012.

[68] K. Padmanabhan and M. Billaud, "Desynchronization of Circadian Clocks in Cancer: A Metabolic and Epigenetic Connection," *Front. Endocrinol. (Lausanne).*, vol. 8, no. June, pp. 1–7, 2017.

[69] A. Luengo, D. Y. Gui, and M. G. Vander Heiden, "Targeting Metabolism for Cancer Therapy," *Cell Chem. Biol.*, vol. 24, no. 9, pp. 1161–1180, Sep. 2017.

[70] Y. Zhao, E. B. Butler, and M. Tan, "Targeting cellular metabolism to improve cancer therapeutics," *Cell Death Dis.*, vol. 4, no. 3, p. e532, Mar. 2013.

[71] Q. Tran, H. Lee, J. Park, S. H. Kim, and J. Park, "Targeting cancer metabolism - revisiting the Warburg effects," *Toxicol. Res.*, vol. 32, no. 3, pp. 177–193, 2016.

[72] Y. Y. Liu *et al.*, "A Small-Molecule Inhibitor of Glucose Transporter 1 Downregulates Glycolysis, Induces Cell-Cycle Arrest, and Inhibits Cancer Cell Growth In Vitro and In Vivo," *Mol. Cancer Ther.*, vol. 11, no. 8, pp. 1672–1682, Aug. 2012.

[73] W. Liu, Y. Fang, X.-T. T. Wang, J. Liu, X. Dan, and L.-L. L. Sun, "Overcoming 5-Fu resistance of colon cells through inhibition of glut1 by the specific inhibitor WZB117," *Asian Pacific J. Cancer Prev.*, vol. 15, no. 17, pp. 7037–7041, Sep. 2014.

[74] S. Panda *et al.*, "Coordinated transcription of key pathways in the mouse by the circadian clock," *Cell*, vol. 109, no. 3, pp. 307–320, 2002.

[75] C. B. Green, J. S. Takahashi, and J. Bass, "The Meter of Metabolism," *Cell*, vol. 134, no. 5. pp. 728–742, 2008.

[76] K. Bozek *et al.*, "Regulation of clock-controlled genes in mammals.," *PLoS One*, vol. 4, no. 3, p. e4882, Jan. 2009.

[77] R. Scrima *et al.*, "Clock-genes and mitochondrial respiratory activity: Evidence of a reciprocal interplay," *Biochim. Biophys. Acta - Bioenerg.*, vol. 1857, no. 8, pp. 1344–1351, Aug. 2016.

[78] O. Cela *et al.*, "Clock genes-dependent acetylation of complex I sets rhythmic activity

of mitochondrial OxPhos," *Biochim. Biophys. Acta - Mol. Cell Res.*, vol. 1863, no. 4, pp. 596–606, Apr. 2016.

[79] Y. Onder and C. B. Green, "Neurobiology of Sleep and Circadian Rhythms Rhythms of metabolism in adipose tissue and mitochondria," *Neurobiol. Sleep Circadian Rhythm.*, vol. 4, no. February, pp. 57–63, 2018.

[80] K. Eckel-Mahan and P. Sassone-Corsi, "Metabolism and the circadian clock converge.," *Physiol. Rev.*, vol. 93, no. 1, pp. 107–35, 2013.

[81] S. Y. Krishnaiah *et al.*, "Clock Regulation of Metabolites Reveals Coupling between Transcription and Metabolism," *Cell Metab.*, vol. 25, no. 4, p. 961–974.e4, Apr. 2017.

[82] K. L. Eckel-mahan, V. R. Patel, R. P. Mohney, K. S. Vignola, P. Baldi, and P. Sassone-corsi, "Coordination of the transcriptome and metabolome by the circadian clock," *Proc. Natl. Acad. Sci.*, vol. 109, no. 14, pp. 10–15, 2012.

[83] T. Hirota, T. Okano, K. Kokame, H. Shirotani-Ikejima, T. Miyata, and Y. Fukada, "Glucose Down-regulates Per1 and Per2 mRNA Levels and Induces Circadian Gene Expression in Cultured Rat-1 Fibroblasts," *J. Biol. Chem.*, vol. 277, no. 46, pp. 44244–44251, Nov. 2002.

[84] H. Oike, K. Nagai, T. Fukushima, N. Ishida, and M. Kobori, "Feeding Cues and Injected Nutrients Induce Acute Expression of Multiple Clock Genes in the Mouse Liver," *PLoS One*, vol. 6, no. 8, p. e23709, Aug. 2011.

[85] F. Dang *et al.*, "Insulin post-transcriptionally modulates Bmal1 protein to affect the hepatic circadian clock," *Nat. Commun.*, vol. 7, no. 1, p. 12696, Dec. 2016.

[86] V. Petrenko and C. Dibner, "Cell-specific resetting of mouse islet cellular clocks by glucagon, glucagon-like peptide 1 and somatostatin," *Acta Physiol.*, vol. 222, no. 4, p. e13021, Apr. 2018.

[87] a Balsalobre *et al.*, "Resetting of circadian time in peripheral tissues by glucocorticoid signaling.," *Science (80-.).*, vol. 289, no. September, pp. 2344–2347, 2000.

[88] R. Salgado-Delgado, M. Angeles-Castellanos, M. R. Buijs, and C. Escobar, "Internal

desynchronization in a model of night-work by forced activity in rats," *Behav. Neurosci.*, vol. 154, pp. 922–931, 2008.

[89] J. Hernández-García, D. Navas-Carrillo, and E. Orenes-Piñero, "Alterations of circadian rhythms and their impact on obesity, metabolic syndrome and cardiovascular diseases," *Crit. Rev. Food Sci. Nutr.*, vol. 0, no. 0, pp. 1–10, 2019.

[90] A. H. Tsang, M. Astiz, B. Leinweber, and H. Oster, "Rodent models for the analysis of tissue clock function in metabolic rhythms research," *Front. Endocrinol. (Lausanne).*, vol. 8, no. FEB, pp. 1–7, 2017.

[91] R. V Kondratov, A. A. Kondratova, V. Y. Gorbacheva, O. V Vykhovanets, and M. P. Antoch, "Early aging and age-related pathologies in mice deficient in BMAL1 , the core component of the circadian clock," *Genes Dev.*, no. 216, pp. 1868–1873, 2006.

[92] R. D. Rudic *et al.*, "BMAL1 and CLOCK , Two Essential Components of the Circadian Clock , Are Involved in Glucose Homeostasis," *PLOS*, vol. 2, no. 11, 2004.

[93] S. Masri and P. Sassone-Corsi, "The emerging link between cancer, metabolism, and circadian rhythms," *Nat. Med.*, vol. 24, no. 12, pp. 1795–1803, Dec. 2018.

[94] A. Ballesta, P. F. Innominato, R. Dallmann, D. A. Rand, and F. A. Lévi, "Systems Chronotherapeutics," *Pharmacol. Rev.*, vol. 69, no. 2, pp. 161–199, 2017.

[95] S. Giacchetti *et al.*, "Sex moderates circadian chemotherapy effects on survival of patients with metastatic colorectal cancer: a meta-analysis.," *Ann. Oncol.*, vol. 23, no. 12, pp. 3110–6, 2012.

[96] M. V Plikus *et al.*, "Local circadian clock gates cell cycle progression of transient amplifying cells during regenerative hair cycling.," *Proc. Natl. Acad. Sci. U. S. A.*, vol. 110, no. 23, pp. E2106-15, 2013.

[97] P. Shukla *et al.*, "Circadian variation in radiation-induced intestinal mucositis in patients with cervical carcinoma," *Cancer*, vol. 116, no. 8, pp. 2031–2035, 2010.

[98] G. a. Bjarnason *et al.*, "Comparison of Toxicity Associated With Early Morning Versus Late Afternoon Radiotherapy in Patients With Head-and-Neck Cancer: A Prospective

Randomized Trial of the National Cancer Institute of Canada Clinical Trials Group (HN3)," *Int. J. Radiat. Oncol. Biol. Phys.*, vol. 73, no. 1, pp. 166–172, 2009.

[99] R. Dallmann, A. Okyar, and F. Lévi, "Dosing-Time Makes the Poison: Circadian Regulation and Pharmacotherapy," *Trends Mol. Med.*, vol. 22, no. 5, pp. 430–445, May 2016.

[100] B. He and Z. Chen, "Molecular Targets for Small-Molecule Modulators of Circadian Clocks.," *Curr. Drug Metab.*, vol. 17, no. 5, pp. 583–592, 2016.

[101] N. Ozturk, D. Ozturk, I. H. Kavakli, and A. Okyar, "Molecular aspects of circadian pharmacology and relevance for cancer chronotherapy," *Int. J. Mol. Sci.*, vol. 18, no. 10, 2017.

[102] G. E. Rivard, C. Infante-rivard, and M. Dresse, "Circadian Time-Dependent Response of Childhood Lymphoblastic Leukemia to Chemotherapy : A Long-Term Follow-up Study of Survival Circadian Time-Dependent Response of Childhood Lymphoblastic Leukemia to Chemotherapy : A Long-Term Follow-up Study of Survival," *J. Biol. Med. Rhythm Res.*, vol. 0528, no. November 2015, pp. 4–8, 2009.

[103] P. F. Innominato, V. P. Roche, O. G. Palesh, A. Ulusakarya, D. Spiegel, and F. a Lévi, "The circadian timing system in clinical oncology.," *Ann. Med.*, vol. 46, no. 4, pp. 191–207, 2014.

[104] F. Lévi, A. Okyar, S. Dulong, P. F. Innominato, and J. Clairambault, "Circadian Timing in Cancer Treatments," *Annu. Rev. Pharmacol. Toxicol.*, vol. 50, no. 1, pp. 377–421, 2010.

[105] A. Sancar *et al.*, "Circadian Clock, Cancer, and Chemotherapy," *Biochemistry*, vol. 54, no. 2, pp. 110–123, Jan. 2015.

[106] Y. Ye *et al.*, "The Genomic Landscape and Pharmacogenomic Interactions of Clock Genes in Cancer Chronotherapy," *Cell Syst.*, vol. 6, no. 3, p. 314–328.e2, 2018.

[107] T. Hirota and S. a Kay, *Identification of small-molecule modulators of the circadian clock.*, 1st ed., vol. 551. Elsevier Inc., 2015.

[108] F. Spörl *et al.*, “A circadian clock in HaCaT keratinocytes.,” *J. Invest. Dermatol.*, vol. 131, no. 2, pp. 338–348, 2011.

[109] J. Bieler, R. Cannavo, K. Gustafson, C. Gobet, D. Gatfield, and F. Naef, “Robust synchronization of coupled circadian and cell cycle oscillators in single mammalian cells.,” *Mol. Syst. Biol.*, vol. 10, no. 7, p. 739, 2014.

[110] S. a. Brown *et al.*, “The period length of fibroblast circadian gene expression varies widely among human individuals.,” *PLoS Biol.*, vol. 3, no. 10, p. e338, Oct. 2005.

[111] M. Kessler *et al.*, “The Notch and Wnt pathways regulate stemness and differentiation in human fallopian tube organoids,” *Nat. Commun.*, vol. 6, no. May, p. 8989, Dec. 2015.

[112] K. J. Livak and T. D. Schmittgen, “Analysis of relative gene expression data using real-time quantitative PCR and the 2(-Delta Delta C(T)) Method.,” *Methods*, vol. 25, no. 4, pp. 402–8, Dec. 2001.

[113] C. A. Schneider, W. S. Rasband, and K. W. Eliceiri, “NIH Image to ImageJ: 25 years of image analysis.,” *Nat. Methods*, vol. 9, no. 7, pp. 671–5, Jul. 2012.

[114] J. Schindelin *et al.*, “Fiji: an open-source platform for biological-image analysis,” *Nat. Methods*, vol. 9, no. 7, pp. 676–682, Jul. 2012.

[115] X. X. Li *et al.*, “RNA-seq identifies determinants of oxaliplatin sensitivity in colorectal cancer cell lines,” *Int. J. Clin. Exp. Pathol.*, vol. 7, no. 7, pp. 3763–3770, 2014.

[116] R Development Core Team, *R: A language and environment for statistical computing*. 2008.

[117] B. S. Carvalho and R. A. Irizarry, “A framework for oligonucleotide microarray preprocessing,” *Bioinformatics*, vol. 26, no. 19, pp. 2363–2367, 2010.

[118] B. M. Bolstad, R. A. Irizarry, M. Astrand, and T. P. Speed, “A comparison of normalization methods for high density oligonucleotide array data based on variance and bias.,” *Bioinformatics*, vol. 19, no. 2, pp. 185–93, Jan. 2003.

[119] R. A. Irizarry, “Summaries of Affymetrix GeneChip probe level data,” *Nucleic Acids*

Res., vol. 31, no. 4, p. 15e–15, Feb. 2003.

[120] A. Kauffmann, R. Gentleman, and W. Huber, "arrayQualityMetrics — a bioconductor package for quality assessment of microarray data," *Bioinformatics*, vol. 25, no. 3, pp. 415–416, 2009.

[121] M. E. Ritchie *et al.*, "limma powers differential expression analyses for RNA-sequencing and microarray studies," *Nucleic Acids Res.*, vol. 43, no. 7, pp. e47–e47, Apr. 2015.

[122] P. F. Thaben and P. O. Westermark, "Detecting Rhythms in Time Series with RAIN," *J. Biol. Rhythms*, vol. 29, no. 6, pp. 391–400, Dec. 2014.

[123] S. Lück, K. Thurley, P. F. Thaben, and P. O. Westermark, "Rhythmic Degradation Explains and Unifies Circadian Transcriptome and Proteome Data," *Cell Rep.*, vol. 9, no. 2, pp. 741–751, Oct. 2014.

[124] B. Warnes, Gregory R. Bolker, W. Bonebakker, Lodewijk Gentleman, Robert Huber, A. Liaw, T. Lumley, and M. Maechler, *gplots: Various R Programming Tools for Plotting Data*. 2016.

[125] M. Izumo, T. R. Sato, M. Straume, and C. H. Johnson, "Quantitative analyses of circadian gene expression in mammalian cell cultures," *PLoS Comput. Biol.*, vol. 2, no. 10, pp. 1248–1261, 2006.

[126] K. Yagita and H. Okamura, "Forskolin induces circadian gene expression of rPer1, rPer2 and dbp in mammalian rat-1 fibroblasts," *FEBS Lett.*, vol. 465, no. 1, pp. 79–82, 2000.

[127] D. Petrocellis *et al.*, "A transcription factor response element for gene expression during circadian night," *Nature*, vol. 418, no. 6897, pp. 534–539, 2002.

[128] K. Oishi, K. Sakamoto, T. Okada, T. Nagase, and N. Ishida, "Antiphase Circadian Expression between BMAL1 and period Homologue mRNA in the Suprachiasmatic Nucleus and Peripheral Tissues of Rats," *Biochem. Biophys. Res. Commun.*, vol. 253, no. 2, pp. 199–203, 1998.

[129] R. González-Fernández, J. Hernández, P. Martín-Vasallo, M. Puopolo, A. Palumbo, and J. Ávila, "Expression Levels of the Oxidative Stress Response Gene ALDH3A2 in

Granulosa-Lutein Cells Are Related to Female Age and Infertility Diagnosis," *Reprod. Sci.*, vol. 23, no. 5, pp. 604–609, May 2016.

[130] S. A. Oppelt, W. Zhang, and D. R. Tolan, "Specific regions of the brain are capable of fructose metabolism," *Brain Res.*, vol. 1657, pp. 312–322, 2017.

[131] Z. Zhang *et al.*, "High expression of hexokinase domain containing 1 is associated with poor prognosis and aggressive phenotype in hepatocarcinoma," *Biochem Biophys Res Commun*, vol. 474, no. 4, pp. 673–679, 2016.

[132] E. D. Montal *et al.*, "PEPCK Coordinates the Regulation of Central Carbon Metabolism to Promote Cancer Cell Growth," *Mol. Cell*, vol. 60, no. 4, pp. 571–583, Nov. 2015.

[133] H. Tang *et al.*, "Pyruvate dehydrogenase B promoted the growth and migration of the nasopharyngeal carcinoma cells," *Tumor Biol.*, vol. 37, no. 8, pp. 10563–10569, 2016.

[134] F. Cammarota and M. O. Laukkanen, "Mesenchymal stem/stromal cells in stromal evolution and cancer progression," *Stem Cells Int.*, vol. 2016, no. i, 2016.

[135] N. Sachs and H. Clevers, "Organoid cultures for the analysis of cancer phenotypes," *Curr. Opin. Genet. Dev.*, vol. 24, no. 1, pp. 68–73, 2014.

[136] S. Kiessling *et al.*, "Enhancing circadian clock function in cancer cells inhibits tumor growth," *BMC Biol.*, vol. 15, no. 1, p. 13, 2017.

[137] L. Fu and C. C. Lee, "The circadian clock: pacemaker and tumour suppressor.," *Nat. Rev. Cancer*, vol. 3, no. May, pp. 350–361, 2003.

[138] S.-J. Kuo *et al.*, "Disturbance of circadian gene expression in breast cancer.," *Virchows Arch.*, vol. 454, no. 4, pp. 467–474, 2009.

[139] A. Gréchez-Cassiau, B. Rayet, F. Guillaumond, M. Teboul, and F. Delaunay, "The Circadian Clock Component BMAL1 Is a Critical Regulator of p21 WAF1/CIP1 Expression and Hepatocyte Proliferation," *J. Biol. Chem.*, vol. 283, no. 8, pp. 4535–4542, Feb. 2008.

[140] M. Geyfman *et al.*, "Brain and muscle Arnt-like protein-1 (BMAL1) controls circadian

cell proliferation and susceptibility to UVB-induced DNA damage in the epidermis," *Proc. Natl. Acad. Sci.*, vol. 109, no. 29, pp. 11758–11763, Jul. 2012.

[141] J. Mullenders, A. W. M. Fabius, M. Madiredjo, R. Bernards, and R. L. Beijersbergen, "A Large Scale shRNA Barcode Screen Identifies the Circadian Clock Component ARNTL as Putative Regulator of the p53 Tumor Suppressor Pathway," *PLoS One*, vol. 4, no. 3, p. e4798, Mar. 2009.

[142] M. G. Vander Heiden and R. J. DeBerardinis, "Understanding the Intersections between Metabolism and Cancer Biology," *Cell*, vol. 168, no. 4, pp. 657–669, Feb. 2017.

[143] T. Colangelo *et al.*, "Friend or foe?: The tumour microenvironment dilemma in colorectal cancer," *Biochim. Biophys. Acta - Rev. Cancer*, vol. 1867, no. 1, pp. 1–18, Jan. 2017.

[144] F. Xing, J. Saidou, and K. Watabe, "Cancer associated fibroblasts (CAFs) in tumor microenvironment.," *Front. Biosci. (Landmark Ed.*, vol. 15, no. 2, pp. 166–79, 2010.

[145] R. Kalluri and M. Zeisberg, "Fibroblasts in cancer," *Nat. Rev. Cancer*, vol. 6, no. 5, pp. 392–401, May 2006.

[146] R. E. Hewitt *et al.*, "Validation of a model of colon cancer progression.," *J. Pathol.*, vol. 192, no. 4, pp. 446–54, Dec. 2000.

[147] A. Provenzani, "Global alterations in mRNA polysomal recruitment in a cell model of colorectal cancer progression to metastasis," *Carcinogenesis*, vol. 27, no. 7, pp. 1323–1333, Feb. 2006.

[148] D. M. Irwin and H. Tan, "Molecular evolution of the vertebrate hexokinase gene family: Identification of a conserved fifth vertebrate hexokinase gene," *Comp. Biochem. Physiol. - Part D Genomics Proteomics*, vol. 3, no. 1, pp. 96–107, 2008.

[149] G. G.-H. Li and J.-F. J. Huang, "Inferring therapeutic targets from heterogeneous data: HKDC1 is a novel potential therapeutic target for cancer," *Bioinformatics*, vol. 30, no. 6, pp. 748–752, Mar. 2014.

[150] J. Hu *et al.*, "Heterogeneity of tumor-induced gene expression changes in the human metabolic network," *Nat Biotechnol*, vol. 31, no. 6, pp. 522–529, 2013.

[151] S. Masri, M. Cervantes, and P. Sassone-Corsi, “The circadian clock and cell cycle: interconnected biological circuits,” *Curr. Opin. Cell Biol.*, vol. 25, no. 6, pp. 730–734, Dec. 2013.

[152] E. E. Vincent *et al.*, “Mitochondrial Phosphoenolpyruvate Carboxykinase Regulates Metabolic Adaptation and Enables Glucose-Independent Tumor Growth,” *Mol. Cell*, vol. 60, no. 2, pp. 195–207, Oct. 2015.

[153] A. Schulze and A. L. Harris, “How cancer metabolism is tuned for proliferation and vulnerable to disruption,” *Nature*, vol. 491, no. 7424, pp. 364–373, 2012.

[154] W. Sakamoto and S. Takenoshita, “[Original Article] OVEREXPRESSION OF BOTH CLOCK AND BMAL1 INHIBITS ENTRY TO S PHASE IN HUMAN COLON CANCER CELLS,” *FUKUSHIMA J. Med. Sci.*, vol. 61, no. 2, pp. 111–124, 2015.

[155] K. C. Carvalho *et al.*, “GLUT1 expression in malignant tumors and its use as an immunodiagnostic marker,” *Clinics*, vol. 66, no. 6, pp. 965–972, 2011.

[156] D. A. Chan *et al.*, “Targeting GLUT1 and the Warburg Effect in Renal Cell Carcinoma by Chemical Synthetic Lethality,” *Sci. Transl. Med.*, vol. 3, no. 94, p. 94ra70-94ra70, Aug. 2011.

[157] O. A. Ojelabi, K. P. Lloyd, A. H. Simon, J. K. De Zutter, and A. Carruthers, “WZB117 (2-Fluoro-6-(m -hydroxybenzoyloxy) Phenyl m -Hydroxybenzoate) Inhibits GLUT1-mediated Sugar Transport by Binding Reversibly at the Exofacial Sugar Binding Site,” *J. Biol. Chem.*, vol. 291, no. 52, pp. 26762–26772, Dec. 2016.

[158] Q. Tang *et al.*, “Circadian clock gene Bmal1 inhibits tumorigenesis and increases paclitaxel sensitivity in tongue squamous cell carcinoma,” *Cancer Res.*, vol. 77, no. 2, pp. 532–544, Jan. 2017.

[159] L. Lu, M. Wei, W. Sui, L. Lv, Y. Liu, and X. Shi, “Inhibition of GLUTs by WZB117 mediates apoptosis in blood-stage Plasmodium parasites by breaking redox balance,” *Biochem. Biophys. Res. Commun.*, vol. 503, no. 2, pp. 1154–1159, 2018.

[160] S. Yokoo, S. Masuda, A. Yonezawa, T. Terada, T. Katsura, and K. -i. K. I. K. -i. Inui,

"Significance of organic cation transporter 3 (SLC22A3) expression for the cytotoxic effect of oxaliplatin in colorectal cancer," *Drug Metab. Dispos.*, vol. 36, no. 11, pp. 2299–2306, Aug. 2008.

[161] F. Lévi, R. Zidani, and J. L. Misset, "Randomised multicentre trial of chronotherapy with oxaliplatin, fluorouracil, and folinic acid in metastatic colorectal cancer," *Lancet*, vol. 350, pp. 681–686, 1997.

[162] T. Alcindor and N. Beauger, "Oxaliplatin: a review in the era of molecularly targeted therapy.," *Curr. Oncol.*, vol. 18, no. 1, pp. 18–25, Jan. 2011.

[163] K. Furudate, T. Imaizumi, H. Kimura, and W. Kobayashi, "Clock Gene Expressions Are Altered By Co-Culture of," *CiNii*, pp. 135–142, 2016.

[164] C. Beaulé, D. Granados-Fuentes, L. Marpegan, and E. D. Herzog, "In vitro circadian rhythms: imaging and electrophysiology," *Essays Biochem.*, vol. 49, no. 1, pp. 103–117, Jun. 2011.

[165] M. G. Vander Heiden, "Targeting cancer metabolism: A therapeutic window opens," *Nat. Rev. Drug Discov.*, vol. 10, no. 9, pp. 671–684, 2011.

[166] Y. Choi and K. Park, "Targeting Glutamine Metabolism for Cancer Treatment," *Biomol. Ther. (Seoul).*, vol. 26, no. 1, pp. 19–28, Jan. 2018.

[167] B. A. Teicher, W. M. Linehan, and L. J. Helman, "Targeting Cancer Metabolism," *Clin. Cancer Res.*, vol. 18, no. 20, pp. 5537–5545, Oct. 2012.

[168] K. Ikegami *et al.*, "Identification of circadian clock modulators from existing drugs," *EMBO Mol. Med.*, vol. 10, no. 5, p. e8724, 2018.

[169] Z. Chen, S.-H. Yoo, and J. S. Takahashi, "Development and Therapeutic Potential of Small-Molecule Modulators of Circadian Systems," *Annu. Rev. Pharmacol. Toxicol.*, vol. 58, no. 1, pp. 231–252, 2017.

[170] G. H. Son, S. Chung, V. D. Ramirez, and K. Kim, "Pharmacological Modulators of Molecular Clock and their Therapeutic Potentials in Circadian Rhythm-Related Diseases," *Med. Chem. (Los. Angeles).*, vol. 6, no. 12, pp. 724–733, 2017.

[171] T. Wallach and A. Kramer, “Chemical chronobiology: Toward drugs manipulating time,” *FEBS Lett.*, vol. 589, no. April, pp. 1530–1538, 2015.

[172] M. P. Antoch and R. V. Kondratov, “Pharmacological Modulators of the Circadian Clock as Potential Therapeutic Drugs: Focus on Genotoxic/Anticancer Therapy,” vol. 217, no. 217, A. Kramer and M. Merrow, Eds. Berlin, Heidelberg: Springer Berlin Heidelberg, 2013, pp. 289–309.

[173] Y. . Hu *et al.*, “Selenium is a modulator of circadian clock that protects mice from the toxicity of a chemotherapeutic drug via upregulation of the core clock protein, BMAL1,” *Oncotarget*, vol. 2, no. 12, pp. 1279–1290, 2011.

6. Supplementary information

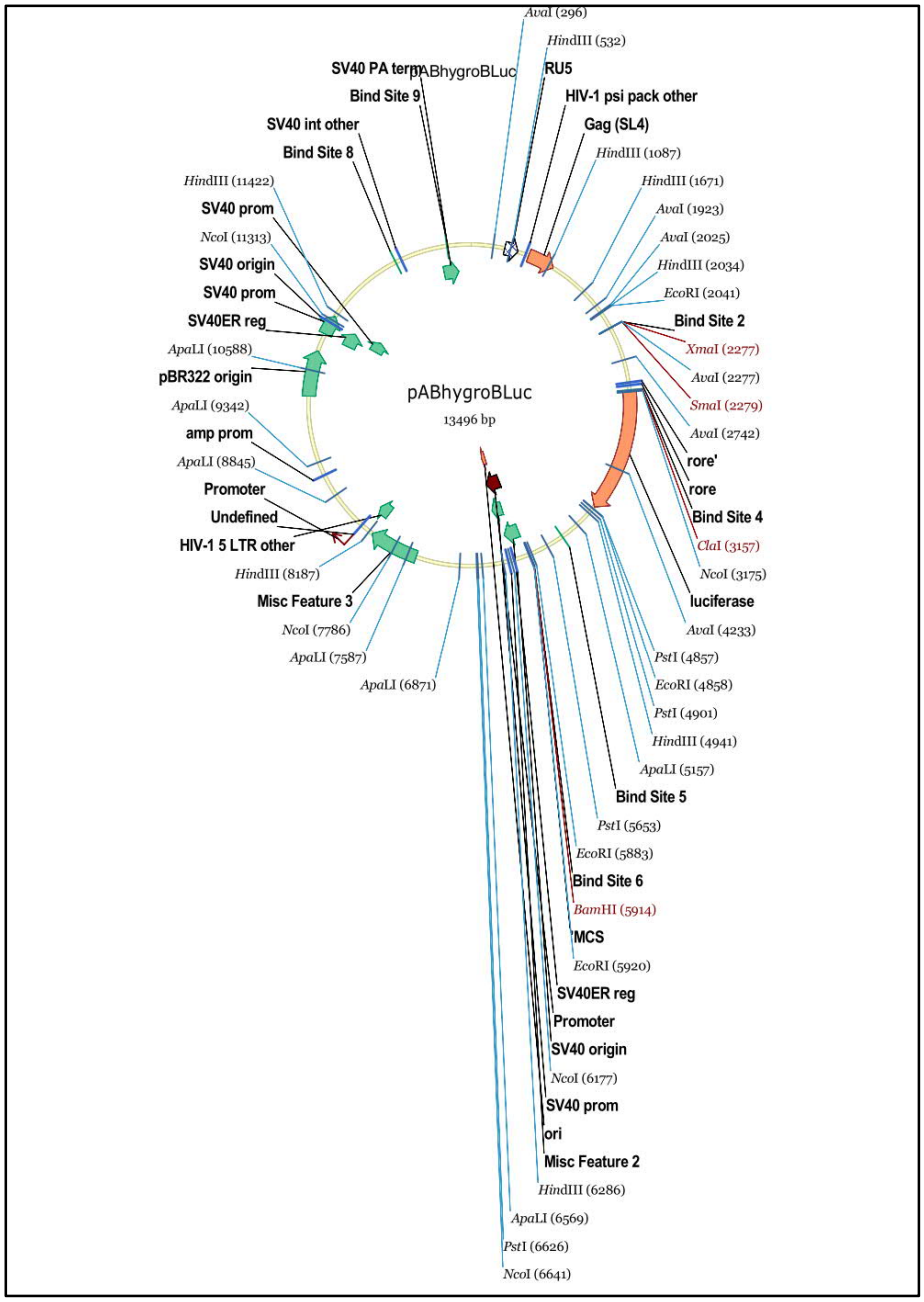

Figure S 1: Vector map of the BLH vector
BLH (*Bmal1*-promoter-Luciferase-Hygromycin) vector. The luciferase is under the control of the *Bmal1*-promoter. The selection marker is hygromycin.

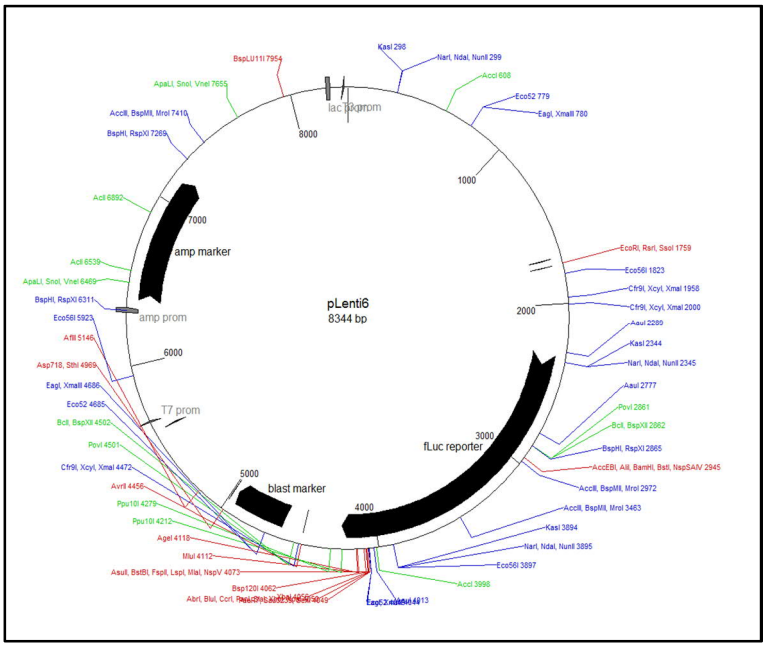

Figure S 2: Vector map of the PLB vector
PLB (*Per2*-promoter-Luciferase-Hygromycin) vector. The luciferase is under the control of the *Per2*-promoter. The selection marker is blasticidin.

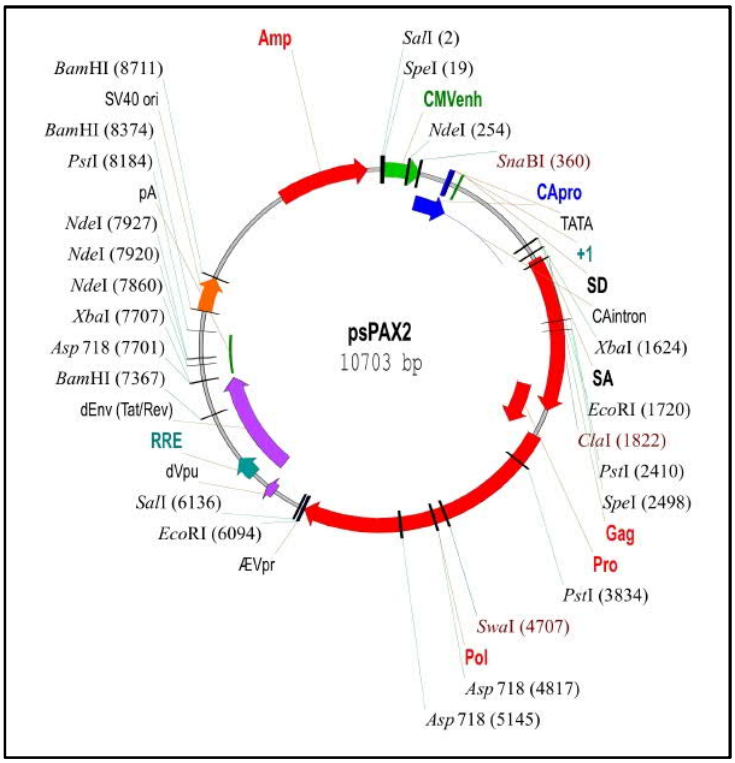

Figure S 3: Vector map of the psPAX2 packaging vector

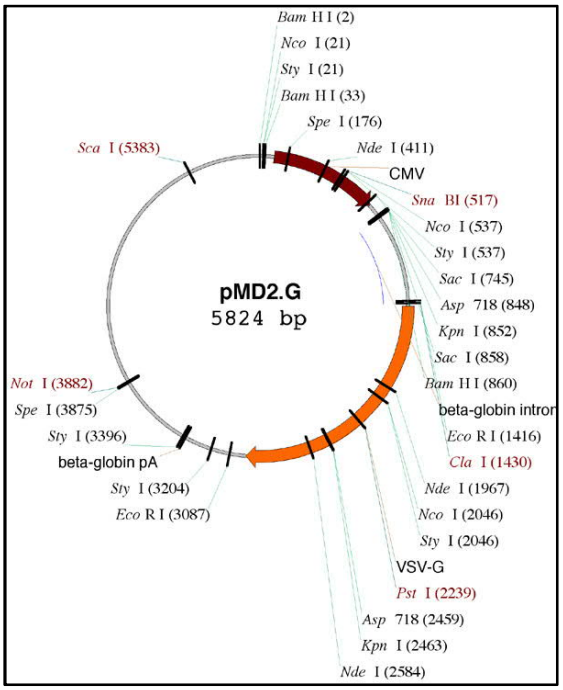

Figure S 4: Vector map of the pMD2.G envelope plasmid

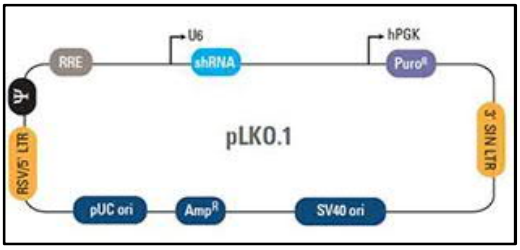

Figure S 5: Vector map of the pLKO.1 plasmid

Table S 1: Mean period with SEM of different tested colorectal cancer cell lines
Cells were lentivirally transduced with a *Bmal1*-luciferase construct (BLH) and synchronised with 1µM dexamethasone for 30 minutes. Bioluminescence was measured over five days. The mean period and SEM were calculated based on three replicates.

Cell line	Period (h)	SEM
CaCo2	45.37	11.81
Colo678	26.70	0.09
DLD1	22.63	0.15
HCT116	23.18	0.31
HT29	26.57	5.12
LIM1215	22.01	0.63
RKO	35.85	1.63
SW480	23.79	0.70
SW620	28.31	1.77

Table S 2: RAIN and harmonic regression analysis of core-clock and metabolic candidate genes.
Data are derived from 45 h time course qPCR. Adapted from **Fuhr** *et al*., 2018 [1].

RT-qPCR Data (Harmonic Regression)												RAIN	
Gene	SW480					SW620					Phase shift (SW480-SW620)	SW480	SW620
	Period	p-value	Relative Amplitude	Phase	Mesor	Period	p-value	Relative Amplitude	Phase	Mesor		p-value	p-value
Bmal1	26.1	2.2E-05	0.385	8.0	1.11	21.2	3.9E-03	0.301	21.3	1.10	-13.3	9.8E-06	2.6E-02
Per2	20.2	2.5E-03	0.346	4.6	1.16	23.1	2.7E-01	0.129	21.4	1.09	-16.8	1.2E-09	3.7E-03
Cry1	28	1.3E-02	0.339	3.4	1.22	28	1.1E-03	0.365	1.0	1.12	2.4	1.8E-04	4.7E-06
Cry2	28	4.3E-01	0.315	8.6	1.53	27.3	2.0E-03	0.552	7.8	1.23	0.9	9.9E-01	6.3E-05
Reverba	20	6.9E-02	0.321	18.3	1.23	28	3.1E-04	0.576	20.8	1.25	-2.5	8.4E-01	3.6E-05
Pdhb	28	1.7E-03	0.465	2.7	1.31	20.1	1.8E-02	0.130	4.7	1.02	-2.1	2.8E-03	2.4E-03
Pck2	20	5.4E-02	0.347	2.7	1.36	21.7	4.2E-02	0.129	1.4	1.03	1.3	8.4E-02	6.4E-02
Aldoc	20.5	2.6E-01	0.297	4.1	1.63	28	1.0E-04	0.284	12.5	1.08	-8.4	1.9E-02	8.8E-04
Aldh3a2	28	1.2E-02	0.465	3.2	1.44	20	3.3E-03	0.228	3.1	1.06	0.1	7.5E-01	1.7E-02
Hkdc1	28	5.7E-04	0.562	3.7	1.48	28	1.6E-05	0.353	16.8	1.10	-13.1	8.3E-04	2.8E-08

Table S 3: Rain analysis of core-clock genes in SW480 and SW620 cells
Rain analysis was performed with 24 h time course microarray data. P-values < 0.05 are marked in green, p-values > 0.05 are marked in red.

Gene	SW480 p-value	SW620 p-value
Bmal1	0.006111224	> 0.05
Bmal2	> 0.05	> 0.05
Cry1	0.012131716	> 0.05
Cry2	> 0.05	> 0.05
Clock	> 0.05	> 0.05
Npas2	> 0.05	0.022373697
Rora	0.043383585	> 0.05
Rorb	> 0.05	> 0.05
Rorc	> 0.05	> 0.05
Rev-erba	0.011438475	> 0.05
Rev-erbb	0.008786381	0.002249272
Per1	0.004265529	0.028788217
Per2	0.031167244	0.004398827
Per3	0.006111224	> 0.05

Table S 4: Over-representation analysis of top differentially expressed genes, pathway based
All differentially expressed genes between SW480 and SW620 cells were taken into account with lfc > 2 and p < 0.001.

p-value	pathway	source
1.41E-05	Validated transcriptional targets of TAp63 isoforms	PID
9.52E-05	Validated transcriptional targets of deltaNp63 isoforms	PID
0.000187427	Extracellular vesicle-mediated signaling in recipient cells	Wikipathways
0.000225801	Axon guidance - Homo sapiens (human)	KEGG
0.000430668	Wnt Signaling Pathway and Pluripotency	Wikipathways
0.000497315	p53 signaling pathway - Homo sapiens (human)	KEGG
0.000724733	Hippo signaling pathway - Homo sapiens (human)	KEGG
0.000910717	Transcriptional regulation of pluripotent stem cells	Wikipathways
0.001235166	Signaling Pathways in Glioblastoma	Wikipathways
0.001604464	Pathways in cancer - Homo sapiens (human)	KEGG
0.001888413	Paclitaxel Action Pathway	SMPDB
0.001888413	Docetaxel Action Pathway	SMPDB
0.002439395	Direct p53 effectors	PID
0.00267005	Cell-cell junction organization	Reactome
0.003196557	retinoate biosynthesis I	HumanCyc
0.003196557	Pravastatin Pathway, Pharmacokinetics	PharmGKB
0.005415293	Adherens junction - Homo sapiens (human)	KEGG
0.005415293	Primary Focal Segmental Glomerulosclerosis FSGS	Wikipathways
0.006753106	il-10 anti-inflammatory signaling pathway	BioCarta
0.006753106	Taxane Pathway, Pharmacokinetics	PharmGKB
0.006753106	Methotrexate Pathway, Pharmacokinetics	PharmGKB
0.007829117	Atorvastatin/Lovastatin/Simvastatin Pathway, Pharmacokinetics	PharmGKB
0.008217788	Urokinase-type plasminogen activator (uPA) and uPAR-mediated signaling	PID
0.009318316	a6b1 and a6b4 Integrin signaling	PID
0.009603683	Cell junction organization	Reactome
0.009993034	Hematopoietic cell lineage - Homo sapiens (human)	KEGG

Table S 5: Over-representation analysis of top differentially expressed genes, GO terms
All differentially expressed genes between SW480 and SW620 cells were taken into account with lfc > 2 and p < 0.001.

p-value	term_category	term_name
1.61E-08	b	positive regulation of cell communication
2.67E-07	b	regulation of programmed cell death
4.73E-07	b	apoptotic process
7.14E-07	b	positive regulation of macromolecule metabolic process
1.07E-06	b	epithelial cell differentiation
1.80E-06	b	positive regulation of cell death
1.99E-06	b	positive regulation of signal transduction
4.29E-06	b	positive regulation of cellular metabolic process
7.35E-06	b	positive regulation of cell differentiation
1.60E-05	b	neurogenesis
2.39E-05	b	neuron differentiation
5.25E-05	b	leukocyte differentiation

5.79E-05	b	positive regulation of biosynthetic process
6.57E-05	b	axon guidance
7.66E-05	c	apical dendrite
0.000100991	b	mammary gland morphogenesis
0.000117053	b	regulation of intracellular signal transduction
0.000218985	b	cell morphogenesis involved in differentiation
0.000226766	b	regulation of epithelial cell proliferation
0.00024409	b	salivary gland morphogenesis
0.000252268	b	kidney epithelium development
0.000274606	b	axon development
0.000314784	b	positive regulation of nervous system development
0.000338907	b	eye morphogenesis
0.000405577	b	stem cell differentiation
0.000430845	b	homophilic cell adhesion via plasma membrane adhesion molecules
0.000477846	b	regulation of cellular protein metabolic process
0.0006051	b	negative regulation of cellular component movement
0.0007661	b	morphogenesis of an epithelial sheet
0.00077592	b	glial cell differentiation
0.00086486	m	transcriptional activator activity, RNA polymerase II core promoter proximal region sequence-specific binding
0.000881994	b	regulation of protein metabolic process
0.00115633	b	regulation of cell development
0.001179953	b	calcium-independent cell-cell adhesion via plasma membrane cell-adhesion molecules
0.001179953	b	branching involved in salivary gland morphogenesis
0.001286036	b	regulation of Wnt signaling pathway
0.001332245	b	regulation of insulin-like growth factor receptor signaling pathway
0.001458414	b	negative regulation of cell proliferation
0.001461174	b	positive regulation of cell adhesion
0.001500647	b	negative regulation of cell communication
0.001568083	b	regulation of secondary metabolite biosynthetic process
0.001570582	b	cell surface receptor signaling pathway
0.001614836	b	negative regulation of leukocyte activation
0.001615225	b	epidermis development
0.001690867	b	regulation of interleukin-8 production
0.001692798	b	negative regulation of response to external stimulus
0.001916087	m	ubiquitin protein ligase binding
0.002075534	b	myelination
0.002078709	b	retinoic acid biosynthetic process
0.002078709	m	axon guidance receptor activity
0.002130877	b	mesenchymal cell development
0.002248714	b	negative regulation of signal transduction
0.002471807	b	epithelial cell migration
0.002679048	b	positive regulation of nitrogen compound metabolic process
0.002850607	b	negative regulation of cell activation
0.002894657	b	positive regulation of cellular component organization
0.002971823	b	negative regulation of cell adhesion

0.003329158	b	regulation of nervous system development
0.003910836	b	intracellular signal transduction
0.003918285	b	mammary gland epithelium development
0.004012977	b	terpenoid biosynthetic process
0.004114258	b	T cell mediated immunity
0.004166679	b	embryonic axis specification
0.004186821	b	regulation of lipid biosynthetic process
0.004186821	b	regulation of epithelial cell differentiation
0.004316752	b	central nervous system neuron development
0.0046561	b	muscle cell differentiation
0.004787853	b	myelin maintenance
0.005743005	b	regulation of cell-cell adhesion
0.006465988	b	negative regulation of cell death
0.006525736	b	astrocyte development
0.006525736	b	tripartite regional subdivision
0.006859973	b	regulation of cytokine secretion
0.007016702	b	cellular response to lipid
0.007229704	b	cell differentiation involved in kidney development
0.008506827	b	cardiac right ventricle morphogenesis
0.008506827	b	renal filtration cell differentiation
0.008645037	b	anterior/posterior axis specification
0.009585771	b	pericardium development
0.009672498	b	negative regulation of behavior

Table S 6: Over-representation analysis of genes oscillating in SW480 and SW620 cells

p-value	pathway	source
2.09E-30	S Phase	Reactome
5.64E-28	Cell Cycle, Mitotic	Reactome
2.47E-26	DNA Replication	Reactome
3.56E-26	Cell Cycle	Reactome
1.07E-25	Synthesis of DNA	Reactome
1.32E-24	DNA strand elongation	Reactome
8.85E-23	DNA replication - Homo sapiens (human)	KEGG
5.80E-20	DNA Replication	Wikipathways
8.18E-20	Chromosome Maintenance	Reactome
7.64E-19	Telomere Maintenance	Reactome
1.02E-17	G1/S Transition	Reactome
2.09E-17	Retinoblastoma (RB) in Cancer	Wikipathways
2.43E-16	Mitotic G1-G1/S phases	Reactome
3.44E-16	DNA Replication Pre-Initiation	Reactome
3.44E-16	M/G1 Transition	Reactome
1.43E-15	Activation of the pre-replicative complex	Reactome
1.21E-14	Extension of Telomeres	Reactome
1.34E-14	Telomere C-strand (Lagging Strand) Synthesis	Reactome
6.78E-14	Unwinding of DNA	Reactome
3.86E-13	Cell Cycle Checkpoints	Reactome
4.39E-13	Activation of ATR in response to replication stress	Reactome
8.10E-13	G2/M Checkpoints	Reactome

1.16E-12	Lagging Strand Synthesis	Reactome
3.36E-12	Resolution of AP sites via the multiple-nucleotide patch replacement pathway	Reactome
3.98E-12	G1 to S cell cycle control	Wikipathways
3.91E-11	M Phase	Reactome
9.10E-11	Processive synthesis on the lagging strand	Reactome
9.10E-11	Gap-filling DNA repair synthesis and ligation in GG-NER	Reactome
9.10E-11	Gap-filling DNA repair synthesis and ligation in TC-NER	Reactome
9.23E-11	PCNA-Dependent Long Patch Base Excision Repair	Reactome
1.75E-10	Mismatch repair - Homo sapiens (human)	KEGG
2.20E-10	DNA Repair	Reactome
2.38E-10	Resolution of Abasic Sites (AP sites)	Reactome
2.38E-10	Base Excision Repair	Reactome
2.48E-10	Removal of the Flap Intermediate	Reactome
2.48E-10	Cell Cycle	Wikipathways
4.65E-10	Removal of licensing factors from origins	Reactome
4.65E-10	Regulation of DNA replication	Reactome
7.97E-10	cdk regulation of dna replication	BioCarta
8.61E-10	Repair synthesis of patch ~27-30 bases long by DNA polymerase	Reactome
8.61E-10	Repair synthesis for gap-filling by DNA polymerase in TC-NER	Reactome
1.02E-09	Parkin-Ubiquitin Proteasomal System pathway	Wikipathways
1.95E-09	Proteasome Degradation	Wikipathways
2.66E-09	Mitotic Prophase	Reactome
4.65E-09	Assembly of the pre-replicative complex	Reactome
6.81E-09	ATR signaling pathway	PID
7.95E-09	Mismatch repair (MMR) directed by MSH2:MSH6 (MutSalpha)	Reactome
7.95E-09	Polymerase switching on the C-strand of the telomere	Reactome
7.95E-09	Polymerase switching	Reactome
7.95E-09	Leading Strand Synthesis	Reactome
2.07E-08	Orc1 removal from chromatin	Reactome
2.07E-08	Switching of origins to a post-replicative state	Reactome
2.21E-08	Mismatch Repair	Reactome
2.37E-08	Processive synthesis on the C-strand of the telomere	Reactome
3.69E-08	Processing of Capped Intron-Containing Pre-mRNA	Reactome
5.83E-08	Translesion synthesis by Y family DNA polymerases bypasses lesions on DNA template	Reactome
6.41E-08	Recognition of DNA damage by PCNA-containing replication complex	Reactome
6.57E-08	Removal of the Flap Intermediate from the C-strand	Reactome
8.15E-08	Base excision repair - Homo sapiens (human)	KEGG
1.23E-07	Transcriptional regulation by small RNAs	Reactome
1.29E-07	Proteasome - Homo sapiens (human)	KEGG
1.52E-07	Pyrimidine metabolism - Homo sapiens (human)	KEGG
1.86E-07	Mismatch repair (MMR) directed by MSH2:MSH3 (MutSbeta)	Reactome
1.98E-07	Global Genomic NER (GG-NER)	Reactome
2.63E-07	DNA Damage Bypass	Reactome
2.81E-07	Cellular Senescence	Reactome
3.11E-07	Packaging Of Telomere Ends	Reactome
3.69E-07	Nucleotide excision repair - Homo sapiens (human)	KEGG
3.69E-07	Transcription-coupled NER (TC-NER)	Reactome
4.00E-07	Cellular responses to stress	Reactome
4.05E-07	Cell cycle - Homo sapiens (human)	KEGG

4.58E-07	DNA methylation	Reactome
5.05E-07	Translesion Synthesis by POLH	Reactome
6.60E-07	Mismatch repair	Wikipathways
7.99E-07	Cytosolic tRNA aminoacylation	Reactome
8.06E-07	Regulatory RNA pathways	Reactome
8.35E-07	Oxidative Stress Induced Senescence	Reactome
9.68E-07	Viral carcinogenesis - Homo sapiens (human)	KEGG
1.16E-06	E2F transcription factor network	PID
1.50E-06	Termination of translesion DNA synthesis	Reactome
1.53E-06	Disease	Reactome
1.73E-06	Nucleotide Excision Repair	Reactome
2.28E-06	RHO GTPase Effectors	Reactome
2.40E-06	Gene Expression	Reactome
3.19E-06	PRC2 methylates histones and DNA	Reactome
3.53E-06	Activated PKN1 stimulates transcription of AR (androgen receptor) regulated genes KLK2 and KLK3	Reactome
3.64E-06	Deposition of new CENPA-containing nucleosomes at the centromere	Reactome
3.64E-06	Nucleosome assembly	Reactome
3.98E-06	Condensation of Prophase Chromosomes	Reactome
4.34E-06	tRNA charging	HumanCyc
4.86E-06	Amyloids	Reactome
4.86E-06	Meiotic recombination	Reactome
4.93E-06	Meiosis	Reactome
6.16E-06	TLR JNK	INOH
6.16E-06	IL-1 JNK	INOH
6.16E-06	RNA Polymerase I Promoter Opening	Reactome
7.23E-06	mRNA Processing	Wikipathways
7.61E-06	BARD1 signaling events	PID
7.77E-06	TLR p38	INOH
7.99E-06	HATs acetylate histones	Reactome
8.84E-06	Pyrimidine metabolism	EHMN
9.74E-06	IL-1 NFkB	INOH
9.74E-06	DroToll-like	INOH
1.06E-05	Glucose metabolism	Reactome
1.06E-05	RMTs methylate histone arginines	Reactome
1.12E-05	RHO GTPases activate PKNs	Reactome
1.12E-05	Mitotic Anaphase	Reactome
1.15E-05	mRNA Splicing - Major Pathway	Reactome
1.15E-05	mRNA Splicing	Reactome
1.17E-05	Meiotic synapsis	Reactome
1.22E-05	Senescence-Associated Secretory Phenotype (SASP)	Reactome
1.30E-05	Mitotic Metaphase and Anaphase	Reactome
1.44E-05	miR-targeted genes in epithelium - TarBase	Wikipathways
1.51E-05	IL-1 p38	INOH
1.51E-05	TNF	INOH
1.51E-05	tRNA Aminoacylation	Reactome
1.63E-05	E2F mediated regulation of DNA replication	Reactome
1.80E-05	Folding of actin by CCT/TriC	Reactome
1.86E-05	Telomere C-strand synthesis initiation	Reactome
1.86E-05	DNA replication initiation	Reactome

1.86E-05	Pyrimidine biosynthesis	Reactome
1.86E-05	SIRT1 negatively regulates rRNA Expression	Reactome
2.36E-05	Gemcitabine Action Pathway	SMPDB
2.36E-05	Gemcitabine Metabolism Pathway	SMPDB
2.53E-05	Chromatin modifying enzymes	Reactome
2.53E-05	Chromatin organization	Reactome
2.56E-05	Translation Factors	Wikipathways
2.75E-05	RNA Polymerase I Chain Elongation	Reactome
2.80E-05	TLR NFkB	INOH
3.35E-05	NoRC negatively regulates rRNA expression	Reactome
3.56E-05	Amino acid synthesis and interconversion (transamination)	Reactome
3.91E-05	Pyrimidine Metabolism	SMPDB
3.91E-05	UMP Synthase Deiciency (Orotic Aciduria)	SMPDB
3.91E-05	MNGIE (Mitochondrial Neurogastrointestinal Encephalopathy)	SMPDB
3.91E-05	Beta Ureidopropionase Deficiency	SMPDB
3.91E-05	Dihydropyrimidinase Deficiency	SMPDB
4.15E-05	Apoptotic execution phase	Reactome
4.22E-05	Resolution of Sister Chromatid Cohesion	Reactome
4.64E-05	Metabolism	Reactome
4.67E-05	Transcription	Reactome
5.20E-05	Homologous recombination - Homo sapiens (human)	KEGG
5.23E-05	RNA Polymerase I Promoter Clearance	Reactome
5.23E-05	Negative epigenetic regulation of rRNA expression	Reactome
5.23E-05	Mitotic Prometaphase	Reactome
5.71E-05	Nucleotide Metabolism	Wikipathways
5.97E-05	Epstein-Barr virus infection - Homo sapiens (human)	KEGG
6.24E-05	Separation of Sister Chromatids	Reactome
6.35E-05	Epigenetic regulation of gene expression	Reactome
6.40E-05	miR-targeted genes in lymphocytes - TarBase	Wikipathways
6.63E-05	Validated targets of C-MYC transcriptional activation	PID
6.95E-05	RNA Polymerase I Transcription	Reactome
7.23E-05	CD4 T cell receptor signaling-NFkB cascade	INOH
7.66E-05	SCF(Skp2)-mediated degradation of p27/p21	Reactome
0.000101	Transport of Mature Transcript to Cytoplasm	Reactome
0.000127	Translesion synthesis by REV1	Reactome
0.000135	Cyclin D associated events in G1	Reactome
0.000135	G1 Phase	Reactome
0.000143	Pyrimidine nucleotides nucleosides metabolism	INOH
0.000144	HDACs deacetylate histones	Reactome
0.000144	Metabolism of amino acids and derivatives	Reactome
0.000149	Hedgehog	INOH
0.000151	Recycling of eIF2:GDP	Reactome
0.00016	Inhibition of replication initiation of damaged DNA by RB1/E2F1	Reactome
0.000167	AndrogenReceptor	NetPath
0.000168	Regulation of HSF1-mediated heat shock response	Reactome
0.000175	Signaling events mediated by HDAC Class III	PID
0.000177	Transport of Mature mRNA derived from an Intron-Containing Transcript	Reactome
0.000181	Protein processing in endoplasmic reticulum - Homo sapiens (human)	KEGG
0.000194	pyrimidine deoxyribonucleosides salvage	HumanCyc
0.000194	superpathway of pyrimidine deoxyribonucleotides de novo biosynthesis	HumanCyc

0.000194	Cyclin E associated events during G1/S transition	Reactome
0.000201	Translesion synthesis by POLK	Reactome
0.000201	Translesion synthesis by POLI	Reactome
0.000202	Fanconi anemia pathway	PID
0.000254	Cellular response to heat stress	Reactome
0.00026	DNA Damage Response	Wikipathways
0.000266	Mitochondrial protein import	Reactome
0.000277	Antigen Presentation: Folding, assembly and peptide loading of class I MHC	Reactome
0.000277	Cyclin A:Cdk2-associated events at S phase entry	Reactome
0.000278	regulation of p27 phosphorylation during cell cycle progression	BioCarta
0.000294	RHO GTPases Activate Formins	Reactome
0.000317	Type I hemidesmosome assembly	Reactome
0.000317	btg family proteins and cell cycle regulation	BioCarta
0.000387	Pyrimidine metabolism	Reactome
0.000392	Infectious disease	Reactome
0.000433	B cell receptor signaling	INOH
0.000453	CDT1 association with the CDC6:ORC:origin complex	Reactome
0.00048	Purine metabolism	EHMN
0.000529	IL-7 Signaling Pathway	Wikipathways
0.000529	cell cycle: g1/s check point	BioCarta
0.000533	Metabolism of nucleotides	Reactome
0.000558	Urea cycle and metabolism of arginine, proline, glutamate, aspartate and asparagine	EHMN
0.000593	Gemcitabine Pathway, Pharmacodynamics	PharmGKB
0.000631	Aminoacyl-tRNA biosynthesis - Homo sapiens (human)	KEGG
0.000632	Apoptotic cleavage of cellular proteins	Reactome
0.000632	Regulation of mRNA stability by proteins that bind AU-rich elements	Reactome
0.000632	miRNA Regulation of DNA Damage Response	Wikipathways
0.000645	Arginine biosynthesis - Homo sapiens (human)	KEGG
0.000645	Urea cycle and metabolism of amino groups	Wikipathways
0.000645	S-Adenosylhomocysteine (SAH) Hydrolase Deficiency	SMPDB
0.000645	Methionine Metabolism	SMPDB
0.000645	Methionine Adenosyltransferase Deficiency	SMPDB
0.000645	Glycine N-methyltransferase Deficiency	SMPDB
0.000645	Hypermethioninemia	SMPDB
0.000645	Methylenetetrahydrofolate Reductase Deficiency (MTHFRD)	SMPDB
0.000645	Homocystinuria-megaloblastic anemia due to defect in cobalamin metabolism, cblG complementation type	SMPDB
0.000645	Cystathionine Beta-Synthase Deficiency	SMPDB
0.000646	Metabolism of proteins	Reactome
0.000773	RNA Polymerase I, RNA Polymerase III, and Mitochondrial Transcription	Reactome
0.000787	Signaling by Rho GTPases	Reactome
0.000823	Fanconi anemia pathway - Homo sapiens (human)	KEGG
0.000823	Apoptosis-related network due to altered Notch3 in ovarian cancer	Wikipathways
0.000824	formation of the beta-catenin:TCF transactivating complex	Reactome
0.000886	Transport of the SLBP Dependant Mature mRNA	Reactome
0.000901	Formation of tubulin folding intermediates by CCT/TriC	Reactome
0.000912	HIV Life Cycle	Reactome
0.00094	Prefoldin mediated transfer of substrate to CCT/TriC	Reactome
0.001003	Triglyceride Biosynthesis	Reactome

0.001015	Nucleotide Excision Repair	SMPDB
0.001048	G2/M DNA damage checkpoint	Reactome
0.00105	G1/S DNA Damage Checkpoints	Reactome
0.001121	Interactions of Vpr with host cellular proteins	Reactome
0.001166	Pathogenic Escherichia coli infection - Homo sapiens (human)	KEGG
0.00119	POLB-Dependent Long Patch Base Excision Repair	Reactome
0.00119	AUF1 (hnRNP D0) destabilizes mRNA	Reactome
0.001201	Glycine Serine metabolism	INOH
0.001203	Methionine and cysteine metabolism	EHMN
0.001208	HDMs demethylate histones	Reactome
0.001225	influence of ras and rho proteins on g1 to s transition	BioCarta
0.001225	Cooperation of Prefoldin and TriC/CCT in actin and tubulin folding	Reactome
0.001362	HIV Infection	Reactome
0.001377	Pathogenic Escherichia coli infection	Wikipathways
0.001377	Notch	INOH
0.001403	Alanine, aspartate and glutamate metabolism - Homo sapiens (human)	KEGG
0.001465	FOXM1 transcription factor network	PID
0.001489	Regulation of retinoblastoma protein	PID
0.001547	CD4 T cell receptor signaling	INOH
0.001574	Regulation of cholesterol biosynthesis by SREBP (SREBF)	Reactome
0.00162	Influenza Infection	Reactome
0.001626	mechanism of protein import into the nucleus	BioCarta
0.001649	cyclins and cell cycle regulation	BioCarta
0.00174	Transport of Mature mRNAs Derived from Intronless Transcripts	Reactome
0.001944	TGF-beta super family signaling pathway canonical	INOH
0.001945	Hypusine synthesis from eIF5A-lysine	Reactome
0.001945	Phosphorylation of proteins involved in G1/S transition by active Cyclin E:Cdk2 complexes	Reactome
0.001996	TSH signaling pathway	Wikipathways
0.001996	Pancreatic cancer - Homo sapiens (human)	KEGG
0.001997	Oncogene Induced Senescence	Reactome
0.002068	Spliceosome - Homo sapiens (human)	KEGG
0.002138	Squalene and cholesterol biosynthesis	EHMN
0.002168	Fluoropyrimidine Pathway, Pharmacokinetics	PharmGKB
0.002187	Organelle biogenesis and maintenance	Reactome
0.002229	Tenofovir/Adefovir Pathway, Pharmacokinetics	PharmGKB
0.002229	CDC6 association with the ORC:origin complex	Reactome
0.002272	Systemic lupus erythematosus - Homo sapiens (human)	KEGG
0.002469	p53 signaling pathway	BioCarta
0.002469	p53-Dependent G1 DNA Damage Response	Reactome
0.002469	p53-Dependent G1/S DNA damage checkpoint	Reactome
0.002469	cholesterol biosynthesis I	HumanCyc
0.002469	Antimetabolite Pathway - Folate Cycle, Pharmacodynamics	PharmGKB
0.002469	cholesterol biosynthesis II (via 24,25-dihydrolanosterol)	HumanCyc
0.002469	cholesterol biosynthesis III (via desmosterol)	HumanCyc
0.002469	Homologous recombination	Wikipathways
0.002506	Trans-sulfuration and one carbon metabolism	Wikipathways
0.002506	HSF1 activation	Reactome
0.002506	Folate metabolism	INOH
0.002506	Vpr-mediated nuclear import of PICs	Reactome

0.002675	RNA transport - Homo sapiens (human)	KEGG
0.002806	skeletal muscle hypertrophy is regulated via akt-mtor pathway	BioCarta
0.002806	regulation of eif-4e and p70s6 kinase	BioCarta
0.002806	superpathway of cholesterol biosynthesis	HumanCyc
0.002806	Fatty Acyl-CoA Biosynthesis	Reactome
0.002806	Alanine Aspartate Asparagine metabolism	INOH
0.002887	Pre-NOTCH Transcription and Translation	Reactome
0.00311	Gluconeogenesis	Reactome
0.00311	Glycolysis	Reactome
0.00311	Rev-mediated nuclear export of HIV RNA	Reactome
0.00311	Thiopurine Pathway, Pharmacokinetics/Pharmacodynamics	PharmGKB
0.00311	Transport of the SLBP independent Mature mRNA	Reactome
0.003287	Small cell lung cancer - Homo sapiens (human)	KEGG
0.003438	Apoptosis	Reactome
0.003578	C-MYC pathway	PID
0.003578	Vitamin B9 (folate) metabolism	EHMN
0.003685	Host Interactions of HIV factors	Reactome
0.003758	Urea cycle	Reactome
0.003758	Sepiapterin reductase deficiency	SMPDB
0.003758	Segawa syndrome	SMPDB
0.003758	Pterine Biosynthesis	SMPDB
0.003758	Dopa-responsive dystonia	SMPDB
0.003758	Hyperphenylalaniemia due to guanosine triphosphate cyclohydrolase deficiency	SMPDB
0.003758	Hyperphenylalaninemia due to 6-pyruvoyltetrahydropterin synthase deficiency (ptps)	SMPDB
0.003758	Hyperphenylalaninemia due to dhpr-deficiency	SMPDB
0.003758	cycling of ran in nucleocytoplasmic transport	BioCarta
0.003818	Copper homeostasis	Wikipathways
0.003821	Fluoropyrimidine Activity	Wikipathways
0.0039	miR-targeted genes in muscle cell - TarBase	Wikipathways
0.004501	One Carbon Metabolism	Wikipathways
0.004501	DNA Damage/Telomere Stress Induced Senescence	Reactome
0.004506	Intraflagellar transport	Reactome
0.004572	Assembly of the RAD51-ssDNA nucleoprotein complex	Reactome
0.004572	dTMP de novo biosynthesis (mitochondrial)	HumanCyc
0.004572	folate polyglutamylation	HumanCyc
0.004572	fructose 2,6-bisphosphate synthesis	HumanCyc
0.004587	Programmed Cell Death	Reactome
0.004912	Alcoholism - Homo sapiens (human)	KEGG
0.005027	TSLP	NetPath
0.005032	Methotrexate Pathway (Cancer Cell), Pharmacodynamics	PharmGKB
0.005032	Early Phase of HIV Life Cycle	Reactome
0.005032	Unfolded Protein Response (UPR)	Reactome
0.005593	Glyoxylate and dicarboxylate metabolism - Homo sapiens (human)	KEGG
0.005615	Lysosome Vesicle Biogenesis	Reactome
0.005615	Transport of Mature mRNA Derived from an Intronless Transcript	Reactome
0.0057	Arginine and proline metabolism - Homo sapiens (human)	KEGG
0.0057	snRNP Assembly	Reactome
0.0057	Metabolism of non-coding RNA	Reactome
0.005869	e2f1 destruction pathway	BioCarta

0.005869	ifn alpha signaling pathway	BioCarta
0.006278	FAS pathway and Stress induction of HSP regulation	Wikipathways
0.006358	Hepatitis B - Homo sapiens (human)	KEGG
0.00645	Simvastatin Action Pathway	SMPDB
0.00645	Hyper-IgD syndrome	SMPDB
0.00645	Cholesteryl ester storage disease	SMPDB
0.00645	Lysosomal Acid Lipase Deficiency (Wolman Disease)	SMPDB
0.00645	Mevalonic aciduria	SMPDB
0.00645	Wolman disease	SMPDB
0.00645	Smith-Lemli-Opitz Syndrome (SLOS)	SMPDB
0.00645	Chondrodysplasia Punctata II, X Linked Dominant (CDPX2)	SMPDB
0.00645	CHILD Syndrome	SMPDB
0.00645	Desmosterolosis	SMPDB
0.00645	Hypercholesterolemia	SMPDB
0.00645	Steroid Biosynthesis	SMPDB
0.00645	Pravastatin Action Pathway	SMPDB
0.00645	Atorvastatin Action Pathway	SMPDB
0.00645	Rosuvastatin Action Pathway	SMPDB
0.00645	Lovastatin Action Pathway	SMPDB
0.00645	Cerivastatin Action Pathway	SMPDB
0.00645	Fluvastatin Action Pathway	SMPDB
0.00645	Alendronate Action Pathway	SMPDB
0.00645	Risedronate Action Pathway	SMPDB
0.00645	Pamidronate Action Pathway	SMPDB
0.00645	Zoledronate Action Pathway	SMPDB
0.00645	Ibandronate Action Pathway	SMPDB
0.00645	Lysine degradation	INOH
0.00645	Terpenoid backbone biosynthesis - Homo sapiens (human)	KEGG
0.006451	Influenza Virus Induced Apoptosis	Reactome
0.006451	glycine/serine biosynthesis	HumanCyc
0.006451	UMP biosynthesis	HumanCyc
0.006451	Cytosolic iron-sulfur cluster assembly	Reactome
0.006659	Lysine metabolism	EHMN
0.006722	Interactions of Rev with host cellular proteins	Reactome
0.006763	Purine metabolism - Homo sapiens (human)	KEGG
0.006841	pyrimidine deoxyribonucleotides de novo biosynthesis	HumanCyc
0.006871	NEP/NS2 Interacts with the Cellular Export Machinery	Reactome
0.006871	Transport of Ribonucleoproteins into the Host Nucleus	Reactome
0.007143	TNFalpha	NetPath
0.007343	Cleavage of Growing Transcript in the Termination Region	Reactome
0.007343	RNA Polymerase II Transcription Termination	Reactome
0.007343	Post-Elongation Processing of the Transcript	Reactome
0.007389	Regulation of Telomerase	PID
0.007389	p53 signaling pathway - Homo sapiens (human)	KEGG
0.007591	Influenza Life Cycle	Reactome
0.007918	Antigen processing and presentation - Homo sapiens (human)	KEGG
0.008145	Biosynthesis of unsaturated fatty acids - Homo sapiens (human)	KEGG
0.008145	Cholesterol biosynthesis	Reactome
0.008145	caspase cascade in apoptosis	BioCarta
0.008145	Deadenylation of mRNA	Reactome

0.008488	EGFR1	NetPath
0.008541	RAGE	NetPath
0.008598	Ubiquitin-dependent degradation of Cyclin D1	Reactome
0.008598	Ubiquitin-dependent degradation of Cyclin D	Reactome
0.008598	γ-glutamyl cycle	HumanCyc
0.008598	TP53 Regulates Metabolic Genes	Wikipathways
0.008598	Presynaptic phase of homologous DNA pairing and strand exchange	Reactome
0.008598	IL-10 signaling	INOH
0.008598	CDK-mediated phosphorylation and removal of Cdc6	Reactome
0.008642	Association of licensing factors with the pre-replicative complex	Reactome
0.008642	Hh mutants that don,t undergo autocatalytic processing are degraded by ERAD	Reactome
0.008642	Hh mutants abrogate ligand secretion	Reactome
0.008642	Interleukin-6 signaling	Reactome
0.008642	il22 soluble receptor signaling pathway	BioCarta
0.008642	Establishment of Sister Chromatid Cohesion	Reactome
0.008879	Direct p53 effectors	PID
0.009061	superpathway of pyrimidine deoxyribonucleoside salvage	HumanCyc
0.009545	HTLV-I infection - Homo sapiens (human)	KEGG
0.009931	Interferon type I signaling pathways	Wikipathways

Table S 7: Over-representation analysis of genes oscillating only in SW480 cells

p-value	pathway	source
4.30E-09	HDACs deacetylate histones	Reactome
9.93E-09	Chromatin modifying enzymes	Reactome
9.93E-09	Chromatin organization	Reactome
1.07E-08	RNA Polymerase I, RNA Polymerase III, and Mitochondrial Transcription	Reactome
1.80E-07	RNA Polymerase I Transcription	Reactome
2.34E-07	HATs acetylate histones	Reactome
3.60E-07	RNA Polymerase I Promoter Clearance	Reactome
4.98E-07	Cell Cycle	Reactome
7.06E-07	Aurora B signaling	PID
1.16E-06	RMTs methylate histone arginines	Reactome
1.35E-06	SIRT1 negatively regulates rRNA Expression	Reactome
1.49E-06	M Phase	Reactome
1.89E-06	RHO GTPase Effectors	Reactome
1.99E-06	Signaling by Rho GTPases	Reactome
2.06E-06	Condensation of Prophase Chromosomes	Reactome
3.43E-06	Negative epigenetic regulation of rRNA expression	Reactome
4.20E-06	RNA Polymerase I Chain Elongation	Reactome
4.20E-06	formation of the beta-catenin:TCF transactivating complex	Reactome
4.52E-06	RNA Polymerase I Promoter Opening	Reactome
4.73E-06	Epigenetic regulation of gene expression	Reactome
5.09E-06	Cell Cycle, Mitotic	Reactome
6.22E-06	EGFR1	NetPath
8.29E-06	Transcriptional regulation by small RNAs	Reactome
8.36E-06	Transcription	Reactome
9.55E-06	Meiosis	Reactome
1.28E-05	Amyloids	Reactome

1.28E-05	Meiotic recombination	Reactome
1.54E-05	NoRC negatively regulates rRNA expression	Reactome
1.94E-05	PRC2 methylates histones and DNA	Reactome
2.03E-05	RHO GTPases activate PKNs	Reactome
2.76E-05	Mitotic Prometaphase	Reactome
2.89E-05	DNA methylation	Reactome
4.02E-05	Polo-like kinase mediated events	Reactome
4.22E-05	Lysosome - Homo sapiens (human)	KEGG
4.48E-05	Cellular responses to stress	Reactome
4.81E-05	Activated PKN1 stimulates transcription of AR (androgen receptor) regulated genes KLK2 and KLK3	Reactome
5.01E-05	G2/M DNA damage checkpoint	Reactome
5.09E-05	PLK1 signaling events	PID
9.06E-05	Recruitment of repair and signaling proteins to double-strand breaks	Reactome
9.06E-05	DNA Double Strand Breaks Response	Reactome
9.68E-05	Regulatory RNA pathways	Reactome
0.000114234	Signaling events mediated by HDAC Class I	PID
0.000145706	Factors involved in megakaryocyte development and platelet production	Reactome
0.000185057	Oxidative Stress Induced Senescence	Reactome
0.000226947	Condensation of Prometaphase Chromosomes	Reactome
0.000241343	Systemic lupus erythematosus - Homo sapiens (human)	KEGG
0.000257463	Cellular Senescence	Reactome
0.000329855	Senescence-Associated Secretory Phenotype (SASP)	Reactome
0.00036891	Gene Expression	Reactome
0.000371421	RNA Polymerase III Transcription Termination	Reactome
0.000424944	FOXM1 transcription factor network	PID
0.000585899	HDMs demethylate histones	Reactome
0.000633043	Resolution of Sister Chromatid Cohesion	Reactome
0.00071913	PKMTs methylate histone lysines	Reactome
0.000792444	Kinesins	Reactome
0.00083642	Clathrin derived vesicle budding	Reactome
0.00083642	trans-Golgi Network Vesicle Budding	Reactome
0.000870163	ATM Signaling Pathway	Wikipathways
0.000944467	RHO GTPases Activate Formins	Reactome
0.001009042	Alpha6Beta4Integrin	NetPath
0.001036295	Mitotic Prophase	Reactome
0.00112716	TCF dependent signaling in response to WNT	Reactome
0.001147993	ATM mediated phosphorylation of repair proteins	Reactome
0.001147993	ATM mediated response to DNA double-strand break	Reactome
0.001147993	Mitotic G2-G2-M phases	Wikipathways
0.001153103	RNA Polymerase III Abortive And Retractive Initiation	Reactome
0.001153103	RNA Polymerase III Transcription	Reactome
0.001160279	BMP2 signaling TGF-beta MV	INOH
0.001386299	G2/M Checkpoints	Reactome
0.001446958	Adherens junction - Homo sapiens (human)	KEGG
0.001453483	Cell cycle - Homo sapiens (human)	KEGG
0.001552102	p53 signaling pathway - Homo sapiens (human)	KEGG

0.00203656	E2F transcription factor network	PID
0.002129523	Spliceosome - Homo sapiens (human)	KEGG
0.002227818	Golgi Associated Vesicle Biogenesis	Reactome
0.00231452	Histone Modifications	Wikipathways
0.002610849	RORA activates gene expression	Reactome
0.002672245	Mitotic G2-G2/M phases	Reactome
0.002678169	Direct p53 effectors	PID
0.002711887	Validated transcriptional targets of TAp63 isoforms	PID
0.002853964	cell cycle: g2/m checkpoint	BioCarta
0.002853964	p38 signaling mediated by MAPKAP kinases	PID
0.002947859	Disease	Reactome
0.002980914	Transcriptional misregulation in cancer - Homo sapiens (human)	KEGG
0.00309782	Spermidine and Spermine Biosynthesis	SMPDB
0.003118515	Validated targets of C-MYC transcriptional activation	PID
0.003284364	Alcoholism - Homo sapiens (human)	KEGG
0.003655759	Aurora A signaling	PID
0.004215335	Synthesis of substrates in N-glycan biosythesis	Reactome
0.004335829	G2/M Transition	Reactome
0.004460154	Meiotic synapsis	Reactome
0.004497353	RNA Polymerase III Transcription Initiation From Type 2 Promoter	Reactome
0.004651555	mRNA Splicing - Minor Pathway	Reactome
0.004680258	Fluoropyrimidine Pathway, Pharmacodynamics	PharmGKB
0.004725101	RNA polymerase - Homo sapiens (human)	KEGG
0.004755542	Validated transcriptional targets of AP1 family members Fra1 and Fra2	PID
0.005423447	RNA Polymerase I Transcription Initiation	Reactome
0.005450451	AP-1 transcription factor network	PID
0.005896613	Arylhydrocarbon receptor (AhR) signaling pathway	Wikipathways
0.005896613	RNA Polymerase III Transcription Initiation From Type 1 Promoter	Reactome
0.00646572	TP53 Network	Wikipathways
0.00646572	RNA Polymerase III Chain Elongation	Reactome
0.00646572	regulation of cell cycle progression by plk3	BioCarta
0.00646572	atm signaling pathway	BioCarta
0.006864214	Separation of Sister Chromatids	Reactome
0.007025465	Signaling by TGF-beta Receptor Complex	Reactome
0.007322169	Vitamin K Metabolism	SMPDB
0.007322169	phospholipase c delta in phospholipid associated cell signaling	BioCarta
0.007354011	Homologous recombination repair of replication-independent double-strand breaks	Reactome
0.007354011	Homologous Recombination Repair	Reactome
0.007354011	1D-myo-inositol hexakisphosphate biosynthesis II (mammalian)	HumanCyc
0.007354011	D-myo-inositol (1,3,4)-trisphosphate biosynthesis	HumanCyc
0.007588053	BMP signaling Dro	INOH
0.007608657	RNA Polymerase III Transcription Initiation From Type 3 Promoter	Reactome
0.007608657	Gastric Cancer Network 1	Wikipathways
0.007694008	apoptotic dna-fragmentation and tissue homeostasis	BioCarta
0.007747909	Apoptosis	Wikipathways
0.008859471	Cell Cycle	Wikipathways

0.008859471	HIF-1 signaling pathway - Homo sapiens (human)	KEGG
0.00887877	superpathway of D-myo-inositol (1,4,5)-trisphosphate metabolism	HumanCyc
0.00887877	tgf beta signaling pathway	BioCarta
0.00944541	ATM pathway	PID
0.00944541	HIF-2-alpha transcription factor network	PID
0.009466005	DNA Damage Response	Wikipathways
0.009544442	Signaling by Wnt	Reactome
0.009674878	Fructose Mannose metabolism	INOH

Table S 8: Over-representation analysis of genes oscillating only in SW620 cells

p-value	pathway	source
1.08E-08	proteasome complex	BioCarta
9.47E-08	The citric acid (TCA) cycle and respiratory electron transport	Reactome
1.04E-06	Warburg Effect	SMPDB
1.28E-05	Huntington,s disease - Homo sapiens (human)	KEGG
1.40E-05	Pyruvate metabolism and Citric Acid (TCA) cycle	Reactome
1.63E-05	Pyruvate dehydrogenase deficiency (E3)	SMPDB
1.63E-05	Pyruvate dehydrogenase deficiency (E2)	SMPDB
1.63E-05	2-ketoglutarate dehydrogenase complex deficiency	SMPDB
1.63E-05	Mitochondrial complex II deficiency	SMPDB
1.63E-05	Fumarase deficiency	SMPDB
1.63E-05	Congenital lactic acidosis	SMPDB
1.63E-05	Citric Acid Cycle	SMPDB
1.84E-05	Protein processing in endoplasmic reticulum - Homo sapiens (human)	KEGG
1.97E-05	Asparagine N-linked glycosylation	Reactome
3.12E-05	TNF	INOH
5.95E-05	Metabolism	Reactome
6.52E-05	RNA transport - Homo sapiens (human)	KEGG
7.66E-05	Mitochondrial Electron Transport Chain	SMPDB
8.23E-05	Thyroid cancer - Homo sapiens (human)	KEGG
0.000102855	Electron Transport Chain	Wikipathways
0.000107415	Respiratory electron transport, ATP synthesis by chemiosmotic coupling, and heat production by uncoupling proteins.	Reactome
0.000119469	Parkinson,s disease - Homo sapiens (human)	KEGG
0.000130335	Organelle biogenesis and maintenance	Reactome
0.000187421	Pravastatin Action Pathway	SMPDB
0.000187421	Atorvastatin Action Pathway	SMPDB
0.000187421	Rosuvastatin Action Pathway	SMPDB
0.000187421	Lovastatin Action Pathway	SMPDB
0.000187421	Cerivastatin Action Pathway	SMPDB
0.000187421	Fluvastatin Action Pathway	SMPDB
0.000187421	Simvastatin Action Pathway	SMPDB
0.000187421	Hyper-IgD syndrome	SMPDB
0.000187421	Cholesteryl ester storage disease	SMPDB
0.000187421	Lysosomal Acid Lipase Deficiency (Wolman Disease)	SMPDB
0.000187421	Mevalonic aciduria	SMPDB
0.000187421	Wolman disease	SMPDB

0.000187421	Smith-Lemli-Opitz Syndrome (SLOS)	SMPDB
0.000187421	Chondrodysplasia Punctata II, X Linked Dominant (CDPX2)	SMPDB
0.000187421	CHILD Syndrome	SMPDB
0.000187421	Desmosterolosis	SMPDB
0.000187421	Hypercholesterolemia	SMPDB
0.000187421	Steroid Biosynthesis	SMPDB
0.000187421	Alendronate Action Pathway	SMPDB
0.000187421	Risedronate Action Pathway	SMPDB
0.000187421	Pamidronate Action Pathway	SMPDB
0.000187421	Zoledronate Action Pathway	SMPDB
0.000187421	Ibandronate Action Pathway	SMPDB
0.000210436	N-Glycan biosynthesis	EHMN
0.000279828	Cholesterol biosynthesis	Reactome
0.00029203	Hedgehog	INOH
0.000297685	Signaling events mediated by HDAC Class II	PID
0.00035078	Recruitment of mitotic centrosome proteins and complexes	Reactome
0.00035078	Centrosome maturation	Reactome
0.000378947	Cholesterol Biosynthesis	Wikipathways
0.000406414	Regulation of nuclear beta catenin signaling and target gene transcription	PID
0.000461683	Alzheimer,s disease - Homo sapiens (human)	KEGG
0.000519086	Metabolism of proteins	Reactome
0.000577583	HIV Life Cycle	Reactome
0.000583689	3-Methylglutaconic Aciduria Type I	SMPDB
0.000583689	Valine, Leucine and Isoleucine Degradation	SMPDB
0.000583689	2-Methyl-3-Hydroxybutryl CoA Dehydrogenase Deficiency	SMPDB
0.000583689	Isovaleric Aciduria	SMPDB
0.000583689	3-Methylcrotonyl Coa Carboxylase Deficiency Type I	SMPDB
0.000583689	Propionic Acidemia	SMPDB
0.000583689	Maple Syrup Urine Disease	SMPDB
0.000583689	3-Hydroxy-3-Methylglutaryl-CoA Lyase Deficiency	SMPDB
0.000583689	Isobutyryl-coa dehydrogenase deficiency	SMPDB
0.000583689	3-hydroxyisobutyric aciduria	SMPDB
0.000583689	3-hydroxyisobutyric acid dehydrogenase deficiency	SMPDB
0.000583689	Isovaleric acidemia	SMPDB
0.000583689	Methylmalonate Semialdehyde Dehydrogenase Deficiency	SMPDB
0.000583689	Methylmalonic Aciduria	SMPDB
0.000583689	3-Methylglutaconic Aciduria Type IV	SMPDB
0.000583689	3-Methylglutaconic Aciduria Type III	SMPDB
0.000583689	Beta-Ketothiolase Deficiency	SMPDB
0.000583689	Citrate cycle (TCA cycle) - Homo sapiens (human)	KEGG
0.000584992	Post-translational protein modification	Reactome
0.000613805	TCA Cycle and PDHc	Wikipathways
0.00062429	Androgen receptor signaling pathway	Wikipathways
0.000726218	Mitochondrial translation	Reactome
0.000758689	Peroxisomal lipid metabolism	Reactome
0.000776677	Mitochondrial translation elongation	Reactome

0.000911746	Processing of Capped Intron-Containing Pre-mRNA	Reactome
0.000950885	TCA Cycle	Wikipathways
0.000950885	Bisphosphonate Pathway, Pharmacodynamics	PharmGKB
0.001035737	Benzo(a)pyrene metabolism	Wikipathways
0.001066306	IL-1 p38	INOH
0.001085127	Pyruvate Dehydrogenase Complex Deficiency	SMPDB
0.001085127	Primary hyperoxaluria II, PH2	SMPDB
0.001085127	Pyruvate kinase deficiency	SMPDB
0.001085127	Leigh Syndrome	SMPDB
0.001085127	Pyruvate Metabolism	SMPDB
0.001085127	Pyruvate Decarboxylase E1 Component Deficiency (PDHE1 Deficiency)	SMPDB
0.001085127	Pyruvate metabolism	Reactome
0.001090671	N-Glycan biosynthesis - Homo sapiens (human)	KEGG
0.001090671	Valine, leucine and isoleucine degradation	EHMN
0.001122506	Respiratory electron transport	Reactome
0.001199999	SUMOylation of DNA damage response and repair proteins	Reactome
0.001199999	SUMO E3 ligases SUMOylate target proteins	Reactome
0.001415586	TGF-beta super family signaling pathway canonical	INOH
0.001415586	mRNA Splicing - Major Pathway	Reactome
0.001415586	mRNA Splicing	Reactome
0.001415586	G2/M Transition	Reactome
0.001418181	TCA cycle	HumanCyc
0.001436718	Late Phase of HIV Life Cycle	Reactome
0.001439725	allopregnanolone biosynthesis	HumanCyc
0.001468946	Glyoxylate and dicarboxylate metabolism - Homo sapiens (human)	KEGG
0.001468946	Signaling by FGFR4 mutants	Reactome
0.001556962	Non-alcoholic fatty liver disease (NAFLD) - Homo sapiens (human)	KEGG
0.001560644	Loss of Nlp from mitotic centrosomes	Reactome
0.001560644	Loss of proteins required for interphase microtubule organizationfrom the centrosome	Reactome
0.001560644	IL-1 JNK	INOH
0.001560644	TLR JNK	INOH
0.001746394	the prc2 complex sets long-term gene silencing through modification of histone tails	BioCarta
0.001754773	Infectious disease	Reactome
0.001778706	RNA Polymerase II Transcription	Reactome
0.001797969	Mitotic G2-G2/M phases	Reactome
0.001847434	TLR p38	INOH
0.001847434	Proteasome Degradation	Wikipathways
0.001856701	Anchoring of the basal body to the plasma membrane	Reactome
0.001867891	HIV Infection	Reactome
0.00196427	Fanconi anemia pathway	PID
0.002029834	Mitochondrial translation termination	Reactome
0.002046936	Citric acid cycle (TCA cycle)	Reactome
0.002068459	Fas	INOH
0.002232855	Oxidative phosphorylation - Homo sapiens (human)	KEGG
0.002350716	Eukaryotic Transcription Initiation	Wikipathways

0.002423989	Cell Cycle	Reactome
0.00251725	Retinoic acid receptors-mediated signaling	PID
0.002547572	SUMOylation	Reactome
0.002658026	Synthesis of bile acids and bile salts via 27-hydroxycholesterol	Reactome
0.002705735	Oxidative phosphorylation	Wikipathways
0.002769849	superpathway of cholesterol biosynthesis	HumanCyc
0.002794736	miR-targeted genes in lymphocytes - TarBase	Wikipathways
0.002897652	superpathway of conversion of glucose to acetyl CoA and entry into the TCA cycle	HumanCyc
0.003084264	Long-chain-3-hydroxyacyl-coa dehydrogenase deficiency (LCHAD)	SMPDB
0.003084264	Fatty Acid Elongation In Mitochondria	SMPDB
0.003084264	Aflatoxin B1 metabolism	Wikipathways
0.003307436	Transcription	Reactome
0.003360227	Regulation of PLK1 Activity at G2/M Transition	Reactome
0.003377534	Ubiquitin mediated proteolysis - Homo sapiens (human)	KEGG
0.003485943	miR-targeted genes in muscle cell - TarBase	Wikipathways
0.003643701	ID	NetPath
0.003643701	Vitamin B9 (folate) metabolism	EHMN
0.004075669	Alpha-oxidation of phytanate	Reactome
0.004084807	Noncanonical Wnt signaling pathway	PID
0.004161687	snRNP Assembly	Reactome
0.004161687	Metabolism of non-coding RNA	Reactome
0.004276984	Proteasome - Homo sapiens (human)	KEGG
0.004637878	TLR NFkB	INOH
0.004666234	Influenza Infection	Reactome
0.004716363	Signaling by FGFR2 mutants	Reactome
0.004716363	Signaling by FGFR2 in disease	Reactome
0.004716363	Synthesis of bile acids and bile salts	Reactome
0.00497158	Mitochondrial translation initiation	Reactome
0.004992114	map kinase inactivation of smrt corepressor	BioCarta
0.004992114	Vitamin B5 (pantothenate) metabolism	Reactome
0.00542558	Wnt Canonical	INOH
0.00542558	Wnt Mammals	INOH
0.00552047	Glycine, serine, alanine and threonine metabolism	EHMN
0.005665197	Gene Expression	Reactome
0.005665335	MAP kinase cascade	HumanCyc
0.005665335	sumoylation as a mechanism to modulate ctbp-dependent gene responses	BioCarta
0.005665335	nuclear receptors coordinate the activities of chromatin remodeling complexes and coactivators to facilitate initiation of transcription in carcinoma cells	BioCarta
0.005833539	Influenza Life Cycle	Reactome
0.005841352	IL-1 NFkB	INOH
0.005995941	AndrogenReceptor	NetPath
0.006142235	Integrin-linked kinase signaling	PID
0.006142235	Aryl Hydrocarbon Receptor	Wikipathways
0.006326131	p38 MAPK Signaling Pathway	Wikipathways
0.006848521	Fanconi anemia pathway - Homo sapiens (human)	KEGG

0.006889913	SHC-mediated cascade:FGFR4	Reactome
0.006889913	Antigen Presentation: Folding, assembly and peptide loading of class I MHC	Reactome
0.007287488	Valine, leucine and isoleucine degradation - Homo sapiens (human)	KEGG
0.007429047	cholesterol biosynthesis I	HumanCyc
0.007429047	cholesterol biosynthesis II (via 24,25-dihydrolanosterol)	HumanCyc
0.007429047	cholesterol biosynthesis III (via desmosterol)	HumanCyc
0.007465324	Cellular responses to stress	Reactome
0.007518024	Activation of gene expression by SREBF (SREBP)	Wikipathways
0.007518024	Activation of gene expression by SREBF (SREBP)	Wikipathways
0.00771552	FGF	INOH
0.00854022	DNA Repair	Reactome
0.008816433	Transcription of the HIV genome	Reactome
0.008816433	SREBP signalling	Wikipathways
0.008875218	Doxorubicin Pathway (Cardiomyocyte Cell), Pharmacodynamics	PharmGKB
0.008875218	Activation of gene expression by SREBF (SREBP)	Reactome
0.008875218	Synthesis of bile acids and bile salts via 7alpha-hydroxycholesterol	Reactome
0.008875218	tumor suppressor arf inhibits ribosomal biogenesis	BioCarta
0.009369013	UDP-acetyl-D-galactosamine biosynthesis II	HumanCyc
0.009369013	spliceosomal assembly	BioCarta
0.009369013	COPII (Coat Protein 2) Mediated Vesicle Transport	Reactome
0.009369013	ER to Golgi Transport	Reactome
0.00940484	pyruvate decarboxylation to acetyl CoA	HumanCyc
0.00940484	Pentose Phosphate Pathway (Erythrocyte)	PharmGKB
0.009405877	TCA cycle	EHMN
0.009405877	IGF1 pathway	PID
0.009409047	Transport to the Golgi and subsequent modification	Reactome

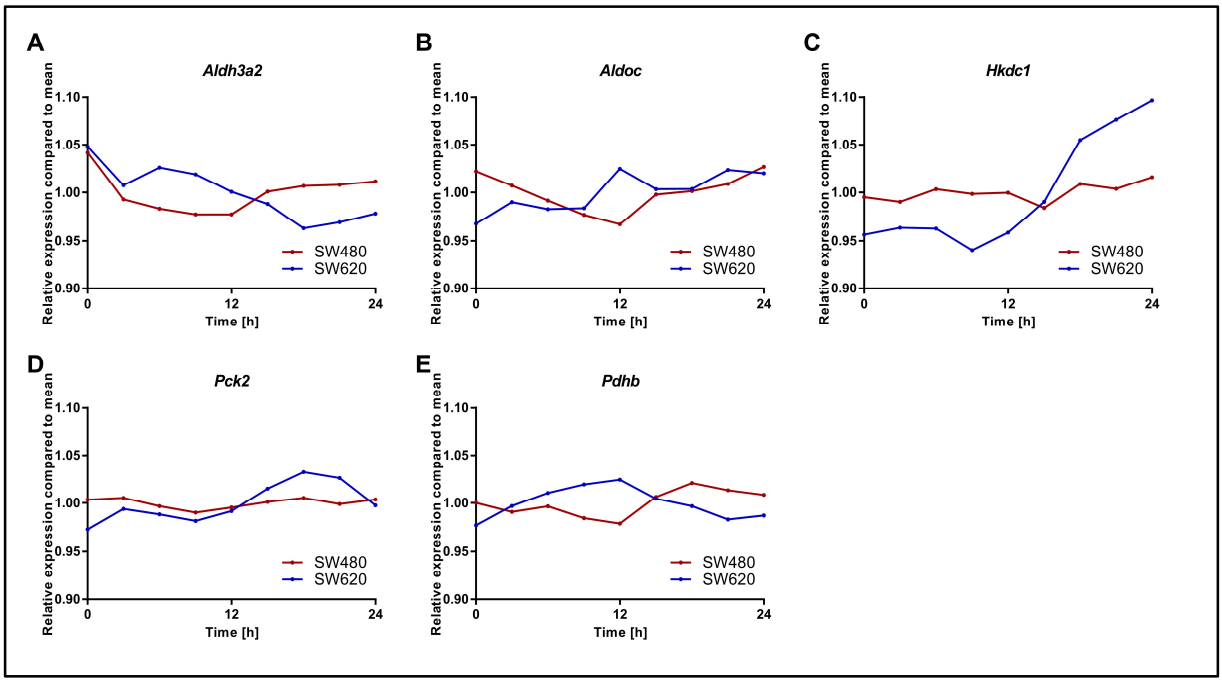

Figure S 6: Expression of metabolic candidate genes

24 h expression patterns of selected metabolic genes in SW480 and SW620 cells. The expression is based on 24 h time course microarray data. Relative expression compared to the mean.

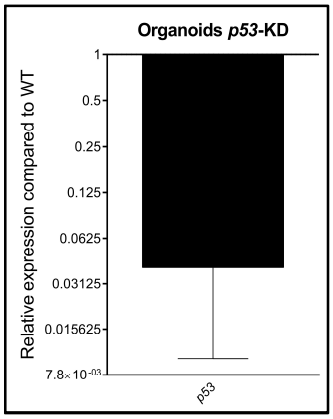

Figure S 7: Knockdown efficiency after shRNA-mediated KD of *p53*
Gene expression analysis of *p53* in human fallopian tube organoids after shRNA-mediated *p53*-KD. Gene expression is shown compared to the corresponding control gene. Mean ± SEM, n = 3. KD efficiency: 96 %.

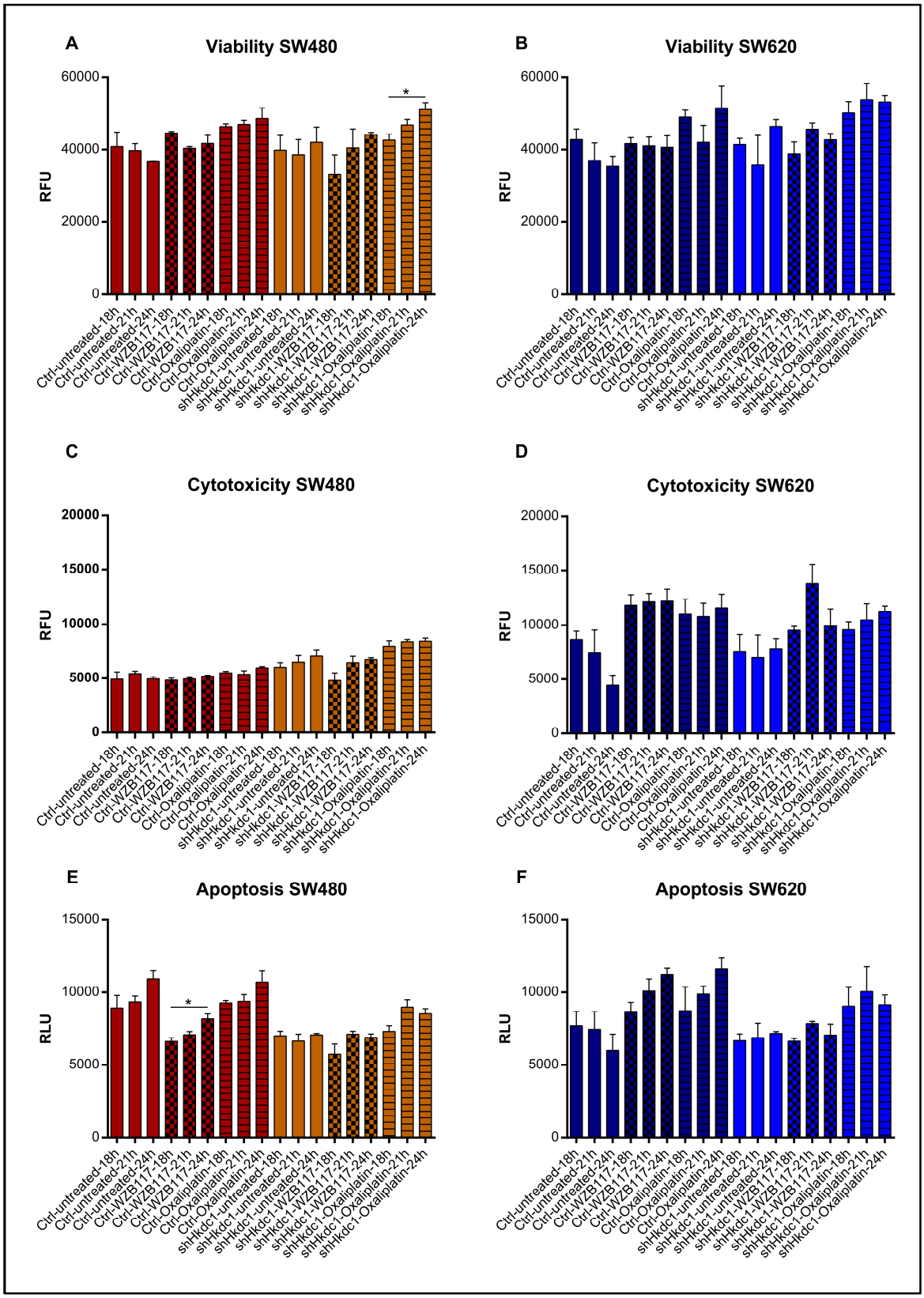

Figure S 8: Viability, cytotoxicity and apoptosis in SW480 and SW620 cells
Viability (**A**, **B**), cytotoxicity (**C**, **D**) and apoptosis (**E**, **F**) in SW480 and SW620 control and *shHkdc1* cells synchronised at different timepoints. Cells were either untreated or treated with WZB117 or oxaliplatin. Mean ± SEM, n = 3. Significant changes ($p < 0.05$) between different synchronisation timepoints of the same condition are marked with *. * = $p < 0.05$, ** = $p < 0.01$, *** = $p < 0.001$.

7. Publications and conference contributions

7.1 Publications

The following publications were published during the time of this doctoral project.

7.1.1 Research articles

Fuhr, L., El-Athman, R., Scrima, R., Cela, O., Carbone, A., Knoop, H., Li, Y., Hoffmann, K., Laukkanen, M.O., Corcione, F., et al. (2018). The Circadian Clock Regulates Metabolic Phenotype Rewiring Via HKDC1 and Modulates Tumor Progression and Drug Response in Colorectal Cancer. EBioMedicine 33, 105–121. IF: 6.183, Citations: 2.

El-Athman, R., **Fuhr, L**., and Relógio, A. (2018). A Systems-Level Analysis Reveals Circadian Regulation of Splicing in Colorectal Cancer. EBioMedicine 33, 68–81. IF: 6.183, Citations: 1.

El-Athman, R., Genov, N.N., Mazuch, J., Zhang, K., Yu, Y., **Fuhr, L**., Abreu, M., Li, Y., Wallach, Thomas, et al. (2017). The Ink4a/Arf locus operates as a regulator of the circadian clock modulating RAS activity. PLoS Biol. 15. IF: 9.163, Citations: 12.

Lehmann, R., Childs, L., Thomas, P., Abreu, M., **Fuhr, L**., Herzel, H., Leser, U., and Relógio, A. (2015). Assembly of a Comprehensive Regulatory Network for the Mammalian Circadian Clock: A Bioinformatics Approach. PLoS One 10, e0126283. IF: 2.766, Citations: 14.

Scrima, R., Cela, O., Merla, G., Augello, B., Rubino, R., Quarato, G., Fugetto, S., Menga, M., **Fuhr, L**., Relógio, A., et al. (2016). Clock-genes and mitochondrial respiratory activity: Evidence of a reciprocal interplay. Biochim. Biophys. Acta - Bioenerg. 1857, 1344–1351. IF: 4.28, Citations: 8.

Cela, O., Scrima, R., Pazienza, V., Merla, G., Benegiamo, G., Augello, B., Fugetto, S., Menga, M., Rubino, R., **Fuhr, L**., et al. (2016). Clock genes-dependent acetylation of complex I sets rhythmic activity of mitochondrial OxPhos. Biochim. Biophys. Acta - Mol. Cell Res. 1863, 596–606. IF: 4.28, Citations: 15.

7.1.2 Reviews

Fuhr, L., Abreu, M., Pett, P., and Relógio, A. (2015). Circadian systems biology: When time matters. Comput. Struct. Biotechnol. J. 13, 417–426. IF: 4.148, Citations: 28.

7.1.3 Book chapters

El-Athman, R., Mazuch, J., **Fuhr, L**., Abreu, M., Genov, N., and Relógio, A. (2017). Methods for the visualization of circadian rhythms: From molecules to organisms. In Fluorescence Imaging and Biological Quantification, (Taylor & Francis Group, 6000 Broken Sound Parkway NW, Suite 300, Boca Raton, FL 33487-2742: CRC Press), pp. 231–257.

7.1.4 Peer-reviewed abstracts

Fuhr, L., and Relógio, A. (2015). Analysis and identification of circadian-regulated metabolic pathways in tumourigenesis. Febs J. 282, 184.

7.2 Conference contributions

40th FEBS Congress, The Biochemical Basis of Life (Berlin)
Poster presentation and speed talk
Analysis and identification of circadian-regulated metabolic pathways in tumourigenesis.

EMBO|EMBL Symposium: Biological oscillators: Design, Mechanism, Function (Heidelberg)
Poster presentation
Circadian-regulated metabolic pathways in tumourigenesis

EMBO Conference: From functional genomics to systems biology (Heidelberg)
Poster presentation
The circadian clock and its role in tumourigenesis

Charité Conference: Sharing radically novel visions in Cancer (Berlin)
Poster presentation
The circadian clock regulates metabolism and influences treatment response in cancer cells